OPUR : Observatoire d'hydrologie urbaine en Île de France
Thème de recherche R3: Gestion à la source des eaux pluviales
Action de recherche R3.2

EFFICACITE HYDROLOGIQUE DES JARDINS DE PLUIE : DE LA MESURE IN-SITU A LA MODELISATION POUR UNE DIVERSITE DE CONTEXTES

Rapport final
Thèse de doctorat de Tinghao HUANG
Mai 2025

Thèse réalisée au sein des laboratoires ENPC/Leesu et Cerema/Team, sous la direction de Marie-Christine Gromaire, Jérémie Sage et Didier Techer

THÈSE DE DOCTORAT

de l'École nationale des ponts et chaussées

TITRE DE LA THÈSE

Hydrologic performances of rain gardens – From *in-situ* monitoring to modelling for a variety of contexts

École doctorale Sciences, Ingénierie et Environnement

Spécialité du doctorat : Sciences et Techniques de l'Environnement

Thèse préparée au sein Laboratoire Eau Environnement et Systèmes Urbains, École nationale des ponts et chaussées | Institut Polytechnique de Paris

Thèse soutenue la 22 mai, 2025, par

Tinghao HUANG

Composition du jury :

Laurent, LASSABATERE Ingénieur des Travaux Publics d'État, ENTPE	*Rapporteur*
Tim, FLETCHER Professeur, University of Melbourne	*Rapporteur*
Adrien, WANKO Professeur, Université de Strasbourg	*Examinateur*
Anna, PALLA Professeure associée, University of Genova	*Examinateur*
Agnes, DUCHARNE Directrice de recherche, Sorbonne Université	*Examinateur*
Marie-Christine, GROMAIRE Directrice de recherche, Leesu - ENPC	*Directeur de thèse*
Jérémie, SAGE Ingénieur des Travaux Publics d'État, CEREMA	*Co-Directeur de thèse*
Didier, TÉCHER Chargé de recherche, CEREMA	*Co-Directeur de thèse*

Table of Contents

List of Figures

List of Tables

List of Abbreviations

Abbreviations	Definitions
BEST-infiltration test	Beerkan Estimation of Soil Transfer parameters single-ring infiltrometer test
BMPs	Best Management Practices
CI	Confidence Interval
ET	Evapotranspiration
FAO56-PM	FAO56 Penman-Monteith equation
GI	Green Infrastructures
HLR	Hydraulic Loading Ratio
IWS	Internal Water Storage
Ks/Ksat	Saturated Hydraulic Conductivity
LID	Low Impact Development
NbS	Nature-based Solutions
OLS	Ordinary Least Squares regression
PET	Potential Evapotranspiration
PI	Prediction Interval
SCF	Surface Coverage Fraction
SCMs	Stormwater Source Control Measures
SuDS	Sustainable Urban Drainage Systems
SWMM	Storm Water Management Model
TA	Alternative Techniques
VRR	Volume Reduction Ratio
WSUD	Water Sensitive Urban Design

Abstract

Nature-based solutions, such as bioretention systems, are in growing use for resilient urban runoff management. A bioretention system includes a vegetated depression to collect and infiltrate runoff, a substrate to provide water filtration and retention/evapotranspiration, and optionally a transition, drainage or storage layer. Bioretention can control runoff volume, delay flow peaks and enhance evapotranspiration (ET), thereby contributing to a more natural local water balance. However, its hydrological performance is likely to vary, depending on system design and local context. The objectives of this research are: i) to elucidate the impacts of various bioretention design characteristics on their hydrological functioning, with a special focus on cases with low exfiltration potential and under an oceanic climate, typically corresponding to the conditions found around Paris; and ii) to assess the reliability and robustness of HYDRUS-1D model in representing different designs and input parameters.

Through a thorough literature review, this research began with a comprehensive overview of bioretention designs, experimental setups and modelling approaches considered in previous studies. The analysis also highlighted the following knowledge gaps: 1) underrepresentation of some local contexts and designs; 2) limited studies on long-term water balance monitoring; and 3) insufficient investigation on subsoil and shallow groundwater interactions.

The PhD relied on continuous monitoring of three bioretention prototypes in Paris region and on field investigations to explore the efficiency of runoff volume reduction under unfavourable subsoil conditions (e.g., limited or forbidden exfiltration), the relative importance of different hydrologic processes and ways to enhance them. The field conditions include: 1) An unlined system with a relatively high hydraulic loading ratio (HLR) of 13over clay soil, examining how IWS may enhance exfiltration; 2) Two lined systems, assessing whether a combination of low HLR (i.e.4), fine-textured substrate and IWS can enhance ET and act as a primary mechanism for volume reduction.

Overall, the three systems achieved significant runoff volume reduction over the monitoring period (43% for JdB1, 48% for JdB2, 63% for SC), despite the lack of exfiltration or low permeability of the subsoil. For the unlined system, the volume reduction performance was largely controlled by the thickness of the IWS (extending IWS from 2 cm to 22 cm increased volume reduction from 27% to 55%). For the lined systems, it is controlled by ET, which was more than doubled in presence of an IWS. In the unlined system, a capillary barrier between the transition and drainage layers promoted soil water retention, yet ET remained lower than potential evapotranspiration (PET). Silt loam substrate in the lined systems supported vegetation but led to clogging and cracking issues which were mitigated by the IWS. A risk of water intrusion from perched lens was also identified when the bottom of the bioretention is connected to a low permeability subsoil.

The final part of this research involved an evaluation of HYDRUS-1D for bioretention modelling. A sensitivity analysis assessed how varying levels of input knowledge impact the model robustness. The results on water balance, especially drainage volume, proved to be robust and accurate and were not significantly affected by uncertainties in input parameters. However, the soil moisture profile results were highly dependent on the bottom boundary condition and, to a lesser extent, on soil hydrodynamic properties. Neither of the two tested boundary conditions allowed for a good description of soil moisture, indicating that the model could not adequately capture the hydraulic behaviour of the system. Besides, for a HLR of 13, vegetation properties had a very limited impact on the water balance.

Key words: infiltration, evapotranspiration, monitoring, modelling, urban runoff, bioretention

Chapter 1: General introduction

From a historical perspective, urban runoff management has always been an important topic in the urbanisation process. As early as more than 4000 years ago, early civilisations, such as Mesopotamian (Eshnunna and Babylonia) and Pingliangtai civilisations (De Feo et al., 2014a) were already starting to use grey infrastructures such as clay or earthen water pipes and drainage trenches to quickly direct floodwaters away from the city. These designs are the early stage of urban grey drainage systems. As time progressed, start from the Middle Age in Europe, the construction of sewers went through an erratic and less coherent phase, due to the inconsistent design and objectives, until the occurrence of modern sewer systems in 1842 in Hamburg, Germany (Eich & Wierecky, 2002). The principle for sewer systems at this stage was focusing on sanitation, i.e., rapid drainage of the wastewater and stormwater from the city (Bertrand-Krajewski, 2021). Thus, they are commonly linked to surface water impairment. With the fast urbanisation around the world, the limits of the capacity of grey infrastructure have been stretched, from the large sewer conduits built in 19th century Paris which allow people to pass through (De Feo et al., 2014b), to the huge underground "temple" in Tokyo (Nakamura & Oosawa, 2021).

Due to the rapid urbanisation and climate change impact, these stationary grey infrastructures are under challenges, not only for extreme events such as the cloudburst event in Denmark in 2011 that caused massive flood damage (Matte et al., 2021), but also for the relatively frequent rain events, such as discharge of polluted stormwater and combined sewer overflow (partly due to the misconnection in the separate sewer system) during the Paris Olympic game in 2024 (Le Monde & AP, 2024). Besides, other issues also exist, e.g., reduction of infiltration (less groundwater recharge), physical impact on the receiving bodies linked to modification of hydrological regime and exacerbated hydrological extremes such as drought, lack of water resources and urban heat islands (Benedict & McMahon, 2002). All these challenges introduce the need for new paradigms in stormwater management.

As a result, a number of more sustainable and flexible concepts of stormwater management have been proposed and refined around the world since last century. For instance, in the US, Low Impact Development (LID) was initially coined by Barlow

et al. (1977) and was later officially documented by Prince George's County Department of Environmental Resources (2000). Best Management Practices (BMPs) existed from the mid-20th century (Ice, 2004), and were further officially defined by USDA Forest Service (1980). Green infrastructures (GI) (Walmsley, 1995), which was originally used in the field of urban planning and focused on ecosystem services, was later found to have potential usage on stormwater management. Nowadays GI is widely spread and adopted around the world as both a concept and process (Fletcher et al., 2015). Out of US, Sustainable Urban Drainage System (SuDS) was coined in UK (Woods-Ballard et al., 2007), Water Sensitive Urban Design (WSUD) was from Australia (Whelans et al., 1994). In addition, similar concepts have also been proposed in non-English speaking countries. Such as Alternative techniques (TA) (STU, 1982) and the later introduced "gestion intégrée des eaux pluviales" (integrated stormwater management) and "gestion à la source" (source control) from France, Sponge City Program from China (MOHURD, 2014), etc. These concepts have great variations in scale, some are more focused on specific practices, and others are planning principles (Fletcher et al., 2015). In addition, although the specific measures are often multifunctional, these concepts have a context-specific focus. Some focus more on the runoff flow control, such as volume and peak flow reduction (TA), reducing impervious surface and enhance infiltration (LID), mimicking natural drainage to manage runoff (SuDS), or absorb and store water (Sponge City), while others refer more to pollution prevention, such as BMPs (US EPA, 1990). There are also some concepts with more multi-benefit and more integrated water management purpose, such as GI which tries to improve biodiversity and climate resilience, WSUD which blends urban planning with sustainable water use. In recent years, nature-based solutions (NbS) have gained increasing attention as a concept to address climate change adaptation and mitigation (Su et al., 2023). By using natural processes and ecosystems, NbS offer resilient alternatives for managing water, climate, and biodiversity while complementing traditional engineering approaches (Seddon et al., 2020).

This thesis focuses on one type of green infrastructures that has a vegetated surface storage, a layer of filter media and optional layers of drainage and underground storage, namely bioretention systems. They can capture, filter, and treat runoff from pervious/impervious surface before infiltration or discharge by mimicking natural

biological and hydrological processes. Bioretention systems can be implemented from a household scale (a garden) up to a neighbourhood scale.

Certainly, the terminology used for bioretention systems varies between regions, languages and design purposes. The term “rain garden” appeared for residential use in the 1990 in Maryland, USA. By 1993, “bioretention” was brought out as a type of BMP and being noted on the use of natural or artificial soil media (Clar, 2010). Other terms such as “biofilter”, “bioswale” and “bio-infilter” have been proposed to distinguish their shape or function (MPCA, 2022). In order to avoid confusion and make the terminology more uniform, this study follows the initiative from previous researchers (Spraakman et al., 2020a) and thus uses the term ‘bioretention’.

Nowadays, bioretention is widely studied around the world for its hydrological performance and quality control (pollutant removal) performance. However, there are still gaps and questions remaining in the long-term performance monitoring, as well as on the detailed understanding of various hydrological processes, especially under different design and local contexts. To fill this gap, this PhD was proposed with the aim of i) elucidating the impacts of various bioretention design characteristics on their hydrological functioning, with a special focus on cases with low exfiltration potential, ii) assessing the reliability of modelling approaches to evaluate these designs. The title of this thesis is *Hydrologic performances of rain gardens – From in-situ monitoring to modelling for a variety of contexts.*

This PhD thesis is funded by OPUR program, and also benefited from specific support from the municipality of Paris. OPUR (https://www.leesu.fr/opur/) is a long-term research program on urban hydrology in Paris region developed in close partnership between researchers and operational services. The PhD was conducted under one of the themes of OPUR-Phase5: *managing stormwater from the source*. The aim of this theme is to optimise the design and management of urban runoff source control measures, with a particular focus on structures that use the ecosystem functions of a vegetated soil or substrate.

The manuscript consists of four main chapters with a conclusion and perspectives chapter. In a nutshell, these main chapters include, i) Chapter 2: literature review; ii) Chapter 3: experiment designs and methodology on three bioretention prototypes, Chapter 4: results from the experimental work; iii) Chapter 5: modelling of one prototype garden and sensitivity analysis.

Chapter 2: literature review part is converted from a review article, namely "*Hydrological performance of bioretention in field experiments and models: A review from the perspective of design characteristics and local contexts"*, which has been published on *Science of the Total Environment* in Feb 2025, DOI: 10.1016/j.scitotenv.2025.178684. This review not only provides the background and state of the art of current research, but also explores an approach to extract knowledge from the existing literature. In this review, bioretention data from 75 field monitoring and modelling studies, including local contexts, detailed design information, performance indicators and other key findings, were extracted into a general database (128 monitored facilities and 9 theoretical modelling cases). The database was used to assess the relationships between bioretention designs, local contexts and their hydrological performance. Additionally, regional guidelines and some studies which focused on specific questions were covered.

While Chapter 2 answers some questions about the thesis topic and objectives, there is a part of the question that cannot be directly obtained from the existing literature. A section of PhD objectives and general approaches is thus presented at the end of Chapter2 and from there the approach of monitoring (Chapter3) and modelling (Chapter4) are drawn out.

Chapter 3 and Chapter 4 are adapted from an article draft, which is planned to be submitted to *Journal of Environmental Management*. The chapter contains the most important part of this study, i.e., all the experimental work based on three bioretention prototypes, including field investigation and monitoring, sensor calibration, data processing (Chapter 3) and analysis of the results (Chapter 4).

Based on the field monitoring and investigation results from Chapter 3 and Chapter 4, Chapter 5 conducts a modelling work on one of the bioretention prototypes using HYDRUS-1D model. The chapter intends to check the model sensitivity to different input parameters, and the robustness of the model when some inputs are not provided (or provided without complete understanding or with limited accuracy).

At the end of the document, the main conclusions and perspectives of this work are presented.

Besides the work itself, this study comes at a time when there is the “explosion” of artificial intelligence (AI) and large language model. However, the regulation for the use of AI in academic research (or PhD dissertations) are still less certain. Therefore, although not required by the Doctoral School, a statement on the use of AI tools within this research is placed in Appendix 1 - AI Usage Statement.

Chapter 2: Literature Review and Further Definition of PhD Approach

This Chapter is adapted from a published review article *Hydrological performance of bioretention in field experiments and models: a review from the perspective of design characteristics and local contexts* (DOI: 10.1016/j.scitotenv.2025.178684). Based on findings from the literature review, further defined scientific objectives and PhD approach are presented at the end of this chapter.

2.1 INTRODUCTION

With the progress of urbanization around the world, the increasing proportion of impervious surfaces in cities has significantly altered urban watershed hydrology (Shuster et al., 2005), exacerbating flood risks and pressures on receiving surface waters. As a countermeasure, Sustainable Urban Drainage Systems (SuDS) have been progressively developed over the last decades to provide on-site management of runoff quantity and water quality control, while potentially promoting groundwater recharge. SuDS are also relevant for urban heat island mitigation, greening, biodiversity enhancement, etc. (Benedict & McMahon, 2002).

Bioretention is one of the typical stormwater source control measures (SCMs) used within SuDS. Based on a concept initially developed for sewage effluent treatment (Roy-Poirier et al., 2010), a bioretention system uses the properties of vegetated soils or engineered substrates to control runoff volume and flow, restore a more natural water balance, improve water quality, but also contribute to urban cooling and amenity (Kridakorn Na Ayutthaya et al., 2023). In this paper, “bioretention” will be defined as a shallow planted depression which collects, temporarily stores, and infiltrates runoff from surrounding urban surfaces (roads, roofs, etc.) through one or multiple adapted media layers (Coffma, et al., 1994). This definition encompasses systems that can be shaped as cells or swales, as well as rain gardens. A bioretention system may be lined or unlined. In a lined system, the water that infiltrates at the surface can only return to the atmosphere through evapotranspiration (ET) or be collected by an underdrain. In an unlined system, the water can additionally be

exfiltrated into the surrounding soil (Fletcher et al., 2013). A bioretention system always contains at least one filtration layer (a layer of natural soil or engineered substrate media) and may have optional top (usually mulch), transition, drainage, or bottom storage layers (Donaghue et al., 2022; MPCA, 2022; Payne et al., 2015b). The transition layer separates fine and coarse materials and may sometimes be replaced by a geotextile. The drainage layer is usually associated with the implementation of an underdrain pipe and refers to a coarse media layer above and around this underdrain (Water by Design, 2014). The bottom storage layer consists of a coarse material layer that can only be emptied through exfiltration or evapotranspiration. In systems with a liner or low permeability native soil, the bottom storage becomes a semi-permanent internal submerged zone (Donaghue et al., 2022). This is referred to as an Internal Water Storage (IWS), which can provide an anaerobic environment for enhanced water purification (Qiu et al., 2019) and act as a water reservoir to sustain plant growth during dry periods (Muerdter et al., 2018).

A well-designed bioretention system benefits the watershed from multiple aspects (Heasom et al., 2006). However, the combination of the various optional features listed above results in a wide variety of possible bioretention system designs. In practice, the design of a bioretention system must be adapted to the local context (e.g., climate, soil type, groundwater depth), local constraints (e.g., available space, underground structures/networks), and device-specific objectives (e.g., groundwater recharge, enhanced water treatment, water recovery).

Design choices related to the presence or absence of features associated with water inflow, storage, or evacuation, such as the presence of a liner, drainage layer or bottom gravel storage, are referred to here as “configurations”. Design characteristics relating to the dimensions of the system or the properties of the above features, such as the thickness of different media or storage layers, are referred to here as “design parameters”. It is clear that the design parameters, configurations, and local context of a bioretention system can have a direct influence on its hydrological performance (Bertolotto & Clark, 2017; Ouédraogo et al., 2022; Spraakman et al., 2020b). However, from a practical perspective, adapting design configurations and parameters to the local context and stormwater management objectives is still not so straightforward.

National or local guidelines for bioretention design exist in North America, Australia or China, for example, but are still lacking in some parts of the world. Even

when such guidelines exist, they are often quite general and do not necessarily take into account all the local context (Bacys et al., 2018). At the same time, guidelines may be very restrictive for some design aspects (e.g., filter media grain size distribution), while other options may be appropriate for some contexts. Some studies have discussed specialized designs for their local contexts (Houdeshel & Pomeroy, 2014; Ouédraogo et al., 2022; Wen et al., 2021). Nevertheless, the extent to which current literature covers the range of possible designs and contexts remains unclear.

Several aspects of bioretention research have already been covered in previous review papers. Bertolotto and Clark (2017) presented the design, function, evaluation indicators and methods of bioretention systems from an implementation (landowner) perspective. In a scoping review, Spraakman et al. (2020) investigated available bioretention studies considering both field and modelling aspects, and how hydrologic and pollutant control performance was defined and reported. Yang et al. (2022) focused on the evolution of bioretention system performance over time and possible research avenues to better predict it. Lisenbee et al. (2021) covered process-based models, detailing their capabilities in describing the different water-balance components, their input/output parameters and their ability to simulate various design configurations. Overall, bioretention design and performance have been addressed mainly through two approaches: 1) scoping reviews that discussed designs and performance separately (Spraakman et al., 2020b); 2) narrative reviews that focused on a few specific design aspects and how they impact the bioretention performance, e.g., media or plants (Skorobogatov et al., 2020; Xiong et al., 2022), or discussed specific water treatment performance aspects such as nitrogen removal (Osman et al., 2019; Zhang et al., 2021). However, several gaps remain: 1) A comprehensive view of the local conditions and bioretention designs for which hydrological analysis (monitoring or modelling) has been conducted is still lacking; 2) The ability of monitoring setups or modelling approaches reported in the literature to address the hydrological performance of bioretention systems, given the diversity of contexts and designs, has not been comprehensively discussed.

The objectives of this review are:

1) Characterise the variety of bioretention designs considered in previous experimental studies in relation to the local context (climate and local guidelines) or research objectives.

2) Synthesize the experimental settings and models used and analyse their suitability for assessing a range of relevant hydrological performance indicators.

3) Build on previous studies to relate hydrological performance indicators to local context and design parameters.

2.2 MATERIALS AND METHODS

2.2.1 Literature Searching Method

Relevant literature was selected using advanced search terms (see Appendix 2 – Searching Terms) on Scopus, based on peer-reviewed paper published between 1999 and 2022 (the articles published after 2022 are still considered in specific analysis or discussion, but not included in the database). The search terms aimed to cover all the papers dealing with the hydrological functioning of bioretention systems (including rain gardens, bioretention cells, bioretention swale and bioretention basins), with either a real experimental device or a modelling case/scenario. The initial search returned 1185 papers. A manual screening based on their abstracts was then performed. By following the inclusion and exclusion rules, the 1185 papers were reduced to 73.

Inclusion and exclusion rules are as follows:

1. The paper should be a monitoring study of a real field case (laboratory studies, such as column experiments, are not considered representative of reality and therefore excluded) or a modelling study (possibly theoretical, but based on environmentally relevant time series/climate conditions).
2. The paper may focus on the water quality function, but should at least mention the hydrological function (which is the only aspect of bioretention considered in this work) in its abstract.
3. Studies of large watersheds are not considered, and research must focus on the bioretention devices themselves.

Based on these rules, large-scale modelling work or water quality aspects are therefore not covered by this study. During the analysis of the 73 peer-reviewed papers, two related documents were added, i.e., one PhD dissertation (Li, 2007), and one conference presentation paper (Brown & Hunt, 2010). Hence, a total of 75 documents were thoroughly reviewed for data collection, synthesis and critical discussion in this study.

2.2.2 Data Extraction

For each document, details were collected on experimental devices (if any), study purpose, local context (i.e., climate, surrounding soil and groundwater conditions), design configuration, design parameters and performance indicators. For experimental work, the monitoring devices (e.g., flowmeter, soil moisture sensor and climate sensor) and field tests (e.g., infiltration test, soil sampling) were also recorded. For modelling work, the type of models (based on their governing equation for water flow within and between the different bioretention layers and the surrounding subsoil), calibration/validation approach (e.g., type of observations, parameters to be calibrated), scenarios tested, and hydrological performance indicators used were recorded. Due to the diversity of indicators and monitored processes, and the lack of consistency in the terms used across studies, groupings were made among the items recorded. Details on the item characterization can be found in Appendix 3 – Literature Database.

Studies that addressed the same bioretention device, but with different research objectives and perspectives, were common. During data extraction, information from these different studies was merged to complete the characteristics of a single bioretention device, unless significant modifications (e.g., the depth of IWS) were noted (Brown & Hunt, 2010, 2011b).

For local conditions, climate types (Köppen climate classification) and annual precipitation were not commonly reported in the literature. Missing data were therefore obtained from the Internet (websites are provided in Appendix 3 – Literature Database) according to their geolocation. For design parameters, those reported as a range (e.g., ponding depth and bottom storage depth) were assigned the mean of their upper and lower bounds.

2.2.2.1 Definition and extraction rules of bioretention performance indicators

Existing studies have proposed a range of indicators in order to evaluate the hydrological performance of bioretention systems. In the selected studies, the same indicators were sometimes found to be given slightly different definitions from one article to another. Therefore, the definitions of the bioretention performance indicators in this study have been standardized as follows. Note that the outflow here refers to underdrain flow and overflow, not exfiltration.

- $Volume\ Reduction\ Ratio = 1 - \frac{V_{outflow}}{V_{inflow}}$

- $Complete\ Retention\ Ratio = \frac{Number_{rain\ events\ without\ outflow}}{Number_{rain\ events}}$
- $Attenuation\ Time = T_{outflow\ peak} - T_{inflow\ peak}$
- $Drain\ Time =$
  $Elapsed\ Time\ Until\ No\ Surface\ Ponding\ and\ No\ Underdrain\ flow\ (if\ it\ applies)$
- $Peak\ Flow\ Reduction = 1 - \frac{Q_{Peak\ out}}{Q_{Peak\ in}}$
- $Exfiltration = \frac{V_{recharge\ into\ surround\ soil}}{V_{total\ incoming}}$

Since the value of the same performance indicators can be presented in different ways (e.g., a range, median, average or separate value for each event), the following rules were applied to make the values of performance indicators consistent across studies:

- The study only gives one value à keep the value
- The study gives a range (e.g., 20% - 80%) à use the average of the upper and lower limits (50%)
- The study gives several values for different single events à use the average
- The study gives a median à keep the median

While such assumptions were necessary to obtain consistent indicators that would allow statistical analysis across relevant studies, the use of a mean or median values may not be fully representative of skewed distributions between rain events. Other potential biases in comparing performance indicators across studies include differences in; 1) the definition of rain events (for event-based indicators), 2) monitoring time steps (for peak flow reduction), or 3) the duration and thus the representativeness of the monitoring period.

2.3 RESULTS AND DISCUSSION

2.3.1 Overview of Selected Documents

The selected literature encompasses 128 different bioretention field devices studied through field monitoring or modelling, and 9 theoretical modelling cases without real devices. Devices investigated through field surveys (e.g., saturated hydraulic conductivity or individual soil moisture measurements) were not included in

the database. However, 58 devices identified during the review process, primarily from two regional studies (Beryani et al., 2021; Spraakman & Drake, 2021), were used as a reference to compare the characteristics of the monitoring devices with those of real-world devices. Of the 128 field devices, 94 bioretention devices were studied by experimental monitoring only, 34 devices were studied by both monitoring and modelling. Due to the selection criteria, the majority of the studies focused on the hydrological function of bioretention (82/128), while remaining devices (46/128) were studied for both hydrological and water quality aspects.

2.3.2 Characteristics of Studied Bioretention Systems

2.3.2.1 Local contexts

The experimental devices in the selected studies are scattered around the world. A number (52/128) of experimental devices are reported in Northern Europe, Eastern, Southeastern, Western and Midwestern United States, where they are distributed among several locations. For the other regions of the world, the experimental facilities tend to be centred in one city (e.g., Xi'an, China and Okotoks, Canada). Figure 2-1 shows the Köppen climate, annual precipitation and groundwater situation of selected studies in relation to their regions.

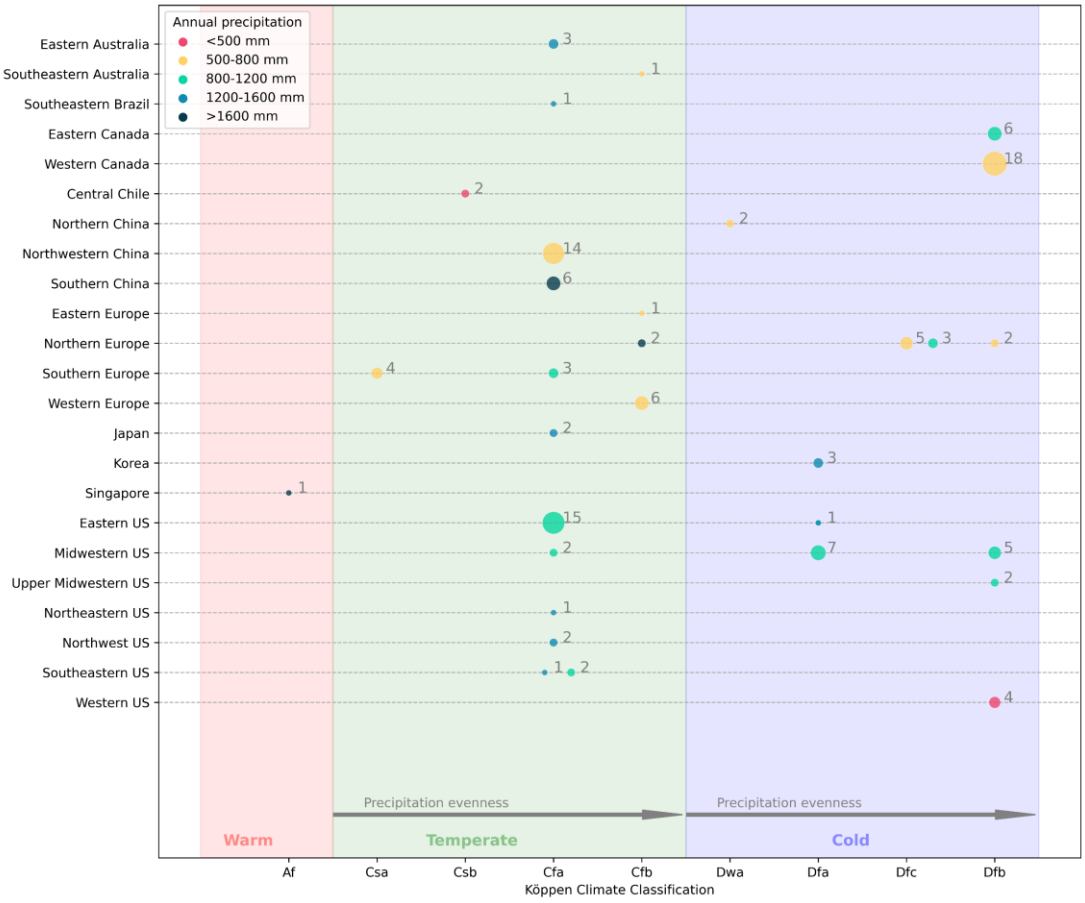

Figure 2-1: Scatter plot on annual precipitation, climate type and region of selected devices. The number next to each dot (also the dot size) represents the number of devices counted in this dot.

A brief definition of the climate classes that were encountered in the selected studies is provided in the following: Af (Tropical rainforest climate); Csa (Mediterranean with dry and hot summers); Csb (Mediterranean with dry and warm Summers); Cfa (Humid subtropical climate); Cfb (Temperate oceanic climate or subtropical highland climate); Dwa (Monsoon-influenced hot-summer continental climate); Dfa (Hot-summer humid continental climate); Dfc (Subarctic climate); Dfb (Warm-summer humid continental climate). These 9 Köppen climate classes can be grouped into 3 temperature types according to their temperature zone (whether they have warm, moderate or cold winters). Within each type, the figure shows, from left to right an increasing evenness of precipitation distribution between seasons. For instance, the Cfb (Oceanic climate) has more evenly distributed precipitation over the year compared to Csa (Mediterranean climate with hot summers).

Cfa (52/128) and Dfb (37/128) were the two most studied climate classes. Except for a few extremely wet (Guangzhou, China and Bergen, Norway) or dry (Lakewood, USA) cities (Guo & Luu, 2015; Mai & Huang, 2021; Zhang et al., 2020), most Dfb,

Cfa and Cfb locations are characterized by relatively even rainfall patterns and moderate drought stress, which is ideal for bioretention systems to control runoff volume and avoid drought threats. The more challenging climate types (Af, Csa, Csb and Dwa) are represented by only one or two studies in Singapore, Southern Europe, Central Chile and Northern China (Aravena & Dussaillant, 2009; Meng et al., 2014; Perales-Momparler et al., 2017; Wang et al., 2019; Zhang & Chui, 2017), and some climates such as BW (Desert climate) or As (Tropical Savanna Climate) are not represented at all.

In addition to climate conditions, other local context aspects such as native soil (or *in-situ* soil) types and local groundwater conditions (e.g., depth and its variability) can influence the design of a bioretention device or affect its performance. For instance, the collapsible native loess (a type of sandy loam soil) in Xi'an (China) required the bioretention system to limit its direct exfiltration to prevent the collapse of nearby infrastructure (Wen et al., 2021). Low-permeability native soils (i.e., clays) can create a "quasi-lined" condition for bioretention systems, limiting exfiltration or even leading to permanent IWS (Géhéniau et al., 2015; Kim et al., 2019). Such conditions were also reported to potentially result the formation of a perched groundwater lens (temporary shallow groundwater) beneath bioretention systems (Schlea et al., 2014). Existing bioretention guidelines took this into account to some extent. For instance, USKH (2008) recommended that for special underground conditions such as impervious soils or bedrock, the bottom of bioretention systems should be kept distant enough from low permeability formations to prevent the buildup of perched groundwater. Furthermore, the hydraulic conductivity of native soils, which controls the exfiltration rate of a bioretention system, was reported to determine the need for an underdrain. (Spraakman & Drake, 2021)Surprisingly, despite its potential influence on bioretention design or performance, native soil has been overall under-reported, even among the studies with unlined bioretention systems. As shown in Figure 2-2, this information was reported for 30.5% of the devices, this proportion was higher for unlined devices (62%). Of the native soil type reported, silt loam, loam and clay were the most common. Based on the limited number of native soil types reported in Figure 2-2, the majority of monitored bioretention systems were not located on highly conductive soil, which may indicate: 1) a bias towards systems better suited for monitoring an outflow (especially

for water quality studies); 2) the current dataset is not representative of bioretention configurations that drain rapidly via exfiltration.

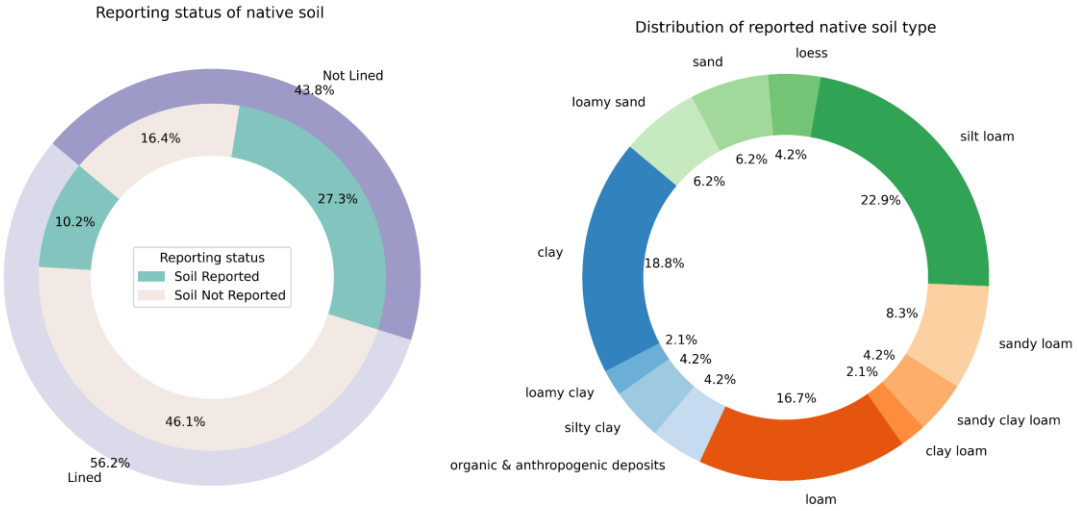

Figure 2-2: Reporting status and distribution of native soil type

Consistent with the limited reporting of native soil types, the presence or absence of groundwater was only rarely mentioned, although a few studies discussed the impact of the bioretention system on groundwater, such as local mounding (Machusick et al., 2011; Stewart et al., 2017) or nearby water table rise (Li, 2007). Those groundwater impact was reported to affect the performance (e.g., negative volume reduction due to more measured outflow than inflow) of studied bioretention system (Kim et al., 2019). Groundwater was also identified as a source of water for plants in bioretention in semi-arid climates (Houdeshel & Pomeroy, 2014). Finally, some cities/regions with special underlying conditions were also reported. For example, Bryggen in Bergen, Norway was reported to have 10 m of organic, anthropogenic waste due to a historical town fire (Venvik & Boogaard, 2020); Collapsible loess soil (mentioned above) was reported in Xi'an, China. But overall, most studies didn't consider subsurface conditions beyond soil type.

2.3.2.2 Configurations

Five configuration aspects were summarized from the 128 field bioretention devices selected: 1. how water enters the device (single or distributed inflow); 2. the presence or absence of an impermeable liner (liner condition); 3. the dominant vegetation type; 4. the presence or absence of a bottom storage layer and/or a drainage layer; 5. the main characteristics of the transition layer (material and thickness, if present).

Transition layer typically refers to a layer that separates two layers with large differences in particle size (e.g., soil media and gravel storage layers). In design guidelines, transition layers have commonly been suggested to be coarse sand (DPU, 2024; Payne et al., 2015a; PUB, 2024) or permeable geotextile fabric (PGCDER, 2007). In its early guidelines Denver's (Colorado, USA) Urban Drainage and Flood Control District recommended the use of geotextile, but later introduced an improved combination of filter media and drainage layer media that eliminated the need for a transition layer (UDFCD, 2015). Consistent with guidelines, bioretention field studies have reported the transition layers to consist of sand (Bonneau et al., 2020; Lisenbee et al., 2020; Lucke & Nichols, 2015; Wang et al., 2019), permeable geotextile (Mai & Huang, 2021; Nocco et al., 2016; Shuster et al., 2017; Zhang & Chui, 2018) or plastic mesh (Muthanna et al., 2008). Since the nature of this transition layer is only reported for a very limited number of devices (27/128), Figure 2-3 shows only the distribution of the first four configuration aspects:

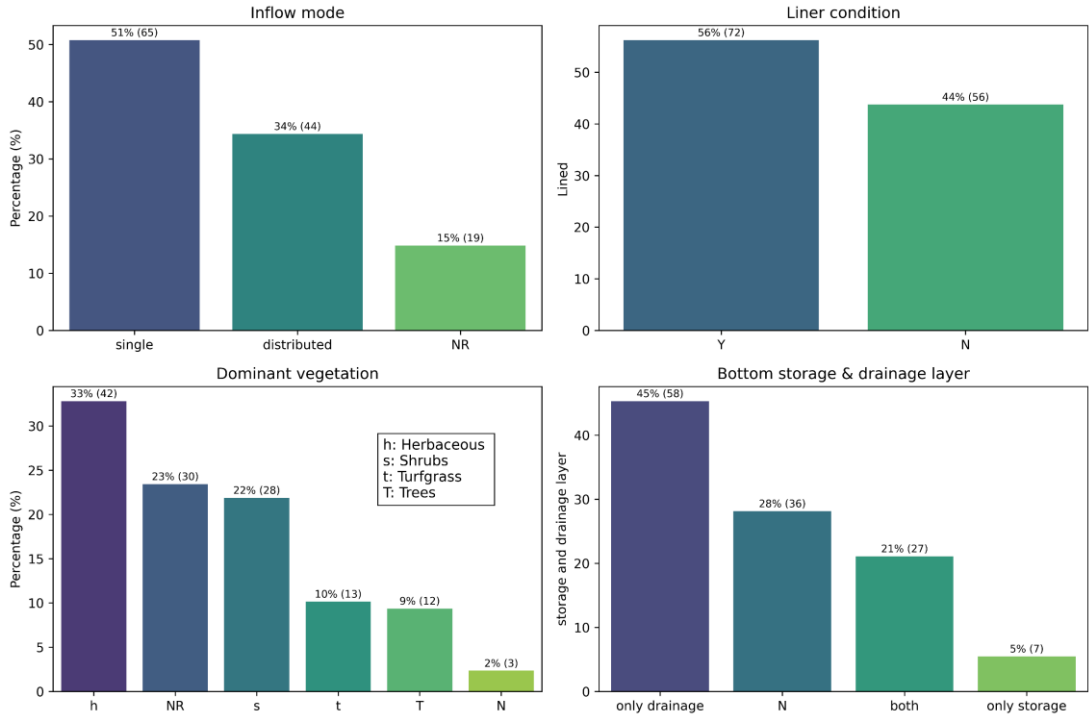

Figure 2-3: The distribution of different bioretention configurations of selected devices (Y: Yes; N: No; NR: Not reported)

The majority (51%) of the bioretention devices studied had a single inflow, while 34% were reported to have a distributed inflow, meaning they receive runoff from multiple inlets or have more dispersed inflows, e.g., direct superficial runoff from adjacent surfaces (Machusick et al., 2011; Zhang et al., 2019), use of a perforated pipe

as an inlet (Dietz & Clausen, 2005; Nocco et al., 2016), or a long distribution gutter inlet to provide a sheet inflow (Li, 2020; Mai & Huang, 2021).

56% of the bioretention devices studied were lined. Lined systems were recommended by guidelines (Dhalla & Zimmer, 2010; NSC, 2008; Payne et al., 2015a; PGCDER, 2007; UDFCD, 2015) in specific contexts to avoid groundwater pollution. For instance, in regions with high groundwater levels, it was recommended to either maintain a sufficient distance between the bottom of the system and the water table (Dhalla & Zimmer, 2010; USKH, 2008), or to use a synthetic liner or compacted clay (DPU, 2024). Guidelines from Australia and Singapore (Payne et al., 2015a; PUB, 2024) also considered the use of liners for rainwater harvesting. However, the high proportion of lined systems in the literature dataset may also reflect the fact that the majority of these bioretention devices were designed/chosen for research purposes, and lined setups facilitated both water balance and water quality assessment. Such an interpretation is consistent with the scarcity of lined bioretention devices reported in field survey studies from Beryani et al. (2021) and Spraakman & Drake (2021), suggesting that non-research purpose bioretention devices are mostly unlined (in Swedish and Canadian contexts). More generally, the adoption of unlined bioretention systems, from which water can be exfiltrated, is presumably the most straightforward option for providing runoff volume control, unless specific constraints preclude exfiltration into the native soil.

Variations were also reported in the implementation of lining components. In some studies with lined systems, clay rings were implemented to prevent preferential flow along the liner boundary (Aravena & Dussaillant, 2009; Dussaillant et al., 2005a; Nocco et al., 2016). Besides, some of the unlined systems were partially lined with rim wall, whose bottoms were connected to the native soil (Bonneau et al., 2020; Smith et al., 2021; Wen et al., 2021). It is noteworthy that the partially lined design can limit lateral flow and restrict lateral exfiltration. This type of partially lined design typically aims at preventing exfiltration damage around buildings and infrastructure (Smith et al., 2021; Wen et al., 2021) or upsloping groundwater intrusion into the bioretention device (Bonneau et al., 2020).

The dominant vegetation type largely varied from one study to another. Herbaceous (ferns, ornamental grasses, herbaceous perennials) (33%) and shrubs (22%) made up for the majority of bioretention vegetation. Despite its herbaceous

affiliation, turfgrass (green lawn) (10%) is classified separately here because it was specifically mentioned in several studies and had different morphometric characteristics (e.g., height, leaf shape) than other ornamental plants or shrubs. 9% of bioretention devices had trees, planted together with other plants (note that the bioretention designs with only a single tree were classified as tree box or tree pit and excluded from this study). Bioretention devices with no vegetation cover were also reported (2%), but this situation only occurred in devices designed for experimental purposes (e.g., reference unvegetated control group) and did not represent real-world bioretention practice. The specific impact of vegetation type was investigated by (Nasrollahpour et al., 2022), who reported higher ET from woody vegetation compared to herbaceous vegetation or turfgrass.

The definitions of drainage and bottom storage layers were not standardized across studies. In this review, a drainage layer is defined as a layer with an underdrain at its bottom. It empties rapidly through the underdrain after the rain event. A bottom storage layer is a layer (usually gravel) which allows water to (temporarily) accumulate and which can empty or drain only by ET or exfiltration. Using this definition, a gravel bottom layer with an underdrain (or outlet) placed in the middle of it is considered as two distinct layers: a drainage layer above the underdrain (or outlet), and a storage layer below the underdrain (or outlet). In some studies, a pipe wrapped in permeable geotextiles was placed directly in the substrate media (Jiang et al., 2020), in which case the pipe itself was considered as the drainage layer. These two layers usually consist of gravel. Other settings included the use of a manufactured alveolar product for the storage layer, as reported in a pilot-scale study (Ouédraogo et al., 2022), and the use of a drainage mat as the drainage layer in a field device (Kanso et al., 2018). On this basis, only 21% of bioretention devices had both storage and drainage layers, 45% of bioretentions had only a drainage layer, and only 5% of devices solely had a bottom storage layer. According to this ratio, drainage was commonly applied in experimental bioretention devices. Drainage may be necessary to prevent water accumulation in the substrate and was recommended by guidelines for low permeability underground. For instance, the Ontario, Canada guideline (Dhalla & Zimmer, 2010) required the installation of an underdrain when the native soil permeability is smaller than 15mm/h. In Ohio, USA, the installation of an underdrain was enforced (DPU, 2024), possibly due to the clay native soil in the region, which

was also consistent with studies in the same region (Schlea et al., 2014). However, designs without drainage and storage appeared to be commonly used in the non-experimental devices reported in the Spraakman & Drake (2021) field surveys, again pointing to a potential bias in the representativeness of experimental systems linked to monitoring constraints.

Table 2-1 presents the different combinations in bioretention typology, and the number of corresponding field devices. Although 5 bioretention configuration elements are discussed in Figure 2-3, only the liner condition, storage layer and drainage layer are chosen to construct this simplified bioretention configuration typology.

Table 2-1: Number of configurations represented by field/modelling devices (Y: exist configuration; N: not exist configuration; NR: Not reported)

Liner condition	Drainage layer	Storage layer	Number of field devices
N	N	N	18
		Y	7
		NR	5
	Y	N	10
		Y	13
	NR	NR	3
Y	Y	N	48
		Y	14
		NR	10

Among the reported field studies, 8 configuration settings were found. The most typical study cases (37.5%; 48 devices) were bioretention devices with impermeable liner, drainage layer and no bottom storage, which was the typical biofiltration/biofilter configuration (Payne et al., 2015b). 14.1% (18 devices) of the bioretention devices studied were unlined and had no specific bottom structures (no drainage or bottom storage layer), and can be classified as bioinfiltration basins (MPCA, 2022). These devices mostly corresponded to real-world operating systems, with only minor modifications to the native terrain or larger bioretention basins. Note that the absence of row corresponding to “liner condition : Y” and “drainage layer : N” in Table 2-1 reflects the systematic inclusion of a drainage layer for lined systems had a drainage layer, consistent with the guidelines (NCDEQ, 2024; USKH, 2008; Woods Ballard et al., 2015).

2.3.2.3 Design parameters

The design parameters include impervious catchment area, bioretention surface area, hydraulic loading ratio, ponding storage thickness, filter media thickness, storage layer thickness and drainage layer thickness. The hydraulic loading ratio HLR is defined here as HLR = impervious catchment area plus bioretention surface area divided by bioretention surface area. Note that some studies used the I/P ratio instead of HLR, where I was the impervious area and P was the bioretention area. However, HLRs in the database were recalculated for all studies for homogeneity.

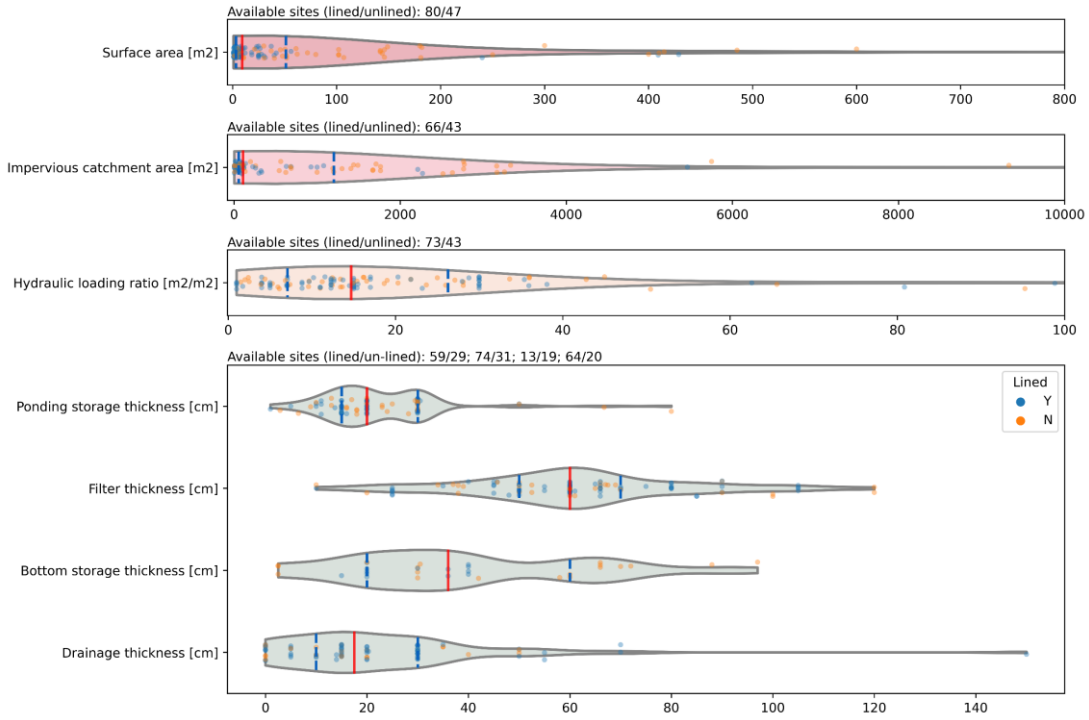

Figure 2-4: Violin plot on bioretention design parameters. The three lines on each violin indicate the lower quarter, median, upper quarter.

The violin plot (Figure 2-4) shows the distribution of these different parameters across experimental studies. The first three violins show area-related parameters with an x-axis limit to exclude large extremes. Most of studied bioretention devices had relatively small surface area (median=9.2m^2) and small catchment area (median=107m^2), although a few bioretention devices with extremely large surface area (up to 4400m^2, 5% > 410m^2) and impervious catchment area (up to 40200m^2, 5% > 5634m^2) were also reported. A large proportion of the smallest bioretention systems (some even < 1m^2) consisted of lined systems. These small devices mostly corresponded to pilot experiments designed for research purposes only, and their area was thus not representative of real-world practice. Large bioretention devices

consisted mostly of unlined retention basin or swales. Large bioretention devices are recommended to have multiple inlets to allow the water to be distributed more evenly (Water by Design, 2014). Design guidelines rarely provided recommendations for bioretention surface and catchment area. Some of the guidelines vaguely mention that bioretention is appropriate for small catchments (PGCDER, 2007; PUB, 2024). Other guidelines suggested an impervious catchment area of less than 4046 m^2 (1 acre) (UDFCD, 2015) or a total catchment area of 100 m^2 to 5000 m^2 (Dhalla & Zimmer, 2010). To size a bioretention, guidelines typically focused on the required capacity of a bioretention device to accommodate design storms (NSC, 2008; PUB, 2024), in other words, the design rainfall pattern and HLR.

The HLR reflects the loading pressure of a bioretention device. From the plot, the HLR of selected devices varies from 1 (no external catchment, used for experimental control group) to 464, with a median of 14.7 (Figure 2-4). The majority (75%) of the devices had an HLR below 26.3 (Figure 2-4). Different issues were reported for extreme HLR values. For the bioretention devices with the lowest HLR values, the inflow was either provided by direct runoff from surrounding surfaces (Hess et al., 2017; Ouédraogo et al., 2022) or showered with a pump (Muthanna et al., 2008). This was partly due to the need to more precisely control the amount of water in these (lysimeter) studies, but may also reflected the difficulty of ensuring a uniform distribution of water across the bioretention area at such low HLRs. For bioretention devices with high HLRs, reported issues included longer drying time (Lee et al., 2022) and excessive sediment loading which eventually led to clogging and overflow (Le Coustumer et al., 2012).

In the lower subplot of Figure 2-4, four thickness parameters are presented. The median thickness of ponding, filter media, bottom storage and drainage layers were 20 cm, 60 cm, 36 cm and 17.5 cm, respectively. These median values are consistent with the range of recommended values from most existing bioretention guidelines (Flanagan et al., 2017). Some extremely low values (< 2 cm) in ponding storage thickness (Zhang et al., 2019, 2020) were calculated by dividing the surface storage volume (originally expressed in m^3) by the bioretention surface area. In the drainage thickness, the few 0 cm values referred to devices that have only an underdrain pipe as the drainage layer, but for which the diameter of the underdrain was not reported. Extreme values in the thickness of the different layers were often associated with

specific design purposes or local contexts. For ponding storage, the high thicknesses came from two large bowl-shaped bioretention basins with large surface storage capacities (Shuster et al., 2017) that were interconnected and collected runoff from a large hillslope catchment (9000 m^2). A bioretention device used for pollutant remediation in Quebec, Canada had a 97 cm IWS layer (bottom storage layer in Figure 2-4) (Géhéniau et al., 2015). Thick filter layers were often justified by the need for improved infiltration (i.e., infiltration basin, bioinfiltration traffic island) systems (Emerson & Traver, 2008) or pollutant treatment (Goor et al., 2021) while the smallest filter layer extents were associated with high outlet elevations (resulting in large storage layer extent) (Mai & Huang, 2021), special shallow depth configurations with large surface area (Li et al., 2019; Zhang et al., 2019). The drainage layer was usually (95%) < 54 cm. The outlier value of 150 cm was a sand layer with a bottom drainage pipe (Aravena & Dussaillant, 2009), which was actually designed as a second filter layer (still considered as a drainage layer in Figure 2-4).

For most devices, the filter layer thickness was within the range of 40 to 100 cm, which was considered acceptable for runoff treatment in guidelines (Flanagan et al., 2017). Some guidelines suggested different design parameters (e.g., thickness of the different layers) based on the configuration of the bioretention device. For instance, a shallower filter layer may be suggested when an IWS is present (NCDEQ, 2024; Payne et al., 2015a), but it should remain at least 30 cm. When trees or shrubs are applied to the bioretention devices, the recommended filter layer thickness often exceeded 90 cm (Dhalla & Zimmer, 2010; NCDEQ, 2024; PUB, 2024).

The bottom storage layer in tested devices were often thicker than the 30 cm value recommended by several guidelines (NCDEQ, 2024; NSC, 2008; Payne et al., 2015a). This may be linked to research objectives to improve performances.

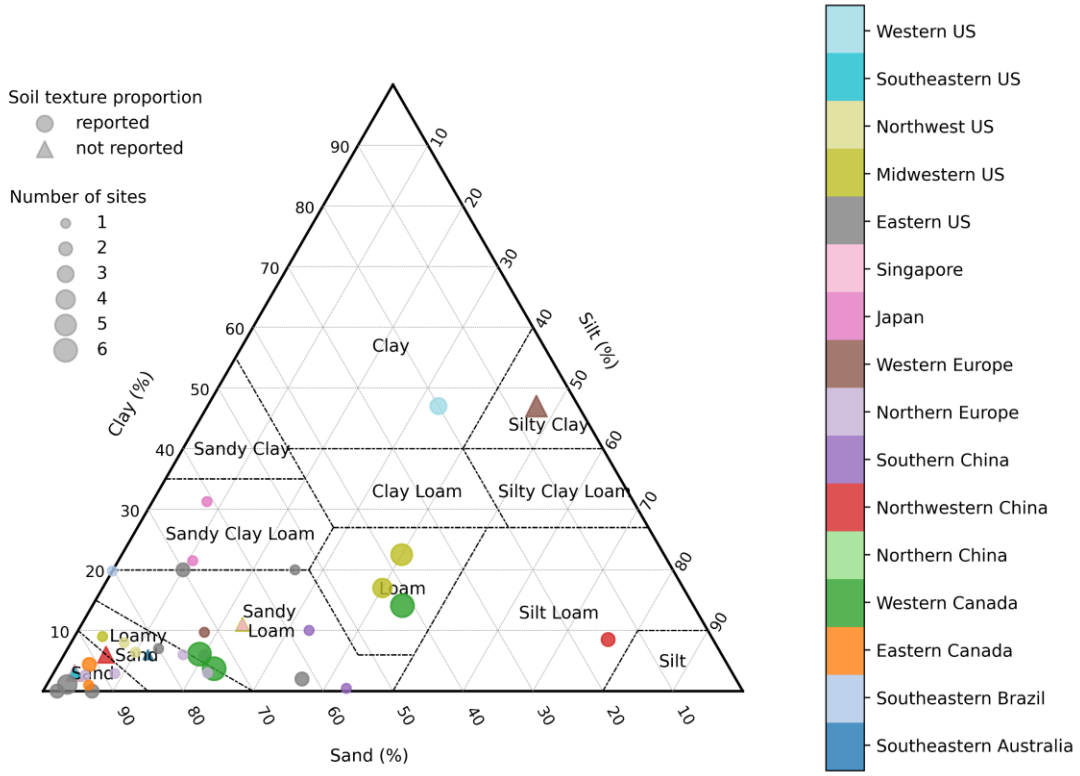

Figure 2-5: Soil texture distribution in bioretention substrates

The media type information was commonly provided as a proportion of sand, silt and clay or a specific USDA soil texture class (e.g., silt clay), which can be standardized and represented on a triangular soil texture classification as shown in Figure 2-5. A total of 84 devices are considered here, excluding ambiguous descriptions (e.g., engineered bio-soil, mixed compost, soil mixed sand) of media type.

In Figure 2-5, the soil type classification is based on USDA soil texture classes, with each point representing a certain proportion of sand, silt, and clay. Figure 2-5 demonstrates a clear clustering of media types used in bioretention devices. The majority of reported devices (59/84) had sandy substrate media (sand > 50%). Reported devices were mostly consistent with the higher proportion of sand (> 75%) commonly recommended by local guidelines (Dhalla & Zimmer, 2010; NCDEQ, 2024; Payne et al., 2015a; PUB, 2024; UDFCD, 2015), but some studies examined medias that differed from the general recommendation. A few bioretention systems reported the use native soils in substrate media, such as silty clay (Ouédraogo et al., 2022), loamy sand (Dietz & Clausen, 2005), sandy loam (Batalini de Macedo et al., 2019), silty sand (native loess) (Guo et al., 2018; Li et al., 2019; Tang et al., 2016) and loam (Mai & Huang, 2021). Loam was also used in a commercially purchased soil with high

organic compost (Schlea et al., 2014). Only three devices from one study used clay as a medium to increase drought resilience (Houdeshel & Pomeroy, 2014). It is worth noting that USDA soil classifications generally give a first indication of a media's infiltration and water-holding capacity, but these properties usually vary within a given soil class. Infiltration and water holding capacity may for instance be affected by plant growth (Skorobogatov et al., 2020) or be enhanced by addition of organic matter, such as wood chips (Nasrollahpour et al., 2022). With the exception of a few studies which focused on the impact of organic matter, organic matter did not exceed 10% in most of bioretention substrates. Filter media characteristics (type, infiltration rate) were often justified by local guidelines or standards (Brown & Hunt, 2011a), which may explain the high concentration of bioretention devices in some specific soil classes (e.g., the large number of dots in the sand class in Figure 2-5).

2.3.2.4 Limitation within the within the studied bioretention characteristics

By summarizing and sorting the currently studied bioretention characteristics, some emerging aspects were not fully (or rarely) covered.

In terms of filter media selection, the vast majority of bioretention devices used sandy-based soils, which was in line with guidelines, but led to limited water retention capacity. The shortages of fine media can be low permeability (which cannot fit with some design requirements on drain time), risk of clogging and potential risk of preferential flow along cracks due to soil shrinking in dry periods (Stewart et al., 2016). However, it may be relevant to consider alternatives to sandy-based substrate, such as finer media with increased organic matter (e.g., addition of compost, wood chips, biochar) (Premarathna et al., 2023; Xiong et al., 2022), or to choose an appropriate of combination of soil and vegetation type to maximize the interaction between roots and soils (Lu et al., 2020). This could allow to balance the water retention capacity and K_{sat}, and still needs to be further tested (Lu et al., 2020). The use of sand, but also of gravel, and possibly concrete, polymeric liners and geotextiles, within multi layered bioretention systems was additionally detrimental to the system’s global environmental impact (Öhrn Sagrelius et al., 2022). Thus, stronger focus should be placed on the evaluation of simpler systems, incorporating local and renewable resources, rather than high environmental footprint materials or scarce natural resources like sand (Zhou et al., 2023).

Most experimental studies focused on lined or partly lined systems, for which the interactions between surrounding underground conditions and the hydrological functioning of bioretention cannot be investigated. Although the risk of groundwater mounding or shallow perched lenses was acknowledged by some studies (Schlea et al., 2014) and guidelines (USKH, 2008), the prevalence of this phenomenon and the extent to which it limited the bioretention performance (i.e., volume reduction ratio) presumably requires further investigation of unlined field devices. Another gap in previous research was the under-representation of devices with high exfiltration capacity (unlined systems with high permeability native soils). While such systems may appear as suitable for meeting runoff reduction targets, they may experience exacerbated drought issues and thus require adaptation to balance hydrological performance with the need to ensure water availability for the vegetation (Bortolini & Zanin, 2018).

2.3.3 Bioretention Monitoring

2.3.3.1 Description of monitoring approaches

Most of the bioretention systems reported in the scientific literature were constructed for research purposes, and most were equipped with monitoring systems. Considering the hydrological processes in the water balance, the following hydrological and meteorological variables were monitored: inflow, outflow (underdrain, exfiltration and overflow), water storage (soil, surface and bottom gravel), precipitation and ET. Depending on the time scale considered (event-based or long-term), different emphasis was placed on the different terms. For instance, although ET was reported to play an important role in the annual water balance (Wadzuk et al., 2015), a previous literature survey indicated that the effect of ET was rarely considered in event-scale approaches (Ebrahimian et al., 2019). Conversely, while changes in surface ponding storage and possibly soil and bottom storage may be ignored in long-term analyses, they became essential for short-term water-balance assessment. Figure 2-6 shows how often and by what means the 9 water balance variables were assessed across the different studies.

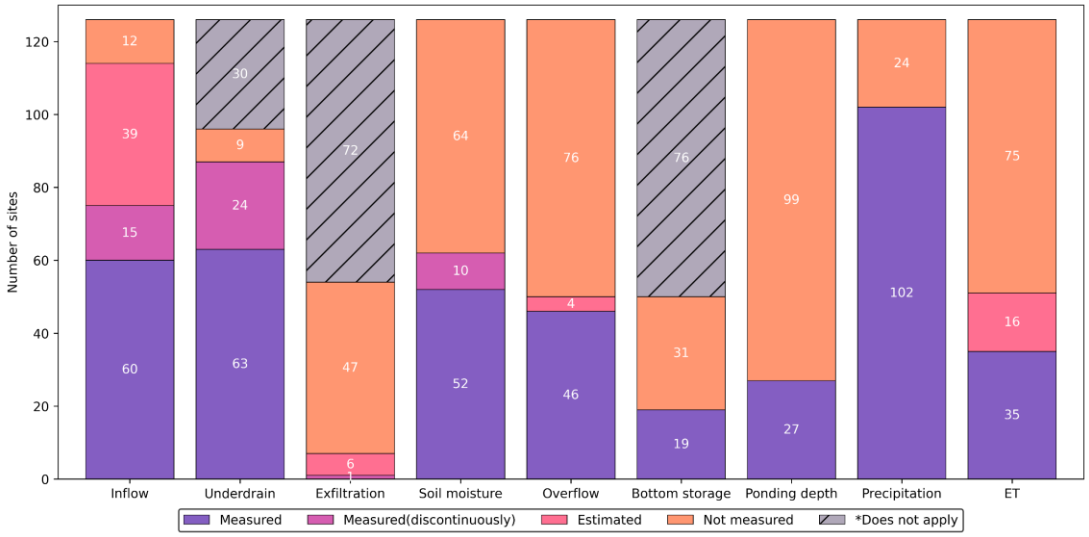

Figure 2-6: Water balance variables for hydrological process (*refer to the monitoring item which cannot be conducted due to the lack of design configuration) in the selected 128 field bioretention devices

In Figure 2-6, the stacked bar indicates the different assessment approaches for each water balance variable. “Measured” means continuously measured; “Measured (discontinuously)” means the measurement is performed at specific time periods (e.g., soil sampling for water content, a container to store and measure cumulative flow volume); “Estimated” means calculated from other variables (by empirical formula, water balance closure). Some water balance variables apply only to specific configurations (e.g., exfiltration occurs only in unlined systems). Therefore, the situation ”does not apply” is introduced for cases where the configuration does not allow the assessment of a given variable. The total number of devices counted in Figure 2-6 is 128, excluding the 9 theoretical modelling cases.

Precipitation was the most commonly reported water balance variable. For 102 out of 128 devices, rain gauges were available. 50 of them were reported to have an *in-situ* rain gauge, while the rest devices were either not reported or used data from nearby weather stations. For inflow, 60 devices had a continuous monitoring system, such as tipping bucket flowmeter or V-weir flowmeter. 39 devices relied on estimations from precipitation with runoff coefficient or Curve Numbers method. In such cases, the calculation of the runoff volume also involved catchment size and land use (Brown & Hunt, 2011a; Davis et al., 2012; Feldman et al., 2019; Olszewski & Davis, 2013). For both rainfall measurement and inflow estimation, relying on a rain gauge from a nearby station (rather than *in-situ* measurements) can introduce

significant uncertainty due to spatial variability in rainfall caused by regional factor, e.g., topography and rain type (O & Foelsche, 2019).

Inflow may be difficult or impossible to monitor if the facility receives unchanneled runoff. In this case, the inflow was estimated based on rainfall and catchment area, or based on measurements for a reference surface (Flanagan et al., 2020; Kanso, 2021; Ramier et al., 2016). However, such estimations may be quite uncertain (due to the difficulty of accurately predicting runoff from rainfall and the spatial variability in the runoff generation process). De-Ville & Deeprose (2024) additionally evidenced the potential of kerb inlet structures, with important flow for high longitudinal road gradients and flow rates. Similarly, some researchers underlined highly uneven distribution of sheet runoff inflows, due to micro-topographic variations near the inflow zone (Tedoldi et al., 2019).

For outlet flux measurement, drainage flow (underdrain in Figure 2-6), when applicable, was quite often monitored (63 out of 95). A large group of devices (24) had discontinuous measurements in underdrain, achieved by cumulative drainage water collection (Dussaillant et al., 2005b; Nasrollahpour et al., 2022; Nocco et al., 2016). Overflow was only monitored for a relatively low proportion of devices (46 out of 128) , although ignoring this term can lead to significant errors in performance evaluations (water balance, but also efficiency for pollutant removal). Since there is no direct way to continuously monitor exfiltration, this term was often not assessed at all (47 out of 54 devices). Few studies (6) introduced indirect estimation methods. The first one was to rely on field infiltration tests on native soil and to validate with the measured drawdown rate of the submerged zone water level (Bonneau et al., 2020). However, such method ignored the possible variability of exfiltration-rate, due to for instance the rise of groundwater at some periods of the year (Vinck & Bock, 2024). Another way to estimate the exfiltration rate was through the closure of the water balance (Batalini de Macedo et al., 2019). Under such approach, the closure term often encompassed both ET and exfiltration (Brown & Hunt, 2011a; Feldman et al., 2019).

Half of the devices did not provide any detail on their soil moisture monitoring, while the other half either reported the use of soil moisture sensor for continuous monitoring (52/128) or field sampling (10/128). Water level, and especially bottom water level was rarely monitored. For bottom water level, a potential reason was the limited accessibility for sensor installation after system construction. The measured

ET in Figure 2-6 represents the actual ET calculated by mass balance of lysimeter experiments. The estimated ET refers to potential ET (PET) calculation by different empirical formulas (e.g., Penman- Monteith FAO56, Priestley and Taylor) and meteorology data. Note that most of "measured ET" studies also involved comparisons with PET estimates.

Measurements of hydrological processes are fundamental to evaluating bioretention performance. The simplest performance indicators (e.g., runoff or peak flow reduction ratio) require measurement of inflow and underdrain/overflow, a condition met by nearly half of the devices studied for research purposes. For a deeper understanding of the hydrological functioning of bioretention devices, especially in the case of unlined systems, further monitoring aspects (ponding depth, bottom storage depth, soil moisture, etc.) are necessary but were not very well addressed in the literature. The sensor coverage ratio of ponding depth and bottom storage depth were still relatively low. For the soil moisture monitoring, only a few devices were equipped with sensors in such a way that they could provide both vertical and horizontal soil moisture variations. In addition, the way in which the different measurements were made can lead to uncertainties in the monitored variables (e.g., limited representativeness of point measurements for soil moisture content), which affected the calculated hydrological performance, but were rarely accounted for in the calculations.

2.3.3.2 Future monitoring needs

Based on the summarised monitoring approaches in the current field bioretention devices, a few insights on future monitoring needs can be drawn.

Previous research on the hydrological behaviours of bioretention systems focused mainly on flow regulation and volume reduction, with relatively little assessment of ET and of soil water content. The resilience of bioretention systems to extreme conditions, especially drought, did not receive much consideration. This may become an issue under increasing concern of climate change.

As for monitoring system design, usual monitoring approaches do not allow studying interactions between the bioretention device and the surrounding soil or groundwater. Most devices were only equipped with inflow/outflow monitoring for hydrological assessment. However, such calculation can be misleading due to

unexpected routes of water biasing the influent and effluent assessment. For instance, Kanso (2021) reported water balance closure issues within a fully monitored bioretention swale, and suspected lateral overflow. Boening-Ulman et al. (2024) reported unmonitored water pathways due to "urban karst" (preferential flows in surrounding soil), which led to low underdrain flux but rapid discharges into the nearby creek. Therefore, a complete monitoring system is necessary for checking water balance closure. Such setup has to be thought of from the start, during the design of the experimental system, and implemented during its construction.

Of course, more comprehensive monitoring systems can only be applied to a limited number of bioretention devices that are designed and controlled for research purposes. Thinking more broadly, how to utilize the large number of real-world devices that were not equipped with a monitoring system is a question worth answering. Existing studies have provided some insights: artificial injection, K_{sat} testing and visual inspection can be used to check the operational status, vegetation condition and performance level (e.g., volume reduction) of a bioretention device (Beryani et al., 2021; Spraakman & Drake, 2021). High-resolution soil sampling with trace metals can help assess the water infiltration distribution in the bioretention surface (Tedoldi et al., 2019). In addition, low-cost sensors with their economic advantages have great potential in bioretention monitoring (Ding et al., 2024; Hamel et al., 2024).

2.3.4 Bioretention Modelling

2.3.4.1 Model overview and local contexts, design parameters and configurations covered

Modelling is a common approach to predict/reconstruct the hydrological behaviour of a bioretention system, which helps assess its performance or review the applicability of a design into different local contexts (Lisenbee et al., 2021). 28 studies, which involved the modelling of 37 bioretention devices, were selected in this review. 28 among the 37 devices were monitored field devices and 9 of them were theoretical cases (without a field device) proposed only for model evaluation (Baek et al., 2015; Dussaillant et al., 2004, 2005a; Herrera et al., 2017) or design recommandations (Bacys et al., 2019; Gao et al., 2018). Although the protocol for selecting documents focused on studies simulating the bioretention device itself, SWMM or PCSWMM, which are primarily dedicated to large-scale modelling and offer a quite conceptual description of bioretention, still account for a high percentage of use (6/28 studies).

Another widely used model was HYDRUS 1D (4/28 studies) which was not specifically intended for the modelling of stormwater management systems. Beyond these two models, MODFLOW, RECHARGE, GIFMOD, DRAINMOD-urban, SUSTAIN and IHMORS were also reported (see Table 2-2). The remaining studies either relied on models specifically developed for their purposes (Guo & Luu, 2015; Li, 2007; Tang et al., 2016b), or on general-purpose finite element simulation software (VS2DI, R2D). Depending on the way each model describes the hydrodynamics of the unsaturated media, these models can be divided into i) physical-based models: GeoStudio-SEEP/W, HYDRUS 1D/2D/3D, VS2DI, R2D, RECHARGE and GIFMOD, which involve numerical resolution of the Richards equation; and ii) conceptual models: LID module of SWMM/PCSWMM, DRAINMOD/DRAINMOD-urban, RECARGA, IHMORS, SUSTAIN, where the different components are described with simple reservoir models. This results in differences as to the description of infiltration or water transfers between the different layers. More details can be found in the review from Lisenbee et al. (2021). Beyond process-based models, statistical modelling (i.e., multiple regression) was used to build empirical predictive models in several studies (Bethke et al., 2022; Tang et al., 2016).

The objectives/uses of these hydrological modelling efforts were diverse and were grouped into the following aspects:

1. Performance evaluation: analysing the effect of substrate characteristics and underlying soil type, i.e., different exfiltration rates of filter media into the underlying soil, porosity and K_{sat}, (Bethke et al., 2022); impact to loess foundation (Wen et al., 2021) and effect of groundwater level on the bioretention hydrology (Dussaillant et al., 2005a; Kim et al., 2019; Zhang & Chui, 2018); evaluating seasonal changes in performance (Nichols et al., 2021); or performance degradation over time due to clogging (William et al., 2019).
2. Design parameters optimization: use sensitivity analysis to determine the design parameters that have the greatest effect on the performance of bioretention systems, and then optimize these parameters to achieve better performance (Li, et al., 2020; Li, et al., 2020; Wang et al., 2019) ; choose an appropriate parameter setting for a not yet precisely designed bioretention system to achieve the performance (e.g., runoff reduction ratio) required by

local guidelines (Bacys et al., 2019; Pan et al., 2022), or optimize an orifice size to improve the operation of the underdrain (Guo & Luu, 2015).

3. Evaluation of a model itself (Bonneau et al., 2021; Dussaillant et al., 2005b; Dussaillant et al., 2004; Massoudieh et al., 2017), or its suitability for specific purposes, such as determining the removal frequency of the top cake layer (Li, 2007).
4. Extrapolate from available measurements to evaluate the hydrological performance of experimental bioretention devices: Zhang et al. (2020) used tank models to investigate the flood mitigation performance when the field monitoring of overflows was unavailable during the experimental periods.

Often, after calibrating/evaluating the model based on available measurements, some changes in local context or design parameters are introduced to construct scenarios and thus to explore the potential impact on hydrological performance. Table 2-2 groups the scenarios that address different local contexts, design parameters, and configurations.

Table 2-2: Different types of model-based scenario analysis conducted in the selected studies

Type	Scenario	Model	References
Local contexts	climate input from different cities	RECARGA; RECHARGE	1, 2
	different rainfall characteristics (duration, intensity)	SWMM; PCSWMM; ABAQUS; HYDRUS 1D; SUSTAIN;	3-10, 12, 15
	initial groundwater depth	VS2DI	12
	cold and warm season (by applying different meteorological data)	HYDRUS 1D	8
	surrounding soil, $K_{in\text{-}situ}$[a] or seepage rate	VS2DI; SWMM; GeoStudio	5, 12, 13
Design parameters	hydraulic loading ratio (controlled by rainfall or inflow)	DRAINMOD; RECHAGRE; VS2DI; HYDRUS 1D	4, 6, 10, 12, 14
	soil mixture (K_{sat}, α[b])	HYDRUS 1D; HYDRUS 2D/3D; RECHAGRE; ABAQUS; SWMM; VS2DI	3, 5, 7, 8
	ponding layer depth	HYDRUS 1D; DRAINMOD; RECHAGRE; PCSWMM	2, 3, 6, 8
	substrate/planting soil thickness	HYDRUS 1D; DRAINMOD	6, 7, 15
	IWS depth	DRAINMOD	6
	detention depth[c]	RECHARGE	14
	underdrain size	VS2DI	12
	storage thickness	RECHARGE; PCSWMM	2, 3
	ponding time	GeoStudio	13
Configurations	with/without an underdrain	VS2DI; RECARGA	12, 16
	supplementary underlying layer	GeoStudio	13

[a]K_{sat} of *in-situ* soil; [b]a fitting parameter in the van Genuchten equation (on the shape of the soil water retention curve); [c]not defined in the study.

1: Dussaillant et al., 2005a; 2: Dussaillant et al., 2004, 3: Bacys et al., 2019; 4: Baek et al., 2015; 5: Bethke et al., 2022; 6: Li et al., 2020a; 7: Meng et al., 2014; 8: Nichols et al., 2021; 9: Tang et al., 2016; 10: Zhang et al., 2018; 11: Zhang et al., 2020; 12: Zhang & Chui, 2017; 13: Wen et al., 2021; 14: Wang et al, 2019; 15: Li et al., 2020b; 16: Gao et al., 2018.

Most of the scenario analysis was based on the adjustment of design parameters, climate, local soil and ground conditions. Only two scenarios (presence of an underdrain) were related to configuration (Gao et al., 2018; Zhang & Chui, 2017). Aside from using the locally monitored rainfall as climate input, studies also involved i) design storm modelling with different return periods and durations for sensitivity analysis purpose (Bacys et al., 2019; Bethke et al., 2022; Li et al., 2020a; Li et al., 2020b; Meng et al., 2014; Zhang & Chui, 2017; Zhang et al., 2018) or ii) multiplying existing rainfall by a factor to assess the impact of climate change (Tang et al., 2016) or to create low/high rainfall scenarios (Nichols et al., 2021). A more limited number of studies used climate data from other cities for scenario analysis (Dussaillant et al., 2004, 2005a). Regarding surrounding underground conditions, the impact of native

soil was more often assessed compared to groundwater level. The influence of initial soil moisture was only discussed in event-based studies. For design parameters, soil mixture was the most studied parameter, but the thickness of different layers of a bioretention system and hydraulic loading ratio were also well studied. Configuration scenarios were the least represented in the current studies, which may reflect a lack of confidence in the ability of the models to describe the functioning of structures with configurations too different from those used for model calibration or evaluation.

2.3.4.2 Limitations in the modelling studies

Model calibration was performed for most of the devices studied (26/37). Calibration was usually based on drainage rate, soil moisture, or ponding level and aimed at adjusting filter media or *in-situ* soil parameters such as K_{sat} (See Appendix 3 – Literature Database). Only one study adjusted daily ET and underdrain size (also filter media and *in-situ* soil K_{sat}) in their calibration based on soil moisture and in/out flow (Zhang & Chui, 2017). While calibration in most cases improved model performance for the calibrated variable, there is no guarantee that the model accurately replicated the other aspects of bioretention functioning. For example, a calibration based on drainage flow was likely to fail correctly predicting ET (Ouédraogo et al., 2022). This can be a problem for variables (e.g., ET, exfiltration) that are often not available as direct measurements.

The simulation period is also notable in this context. Event-based simulations, commonly lasting from 2h to 72h, were conducted for most (25/37) of the studied devices. Such simulations barely focused on the drying period after the rain event. Long-term simulations were less represented (16/37), with durations ranging from 5 months to 6 years. The lack of long-term studies also led to a lack of results on performance indicators such as annual runoff control, overflow occurrence frequency, or the role of ET. The predominance of event-based approaches might additionally raise questions as to the reliability of corresponding event-based performance indicators which are likely to be very sensitive to initial conditions. Within long-term simulations, ET was often represented as a constant flux (Dussaillant et al., 2004, 2005a) or calculated from PET using a simple multiplicative factor (Herrera et al., 2017; J. Li, Liu, et al., 2020; Meng et al., 2014; Stewart et al., 2017). The diversity of plant functional types has been documented to influence bioretention hydrological function, particularly infiltration (Técher & Berthier, 2023) or evapotranspiration

(Ebrahimian et al., 2019), but it was generally not considered in those bioretention studies. Finally, the difficulty of ensuring good model performance over short time periods when the model has only been calibrated to long-term water balances was highlighted, since the long-term water balance did not provide information on the drainage dynamics (Lisenbee et al., 2020).

Models are generally not able to describe all possible configurations (Lisenbee et al., 2021). Researchers have reported limitations in the representational ability of some models and have tried to improve these models on some specific aspects. Viviani and Iovino (2004) used the logistic regression instead of empirical clogging factor in SWMM to improve the representation preciseness. Wen et al. (2021) extended the modelling boundary to include the underlying soil in GeoStudio SEEP/W. Combining or coupling two models was another common way to extend the applicability domain of the model. ABAQUS (a finite element analysis software) was used to determine the input (initial moisture content and suction head) parameters of SWMM-LID module (Zhang et al., 2018). Kim et al. (2019) added a groundwater module to improve the SWMM model prediction accuracy in shallow groundwater contexts. Further development based on an existing model also was conducted. For instance, DRAINMOD-Urban was developed to achieve high time resolution simulation based on the DRAINMOD (Lisenbee et al., 2020).

However, while 2D/3D finite-element models have higher ability to represent a bioretention system, most studies were still based on 1D model. Hence some aspects of the bioretention system such as lateral flow, non-uniformly distributed inflow, elongated shapes (like bioretention swales) or surface topography were still not well understood and their effects on hydrological performances was difficult to predict. Even when 2D modelling was used, the surface of the bioretention device was usually considered flat, e.g., in the work of Stewart et al. (2017) and Zhang & Chui (2017). Modelling of sloped systems, like bioretention swales, with time varying surface storage and infiltration area was still challenging (Durmont et al., 2024). Neglecting lateral flow in 1D models, for instance, was reported to potentially result in an under-representation of storage thickness effect on the maximum saturated duration of the root zone (Dussaillant et al., 2004). However, whether and in which cases the simplified representation of the bioretention system in the 1D model affects its results regarding the performance remain yet unclear. 2D effects could be especially

important when the surrounding soil is stratified, with a high permeability topsoil and low permeability in deeper layers. In such a case, depending on the depth of the low permeability layer relative to the bottom layer of the bioretention system, strong lateral flows (in both ways) can be observed and possible sub-surface flow of the exfiltrated water rather than vertical exfiltration. This may lead to malfunctions that currently are not documented sufficiently.

2.3.5 Bioretention Performance

Table 2-3: Performance indicator and associated field devices/modelling studies number

Performance indicator	Liner condition (No. of devices)	No. of devices with suitable monitoring systems	No. of devices with monitored indicators	No. of devices with modelled indicators
Volume reduction ratio [%] (total)	Lined (72)	38	12	0
	Un-lined (56)	33	15	3
Volume reduction ratio [%] (event scale)	Lined (72)	70	21	7
	Un-lined (56)	33	16	4
Complete retention ratio (event) [%]	Lined (72)	38	4	1
	Un-lined (56)	33	17	1
Attenuation time [h]	Lined (72)	38	7	0
	Un-lined (56)	33	2	1
Drain time [h]	Lined (72)	38	1	1
	Un-lined (56)	33	4	1
Peak flow reduction [%]	Lined (72)	38	8	2
	Un-lined (56)	33	6	0
Exfiltration [%]	Un-lined (56)	33	9	2
ET [%]	Lined (72)	36	18	0
	Un-lined (56)	0	7*	3

*ET reported in unlined system were estimated from PET and empirical formula.

Table 2-3 shows the occurrence of different performance indicators in monitoring and modelling studies. Each indicator is discussed under two conditions (lined and unlined) except for exfiltration. The third column shows the number of devices with a configuration and monitoring system allowing to assess the associated indicator. The fourth column shows the number of devices for which the indicator was provided in the articles. The last column shows the number of modelling studies that provided the indicator. Overall, of the 72 lined devices and 56 unlined devices covered by our literature review, only 38 lined and 33 unlined devices had a continuous monitoring system at both inflow and outflow that allowed observation of long-term volume reduction ratio, attenuation time, drain time, and peak flow reduction. For event-scale volume reduction ratio and complete retention ratio, the requirement for

monitoring continuity is lower, a single measurement after each event on the outflow volume is sufficient, therefore the number of devices for which calculation of these two indicators would be possible was higher (70 for lined and 33 for unlined conditions). Exfiltration rates estimation could have been provided by closing the water balance for 33 devices, but this indicator was reported in the papers for only 9 devices. ET measurement requires a lysimeter system; 36 lined devices met the requirements, 18 devices have reported values. Among the devices whose monitoring system allowed evaluation of different hydrologic performance indicators, the number of devices that provided associated performance indicators is relatively low. This was especially true for lined devices. The high proportion of water quality research in the selected publications could be the reason. These studies often used discontinuous measurements for outflow (e.g., using a bucket for water sampling instead from time to time). Surprisingly, modelling studies provided even fewer performance indicators (even relative to their proportion of the total number of studies). This may be due to the wide range of research objectives (as mentioned in 3.4), or the impossibility to compare some performance indicators due to differences in their terminologies.

In both the monitoring and modelling work, the volume reduction ratios (event scale and total scale) were the most frequently reported performance indicators, while drain time was the least frequently reported indicator. The distribution of performance indicator values retrieved from selected studies could be examined in relation to different design configurations and parameters, as shown in Figure 2-7:

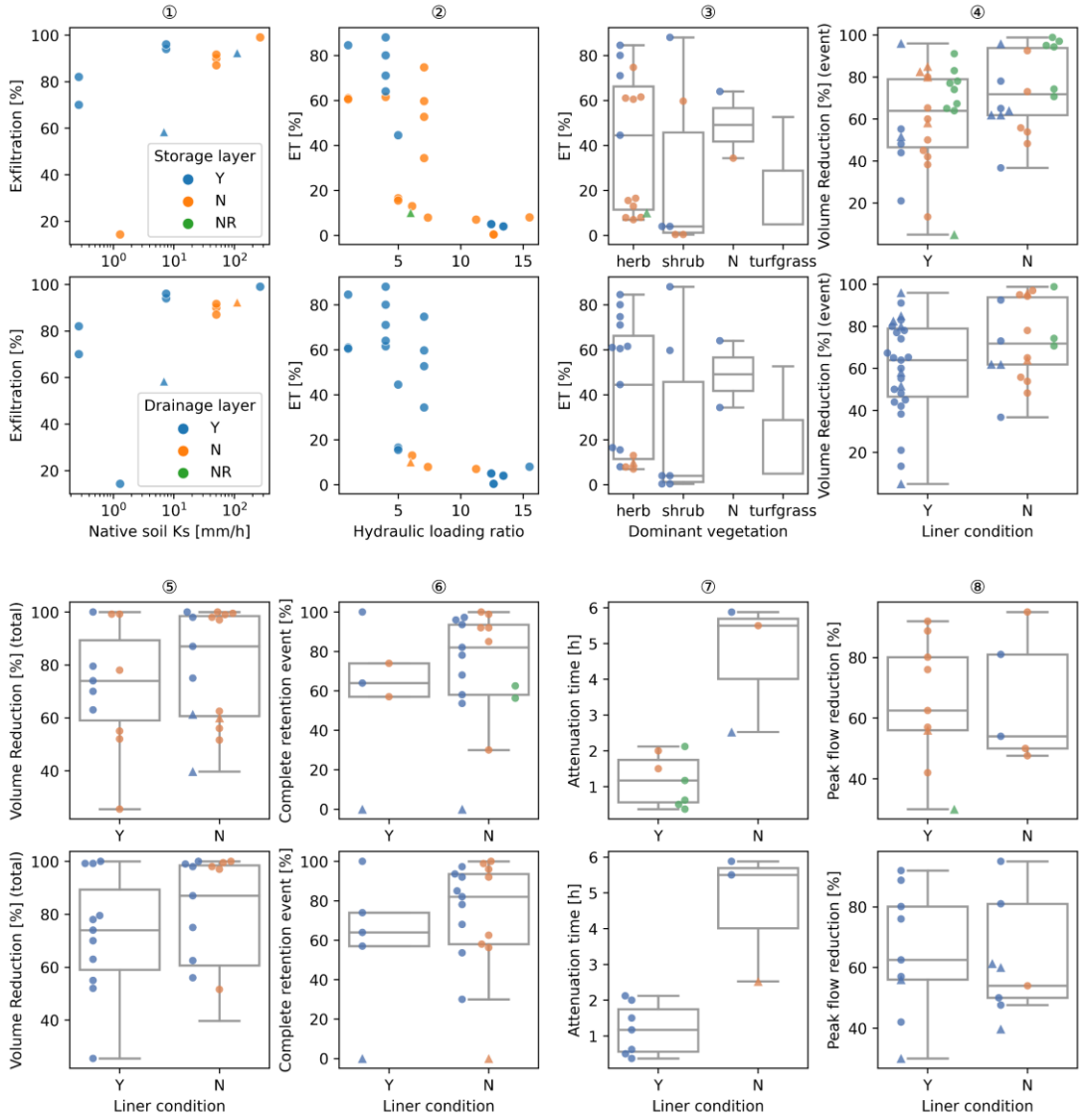

Figure 2-7: Performance distribution based on different configurations and design parameters (○: field monitoring; Δ: modelling; Y: Yes; N: No; NR: Not reported)

Figure 2-7 presents seven performance indicators for monitoring and modelling studies and shows the impact of the presence or absence of a storage layer, drainage layer and liner condition on the distribution of these indicators (except for exfiltration, which is discussed in relation to the K_{sat} of native soil, and ET which is discussed in relation to the hydraulic loading ratio and the dominant vegetation instead of liner condition). Each subplot is divided into two parts, focusing on the presence of a storage layer (the upper plot) or a drainage layer (the lower plot). Drainage time is not considered here, due to the differences in the definition and the small number of studies reporting it.

Expectedly, higher K_{sat} of the underlying soil can contribute to a higher exfiltration ratio, but for low K_{sat} native soil, the presence of a storage layer can lead to high exfiltration ratios (as shown in Figure 2-7①). From Figure 2-7②, the relative contribution of ET to the water balance showed scattered values for low hydraulic ratios, reaching to very high values in some cases, while for high loading ratios (> 10), the relative ET contribution was always very low. High hydraulic loading ratios increased the total amount of incoming water, resulting in relatively low relative ET ratio (Brown & Hunt, 2011a). Moderate hydraulic loading ratios (5-10) showed large relative ET variability that might result from different factors, e.g., substrate media characteristics, presence of IWS (Hess et al., 2017) or climate. This variability was also observed at lower loading ratio, with the possible impact of storage layer (as shown in the Figure 2-7②). Therefore, ET contribution can hardly be anticipated based on isolated factors.

Figure 2-7⑤ does not show any clear effect of storage and drainage conditions on the distribution of total volume reduction ratios, probably due to the cross effect of other context (e.g., underlying soil conditions) or design parameters (e.g., loading ratio). As expected, the unlined bioretention devices had higher total volume reduction ratio, complete retention ratio and attenuation time (Figure 2-7⑤⑥⑦). The distribution of event-based volume reductions did not show any specific pattern for the investigated factors (as shown in Figure 2-7④). It should be noted that this event-scale volume reduction ratio is not robust because it depends on several factors (e.g., size of sample, definition of the event, initial soil moisture and rain depth). The results associated with total (i.e., long-period) volume reduction are expected to be more robust and representative.

For peak flow reduction (Figure 2-7⑧), lined devices had a slightly higher median value than unlined devices, but such a difference was unlikely to be significant due to the small number of samples for unlined conditions. Besides, as an event-based indicator, peak-flow reduction exhibited the same representativity issues as event-based volume reduction. More generally, the relevance of peak flow reduction as a local performance indicator may be questionable. Peak flow reduction is primarily considered to mitigate flooding risks downstream of the sewerage system, or to mitigate physical impact of runoff discharges in receiving waters. However, due to

attenuation during pipe flow, there is no direct link between the level of peak flow reduction at the temporal and spatial scale of a monitored bioretention system and at larger catchment scales (Petrucci et al., 2013a) nor is it be best indicator for impact on receiving waters (Petrucci et al., 2013b). In some countries, regulation limits peak flows for discharges to sewerage systems (Sage et al., 2015), but the better relevant indicator to verify compliance with such regulation is the return period of peak outflows. Further consideration of the rationale for using peak flow reduction ratio as a performance indicator for local scale SuDS evaluation is required.

The local context, such as the underlying soil and the local rainfall pattern, can affect the performance of bioretention, so these local contexts need to be considered during the design. For bioretention systems with low permeability subsoil (<15mm/h), installing an underdrain was recommended (Spraakman & Drake, 2021). Batalini de Macedo et al. (2019) suggested that the hydraulic conductivity of the substrate should be compatible with the local rainfall intensity. As reported by Tansar et al. (2023), other design parameters such as maximum ponding depth and substrate depth can also be used to compensate different rainfall conditions. For regions where local bioretention guidelines exist, local rainfall pattern has already been considered. However, such recommendations may not be directly applicable to other parts of the world. Regarding climate, the current selected publications did not really allow to understand how rainfall or PET characteristics affect bioretention systems, but allow to evidence the potentially strong seasonality in the functioning of these solutions. In a study in Eastern Canada (Dfb climate), the volume reduction rate was reported to be higher and less variable in the summer (Goor et al., 2021). Similarly, in a study in Eastern United States, storage capacity was reported to be much lower in winter than in summer (Nichols et al., 2021). These studies demonstrated that bioretention functioning can undergo strong seasonal variations due to the seasonal variability in precipitation and ET, but also due to changes in their physical characteristics such as hydraulic conductivity (water viscosity can change when the temperature changes) and soil freezing effect (Davis, 2008; Stewart et al., 2017). The strong seasonality of water conditions within a bioretention system may require design adaptations. In Italy (Mediterranean climate), for instance, the need to compromise higher hydraulic loading ratios for a bioretention system to ensure sufficient water supply to the

vegetation was highlighted, even if it resulted in a lower runoff control ability (Bortolini & Zanin, 2018).

Obviously, the factors controlling bioretention performance are not limited to those shown in Figure 2-7. For instance, the storage layer may affect bioretention performance differently depending on the bottom liner condition. For the unlined systems, storage layers were reported to enhance volume reduction by exfiltration during the inter-event periods, even for low-permeability native soils (Winston et al., 2016). For lined systems, the storage layer can enhance ET, increase drought resilience and have benefits for vegetation recovery and growth (Hanley et al., 2023). Regarding the substrate media, Mai and Huang (2021) suggested adding biochar in the filter media (to improve the soil aeration and water holding ability). Proper selection of the filter media can limit clogging (Smith et al., 2021), also with or without maintenance could lead to a huge difference in soil K_{sat} in the bioretention system (Batalini de Macedo et al., 2019; Smolek et al., 2018). Tahvonen pointed out that the fines and organic matter content of the media could influence vegetation growth (2018). Meng et al. suggested using loamy sand or sandy loam for the filter media, which was good for both retention function and vegetation growth (Meng et al., 2014).

Besides, the maturation and aging of the system is also a concerning aspect. Vegetation has a non-negligible effect on soil water balance (Nocco et al., 2016). Nasrollahpour et al. (2022) investigated the main influential factors on ET. They found that the role of vegetation became more important over time compared to the media type factor. Guo et al. (2018), in a seven-year long-term experiment, noted a decrease of the annual runoff reduction rate over time due to clogging. However, the study by Kluge et al. (2018), which focused on bioretention device aging, proved that hydraulic conductivity remained in the range of recommendations even after > 10 years of operation (Kluge et al., 2018). Vegetation was also reported to be able to counteract the problem of clogging at the soil surface (Skorobogatov et al., 2020). Another way to prevent clogging was to install a settling tank/forebay at the inlet of the bioretention system, to remove solids (Karnatz et al., 2019; Kasprzyk et al., 2022).

Overall, some design characteristics (e.g., native soil K_{sat}, loading ratio, liner condition) have a relatively obvious impact on performance indicators. However, due to the lack of data for some contexts, designs or performance indicators, the current selected literature database remained insufficient for drawing reliable suggestions on

how to best combine and adapt different design aspects to local conditions and requirements.

2.4 CONCLUSION: NEEDS FOR FUTURE RESEARCH

In this study, a systematic review of bioretention field and modelling studies was conducted by using a literature database constructed based on a standardized literature search and data extraction method. The characteristics of various bioretention devices considered in hydrological monitoring or modelling studies were analysed, taking into account the local context (climate, soil, water table), design configuration (e.g., lined/unlined, drained/un-drained, with/without IWS), design parameter values (depth and nature of the different layers), in order to identify knowledge gaps and needs for future research. The ability of the experimental setup and modelling approaches to evaluate different hydrological performance indicators was discussed. The relationships between the identified bioretention device characteristics and these hydrologic performance indicators were also explored.

As shown is this review, the current literature did not cover the full range of possible designs and local contexts. A few regions of the world accounted for the majority of monitoring or modelling studies. These were also the regions with the most advanced guidelines for the design and maintenance of bioretention facilities. In terms of climate, regions with relatively uniform precipitation were relatively well studied, whereas regions with more challenging rainfall patterns still require further investigation. Design characteristics were often adapted to the local context of each site (e.g., liner condition, hydraulic loading ratio, presence of an underdrain), as well as to the specific purpose of the study. These characteristics may be strongly influenced by regional guidelines. This was for instance the case of filter media type that exhibited specific values for some regions of the world. However, these locally specific parameters may not be meaningful or transferable to other regions with different climatic conditions. Finally, a significant proportion of studies did not comprehensively report local context or design characteristics, which may limit the interpretation of their outcomes.

Most guidelines provided general design recommendations and incorporated context-specific recommendations tailored to local conditions. However, the implementation of bioretention systems in constrained climates or the optimization of

their design to the local context still requires further investigation (ideally through field pilot studies or advanced modelling approaches), especially for regions without their own local design guidelines.

In the bioretention monitoring studies, inflow, outflow and to a less extend soil moisture received more attention than ponding depth and or water level within bottom storage layer. Exfiltration and ET were also less documented due to the technical challenges in reliably quantifying them. There was a notable oversight regarding heterogeneities in bioretention, such as the uneven distribution of incoming water, the variability in soil water content, and the potential impact of urban karst on exfiltration. These gaps highlight the need for further research to better understand these critical factors. For better understanding the hydrological performance of bioretention systems, comprehensive and continuous monitoring of water transfers in the soil-plant-atmosphere continuum is necessary, along with thorough water-balance assessment to ensure there are no unexpected water pathways. The long-term behaviour and maturing of bioretention may as well deserve further attention. Currently, long-term monitoring (5 years or more) has only been conducted for very few sites (C. Guo et al., 2018; Kluge et al., 2018), which limits our understanding of the evolution of performance over time. Furthermore, to increase the number of study sites (and in particular to facilitate the inclusion of existing real-world devices), low-cost measurement systems (Ding et al., 2024) or high-efficiency field surveys (e.g., portable X-ray fluorescence spectrometry as suggested in Tedoldi et al (Tedoldi et al., 2019) could also be valuable directions.

Modelling approaches have been used to address different issues such as performance evaluation, design parameter optimization or extrapolation, on available measurements to extend further knowledge). From the perspective of devices coverage, modelling was only applied to a limited number of the monitored field devices, and in most cases through event-based approaches. This lack of long-term modelling is problematic, as it is generally needed to fully capture the hydrological functioning of bioretention. Moreover, the use of modelling tools is also associated with different challenges, for instance, whether a model calibrated on one variable can give reliable predictions of another variable. The same doubt also applies for a model used to represent design configurations that differ from the one considered for calibration or validation. Other obstacles include the effect of the potentially high uncertainty

associated with some parameters (e.g., K_{sat} that can vary widely within one device), description of bottom boundary conditions (e.g., seepage face or free drainage depending on the underlying media), or shortcomings in the representation of the system (e.g., the 1D assumption that neglects lateral flow, or simplifications regarding the shape of the device).Furthermore, both monitoring and modelling studies largely omitted discussing the impact of uncertainties on their findings. For modelling applications, which often aimed to improve bioretention design, the identification of uncertainty sources and the assessment of their implications for model results would be worth considering.

Performance indicators have been extracted from the selected publications, homogenised and analysed. Many of these indicators were often not investigated, even though the monitoring systems allowed for their calculation. In addition, the interactions between design parameters and the great variety of situations (combining local context with design configurations and design parameters) make it difficult to draw general design recommendations based on the current available data. Available data on bioretention performance mainly focused on runoff retention efficiency, with less information on flow dynamics. Moreover, the most commonly used performance indicator for flow control efficiency, peak flow reduction, may not be the most relevant. Stovin et al. (2023) introduced a flow control indicator for a different type of SUDS (rainwater harvesting) corresponding to the predevelopment runoff rate. Other possible approaches include the use of flow duration curves(Quinn et al., 2021) to characterise the ability of a system to control stormwater runoff rate, as suggested by Petrucci et al. (2013) and Quinn et al. (2021) . Moreover, as also underlined by Stovin (2024), additional metrics accounting for the whole water balance like exfiltration or evapotranspiration rates would need to be more systematically evaluated. For a better assessment of hydric conditions in the bioretention system, and vegetation resilience to climate extremes like drought or water logging, we would suggest also introducing indicators based on filter substrate water content exceedance probabilities.

Some designs and local contexts were also found to be underrepresented in the existing studies. For filter media, alternatives to sandy materials, could be worth being studied, especially for balancing the rapid percolation of water through the system and the maintenance of water availability for vegetation. Most studies focused on lined systems and whereas interactions with surrounding soil or groundwater were seldom

mentioned and not fully investigated. Specific investigations focusing on the performance (volume reduction and drought resilience) of bioretention systems with highly permeable or heterogeneous (prone to preferential flow) underlying soils were also lacking. Most bioretention monitoring systems focused on outflow rate and volume, rather than on other components of the water balance (e.g., ET and water distribution in soil). While a limited number of studies specifically examined these components (notably ET), the designs of corresponding experimental devices may not be completely representative of real-world configurations. Hence, this underscores the importance of finding a balance between representativeness and experimental goals.

Finally, this review suggests that the relationships between design configuration and performance can hardly be established on the basis of current literature data alone, due to inadequate/insufficient sample sizes at this time and lack of comparability between the different studies. One possible approach is to keep extracting information from the adequately representative modelling and monitoring work, which requires an initiative from the entire research community to work and publish their study cases and results in a standard way (filling up standardised tables) as already suggested by Spraakman et al. (2020), and also to supplement it with an uncertainty assessment. Another possibility is to design experiments to specifically address some design issues (e.g., replicate experimental bioretention devices with design variations). Due to space, time and funding limitations, knowledge gaps cannot be addressed by monitoring alone. Models that have been previously validated based on field monitoring could be used to explore a range of potential designs in the same context, or to evaluate the performance of a single design in different contexts. They would also allow for continuous simulations over longer climate records, providing insights into long-term performance trends and responses to rare climate events (e.g., extreme wet or prolonged dry events), or to explore the impact of climate change.

2.5 OBJECTIVES AND GENERAL APPROACH

2.5.1 Research Needs and Objectives

The literature review in the above summarised some of the current status in bioretention studies. Very limited studies on bioretention performance were found under Western Europe climate. For bioretention monitoring, the complete water balance monitoring (on all the fluxes and stocks) was not often available. Especially for unlined system, the potential issue from the local underground condition may introduce large error into the water balance. In addition, design guidelines are currently missing in France, considering the international design guidelines are often very local specified, direct references or adaptations from these guidelines will ignore the local contexts of Paris region. Hence, in this PhD, a specific focus was put on some design choices to adapt to local constraints in Paris region:

1) In the case that underground conditions that are not very favourable to exfiltration, e.g., low permeability (clay) or no allowed to exfiltrate, it is necessary to explore whether design choices can still improve the water balance. Two bioretention system designs were considered here: a. enhancing exfiltration with an unlined IWS below the drain; b. enhancing ET with an IWS in lined systems.

2) With climate change, drought resilience will become a challenge in Paris region. The use of finer textured substrate could offer some opportunities (especially when facing drought and enhancing ET) but is not well enough documented. Therefore, this study tested the relevance and limits of such designs based on field experiments.

In addition, in order to develop further adapted design guidelines, modelling tools can be used to simulate various design scenarios. However, it is crucial to assess the reliability and robustness of these modelling approaches. Thus, testing the robustness of a physical based modelling approach with Hydrus 1D based on the data monitoring on a representative bioretention cell is necessary.

The main objective of this PhD project is to elucidate the impacts of various bioretention design characteristics on their hydrological performance, with special focuses on their ability to limit runoff volumes and potential for restoring the natural hydrologic balance. Considering gaps and future research directions highlighted in the literature review, the objectives of this PhD can be further detailed as following:

- Objective 1: To have a better understanding of the dominant hydrologic processes (water movement in the substrate media, the role of vegetations) and establish the linkage between bioretention designs, local contexts and hydrological performance, especially for the local contexts in Paris.
- Objective 2: To represent one of the experimental bioretention systems in HYDRUS-1D model, understand the limitations and representing capability of HYDRUS-1D model.
- Objective 3: To evaluate the robustness of modelling a system's performance and hydrodynamics in HYDRUS-1D under the limited or uncertain knowledge of inputs (e.g., boundary condition, soil and vegetation properties, underground conditions, etc.).
- Objective 4: To provide scientific recommendations for bioretention design and implementation, considering local context constraints in Paris region (e.g., controlled exfiltration) and design objectives (performance priorities).

2.5.2 General Approach

To achieve the above objectives, an approach consisting of three parts was adopted (as shown in Figure 2-8). Part I involved a literature review, in which current studies on bioretention monitoring and modelling were investigated. Through this review, some linkages between bioretention design, local contexts, and performance were established (for Objective 1), and research gaps related to Objective 1 were identified as well. Part II comprised monitoring and field measurements based on three bioretention prototypes with different designs and local contexts in Paris region, where Objective 1 and the research gaps from Part I were further explored. Part III involved representing one field bioretention prototype in HYDRUS-1D to evaluate the model's capability in representing different hydrological processes (Objective 2). Additionally, different levels of input parameter knowledge from Part II were used for sensitivity analysis, to evaluate the robustness of HYDRUS-1D modelling results on the water balance performance and soil moisture dynamics (Objective 3). By combining conclusions from all three parts, design recommendations were formulated (Objective 4).

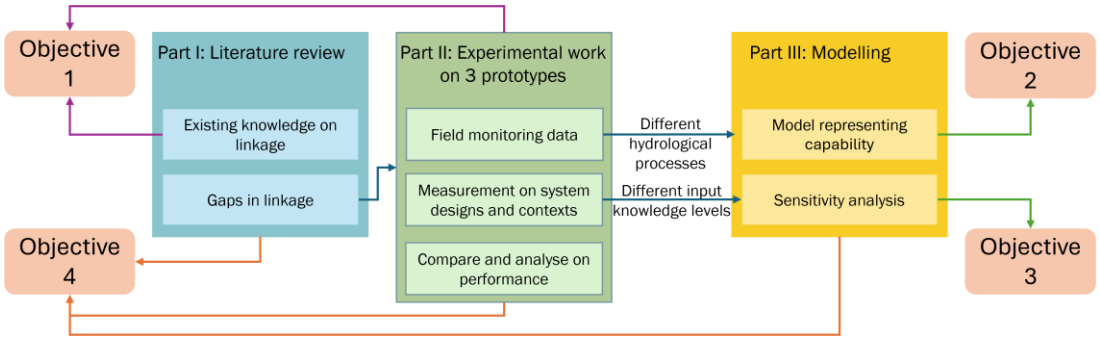

Figure 2-8: Schematic of the general approach

Chapter 3: Experimental Devices and Monitoring Setup

This chapter and the next chapter are adapted from an article draft, with a title of *Hydrological performance of bioretention systems under unfavourable subsoil: a study based on 3 rain garden prototypes in Paris, France*. The introduction is thus already partly covered by the previous chapters.

3.1 INTRODUCTION

Urbanisation significantly affects catchment hydrology (W. D. Shuster et al., 2005). Compared to natural surfaces, urbanized surfaces have lower infiltration and evapotranspiration (ET) rates and can result in significant discharges of runoff and associated pollutants to surface waters (Trowsdale & Simcock, 2011). To address these issues, stormwater management is increasingly relying on nature-based solutions (NbS) that promote natural processes to control runoff and pollution while providing additional environmental and social benefits. Bioretention is one of the typical NbS used in urban areas, to both restore the natural water cycle and reduce the pollutant loads (Trowsdale & Simcock, 2011).

A typical bioretention design includes a depressed surface (allowing ponding), vegetation layer, filter media layer, transition layer and optional drainage and bottom storage layers (Donaghue et al., 2022; Payne et al., 2015b). Depending on its design purpose and local contexts, the bioretention system can be separated from the native soil by a liner or directly in contact with the surrounding soil. In some practices, the height of the underdrain outlet is elevated to create a submerged zone to supply vegetation with water during long dry periods (M. Wang et al., 2018; K. Zhang et al., 2021), to enhance exfiltration in systems with low permeability underground (Brown & Hunt, 2011b), or to allow longer hydraulic retention time and create an anaerobic environment for water purification (Qiu et al., 2019). The volume (or fraction of the system) below the underdrain outlet is named Internal Water Storage (IWS). IWS is normally implemented in a lined system, or an unlined system with low permeability soil (Géhéniau et al., 2015). The functioning of a bioretention system usually involves multiple hydrological processes, for instance collection of direct rainfall and runoff

from its catchment, water retention via ponding, infiltration within the filter media, ET, filter media and bottom storage, exfiltration into the surrounding soil, or discharge through an overflow pipe and/or an underdrain. Due to the variety of possible designs and the relative complexity of bioretention as compared to other techniques, the relationships between processes and biorientation characteristics are yet not fully understood (Huang et al., 2025).

Various studies have been conducted to investigate bioretention performance under different designs or local contexts (Huang et al., 2025). The influence of bioretention cell design components such as media type (Nasrollahpour et al., 2022), media depth (Hunt et al., 2008), vegetation type (Nasrollahpour et al., 2022; Nocco et al., 2016; Ouédraogo et al., 2022) and infiltration capacity of filter media (Venvik & Boogaard, 2020) has been investigated. Hess et al. (2017) and more recently Ouédraogo et al. (2022) reported that IWS could enhance ET. The same studies also focused on the effect of substrate type or vegetation type on ET.

Except from direct impact brought by the design of bioretention, the external limitation, such as unfavourable subsoil conditions (low permeability soil or polluted soil) that may limit exfiltration also leads to issues. Therefore, for a bioretention system with low permeability native soil, it is commonly recommended to use an underdrain (J. Huang et al., 2021; Spraakman & Drake, 2021). However, raising up the underdrain may in this case open up some possibilities to enhance exfiltration. William et al. (2021) indicate that bioretention on clayey native soil can still function effectively (with more than 80% event-based volume reduction ratio), unless the period between two large events is too short to recover storage capacity (Brown & Hunt, 2011b; H. Li et al., 2009).

Another issue is linked to drought challenge. Sandy substrates are commonly used in bioretention systems due to the requirement/suggestion from local regulations (Tirpak et al., 2021). However, sandy substrate may lead to drought stress for a bioretention system. Yet, some specific studies used local soil such as sandy loam (Batalini de Macedo et al., 2019), silty clay (Ouédraogo et al., 2022) or even clay loam (Nasrollahpour et al., 2022). The use of these soils reduces the hydraulic conductivity of the bioretention substrate, but also implies a higher water retention capacity, which in turn can support plant growth and drought tolerance.

In such a case with special substrate or underlying condition, the performance e.g., runoff reduction, ET promotion (for runoff management but also for potential urban comfort) and sustainable urban greening (resilience to drought) is remaining unknow.

From the region and climate perspective, most studies in the past decade were conducted in North America, East Asia and Australia, whereas some contexts such as Western Europe climate are less (or not) represented (Spraakman et al., 2020a). In addition to the limitations on the number of studies that has been conducted in the region (climatic zone), limitations can also be brought by experimental settings. Most studies rely on event-based approaches, which do not allow fully capturing the performance of bioretention over the diversity of conditions they may encounter. Therefore, long-term monitoring is necessary to evaluate volume reductions across various time scales, e.g., annual or seasonal (Muthanna et al., 2008; William et al., 2019), or to provide insights into system behaviour during drought periods (Batalini de Macedo et al., 2019). In addition, these event-based studies are often not able to close the water balance, which prevents detailed understanding of the relative contribution of each process and sometimes leads to ignoring an important part of the water flux, e.g., urban karst (Boening-Ulman et al., 2024), which may even give rise to erroneous estimation of bioretention performance (Huang et al., 2025). In studies that assessed the relative importance of processes like exfiltration (Brown & Hunt, 2011b) and evapotranspiration (Hess et al., 2017; Nasrollahpour et al., 2022; Ouédraogo et al., 2022), IWS drawdown rate or weight lysimeter were applied to better characterise water losses. Therefore, for an accurate evaluation of the hydrologic performance, continuous and relatively long-term monitoring (e.g., several months or at least one year covering seasonal variations) and complete monitoring of flows and storages are needed.

The objective of this study is to evaluate the hydrological performance of bioretention based on the long-term continuous monitoring of all the water flux and storages for three prototype bioretention devices with unfavourable underground conditions (two of them are lined, and one has a low exfiltration capacity) in Western Europe climate, with a focus on their diversity of designs, such as hydraulic loading ratio, role of IWS and filter media types.

3.2 MATERIALS AND METHODS

3.2.1 Case Study

The three bioretention prototypes studied are located in Paris region, France. Paris has a degraded Oceanic climate according to Météo-France (2023), classified as Cfb in Koppen climate classification with relatively low annual precipitation (641mm) and large seasonal temperature difference. Rainfall is distributed relatively uniformly over the year (as shown in 3.2.4, Figure 3-3). According to Météo-France, the design rainfall intensity for 5-year return period (event duration of 120 min) is 21mm/h and the annual potential evapotranspiration PET (850mm) is higher than annual precipitation. Paris has mild winters (barely below the freezing point), and not very hot summers (the mean daily maximum in the summer months is less than 30°C). Potential challenges for bioretention systems under this climate include the water stress in summer dry periods and few heavy events which may cause waterlogging or even overflows. Local underground condition also often limit the possibilities for implementing bioretention systems and pose constraints to their design: the native gypsum-rich soil in Parisian basin has dissolution risk; the prevalence of clay underground leads to low permeability and risk of swelling or shrinkage in some places (Dumont et al., 2023); many underground infrastructures (e.g., metro lines) and old quarries prohibit deep infiltration; some locations with polluted soil are also not recommended for applying extra infiltration. Thus, efforts are often made to minimize exfiltration volumes (by maintaining low hydraulic loading ratios and prioritizing fine-textured materials for the filter media layer), when exfiltration is not simply prohibited.

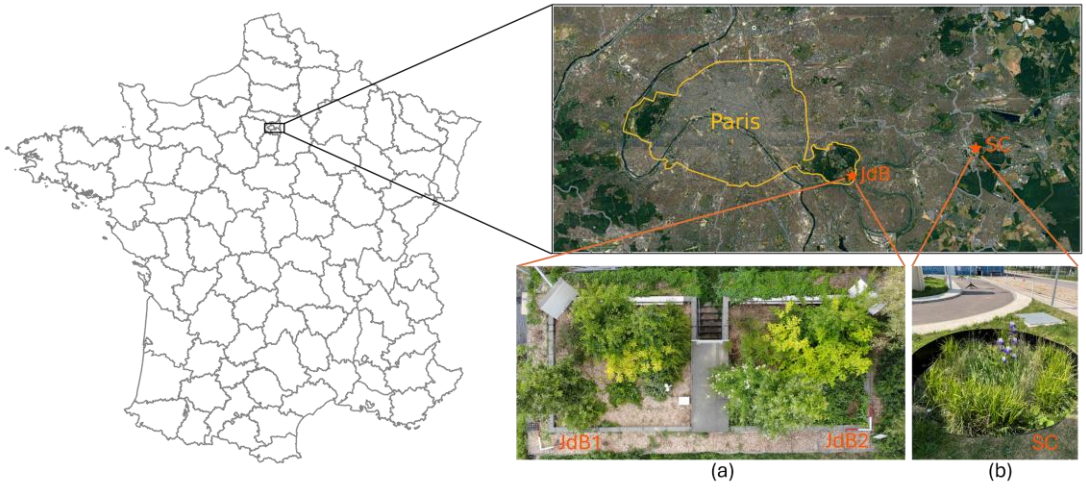

Figure 3-1: Location of the three experimental bioretention cells; (a) the two Jardin du Breuil (JdB) device (photographed by an drone in June 2023); (b) Sense City (SC) device (photographed with a hand-held camera in May 2022)

The experimentation of JdB (JdB1 and JdB2, Figure 3-1a) is initiated by the municipality of Paris, with a support from Cerema for system design and preliminary data analysis. Two of the three experimental devices are located within the Vincennes Park in Paris as shown in Figure 3-1. Each device collects a 72.5 m^2 metal roof catchment area into a 25.2 m^2 rectangular bioretention cell, with a hydraulic loading ratio (total rainfall receiving area/bioretention area) of 4. The two bioretention cells were built and planted in November 2020 and the monitoring was conducted from November 2020 until the present (the inflow system have been replaced once in Spring 2023). The third bioretention system (SC, Figure 3-1b) is located at Champs-sur-Marne, 15 km east of Paris within the Sense City equipment (a 400 m^2 city model equipped with various sensors and a movable climate chamber, https://sense-city.ifsttar.fr/en/). The system consists of an 85 m^2 asphalt pavement catchment area and a 7 m^2 circular bioretention cell (hydraulic loading ratio = 13). The system was built at the end of 2019. Its monitoring was completed progressively until March 2022, and is ongoing until the present. Weekly maintenance was done to remove the aerial part of weeds during the growing season (April to September) of 2022 and 2023 for SC bioretention; for JdB bioretention cells, maintenance (weed removal, checking and cleaning of the different sensors) was done every two weeks.

SC cell is a representative of conventional bioretention cell design, featuring sandy loam filter media and bottom exfiltration, underlain by a low-permeability clay layer, but has clay underground with low permeability. JdB cells are representative of

configurations that may be considered in Paris due to underground constraints (gypsum and quarries); they are lined to prevent exfiltration, feature small loading ratios (collecting only surrounding roofs or a small portion of the road), and have a filter substrate corresponding to the typical planting soil (silt loam) used in public gardens in Paris today

3.2.2 Bioretention Design and Monitoring

3.2.2.1 System design and sensor information

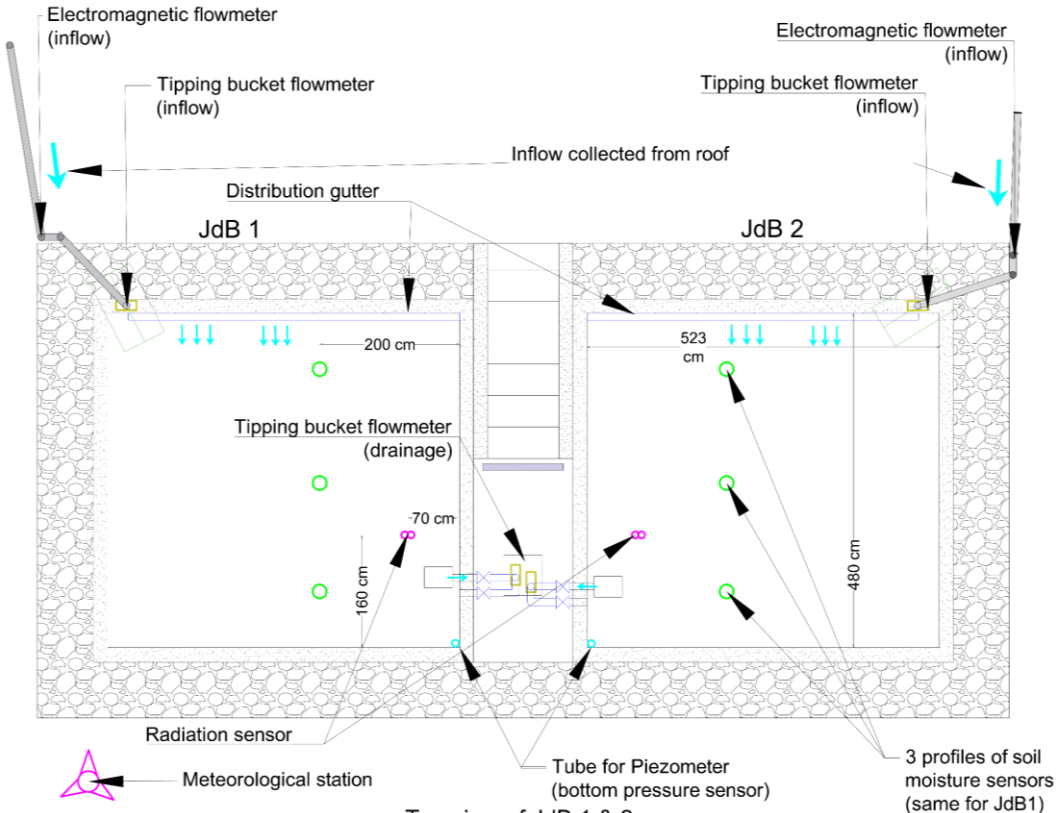

a. Top view of JdB 1 & 2

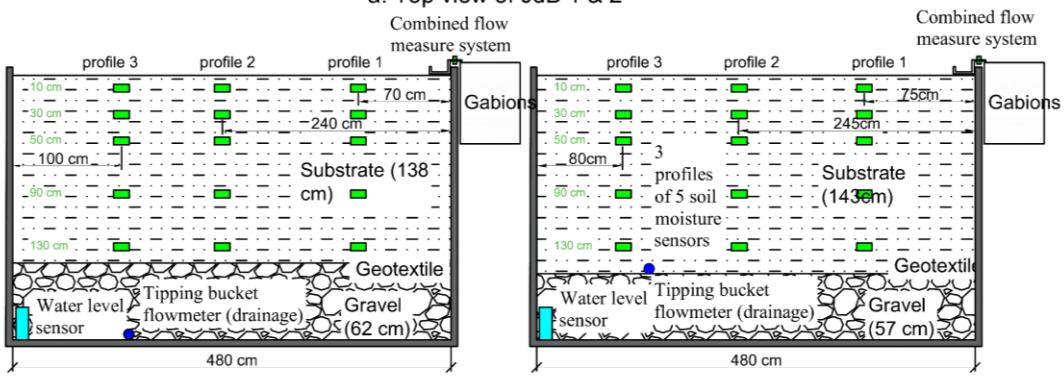

b. JdB 1 profile (along soil sensors)

c. JdB 2 profile (along soil sensors)

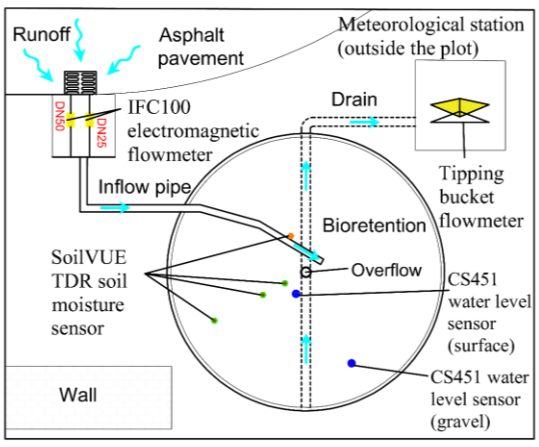

d. Top view of SC

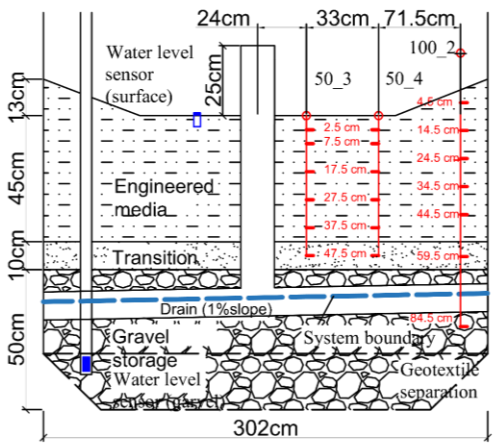

e. SC profile

Figure 3-2: Bioretention sensors setup in Ecole du Breuil (JdB1 & JdB2) and Sense City (SC)

As shown in Figure 3-2b and Figure 3-2c, JdB1 and JdB2 are lined (concrete box) bioretention cells with similar design configuration, the only difference being the drainage conditions (depending on the outlet position). Each device can be described as a 3 layer-system; a 10 cm surface storage layer, a 138 and 143 cm substrate layer for JdB1 and JdB2 respectively, and a 62 and 57 gravel layer for JdB1 and JdB2 respectively (substrate and gravel layer being separated by a geotextile). The outlet of the two cells is located within a vertical gravel well, adjacent to the edges of the system (depicted by the two grey boxes next to the radiation sensor in Figure 3-2a). For JdB1, the outlet is set at the bottom of the gravel layer. The gravel layer can therefore be considered as a drainage layer that empties within a few hours after each rain event. For JdB2, it is located right above the gravel layer. The gravel layer therefore acts as an IWS. The runoff collected from each 72.5 m² roof portion is evenly distributed over one side (5.25 m) of the corresponding bioretention cell, via a horizontal distribution gutter. The vegetations species in JdB1 and JdB2 are the same, each cell is planted with ornamental ground-covering plants (*Geranium sanguineum, Vinca minor and Hedera helix*), shrubs or low trees (*Abelia x grandiflora, Cornus sanguineum, Ligustrum vulgare, Lonicera nitida* and *Carpinus betulus*) and one tree (and *Pyrus calleryana*).

The SC bioretention cell (as shown in Figure 3-2e) consists of 3 layers: 45-58 cm substrate (sandy loam engineered media), 10 cm transition layer (sand), 8 cm drainage layer and 42 cm bottom storage layer (gravel). The cell is lined vertically, the bottom is set on surrounding low-permeable clay soil with a geotextile separation, which allows slow exfiltration. An overflow pipe rises 25.5 cm above the lowest point of the bioretention cell surface and is connected to a horizontal perforated drain situated in the upper part of the gravel layer (100 mm wide slots at the top, covering one-third of the diameter). The deep gravel depth below the level of the drain slots (approximately 42 cm) was aimed at promoting exfiltration into the underlying soil. The inlet flow is directed to the centre of the cell by a pipe, where a stone slab was placed to prevent erosion. The perforated part of the drain (blue line in Figure 3-2e) is considered the system's lower boundary during the water balance analysis. All of the vegetation in SC bioretention is herbaceous and ornamental, including *Carex oshimensis* Evergold, *Miscanthus Sinensis*, *Carex grayi*, *Iris*, *Lobelia fulgens*,

Rudbeckia, *Lychnis coronaria* and *Hemerocallis*. A summary of the three bioretention cell design is provided in Table 3-1, and detailed soil characteristics are presented in Table 3-2.

Table 3-1: Design configuration and parameters comparison for JdB1, JdB2 and SC bioretention systems

	JdB 1	JdB 2	SC
Catchment area	72.5 m2		85 m2
Surface area	25.1 m2		7 m2
Hydraulic loading ratio	3.9		13.4
Linner condition	Lined		Partly lined (bottom open)
Berm/overflow height	Approximately 10 cm		25.5 cm
Vegetation type	Herbaceous, shrubs and tree		Herbaceous
Mulch layer	Yes		No
Substrate type	Silt loam		Sandy loam
Substrate thickness	138 cm	143 cm	45cm (centre) to 58 cm (edge)
Transition layer	Geotextile		Sand (10 cm)
Drainage type	Outlet hole (Diameter=11cm) in gravel well		100 mm Perforated HDPE pipe
Drainage layer thickness	62 cm	-	8 cm (thickest point)
Storage type	Gravel		Gravel
Storage layer (IWS) thickness	-	57 cm	42 cm
Underlying soil	-	-	Native Clay

3.2.2.2 Monitoring period

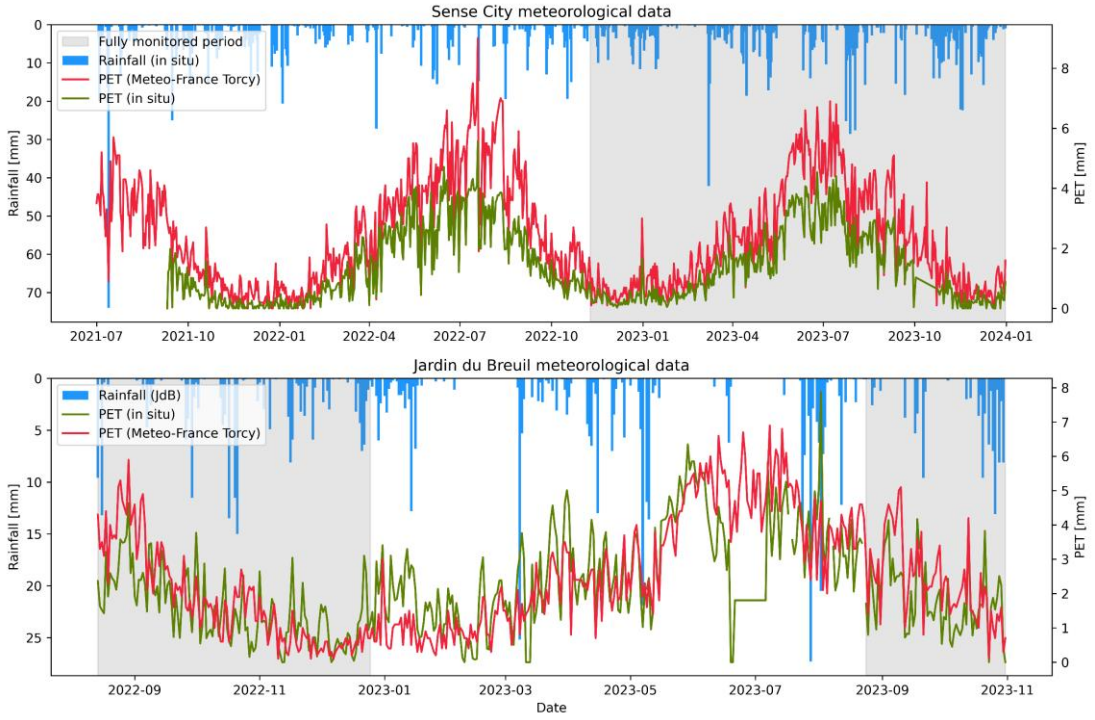

Figure 3-3: Meteorological data and observation period for SC and JdB (daily time step)

Due to the sensor installation time difference, maintenance and replacement, the periods fully covered by the monitoring system differ between the two sites. As shown in the shaded area in Figure 4, the full monitoring period for SC is 2022/11/09 - 2023/12/31 (later been extended to 2021/07/01 – 2023/12/10 through a complementary reservoir model); for JdB, the full monitoring periods are P1: 2022/08/14 - 2022/12/25 and P2: 2023/08/24 - 2023/10/31. Figure 4 also shows the potential evapotranspiration (PET) and precipitation during the study period, the PET (*in-situ*) is calculated by FAO56 Penman-Monteith equation (FAO56-PM) (Allen et al., 1998), with the net radiation/global solar radiation, wind speed, relative humidity, air temperature and atmosphere pressure measured by the *in-situ* meteorological stations, the detailed equation is presented in 3.2.5.5.

3.2.3 Field Investigation

3.2.3.1 Soil hydrodynamic characteristics

Soil hydrodynamic characteristics were investigated through field/lab tests, including granulometric analysis and bulk density measurements, hydrodynamic parameter predictions with Rosetta 3 (Zhang & Schaap, 2017), BEST-infiltration (Beerkan Estimation of Soil Transfer parameters) single-ring infiltrometer test

(Lassabatere et al., 2013), Chameleon saturated conductivity (Ks) test (SOILMOISTURE EQUIPMENT CORP., 2016) and surface ponding drawdown rate based on the surface water level measurement (in this case, the infiltration rate is the average over the whole bioretention surface). Details on these approaches are presented as follow.

3.2.3.1.i Granulometric analysis and Rosetta prediction

Granulometric analyses were done on the media of the three bioretention devices by an external lab. According to the analyses results, the substrate media in Sense City rain garden has 10.4% clay, 23.7% silt and 65.9% sand, the native soil under the bottom of SC rain garden has 58.8% clay, 14.8% silt and 26.4% sand, the substrate media in JdB has 23.25% clay, 61.06% silt and 15.69% sand.

Rosetta (Schaap et al., 2001) is an artificial neural networks program which can predict soil hydraulic parameters based on the proportion of soil particles (as written above) and bulk density (1.50g/cm^3 –1.73g/cm^3 for SC substrate; 1.24g/cm^3 – 1.47g/cm^3 for JdB substrate) The tool used in this study is a webtool Rosetta (handbook60.org) based on Rosetta 3 (Y. Zhang & Schaap, 2017).

3.2.3.1.ii BEST-infiltration tests

The BEST (Beerkan Estimation of Soil Transfer parameters) infiltration method is a single cylinder infiltrometer test used to determine the infiltration capacity of the soil and its hydraulic characteristic curves, i.e. the retention curve (matrix potential as a function of water content) and hydraulic conductivity (hydraulic conductivity as a function of water content). The method integrates the soil retention curve from van Genuchten (1980), Eq. 3-1, and the hydraulic conductivity curve from Brooks and Corey (1964), Eq. 3-3, Eq. 3-4 with Burdine's capillary model (1953), Eq. 3-2.

$$\frac{\theta - \theta_r}{\theta_s - \theta_r} = \left[1 + \left(\frac{h}{h_g}\right)^n\right]^{-m} \quad \text{Eq. 3-1}$$

$$m = 1 - \frac{2}{n} \quad \text{Eq. 3-2}$$

$$\frac{K(\theta)}{K_s} = \left(\frac{\theta - \theta_r}{\theta_s - \theta_r}\right)^{\eta} \quad \text{Eq. 3-3}$$

$$\eta = \frac{2}{mn} + 2 + p \quad \text{Eq. 3-4}$$

$$K(\theta) = Ks \cdot S(\theta)^{\frac{1}{m}}\left[1 - \left(1 - S(\theta)^{\frac{1}{m}}\right)^m\right]^2 \quad \text{Eq. 3-5}$$

Where:

- θ: volumetric water content of the soil
- θ_s: saturated volumetric water content
- θ_r: residual volumetric water content
- Ks: saturated hydraulic conductivity
- h: potential matrix of soil (soil water suction)
- K: hydraulic conductivity
- n, m, η: curve shape parameters
- p: tortuosity parameter (equal to 1 when the relationship between n and m is described by the Burdine model)
- h_g: air entry suction, the suction at which air enters the soil pores and water begins to be retained; in some expression, α is used to represent $\frac{1}{h_g}$

During the summer of 2022 and 2023, 11 valid BEST-infiltration tests have been conducted on SC (6 tests) and JdB (5 tests). These testing results were calculated by BEST-slope and BEST-intercept algorithms in an Excel interface (Lassabatere et al., 2013).

3.2.3.1.iii Chameleon test and surface ponding drawdown rate

Chameleon saturated conductivity (Ks) test is a lab equipment which allows to measure saturated soil hydraulic conductivity on a cylindric soil sample (SOILMOISTURE EQUIPMENT CORP., 2016). For the media samples in this study, the fixed pressure head configuration was used (as shown in Figure 3-4). The configuration establishes a fixed pressure head (through a Mariotte tube structure) and uses a pressure sensor to count the volume of water flow through the pre-saturated soil sample (orange copper cylinder) and thus get the saturated conductivity when the flow rate is stable.

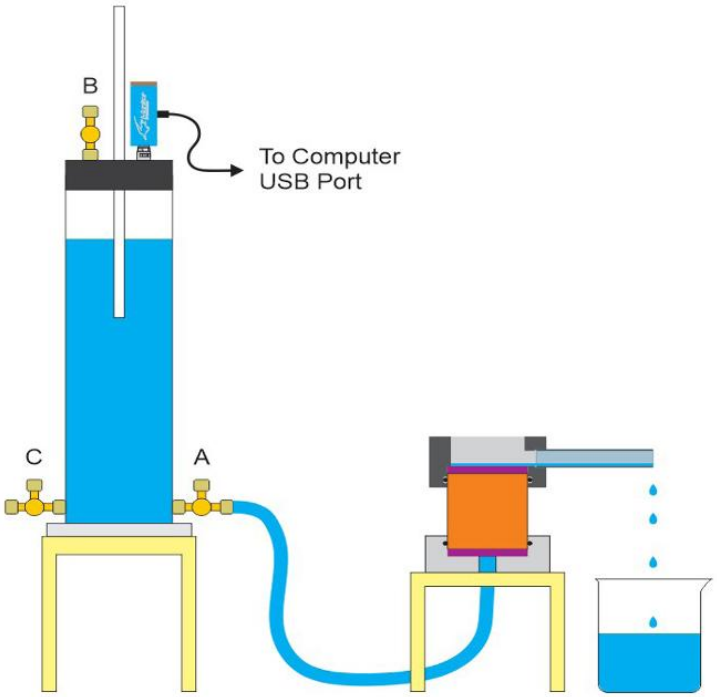

Figure 3-4: Schematic of the Chameleon equipment (fixed pressure head mode), Source: Operation instructions of Chameleon 2816G1/G5

The surface ponding drawdown rate is calculated mainly based on the surface water level measurement (only for SC). In the case where the ponding water floods the whole surface of the bioretention cell, the rate of decline of the water surface is considered to represent the average infiltration rate of the entire cell, i.e., K_{sat} (we assume the filter media was saturated during the ponding period). A water balance equation, accounting for inflow and precipitation during the drawdown process, is applied to calculate the drawdown rate (introduced in 4.1.2.2, Eq. 4-2).

Hydrodynamic curves and characteristics of filter media

The hydrodynamic characteristics parameters can be used to construct the soil water retention curve and hydraulic conductivity curve. Based on the governing equation, the BEST-infiltration test results provide a retention curve based on Van Genuchten Eq. 3-1 and a hydraulic conductivity curve based on Brooks & Korey Eq. 3-3, Eq. 3-4. Rosetta predictions however are based on the Van Genuchten equations for both curves (Eq. 3-1 and Eq. 3-5). By observing the soil water content at different matric potential (soil suction or soil moisture tension), field capacity (water content at 330hPa) and wilting point (water content at 1500hPa) can be identified. The following

figures present the soil characteristics curves obtained by different tests for JdB substrate (Figure 3-5) and SC (Figure 3-6).

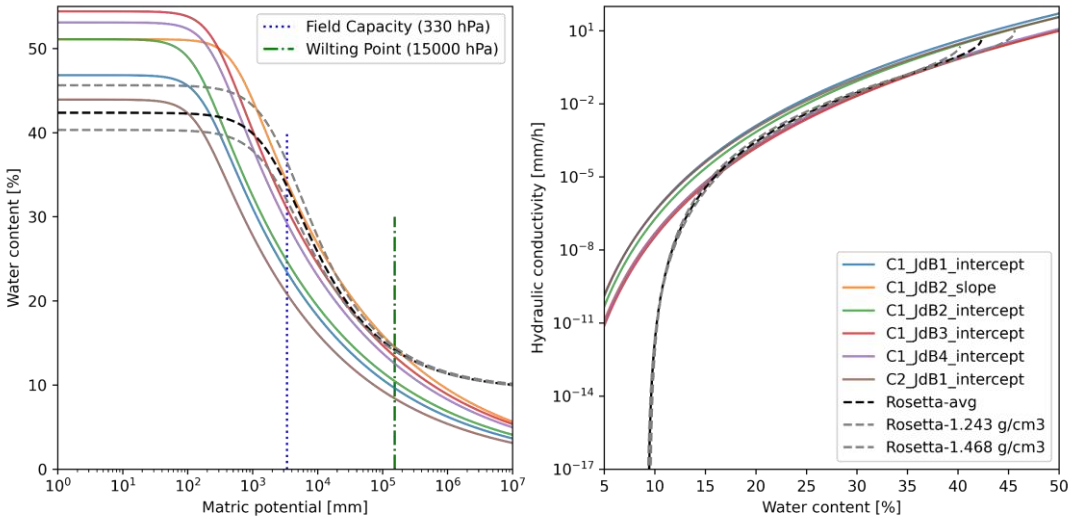

Figure 3-5: Soil retention curve (left) and hydraulic conductivity curve (right) for JdB

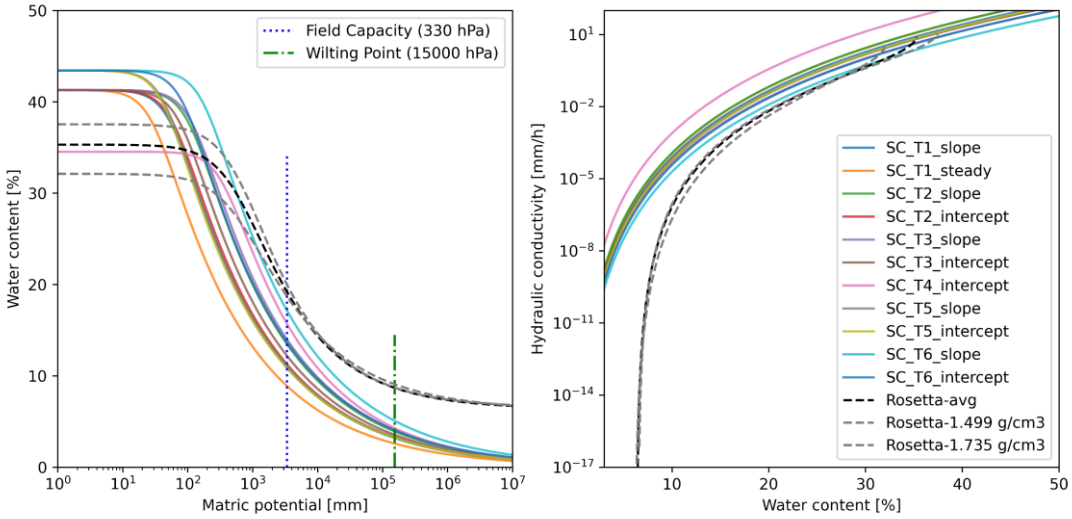

Figure 3-6: Soil retention curve (left) and hydraulic conductivity curve (right) for SC

Aside from Rosetta (which only involves particle distribution and bulk density), for the other three methods, the hydraulic conditions under which they operate and the surface area over which they apply differ. Chameleon test is a constant head Darcy experiment on a small cylindrical soil sample (diameter = 5.38 cm) ; BEST uses a slightly bigger infiltration ring (diameter > 10cm); ponding drawdown rate is based on the whole surface of SC (7 m²).

Based on the spatial extent of measurement, Chameleon is the smallest, which means its result can be very localised, also it relies on a soil sample collected in the field which may have undergone some modification during the sampling process (possible compaction). BEST-infiltration test can sometimes cover a whole plant (and its roots); therefore, it gives larger range. The use of these different methods can provide an idea on different uncertainty sources and variability brought by measurement location and scale. The measured hydrodynamic characteristics are shown in Table 3-2, the range of Rosetta was calculated from the same grain size distribution and different bulk density.

Table 3-2: Field capacity (330 hPa), wilting point (15000 hPa) and Ks on the case study predicted by different methods

Methods / Parameters	BEST-range	BEST-geomean	BEST-median	Rosetta	Chameleon	Ponding drawdown rate
JdB-Field capacity [%]	21-34	27	27	32-37	-	
SC-Field capacity [%]	8.9-17	12	13	19-20	-	
JdB-Wilting point [%]	8.4-14	11	11	14-15	-	
SC-Wilting point [%]	2.6-5.1	3.6	3.7	8.7-9.1	-	
JdB-Ks [cm/h]	0.83-4.8	2.1	2.4	0.40-1.2	-	
SC-Ks [cm/h]	1.6-5.2	3.4	3.6	0.61-1.7	0.07-1.9	0.48-4.5

Grain size distribution	Clay (%)	Silt (%)	Sand (%)	Bulk density (g/cm^3) - range	Bulk density (g/cm^3) - mean
JdB substrate (2020)	23.25	61.06	15.69	1.24-1.47	1.38
SC substrate (construction)	10.40	23.70	65.90	-	-
SC substrate (2022)	-	-	-	1.50-1.73	1.60
SC transition (construction)	4.60	4.90	90.50	-	-
SC transition (2023)	4.60	7.70	87.70	1.37	1.37
SC underlying (2021)	58.80	14.80	26.40	-	-

3.2.3.2 Monitoring systems

The three bioretention cells were monitored for inflow, drainage, bottom gravel water level, soil moisture (as shown in Table 3-3). JdB1 and JdB2 have same sensor settings. Precipitations and other meteorological variables were also monitored at both sites (JdB and SC). For the latter, the inflow is measured for each cell with a combination in series of a tipping bucket flowmeter for low flowrate and an electromagnetic flowmeter for high flowrate (with overlap in measurement ranges). For SC, it is measured by a combination in parallel of two electromagnetic flowmeters that activate for different flowrates. For soil moisture, each JdB cell has 15 sensors

distributed along 3 vertical profiles situated at 70/75 cm, 240/245 cm and 380/400 cm from the inlet gutter (the two values are applying to JdB1/JdB2). Each profile observes 5 depths (10 cm, 30 cm, 50 cm, 90 cm, 130 cm) from the surface to the bottom of the substrate layer, the measurement volume of each probe is approximately 7800 cm^3 (~7.5 cm radius around each probe rod and 4.5 cm beyond the end of the rods). In SC, three water content profile sensors are distributed from the centre of the cell (inlet pipe) to the outside. The two sensors near the centre (24 cm and 57 cm) have 6 probes each (2.5 cm, 7.5 cm, 17.5 cm, 27.5 cm, 37.5cm probes within the substrate layer, 47.5cm within the transition layer). In 2022-11-09, the sensor with 24 cm to the centre was replaced with a new sensor at a new location 45 cm to the centre (the red SoilVUE sensor shown in Figure 3-2d). The outer sensor (128.5cm away from the centre) has 7 probes (4.5 cm, 14.5 cm, 24.5 cm, 34.5 cm, 44.5 cm within the substrate, 59.5 cm in the transition layer, 84.5 cm in the gravel storage layer). Each SC probe measured the soil moisture in a 2cm wide cylindrical zone around the 5cm-diameter probe rod, and over a 5cm height depth. Drainage is monitored on both sites with tipping bucket flowmeters. For SC bioretention the underdrain also collects overflow, however the measurement range of the tipping buckets does not allow to correctly measure these overflow peaks. For JdB, overflow and surface ponding were expected to remain insignificant due to the very low hydraulic ratio of the two cells, and were thus not monitored. All the monitoring data was recorded every 2 min in JdB. SC data were recorded every 1 min for climate data, inflow and water levels, every 15 min for soil moisture and was time-stamped for tipping bucket rain gauge and tipping bucket flowmeter. The sensors have been calibrated in the lab and have undergone field testing for verification and measurement uncertainties evaluation. The details in sensor measurement uncertainties can be found in 3.2.4.

Table 3-3: Monitored items and instrumentations for JdB1, JdB2 and SC

	JdB1 & JdB2	SC
Inflow	tipping bucket (Précis Mécanique 2*1 L) + electromagnetic flowmeter (KOBOLD MIM)	2 electromagnetic flowmeters (Krohne OPTIFLUX2000 –DN25 and DN50)
Drainage	tipping bucket flowmeter (Précis Mécanique 2*1 L)	tipping bucket flowmeter (Précis Mécanique 2*1 L)
Surface ponding depth	-	pressure sensor (Campbell Scientific CS451)
Bottom gravel water level	pressure sensor (Paratronic CNR1.5)	pressure sensor (Campbell Scientific CS451)

Soil moisture	3 profiles of 5 soil moisture sensors each (Campbell Scientific CS650-VS)	3 soil moisture profile sensors with multiple probes (Campbell Scientific SoilVUE^{TM}10 , 50cm and 100cm)
Precipitation	rain gauge (Campbell Scientific TE525MM)	rain gauge (Précis Mécanique 0.2 mm)
Meteorological data	meteorological station + separate solar radiation sensor (Campbell Scientific CS100 + NR01)	2 meteorological stations (Vaisala WXT536 + Campbell Scientific ClimaVUE50) + Météo-France Torcy

3.2.3.3 Vegetation observation methodology

3.2.3.3.i Vegetation types in JdB and SC

As previously mentioned, the three rain garden prototypes have a variety of different plants. The growth and development of these plants, the seasonal changes they undergo throughout the monitoring period. The two figures below show the different plant species grown in JdB and SC.

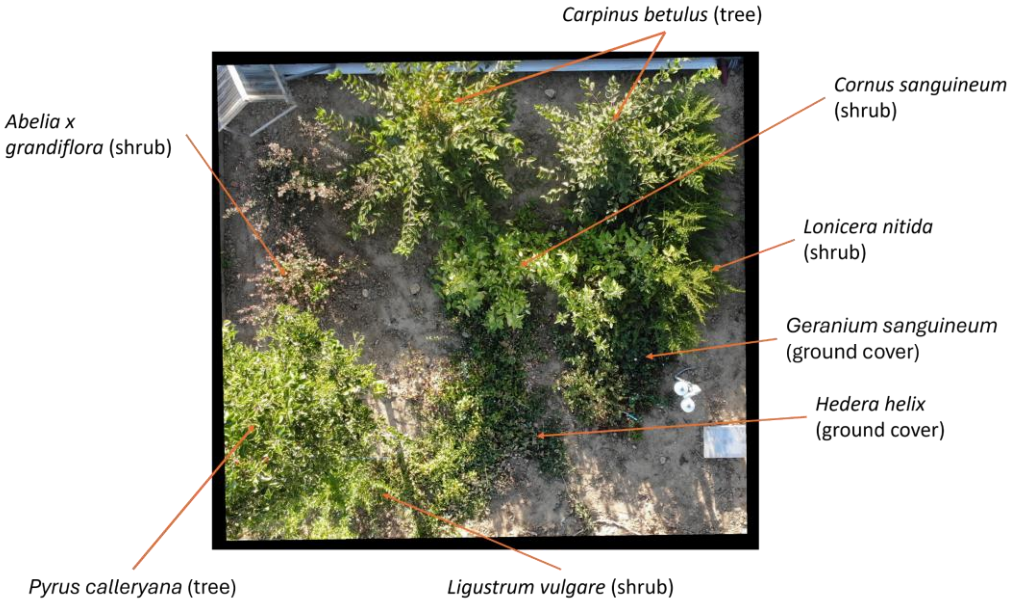

Figure 3-7: Vegetation in JdB (same species setting for JdB1 and JdB2), photo taken on 2022-08 on JdB1

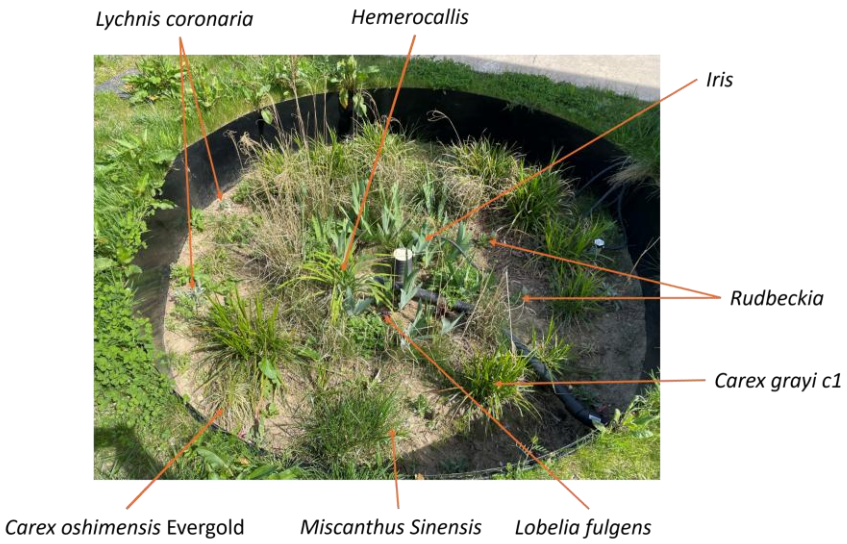

Figure 3-8: Vegetation in SC; photo taken on 2022-04

The observation on vegetation growth for JdB and SC rain gardens was conducted via direct visual observation, photography and field plant height measurements. For JdB, top-view drone photos were taken in 2021-05, 2021-08, 2021-09, 2022-08, 2022-11, 2023-06, 2023-11). For SC, the top-view photos were taken manually every month from 2023-02 to 2023-11, plant height for each species was also measured for the same period.

3.2.3.3.ii Image analysis (Trainable Superpixel Segmentation method) on JdB drone photos

The top-view photos of JdB were processed with an image classification method (Técher, 2022), which allows to identify the surface coverage proportion for different types of plants. The Trainable Superpixel Segmentation was conducted with Fuji-ImageJ free software (https://imagej.net/software/fiji/downloads), «trainable superpixel segmentation» (https://github.com/CVPD/Trainable_Superpixel_Segmentation) plugin and jSLIC plugin (to segment pictures into superpixel-ones, https://biii.eu/jslic, https://imagej.net/plugins/cmp-bia-tools/). The calibration involves to manually choose several areas of pixels for each type of ground covering (bare land, trees, shrubs, ground-covering, weeds and others) as the training set, and classify the whole image based on the training set.

Due to the light effect (especially shadow effect over the different shotting dates), the calibration of the selected 8 photos was done independently. Here shows an example of an overlay image (Figure 3-9, where the results of the classification method

for the different categories of image elements, e.g., background, soil, shrubs, tree and ground cover species, are transparently overlaid on the original drone photo) and the corresponding classification results (Figure 3-10, a "mask-image" without overlay).

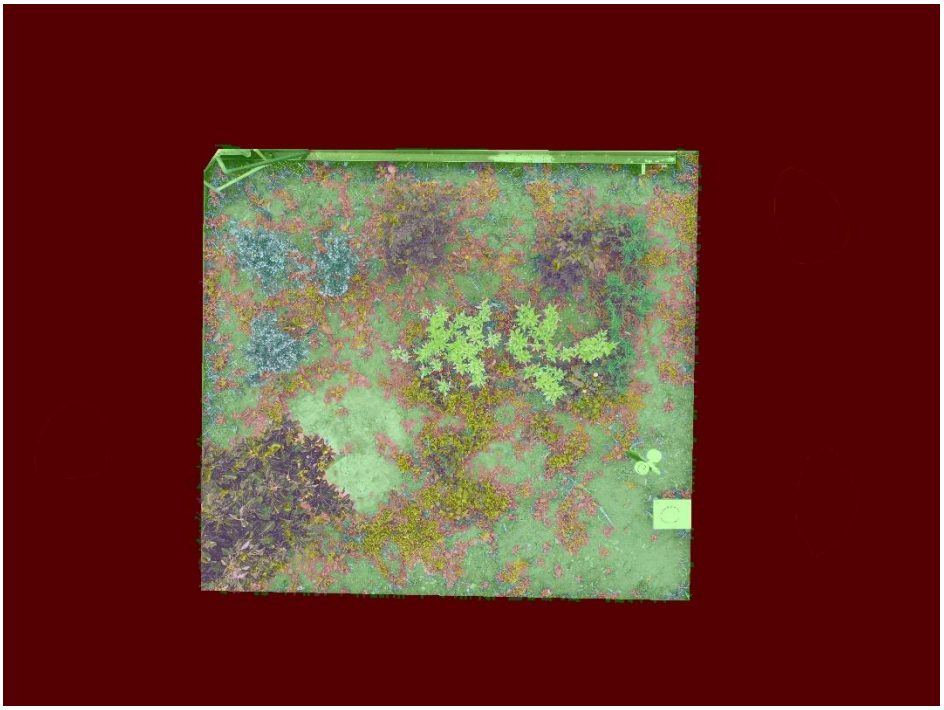

Figure 3-9: Example of an overlay of classified image on the original aerial photo

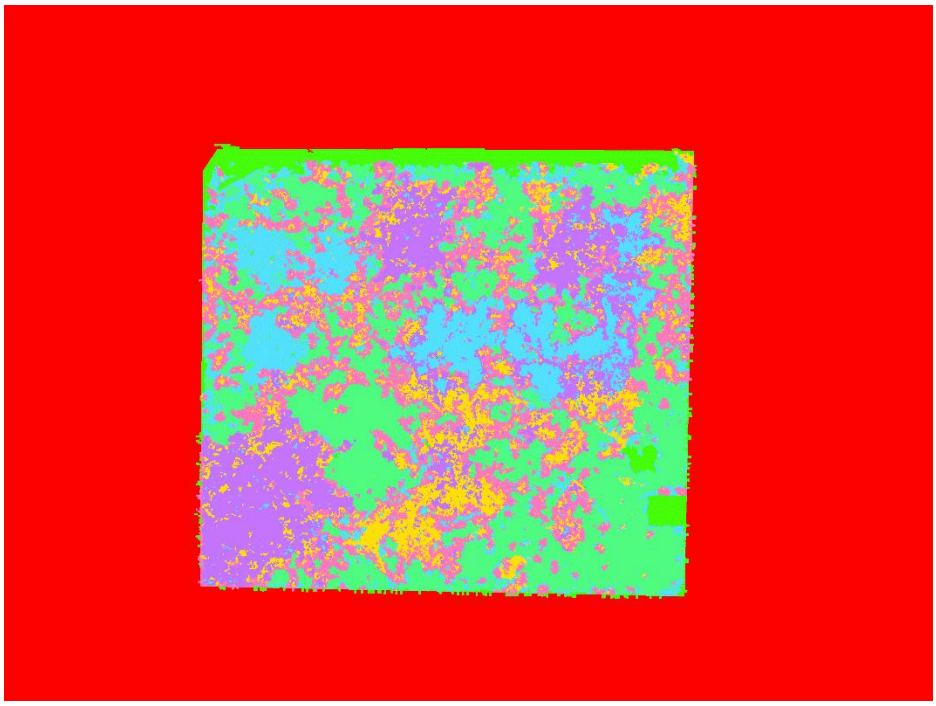

Figure 3-10: Example of classified surface coverage types

By applying the image segmentation and classification method on all the eight drone photos (four months for the two cells), the ratio of different surface coverage

pixels to the total number of pixels is summarized for each month and each cell to analyse the vegetation development of JdB1 and JdB2.

3.2.3.3.iii Vegetation measurement in SC

Unlike JdB, the top view photos could not discriminate between different plant species due to the huge development of a dominant plant species (*Miscanthus Sinensis*) shading all other plants in the SC and were only used to measure the proportion of total plant cover (in 5.2.3.4). Specific growth observations for each SC plant species were more dependent on monthly field measurements on the average green part height of each species. Results of vegetation picture analysis and observations are presented in 4.2.2.

3.2.4 Sensor Calibration and Measurement Uncertainty Evaluation

Sensors in SC and JdB normally have been pre-calibrated or factory-calibrated before their installation. However, the field conditions are difficult to control and may differ from those for which the sensors are expected to operate; some sensors are not working under their optimal design measurement range (i.e., the electromagnetic flowmeters), some sensors are not placed in an ideal environment (SoilVUE in an inhomogeneous media). Hence the accuracy which was set by the manufacturer cannot represent the overall measurement uncertainty.

The overall measurement uncertainty can be defined as a systematic uncertainty (constant error) and a random uncertainty (Attivissimo et al., 2011). The field/laboratory tests carried out in this study are intended to calibrate the sensors to adjust/minimize their systematic uncertainty and also to find the range of random uncertainties.

3.2.4.1 Calibration experiment design

The uncertainties of sensors were evaluated from the following laboratory tests and field experiments.

For Ecole du Breuil (JdB1 and JdB2):

- Soil sampling test: 54 soil core samples (9 in 2022, 45 in 2023) were collected in the field with 100 cm3 calibrated cylinders at depths from 0 cm to 130 cm next to the 6 monitored soil moisture profiles. The water content of the soil cores was determined in the lab by subsequent weighting/drying/weighting.

Each sensor reading was associated to 1 or 2 soil sample. The soil moisture ranged from 0.131 m3/m3 to 0.411 m3/m3.

For SC:

- Water level measurements with the pressor sensor were controlled in the laboratory, in a Perspex column. 33 to 59 sensor measurements were repeated for each water level tested. The 8 water levels reached from 29.8 mm to 500 mm.
- Electromagnetic flowmeter: a water tube based on Mariotte's bottle principle was used to inject adjustable constant flow to be compared with the one measured by the electromagnetic flowmeters. 4 to 205 sensor measurements were taken during each simulated flow rate depending on the tested flow rate. The 8 simulated flow rates reached from 0.03 L/min to 2.4 L/min.
- Soil sampling test: 15 soil core samples were collected in the field with 100 cm3 calibrated cylinders at different depths next to the sensors. The water content of the soil cores was determined in the lab by subsequent weighting/drying/weighting. 1 or 2 sensor readings were associated to each soil sample. The soil moisture ranged from 0.092 m3/m3 to 0.276 m3/m3.

3.2.4.2 Statistic methods

3.2.4.2.i Ordinary Least Squares regression

The calibration and uncertainty evaluation are based on a common linear regression model Ordinary Least Squares regression (OLS) (Craven & Islam, 2011). In this case, OLS estimates the coefficient a and offset b of a linear regression equation which describes the relationship between one independent variable x (sensor readings) and one dependent variable $y_{observed}$ (reference values):

$$y_{predict} = \mathrm{a}x + \mathrm{b} \quad \text{Eq. 3-6}$$

$$y_{observed} = \mathrm{a}x + \mathrm{b} + \varepsilon \quad \text{Eq. 3-7}$$

Where:

- ε = random error (supposed in the following to be normal, with an average of 0, and a standard deviation that does not depend on x.)

Intuitively, OLS is trying to minimize the sum of square errors between the $y_{observed}$ and $y_{predict}$ by changing the coefficient a and the constant b. $y_{predict}$ is considered as the sensor readings after correction, in other words, calibration.

3.2.4.2.ii Confidence interval

A Confidence Interval (CI) is an interval which describes the accuracy of the mean of predictions for a given x_{sensor} level based on the standard error of the predicted mean:

$$MSE = \frac{1}{n-2} i = 1n\left(y_{observedi} - y_{predict}\right)^2 \quad \text{Eq. 3-8}$$

$$y_{predict} \pm t(1-\alpha/2,\, n-2) \times \sqrt{\left\{MSE \times \left(\frac{1}{n} + \frac{(x-\bar{x})^2}{\sum\{(x_i\} - \bar{x})^2}\right\}\right)} \quad \text{Eq. 3-9}$$

Where:

- n is the sample size
- MSE is the mean square error with n-2 denominator.
- $t(1-\alpha/2,\, n-2)$ is Student t-value with n-2 degree of freedom, $1-\alpha$ equals to the confidence level.
- $\sqrt{\left\{MSE \times \left(\frac{1}{n} + \frac{(\{x-\bar{x})\}^2}{\sum\{(x_i\} - \bar{x})^2}\right\}\right)}$ represents the standard error of the fit.

3.2.4.2.iii Prediction interval

A Prediction Interval (PI) is an estimated range at a given confidence level in which the reference value $y_{observed}$, associated to an individual sensor measurement is likely to be. Different than the CI, the PI predicts an individual value rather than the mean value, and it focuses on the real "prediction" for the future while the CI is the statistic of current available data. A PI is wider than CI but with less certainty.

The equation of PI is similar with the CI equation:

$$y_{predict} \pm t(1-\alpha/2,\, n-2) \times \sqrt{\left\{MSE \times \left(\frac{1}{n} + \frac{(x-\bar{x})^2}{\sum\{(x_i\} - \bar{x})^2}\right\}\right)} \quad \text{Eq. 3-10}$$

Where:

- $\sqrt{\left\{MSE \times \left(1 + \frac{1}{n} + \frac{(x-\bar{x})^2}{\sum\{(x_i\}-\bar{x})^2}\right\}\right)}$ represents the standard error of the prediction.

Compared with the CI equation, the last term of PI equation actually only adds an extra MSE term. The further explanation can be found in: [3.3 - Prediction Interval for a New Response | STAT 501 (psu.edu)]

The PI here is used to represent the measurement uncertainty of sensors, at the significance level of 95% (α=0.05). Another thing that needs to be noted is that since the PI range is estimated, even if we choose 95% significance level for PI, the PI eventually will not cover exactly 95% of current observations.

3.2.4.3 Calibration results

3.2.4.3.i Water level test: CS451 pressure water level sensor (SC)

Figure 3-11: *CS451 pressure sensor*

The water level test for CS451 pressure sensor was done in the laboratory. The sensor contained a nose cone in the front of probe, its technical manual indicates that there is 2.3 cm distance from pressure sensor interface to the end of nose cone. During the water level test, the end of the nose cone was placed at the bottom of the Perspex column. Therefore, the 2.3 cm offset was removed from all the sensor measurements before doing the regression.

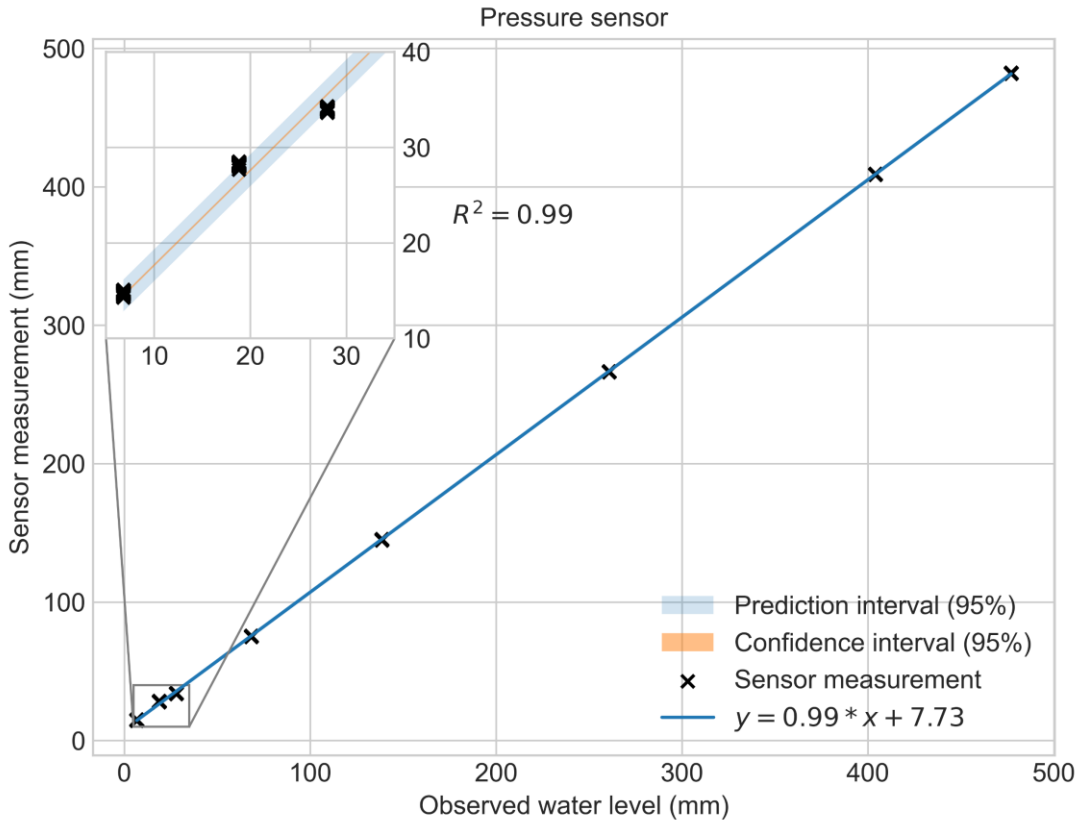

Figure 3-12: *Calibration on CS451_4 water level sensor*

The prediction interval of CS451_water level sensor is small (less then 2mm), but the simulated water level at 18.8 mm and 28.0 mm show a slight deviation (<10%) from the regression line. In addition, the regression result indicates -7.78 mm offset, which means the assumed offset (23 mm) was too much, the real offset should be 15.22 mm.

3.2.4.3.ii Injection test: Q_IFC100 electromagnetic flowmeter (SC)

The injection tests generated 8 different constant flows from 0.026L/min to 2.435L/min. The simulated flows are measured by the Q_IFC100_DN25 flowmeter with 1 minute time step. In each test, the first and last two measurements are excluded to ensure that comparisons between measurements and the targeted flow rate are conducted under stabilized conditions. Due to the limited volume of Mariotte tube, the number of recorded measurements is significantly different between small flows and higher flows. To avoid overweighting on the low flow tests caused by their large amounts of measurements (205 measurements for 0.026L/min flow, 68 measurements for 0.132L/min flow), 20 consecutive measurements (in the middle of whole test period) were kept for each low flow test.

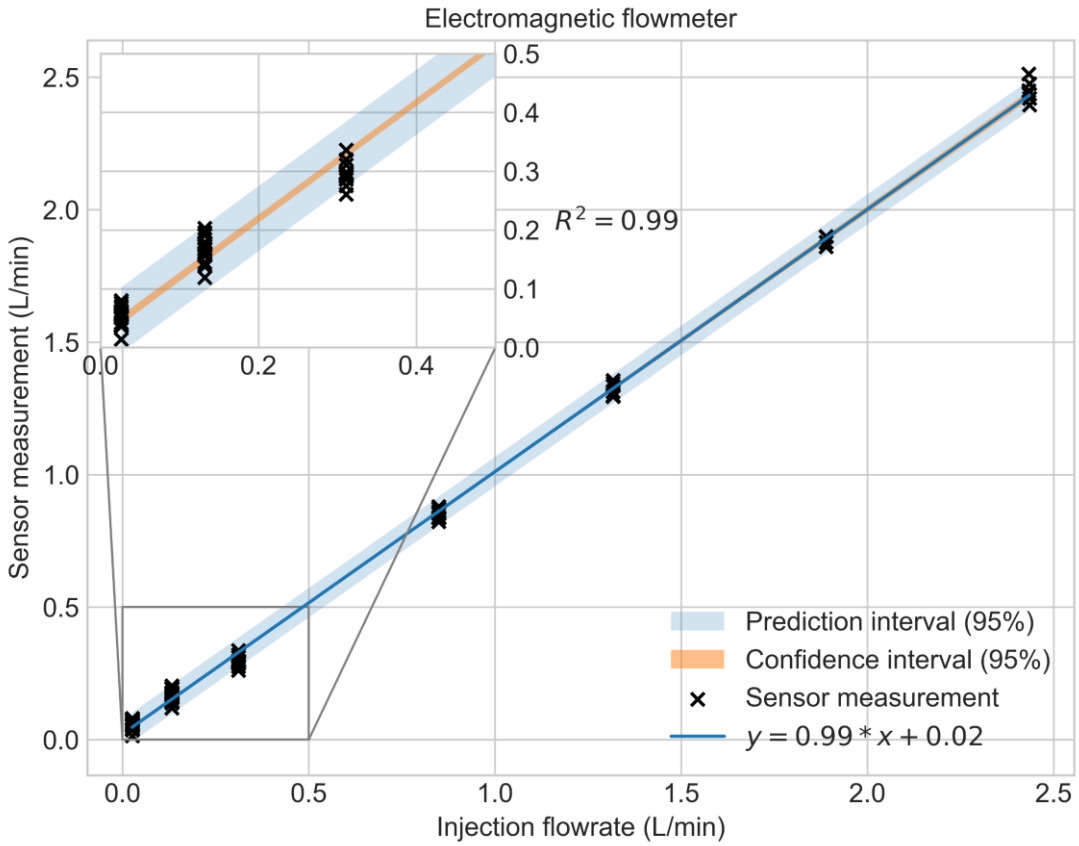

Figure 3-13: *Calibration on Q_IFC100_DN25 flowmeter*

The regression fits well except at 0.311 L/min, where the prediction value is slightly lower than injection flow rate. It is probably due to experimental operation uncertainties, or the flowmeter performance non-linearity under 0.3 L/min. The following table shows the difference within injection flow, prediction flow and sensor average.

3.2.4.3.iii Soil sampling test: SoilVUE soil moisture sensor (SC)

SoilVUE sensors have the largest measuring uncertainty (especially for SoilVUE50_3). Based on the sampling results and measurements from SoilVUE50_3, SoilVUE50_4 and SoilVUE100_2, the “regression” can be implemented as follows.

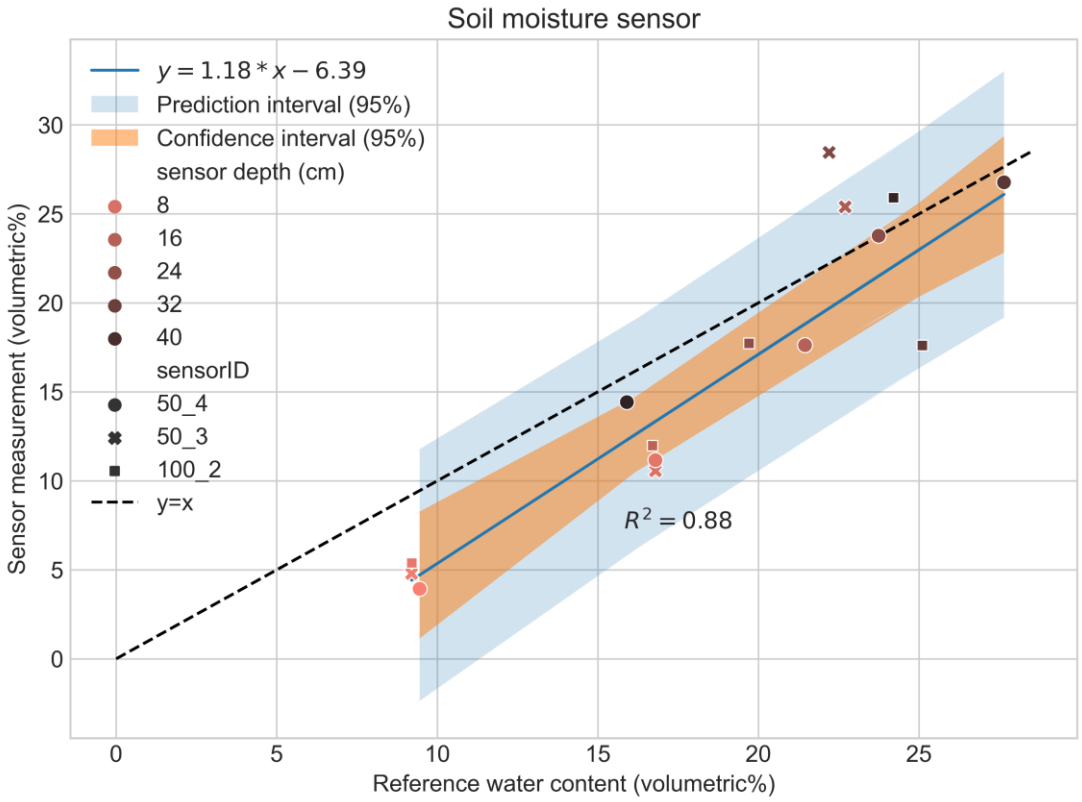

Figure 3-14: Calibration on SoilVUE moisture sensors

Before the regression, all the explainable outliers (i.e., samples with rocks or planting soil) have been removed. In Figure 3-14, regressions were done without the problematic sensor 50_3 (marked as cross). The cross, dot, and square represent the measurements from 50_4, 50_3 and 100_2, and the colour of markers indicates different depths of the correlated sensor, the darker the colour, the deeper the sensor. As shown in Table 7-3 (in Appendix 4), large uncertainties, both systematic and random, are obtained. The dispersion of the points is too important to rely on the results of the regression. However, Figure 3-14 shows all the sensors that are close to the surface are underestimating the moisture under dry conditions, which may originate from an imperfect contact between the surface probe and the surrounding material, especially under dry conditions.

The regression laws suppose that all the different sensors have the same behaviour/error. However, in reality, the sensor behaviour is highly linked to the media condition (e.g., organic carbon) as well as the contact between sensors and surrounding media. Hence, aggregating all monitoring and sampling data for regression is not suitable for this situation, and regression for individual sensors is impractical due to limitations in the number of samples taken. In this case, rather than using regression,

it is more intuitive to directly compare monitored and sampled soil profiles (as shown in Figure 3-15).

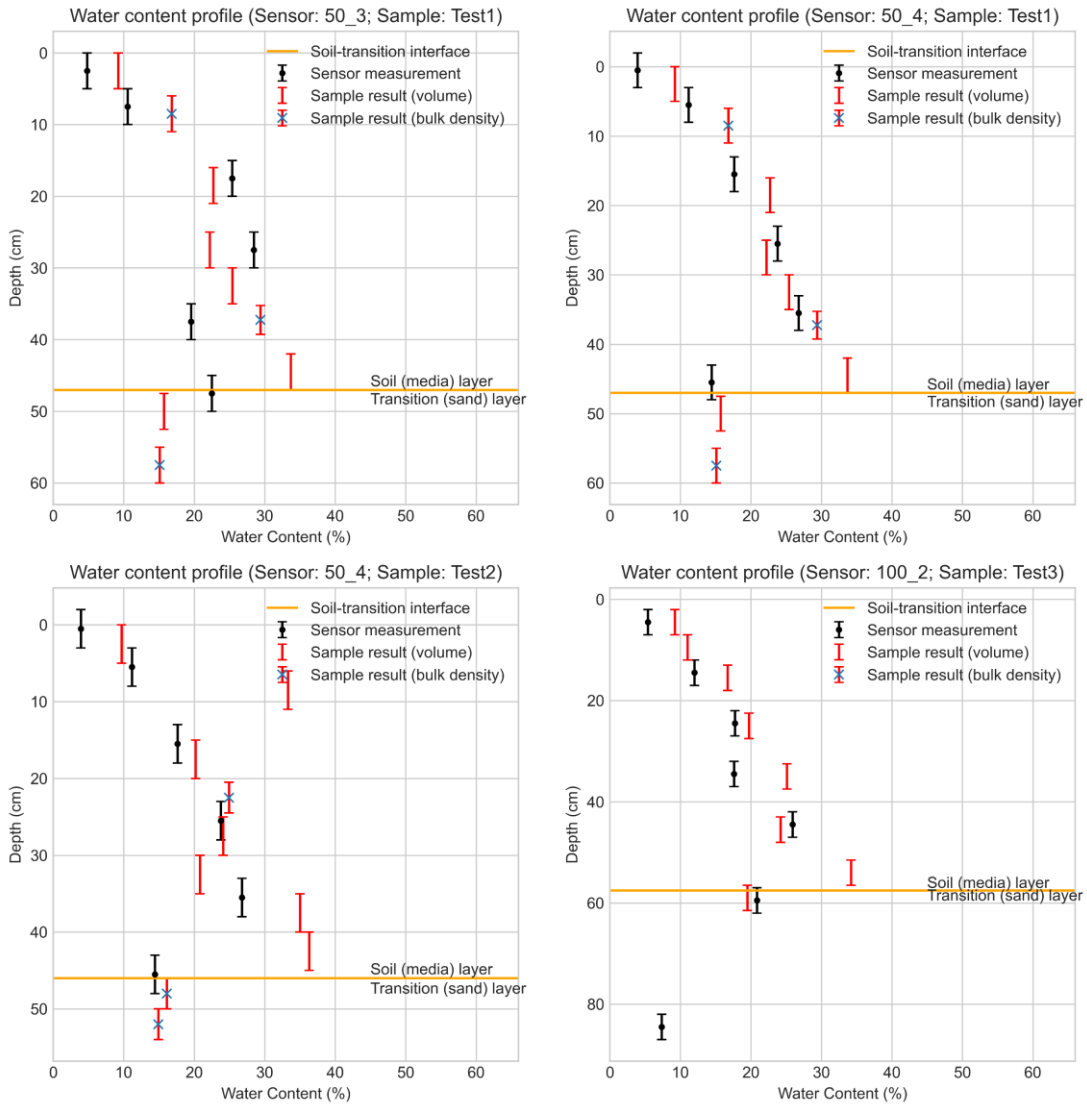

Figure 3-15: Comparison between SoilVUE measured and field sampled soil profiles

In Figure 3-15, each subplot compares a sensor measured profile and a sample results profile. The Test 1 profile was located between the two sensors SoilVUE50_3 and 50_4, thus it is being compared twice. The black bars represent the sensor measured soil moisture and the corresponding monitoring range. Similarly, the red bars indicate the sampled soil moisture and sample range. The moisture of most samples is calculated based on their volumetric percentage of soil water over the cylinder volume. For some samples which were not full in the cylinder during sampling, soil moisture is calculated based on average bulk density of the soil (red bar with blue cross). For the comparison of soil moisture profiles, except for the

problematic sensor SoilVUE50_3, the other two sensors SoilVUE 50_4 (Test1) and 100_2 (Test3) show good consistency between sensor measurements and sampling results. High moisture samples were found in all profiles right above the interface between filter media layer and sand transition layer, which indicates the existence of a capillary barrier. Unfortunately, for the sensor probes located near this interface the monitoring volume partly enters the transition layer, and therefore could not capture the existence of this capillary barrier.

3.2.4.3.iv Soil sampling test: CS650-VS soil moisture sensor (JdB)

The sampling profiles were taken 20-50 cm away from the sensor profiles. Due to the inhomogeneous texture of the filter media, the sampling work was often interrupted by rocks, therefore the number of surface samples is higher than that of deeper samples.

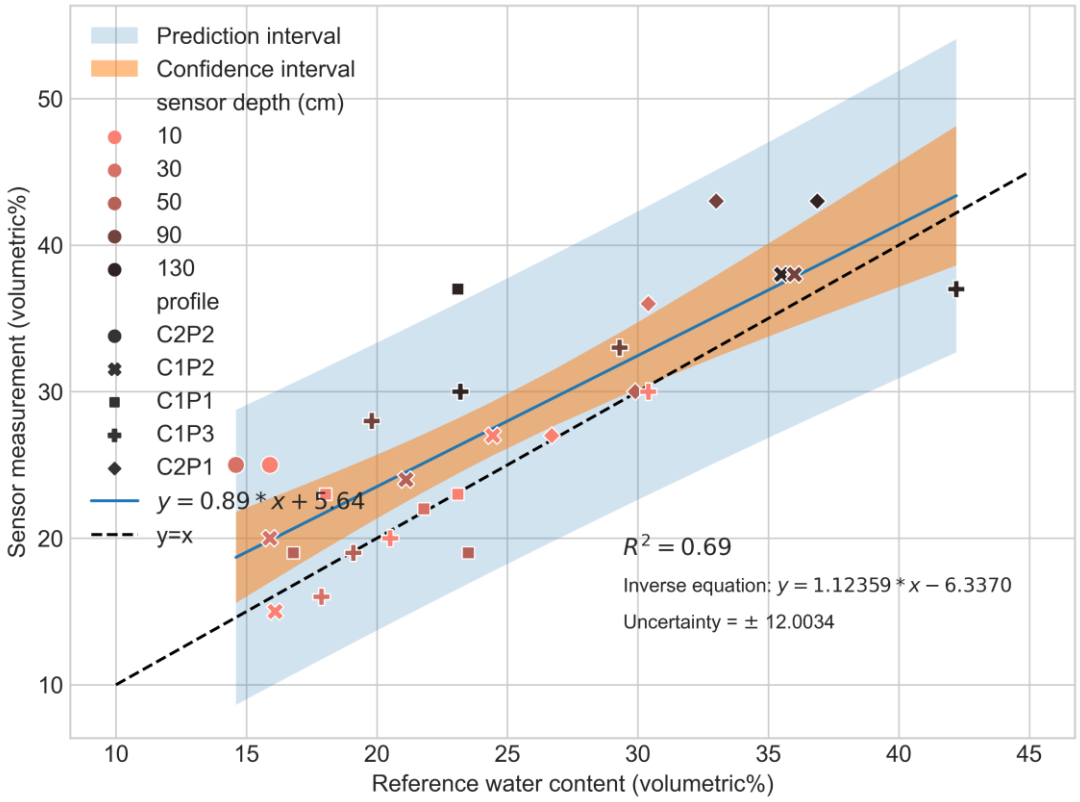

Figure 3-16: Calibration on CS650-VS soil moisture sensor

Similarly to the calibration result from SoilVUE sensors in SC, the CS650-VS sensors in JdB show large dispersion, also since each probe has its independent surrounding situation, the regression presented in Figure 3-16 and Table 7-4 (Appendix 4) can be used to provide an order of magnitude of the error (assuming that

the error has the same behaviour for each sensor), instead of being considered as calibration of all the sensors.

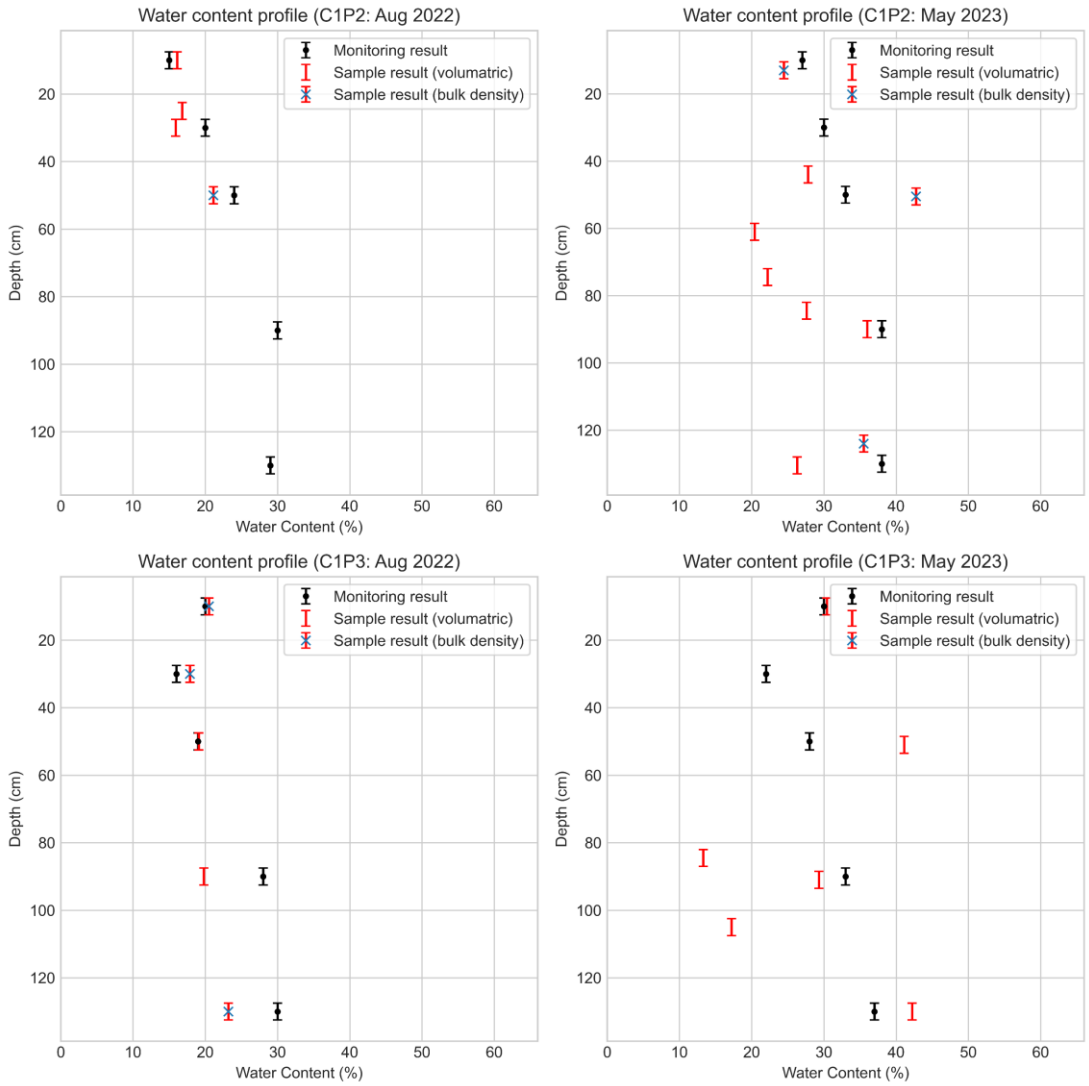

Figure 3-17: Comparison between CS650-VS measured and field sampled soil profiles (C1: JdB1 cell, P2: mid-stream soil moisture profile, P3: down-stream soil moisture profile)

Due to the thickness of filter substrate layer and the type of media (silt loam), the sampling work was difficult especially to reach to the deeper layer (>70 cm). For JdB2, it was only possible to use a very limited number of samples. Therefore, profiles for JdB2 are not able to be showed, thus only two profiles for JdB1 are presented in Figure 3-17. For the two subplots based on measurements in Aug 2022, the soil moisture shows a good consistency between monitored and sampled soil on the top three probes for each profile. However, the comparison between sensors and samples in deeper positions is less satisfactory. In May 2023, due to the implementation of a surface mulch layer and shorter antecedent dry periods, the two profiles show higher

moisture, especially for surface sensors and surface soil samples. Within a same profile, two measurements (50cm and 90 cm for C1P2 samples) sometimes showed abnormal variations and that ii) between two profiles (P2 and P3), sometimes large differences at similar depths can be found. This is possibly due to some local "dry pockets" within the filter substrate, which are created by the fine media and the preferential flow along sensor cables.

3.2.4.3.v Inverse equation and uncertainty

The application of calibration results needs to extrapolate the calibrated values from direct sensor measurements. Table 3-4 presents inverse equations and uncertainty for each type of measurement. However, as explained earlier, the inverse equations for soil moisture are not really reliable and thus were not applied during the data processing. The inverse equations of inflow and gravel storage level demonstrate high consistency with the uncalibrated equation (direct reading), thus only the offset of gravel storage level was applied in the data processing.

Table 3-4: Inverse equation and uncertainty

Type of measurement	Inverse equation	Uncertainty
Runoff (inflow) rate (SC)	y=1.01*x - 0.02	±0.06 L/min
Gravel storage level (SC)	y=1.01*x – 7.78	±1.68 mm
Soil moisture (SC)	y=0.85*x + 5.42	±6.01 m^3/ m^3
Soil moisture (JdB)	y=1.12*x – 6.34	±12.00 m^3/ m^3

3.2.5 Data Pre-processing

3.2.5.1 Inflow monitoring system noise and failure (JdB)

3.2.5.1.i Problems identified

As introduced in 3.2.2.1, the inflow measurement system of each JdB cell consisted of an electromagnetic flowmeter and a tipping bucket flowmeter installed in series (each cell has its own flowmeter system). During the two validated periods, the two measurement systems have experienced multiple interruptions. The following figure presents the function of cumulated inflow (the max value of the two flowmeters at each time step) on the cumulated rainfall.

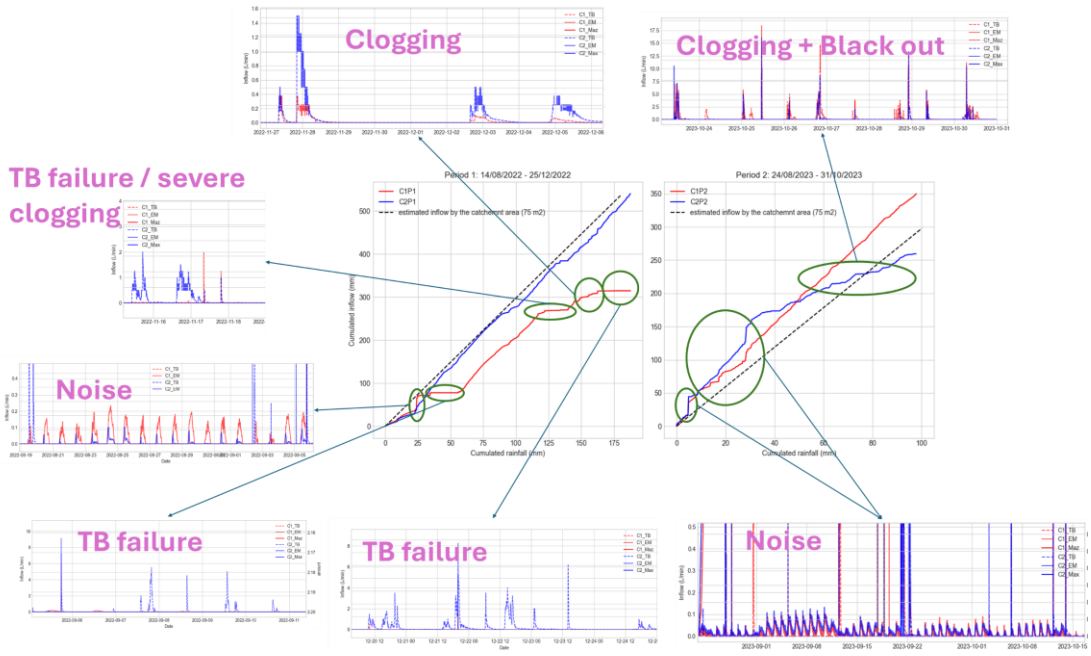

Figure 3-18: Problems identified in the cumulated inflow – rainfall function curve (C1, C2: JdB1, JdB2; P1, P2: valid period1, valid period2; TB: tipping bucket flowmeter)

In Figure 3-18, cumulated inflows are represented for each monitoring period (P1 and P2), and values from raingarden JdB1 and JdB2 are compared to the cumulated volume of rainfall received by the 75 m² theoretical roof catchment of each raingarden. For a slopped metal roof, initial water losses should be relatively limited and we can assume that the runoff coefficient of this roof is close to 1. As shown in the figure, several abnormalities have been identified. Sudden increases in the cumulated inflow while there was no rainfall were observed during some periods (subplot x), they could be explained by noise in the electromagnetic flowmeter data. The flat parts of the curves where cumulated rainfall increased while no inflow accumulated (subplots y and z) are related to tipping bucket failure or severe clogging. In addition, in the second observation period, the inflow sensor "blackout" (recorded Nan data while other sensors were still working, but recovered to normal after a few hours) happened several times on both electromagnetic flowmeters. The reason for this "blackout" is still unclear, it could possibly be due to the low electronic conductivity of the roof runoff which might sometimes be too low (for large events) and thus beyond the measuring range of electromagnetic flowmeter.

3.2.5.1.ii Noise in electromagnetic flowmeter

The electromagnetic flowmeter has noise with low value (<0.25L/min) during some dry periods. The noise is not continuous over the observation periods but always

shows a daily variation pattern (possibly reflecting the impact of temperature). Since actual inflow-rate is taken as the maximum between the tipping bucket and electromagnetic flowmeter measurements, the noise can be counted as real flow during the period when the tipping bucket flowmeter has no readings. Therefore, a simple filter can be applied with the rule:

When both tipping bucket flowmeters give flowrate < 0.05L/min, and both electromagnetic flowmeters have value < 0.25L/min, the real flowrates of the two cells are replaced to 0 L/min. Here these thresholds are not sensitive. 0.05L/min means this filter will stop 10min before a real event (second tip of an event); and 0.25L/min is higher than the highest noise identified by manually checking.

By applying this filter, the noise under dry weather can be removed, while in wet weather the noise value remains lower than the tipping bucket measurements therefore does not need to be removed.

3.2.5.1.iii Rebuild the missing period for inflow

After removing the noise, the "flat" parts (due to tipping bucket failure and electromagnetic flowmeter blackout) in the cumulated inflow-rainfall figure remain. Considering the two bioretention cells are receiving water from a metal roof (runoff coefficient equals to 1), the inflow theoretically can be estimated by the precipitation and catchment area. In Figure 3-19, segment curve fitting is applied on several periods with no identified issues to get the slope in the cumulative rainfall-inflow function, i.e., the contributing catchment area.

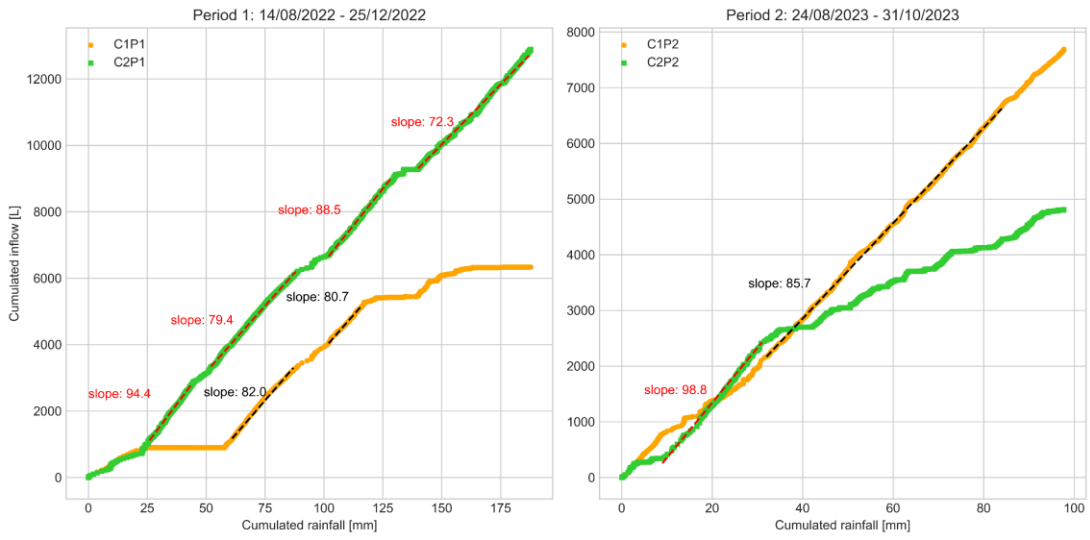

Figure 3-19: Curve fitting on the cumulative rainfall-inflow function (C1, C2: JdB1, JdB2; P1, P2: valid period1, valid period2)

Figure 3-19 The projected area of the whole roof catchment is 150 m^2 (75 m^2 for each cell). Due to the wind effect and other potential reasons, the area calculated by segmented regression vary from a period to another and are higher than the projected area. The average contributing roof area estimated from the two observation periods for JDB1 is 81.3 m^2 (period 2022) and 85.7 m^2 (period 2023); for JDB2 it is 83.6 m^2 (period 2022) and 98.8 m^2 (period 2023).

Based on the estimated contributing area, the inflow during the tipping bucket failure, electromagnetic flowmeter blackout and part of tipping bucket clogging is rebuilt from the rainfall. (refer to figure below?)

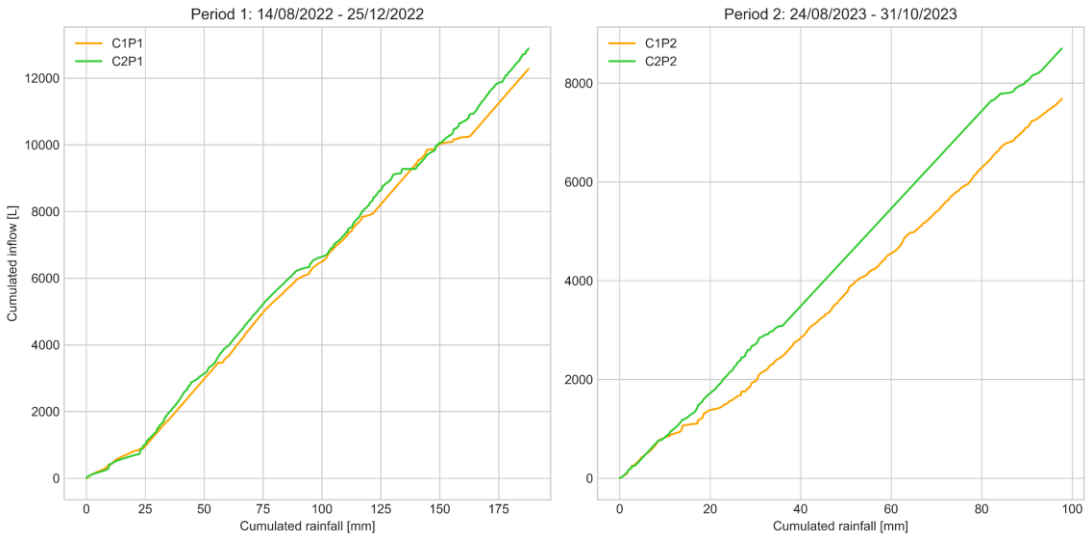

Figure 3-20: Rebuilt cumulative rainfall-inflow function (C1, C2: JdB1, JdB2; P1, P2: valid period1, valid period2)

In Figure 3-20, most of the issues identified in inflow measurements have been solved. For the clogging issues, two types of situations can be identified depending on the readings given by the electromagnetic flowmeter:1) if the latter have high flowrate values, it can be assumed that clogging occurred in the section between the electromagnetic flowmeter and the tipping bucket, or was due to a mechanical failure of the bucket (e.g., the bucket got stuck and did not flip), in which case the incoming water could still enter the cell via the overflow in the inlet. 2) otherwise, it suggests that clogging happened upstream of the electromagnetic flowmeter (on the roof gutter for instance), in which case not only a fraction of the runoff volume part of the roof runoff might have been discharged outside of the bioretention cell. Rebuilding the inflow from rainfall measurements is only relevant for the first situation, the second type needs to be further verified in the event-based water balance in the next step.

3.2.5.1.iv Inflow problem characterization based on event water balance

The event-based water balance analysis was conducted with the following variables (all volume related units are converted to L):

- measured_inflow: measured inflow
- estimated_inflow: inflow estimated by precipitation * roof area
- dir_rainfall: direct rainfall over the cell surface
- in_measure: dir_rainfall + measured_inflow
- in_simulate: dir_rainfall + estimated_inflow
- outflow: measured outflow
- delta_soil: the soil storage difference between the start and the end of event
- delta_wl: the gravel water storage difference between the start and the end of event
- out: total outwards flow (outflow + delta_wl + delta_soil)

Based on the above parameters, the event can be characterized by the following groups and actions as shown in Table 3-5. Based on the "Action" column, the inflow of each event can be kept, removed (together with the whole event) or rebuilt with the rainfall and roof area estimated in the previous curve fitting.

Table 3-5: Event-based inflow problem identifying and fixing criteria (the coefficient 0.7 in this table is used to digitally represent "<<")

No.	Inflow Characteristic	Category	Action
1	in_measure >= out and measured_inflow > estimated_inflow * 0.7	normal inflow well measured	keep the measured inflow
2	in_measure < out and in_simulate > out	normal inflow incompletely measured	rebuild the inflow
3	measured_inflow = 0 and in_simulate > out	0 inflow (total bypass)	keep the measured inflow
4	measured_inflow = 0 and in_simulate > out and dir.rainfall < 10 L	tiny event without inflow	keep the measured inflow
5	in_measure > out and measured_inflow < estimated_inflow * 0.7	limited inflow (partial bypass) well measured	keep the measured inflow
6	in_measure < out and measured_inflow < estimated_inflow * 0.7 and in_simulate > out	limited inflow (partial bypass) incompletely measured	remove the event
7	in_simulate < out and measured_inflow > 0.7 * estimated_inflow	abnormal inflow well measured	keep the measured inflow
8	in_simulate < out and measured_inflow < 0.7 * estimated_inflow	abnormal inflow incompletely measured	rebuild the inflow
9	dir_rainfall = 0	injection test	remove the event

3.2.5.1.v Uncertainty on the wind impact on the receiving runoff volume

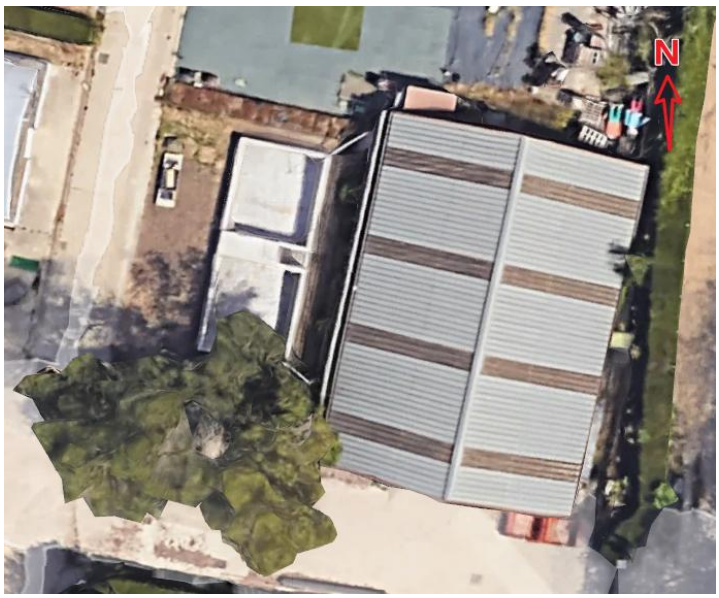

Figure 3-21: Top view of JdB catchment (metal roof)

Due to the slope of the roof and the tree nearby (as shown in Figure 3-21), the wind direction and velocity are supposed to have impact on the runoff volume. The following figure plots the wind direction on cumulative rainfall-inflow curve of the

JdB1 cell at period 2023 and JdB2 cell at period 2022 (these two curves have few modifications).

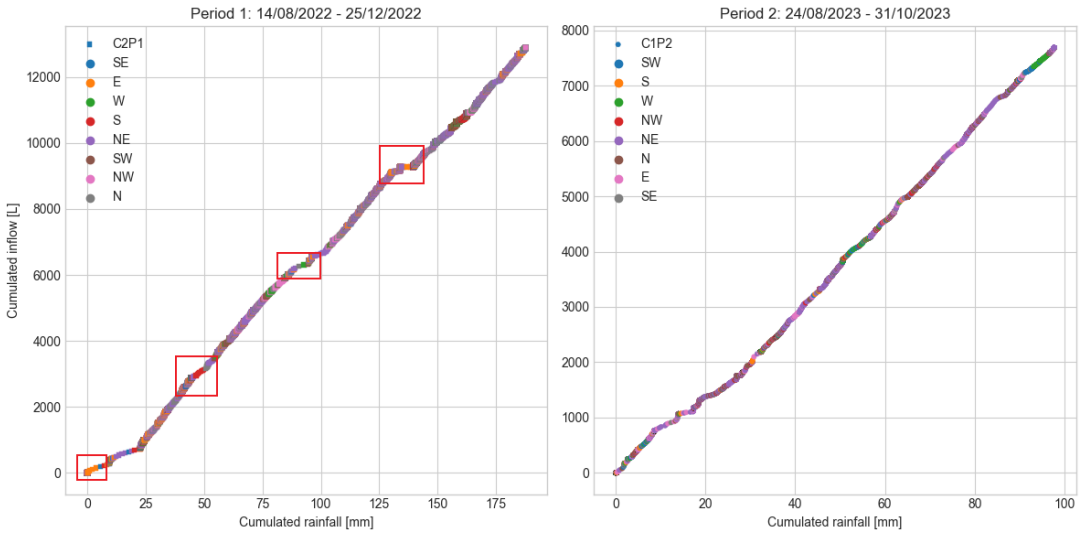

Figure 3-22: Cumulative rainfall-inflow curve with wind direction

For both periods, the dominate wind direction is North-East during the rainy days. On the left subplot, JdB2 received less runoff when the wind direction is from South (red), East (yellow) and West (green), while the inflow in JdB1 cell in 2023 seems not affected by the wind direction. Therefore, the rebuilding of inflow based on rainfall data and catchment area can introduce extra uncertainty, especially for JdB2.

3.2.5.2 Flowmeter noise (SC)

On Sense-City raingarden, two electromagnetic flowmeters (Krohne OPTIFLUX-25) implemented in parallel are used to measure the runoff which enters the bioretention cell. However, both measurements contain a lot of noise. Several attempts have been tried including cut-off threshold, Fourier transformation and Wavelet filter. The cut-off method with a stationary threshold cannot completely remove all the noise and often miss cut the beginning of a runoff event. The Fourier transformation method can filter the frequency of dry noise but is not working when the real flow data is involved. The Wavelet filter can smooth the data but cannot well fit the beginnings of events. Overall, none of the above methods is able to achieve a satisfactory result.

3.2.5.2.i Stationary cut-off

Statistically, the dry weather noise appears to be higher in the winter and lower in the summer. The noise from the DN25 flowmeter is lower but with higher variation compared to the DN50 noise (as Figure 3-23 shows).

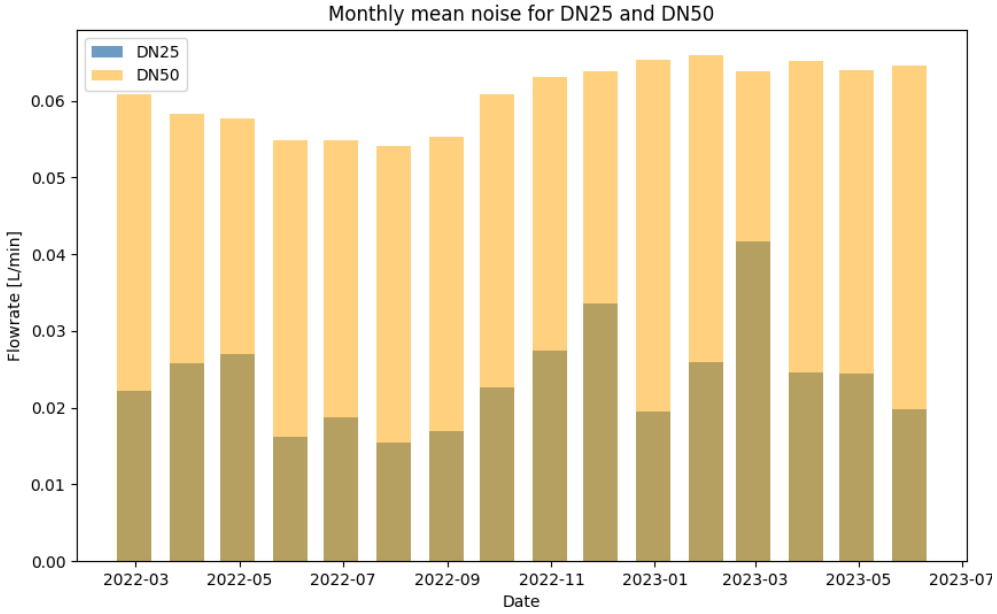

Figure 3-23: Monthly mean noise for the two flowmeters in Sense City

The mean values of the dry noise are 0.024 L/min (for DN25) and 0.060 L/min (for DN50), the maximum of monthly noises are 0.042 L/min (for DN25) and 0.066 L/min (DN50). Based on the distribution of the occurrence of different values of noise, Figure 3-24can be obtained.

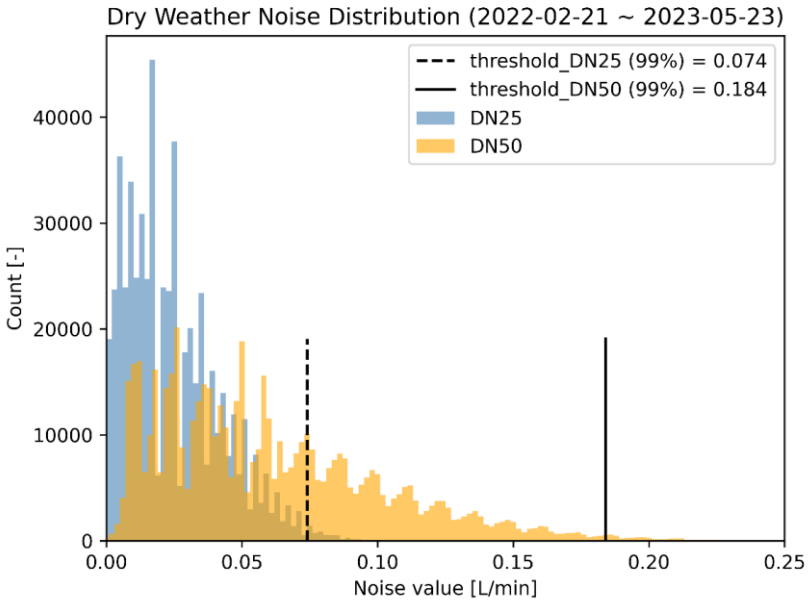

Figure 3-24: Dry weather noise distribution (2022-02 to 2023-05)

99% of dry noise can be cut under the threshold 0.074 L/min (DN25) and 0.184 L/min (DN50).

According to the injection test on the flowmeter DN25 and the evidence on some cases with slow start and end, the cut-off value (0.074 L/min) for DN25 sometimes cuts the beginning and end of a runoff event, therefore this method can underestimate the volumes of some events. In addition, some unusual noises (higher than the threshold) can create false "events" during the drying period, especially for DN50.

3.2.5.2.ii Identification of runoff periods (dynamic conditions judgement method)

A dynamic conditions judgement method was developed based on the work from Ramier (2005) and Kanso (2021) to determine the start and end of the runoff events.

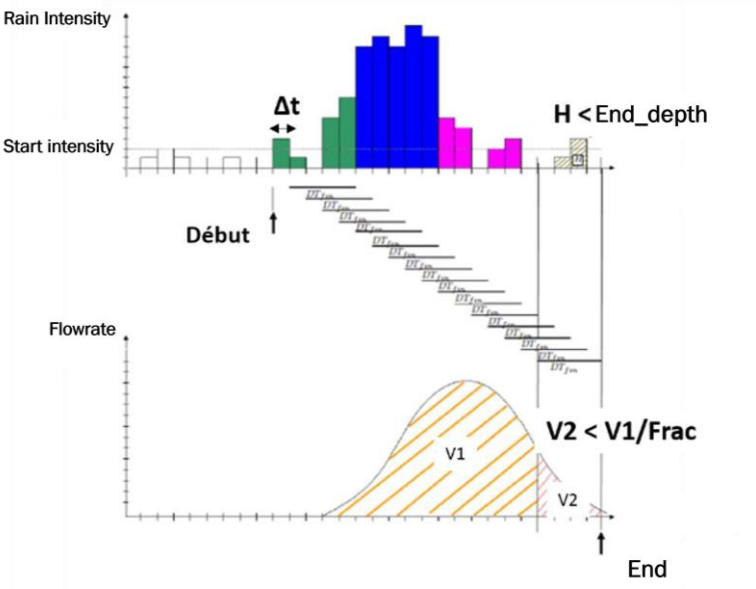

Figure 3-25: Diagram of the steps in the determination of rainfall-runoff events (adapted from Tala Kanso, 2021)

In this method, a rainfall-runoff event starts when the rainfall intensity exceeds a certain threshold start_intensity (mm/h). Then a rolling window judgement is applied to identify the end of the event from rainfall and runoff measurements. The cumulated volume of inflow within the rolling window (V2) is compared with the total cumulated inflow volume from the start of the event (V1): if the proportion V2/V1 is under a certain threshold (frac), and if the rainfall depth within the window (H) is lower than a threshold end_depth (mm), the event will be considered as finished. The window size (window_size) (min) can be customized. The procedure can be described as follows:

- Start condition: rain intensity > start_intensity (mm/h)

- End condition1: rain depth H < end_depth (mm)
- End condition2: V2 < V1 * frac
- End condition3: average inflow within the window < noise_threshold (L/min)

The judgement should meet the end condition1 (essential) and condition 2 or 3 (one of them). Parameters for thresholds are as follow:

window_size=20min, start_intensity=0.4 mm/h (1 tip of 0.2mm per 30 min), frac=0.5% and end_depth=0.1mm (1 tip within 40 min), noise_threshold =0.037L/min (half of the 99% dry noise cut-off).

Based on this method, the runoff event can be identified and inflow outside corresponding periods be considered as 0 flow (for both DN25 and DN50). For the measurement within the runoff period, all DN25 measurements are kept. For DN50, since it only activates during the high flow situation, the data out of runoff events are first removed, and a 0.3 L/min cut-off is applied for the measurements within runoff events, which is high enough to ensure the removal of all the noise.

3.2.5.3 Substrate water storage estimation (JdB)

The soil water storage is generally estimated by cutting the substrate layer into 15 soil blocks which correspond to the 15 soil moisture sensors. Then storage of each block is estimated as the block volume multiplied by moisture given by the sensor (script developed by Emmanuel BERTHIER).

However, due to the clogging issue at its outlet, water level inside JdB2 frequently exceeded the level of the outlet (presence of a “water table” in the substrate layer). The fluctuations of water table levels within the substrate layer may cause issues in the previous soil storage estimation method. For instance, once a soil moisture probe is submerged, the volume associated with corresponding soil block will show a sudden increase. Therefore, another soil storage estimation method based on the water level (from Paratronic CNR1.5 sensor) and soil moisture measurements was developed. In this approach, the soil below the water table is considered as fully saturated, and only the original method only applies to soil moisture sensors located above the water table

When comparing this new method to the original method, almost no difference was found. The limited difference between the two approaches presumably originates from the presence of a "capillary fringe" extending well beyond the water table; the whole substrate is near saturation when the water table is entering the substrate. Considering the calculation speed, the method used in this study is the original method.

3.2.5.4 Hydrological events identification method

JdB and SC have difference on their catchment (metal roof vs. alphas pavement), substrate and drainage condition. This results in significant differences in the rainfall intensity to start generating runoff, event duration, and drainage duration. Thus, their methods for identifying hydrological events vary from each other.

3.2.5.4.i Drainage flow based method (JdB)

JdB has reliable drainage flow measurement, hence the hydrological event can be ended based on drainage flow data (similarly to the work from Ramier (2005)). However, as expected, the silt loam substrate makes the drainage flow occur not instantly after the inflow (with a time lag). This lag can cause that the drainage from the previous event beginning after the start of inflow from the current event, or sometime the drainage does not happen at all. Moreover, in autumn 2023, outlet clogging was observed on JdB2, which caused long and endless low drainage flow. To address those issues, additional end conditions were applied.

Before starting the condition judgement, rainfall intensity is all converted to mm/h; flowrate is converted to L/min; flow volume is converted to mm/h (volume divided by the sum area of cell and roof).

Conditional judgement is conducted in a loop judgement based on a fixed rolling window. For the starting condition for the system to receive runoff, it is defined as when rainfall intensity is > 0.2 mm/h (equivalent to 1 tip in the rain gauge within 1 hour), based on the assumption that the sloped metal roof does not have much water losses.

For the ending condition (as shown in Table 3-6), it is either based on drainage flow or runoff (for small events which do not generate drainage flow). The size of the rolling windows (window size for end condition 1; 180 min) is greater than both the maximum time between start of event and start of runoff, and the maximum time between end of rainfall and beginning of outflow. The window size for end condition

2 (20 min) is considered to be longer than the travel time from the metal roof to inlet flowmeters. The rule 3 in drainage-based end conditions is set to separate the endless low drainage flow period in the autumn 2023.

For each window check, judgement rule is applied. Note that the runoff-based end will be considered as hydrological event end only when the drainage-based end condition judgement is not met.

Table 3-6: Condition judgement for hydrological event ending in JdB

End condition	Window size		Rule (in the window)	Meaning	Judgement rule
1. Drainage-based end conditions	360 min	1	max rain intensity <= 0.2mm/h	no rainfall	1 and (2 or 3)
		2	drainage volume <= 1% * total cumulative drain since the start	no outflow	
		3	max drainage flow rate < 2 * the initial drain flowrate from the start	no outflow	
2. Runoff-based End Conditions	20 min	4	max rain intensity <= 0.2mm/h	no rainfall	4 and 5
		5	runoff volume in window < 1%* total cumulative runoff volume	no runoff	

3.2.5.4.ii Soil moisture based method (SC)

Different than JdB cells which have reliable drainage measurements, SC does not have usable drainage flow measurements due to the groundwater intrusion. Thus, the method for SC is to identify the end of an event by observing the change of soil water content: use average water content changes over specific depths (7.5 cm, 17.5 cm, 27.5 cm, 37.5 cm) to identify the movement that water no longer dripping (end of seepage flow).

Before starting the condition judgement, the data of SC is pre-processed as:

- Rainfall intensity is converted to mm/h, all flowrates are converted to L/min
- Calculating the average of water content measurement from SoilVUE50_4 (excludes the top and bottom probes of the, since their locations were at the soil-air interface or soil-sand interface before Oct-2022).
- Inflow noise is removed by the previous runoff distinguish method (in the previous section 3.2.5.2)
- A rolling window average was applied to water content to smooth the data, window size is 75 min (5 data points, which is enough according to the direct observation in the moisture dynamic).

- All the data are resampled to 15 min to match with maximum monitoring step (15 min for soil moisture sensor)

Step2: Condition judgement

Similar to JdB, conditional judgement in SC is conducted in a loop judgement based on a fixed rolling window. However, due to the fact that the asphalt pavement has more capacity to store water at the beginning of a rain event, the starting condition for SC to receive runoff is defined as when rainfall intensity is > 0.4 mm/h (equivalent to 2 tips in the rain gauge within 1 hour).

Unlike JdB, SC conducts the first end condition judgement to only identify the runoff event and thus remove the noise in the inlet flowmeter (as introduced earlier in the flowmeter noise remove for SC). After that, the inflow data without noise are used to identify the hydrological event with seepage-based end condition (as shown in Table 3-7). For seepage-based end condition, the window is defined as 60 min, it is shorter since it is based the higher conductivity substrate media in SC. Within each window, condition 4 checks the flat slope which is supposed to be drying period. However, sometimes long wetted periods (where seepage can occur) can be associated with seepage interruptions since the moisture remain stable in high moisture. Hence, condition 5 is added to avoid this situation. If both conditions 4 and 5 are met, then the hydrological event is considered complete. In this step, the 0.001 $m^3/m^3/h$ slope of "flat" soil moisture variation and the 0.3 m^3/m^3 were all based on direct observation at the moisture time series.

Table 3-7: Condition judgement for hydrological event ending in SC

End condition	Window size		Rule (in the window)	Meaning	Judgement rule
1. Runoff-based End Conditions	20 min	1	max rain intensity <= 0.2 mm/h	no rainfall	1 and (2 or 3)
		2	runoff volume in window < frac * total cumulative runoff volume	no runoff	
		3	max runoff flowrate < 3 * highest monthly noise	no noise	
2. Seepage-based End Conditions	60 min	4	the regression slope of media moisture change < 0.001 $m^3/m^3/h$	no longer dripping	4 and 5
		5	average media moisture < 0.3 m^3/m^3	low soil moisture	

After this condition judgement, some "tiny" events (the duration is < 150 min, and the soil moisture change cannot be found by direct observation) are identified. These "tiny" events do not affect water content (and thus, they end after inflow stops),

therefore were removed for event-based analysis, but still kept for long-term cumulative water balance.

3.2.5.4.iii Parameter choosing and uncertainty evaluation for the two methods

The parameters choosing for this hydrological event identification is indeed heavily based on direct observations of the timeseries (inflow, outflow or media moisture). This is partly due to the fact that smaller intervals between events can lead to the problem that direct counting of identified events often hidden the issue from individual identified events, while manually check on the timeseries works better. Another reason is that based on a finite number of attempts, the start and end of the event is not sensitive to many parameters, but more important is the combination between the end conditions.

However, a simple sensitivity analysis was conducted for SC, which assesses the additional volume gained by extending the ending time of identified events by 0.5h, 1h, 2h, 3h (as shown in Figure 3-26). Since some events are close to each other, the extended ends caused some high outliers.

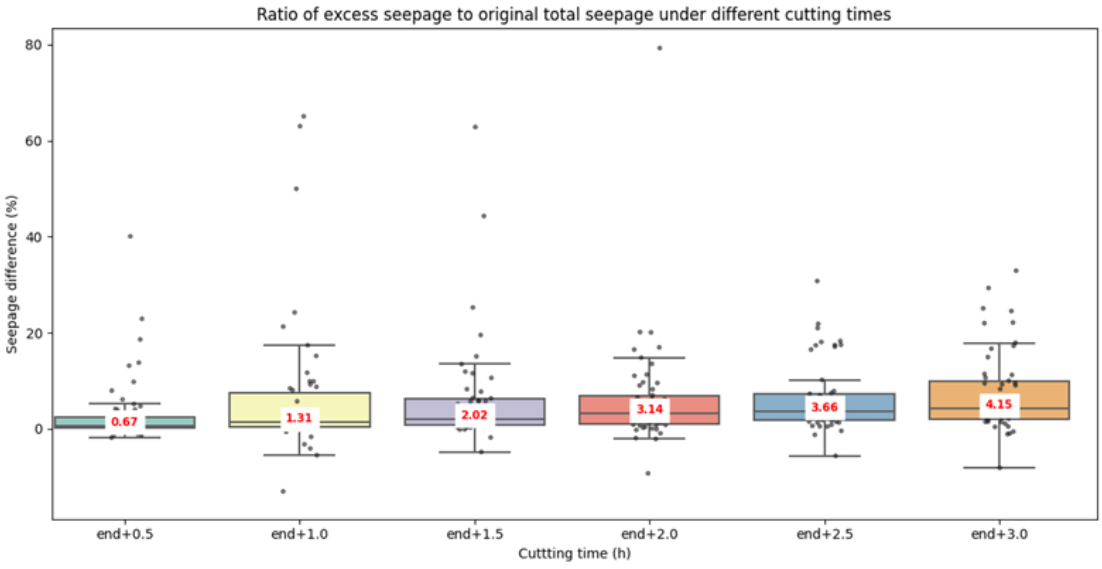

Figure 3-26: Gained seepage volume of different extended event end compared to the current event end

According to this sensitivity analysis, the current end time leads to a loss of less than 5% of the seepage volume when compared to an end time extended by 3 hours. Considering the potential impact of overlapping events and ET when extending the end time, the end time in this method is kept as previously defined.

3.2.5.5 Other preprocessing on data

The inflow measurement systems in JdB were subject to occasional sensor failure and clogging issues due to fallen leaves. A specific procedure was therefore applied to the inflow data to validate the measurements and rebuild when appropriate the runoff-rates from rainfall measurements and catchment area estimation. For SC, the inflow flowmeters have continuously noise, a method with rolling window judgement was thus developed to determine the start and end of runoff (inflow), and inflow was put to zero outside of these periods. In addition, due to the high gravel water level in JdB2 during 2023, part of the soil moisture sensors was submerged by the gravel water table, which causes potential uncertainty in the soil water storage estimation. Hence, two different methods for estimating soil water storage from multiple soil sensors or from both soil moisture and gravel water level were applied and compared. The hydrological event identification, inflow issue characteristic, noise removal and soil storage estimation can be found in 3.2.5.

Based on the pre-processed data, hydrological events are defined and distinguished as follows: the event starts with rainfall and ends when substrate seepage (for SC) or drainage (for JdB) stop (for event without drainage, the event stops if the drainage flow does not occur after 360 min). For JdB, 37 (JdB1) and 39 (JdB2) events are identified during P1, 21 (JdB1) and 19 (JdB2) events during P2; for SC, 195 events are identified for the whole study period (the detail on the method used to distinguish hydrological events can be found in 3.2.5).

3.2.6 PET Calculation

PET represents the evapotranspiration capacity of a field with no limitation on available water, it can be a reference for ET. To calculate PET, a commonly used mathematical method is the Penman-Monteith equation (PM) developed by Penman (Penman, 1948) and Monteith. Later the Food and Agriculture Organization of the United Nations (FAO) adapted PM to a derivative FAO56 Penman-Monteith equation (FAO56-PM) for easier calculation with simplified constants and standardized terms at a daily time step (Allen et al., 1998). Note that in FAO56-PM, the simplified constants are chosen by using a reference grass cover with a crop height of 0.12 m and a surface resistance of 70 s/m and an albedo of 0.23. The equation of FAO56-PM is displayed as follow.

$$ET = \frac{0.408\Delta(R_n - G) + \gamma \frac{900}{T + 273}(e_s - e_a)\mu_2}{\Delta + \gamma(1 + 0.34\mu_2)}$$ Eq. 3-11

Where:

- R_n is the net radiation [MJ/m^2/day]
- G is the soil heat flux [MJ/m^2/day]
- $e_s - e_a$ represents the vapour pressure deficit of the air [kPa]
- Δ is the slope of the saturation vapour pressure temperature relationship [kPa/°C]
- γ is the psychrometric constant [kPa/°C]
- μ_2 is wind speed at 2m height [m/s]
- T is air temperature at 2m height [°C]

The FAO56-PM requires daily resolution input data. At daily scale, the soil heat flux G can be approximated to 0. The $e_s - e_a$ vapour pressure deficit can be calculated from daily maximum and minimum air temperature and daily maximum and minimum relative humidity through the Eq.11, 12, 17 in FAO56 report (Allen et al., 1998).

For JdB, the *in-situ* R_n are provided by the radiation sensor (NR01) within each cell, and another R_n is provided by an *in-situ* meteorological station (Campbell Scientific CS100). Considering the data availability in SC, R_n is not always available by directly calculated from the longwave and shortwave radiation sensors (as Eq. 3-12). Therefore, R_n is estimated from R_s (measured by ClimaVUE50) using equation (Eq. 3-13 and Eq. 3-14), with a default albedo parameter α (0.23).

$$R_n = R_{ns} - R_{nl}$$ Eq. 3-12

$$R_{ns} = (1 - \alpha)R_s$$ Eq. 3-13

$$R_{nl} = \sigma \left[\frac{{T_{max,K}}^4 + {T_{min,K}}^4}{2}\right](0.34 - 0.14\sqrt{e_a})\left(1.35\frac{R_s}{R_{so}} - 0.35\right)$$ Eq. 3-14

Where:

- R_{ns} is the net shortwave radiation
- R_{nl} is the net outgoing longwave radiation
- α is the surface albedo, representing the fraction of solar radiation that is reflected

- R_s is the incoming global radiation
- σ is the Stefan-Boltzmann constant
- $T_{max,K}$ and $T_{min,K}$ is the maximum and minimum absolute temperature during the 24-hour period [K = °C + 273.16]
- e_a is the actual vapour pressure
- R_{so} is the calculated clear-sky radiation

Chapter 4: Experimental Evaluation of Bioretention Performance

4.1 HYDROLGICAL ANALYSIS

The methodology for data analysis is overall the same for the 3 study cases, and involves the following steps: 1) long-term cumulative water balance, 2) event-based hydrological performance, 3) dry period analysis (mainly focusing on ET) and 4) evaluation of vegetation development. Meanwhile, due to the difference in the system design and monitoring variables, the processing methods can sometimes vary between JdB and SC. The following content presents the detailed processing methods, the definition of wet/dry events and the considered performance indicators.

4.1.1 Water Balance Equation

In this study, the long-term water balance is calculated by Eq.1 (JdB) and Eq.2 (SC):

$$\sum_{i=0}^{n}(Q_{\text{in}}(t_i)+P(t_i)\cdot A)\cdot\Delta t=\sum_{i=0}^{n}(Q_{\text{out}}(t_i)+PET(t_i)\cdot A)\cdot\Delta t+\left(V_{\text{soil}}(t_n)-V_{\text{soil}}(t_0)\right)+\left(V_{\text{gravel}}(t_n)-V_{\text{gravel}}(t_0)\right)+\Delta V_{closure} \quad \text{Eq. 4-1}$$

Where:

- Q_{in} = the total inflow volume through the flowmeter (L)
- A = Surface area of the bioretention (m2)
- P = direct rainfall onto the bioretention surface (mm)
- Δt = the measurement time step, can be resampled from 1 minute to 1day
- Q_{out} = the total outflow volume (underdrain and overflow) measured by the tipping bucket flowmeter(L)
- V_{soil} = the soil water storage volume (estimated by the soil moisture sensors)
- PET = Potential ET (mm) calculated by PM-FAO56

- V_{gravel} =the gravel water storage volume (estimated by gravel porosity and water level measurement)
- $V_{closure}$ = the closure of the water balance. For JdB, it represents the water balance errors (i.e., sensor uncertainty, extrapolation errors and difference between PET and ET); For SC, it additionally represents the exchange volume between the bottom of bioretention cell and the underlying soil (i.e., exfiltration and intrusion)

Ro address the gaps (removed events or missing data) in observation periods, the following approach is adopted: Eq. 5-7 is applied for each continuous valid period, and for the cumulative values obtained at the end of each period valid are used at the beginning of the subsequent valid period. The invalid periods are presented as gaps in the cumulative curves. The two periods for JdB are considered as two consecutive cumulative periods. For event-scale analysis, t_0 and t_n are considered as the start and end for each event, with neglecting $ET(t_i) \cdot A$.

4.1.2 Reservoir Model for Exfiltration and Overflow Data Reconstruction and Scenario Analysis on SC

4.1.2.1 General principle

The data showed evidence of groundwater intrusion at the bottom of the SC garden during the wet season, with i) continuous underdrain flow even long time after rain events and ii) abnormally high water level in the inspection well at the inlet of the system. The situation presumably originates from the specific conditions of the underlying soil in Sense City, which may be described as a Technosol (a soil modified by human activities and containing a large number of artefacts; IUSS WG, 2014). The site is not only clayey but was used in the past as a parking lot and thus underwent compaction. Some slabs were also found at 1.5m depth and removed during the construction of the bioretention cell. Similar low permeability layers may still exist in the surrounding area, potentially leading to a temporary perched aquifer.

Since the underground water is entering the system and leaving via the underdrain, the drainage flow and water level measurement in the bottom gravel are no longer representative of bioretention inputs during these intrusion periods. Therefore, in this study, a three-part reservoir model (Figure 4-1) was developed, based on the reliable measures in no-intrusion periods. It allows reconstructing

drainage flow and gravel storage during intrusion periods as they should be without groundwater intrusion. It also allows for the calculation of overflow collected via the underdrain (which, even without groundwater intrusion, cannot be adequately measured by the outflow tipping bucket).

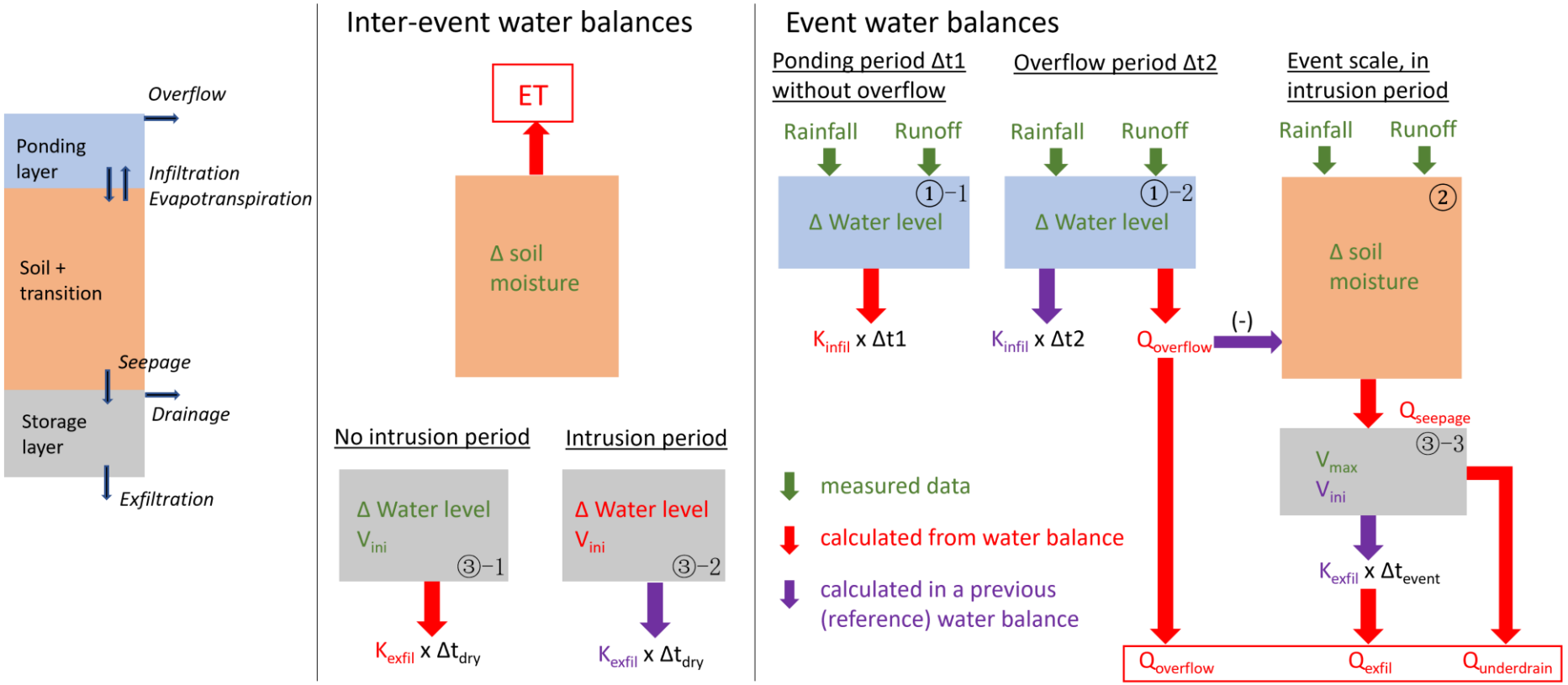

Figure 4-1: Schematic of the three-part reservoir model

As shown in Figure 4-1, the model consists of a simple 3-component reservoir model: surface ponding model (for overflow), substrate+transition layer model (for seepage), bottom storage model (for drainage and exfiltration). Since the intrusion water cannot reach up to the transition layer (it is discharged by the underdrain in the middle of gravel layer), the measurements of surface ponding level, total incoming water, soil moisture profile are still reliable, as well as bottom gravel water level during long dry periods.

4.1.2.2 Computation process – surface ponding overflow model

To assess overflow volumes, a surface reservoir model (blue box in Figure 4-1 is built based on reliable inflow, precipitation and surface ponding depth measurements. The model considers overflow only when the surface ponding depth exceeds the overflow level, in which the water balance (Figure 4-1: ①-2) is given by:

$$Q_{runoff} + Q_{rain} = \widehat{K}_{infil} \times (T_{start} - T_{end}) + \hat{Q}_{overflow} \quad \text{Eq. 4-2}$$

Where Q_{runoff} and Q_{rain} are directly measured inflow volume and rain amount; $\widehat{K}_{infil}$ is estimated from the ponding level decrease after the overflow of each event (Figure 4-1: ①-1); T_{start} and T_{end} stand for the start and end time of an overflow event. Since they cannot be precisely identified from water depth measurements, a "dummy" start is introduced and the overflow volume $\hat{Q}_{overflow}$ is computed from:

$$\hat{Q}_{overflow} = Q_{runoff} + Q_{rain} - \widehat{K}_{infil} \times (T_{dummy\ start} - T_{end}) - \Delta(V_{real\ start} - V_{dummy\ start}) \quad \text{Eq. 4-3}$$

Where: $\Delta(V_{real\ start} - V_{dummy\ start})$ is the water storage (level) difference of the dummy start and real start.

4.1.2.3 Computation process – substrate & transition layer seepage model

The [substrate + transition reservoir] receives measured inflow and rain volumes, from which overflow volume calculated by the surface reservoir is subtracted. Using the soil water storage change $\Delta Q_{soil\ water}$ that was measured by soil moisture sensor, the seepage volume $\hat{Q}_{seepage}$ that leaves from the substrate and transition part (Figure 4-1: ②) can be calculated by the water balance equation:

$$\hat{Q}_{seepage} = Q_{runoff} + Q_{rain} - \hat{Q}_{overflow} - \Delta Q_{soil\ water} \quad \text{Eq. 4-4}$$

4.1.2.4 Computation process – bottom storage model

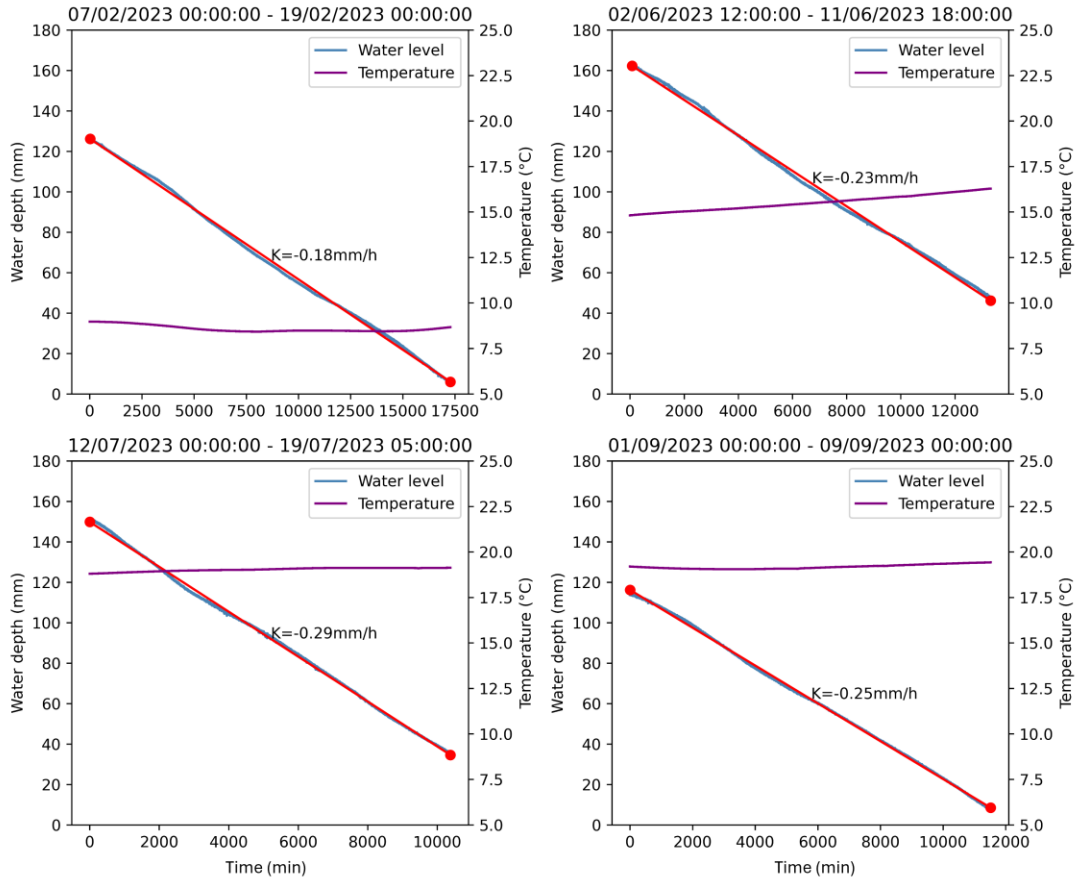

Figure 4-2: Kexfil calculation based on the four non-intrusion periods in 2023

Bottom exfiltration rates have been calculated for 4 dry periods without water intrusion, based on the decrease rate of the water level measured in the gravel storage layer. A porosity of 0.437 has been considered for this gravel layer. water level decrease rate is linear for all 4 periods, decrease rates are consistent between the 4 periods and range from 0.18 mm/h to 0.29 mm/h, with an average value of 0.2175 mm/h. Thus, during intrusion periods (Figure 4-1: ③-2), the average value of these four periods is used to estimate exfiltration. The water balance calculation for the bottom storage is separated in two steps: during the event and inter-event.

For water balance during the event (Figure 4-1: ③-3), the water storage at the end V_{end} can be calculated by closing the water balance of the seepage volume, initial water storage V_{ini} and the exfiltration loss during the event Q_{exfil_during} (calculated from K_{exfil}).

$$\hat{Q}_{seepage} + V_{ini} = Q_{exfil\_during} + V_{end} = Q_{exfil\_during} + Q_{underdrain} + V_{max} \quad \text{Eq. 4-5}$$

If V_{end} exceeds the maximum storage capacity V_{max} of the system (water level higher than the location of underdrain), the excess part is assigned to the volume of underdrain flow $Q_{underdrain}$; else the V_{end} remains the same.

Since $\widehat{K}_{exfil}$ is very low, Q_{exfil_during} in any case remain very low (and the impact of the asumption on the start of inflow is thus very limited). Thus. if V_{ini} is not 0, exfiltration is assumed to occur during the whole event. Otherwise, as the time of beginning of seepage is not known, exfiltration is assumed to start at the end of inflow.

For water balance in between two events (Figure 4-1: ③-2), it is necessary to check whether the V_{end} will be completely exfiltrated before the next event or not. As for Q_{exfil_during}, the amount of exfiltration in between events can be calculated from the dry period between two events (T_{dry}) and K_{exfil}. Hence the initial water storage of the next event can be calculated:

$$V_{ini,next} = \max\left(V_{end} - T_{dry} \times K_{exfil}, 0\right) \quad \text{Eq. 4-6}$$

4.1.2.5 Summary and scenario analysis

Based on the above computation processes, overflow, seepage flow and drainage can then be calculated for each hydrological event. For dry period, the exfiltration not the subsoil as well as the ET (calculated from $\Delta Q_{soil\ water}$). It is therefore possible to reconstruct the behaviour of the system as if groundwater intrusion had not occurred. The model also allows different scenarios analysis on different gravel storage layer thickness and different underlying subsoil permeability by simply modifying V_{max} and K_{exfil}.

4.1.3 Dry Period Analysis

Based on observed drainage dynamics, we defined the start of a dry period as at the midnight the day following the end of the previous hydrological event for SC or the midnight of the next day of the end of previous hydrological event for JdB. Rainfalls are here considered as periods with daily rain depth ≥ 0.2 mm. Note that for SC bioretention, the analysis is conducted over the period during which seepage is assumed to be negligible (in between two hydrological events), and the water balance is limited to the substrate and transition layers. All the dry periods which contain human impact (e.g., injection tests, sensor installation, soil sampling) were removed from the analysis.

The daily and the total ET over each dry period is estimated based on the water balance equations Eq. 4-7 (JdB) and Eq. 4-8 (SC). Because drainage often extends long after the end of rainfall for JdB (especially on JdB2), it is necessary to consider the underdrain flow volume and gravel water storage change for ET calculation in Eq. 4-7.

$$\sum_{i=0}^{n}(ET(t_i)\cdot A)\cdot \Delta t = -\left(V_{\text{soil}}(t_n) - V_{\text{soil}}(t_0)\right) - \left(V_{\text{gravel}}(t_n) - V_{\text{gravel}}(t_0)\right) \pm \Delta error \quad \text{Eq. 4-7}$$

$$\sum_{i=0}^{n}(ET(t_i)\cdot A)\cdot \Delta t = -\left(V_{\text{soil}}(t_n) - V_{\text{soil}}(t_0)\right) \pm \Delta error \quad \text{Eq. 4-8}$$

Where:

- A = Surface area of the bioretention (m^2)
- Δt = the measurement time step, can be resampled from 1 minute to 1day
- V_{soil} = the soil water storage volume (estimated by the soil moisture sensors) [L]
- ET = ET estimated from this equation (mm)
- V_{gravel} = the gravel water storage volume (estimated by gravel porosity and water level measurement) [L]
- $\Delta error$ = the measurement uncertainty error [L]

Based on this definition, 72 dry periods could be identified for SC, 45 out of them are longer than 2 days, with a maximum duration of 16 days. 29 dry periods were defined for JdB over the two observation periods, 21 out of them are longer than 2 days, with a maximum duration of 28 days. More detailed information on the characteristics of these periods (duration, soil moisture, etc.) is shown in the Appendix 5 – Tables of Dry Periods Statistics).

For each dry period, daily and average ET (estimated from water balance Eq.3 and Eq.4) are compared to PET, along with a reference indicator of soil moisture at different depth of substrate.

4.1.4 Performance Indicators

Different hydrologic performance indicators were used during the result analysis, e.g., average volume reduction ratio of all the events ($\overline{\mathrm{VRR}_{\mathrm{Event}}}$), total volume reduction ratio in long-term scale (VRR_{Total}), ratio of events that are completely retained in the system (R_{100}), ratio of event with >80% VRR (R_{80}), peak flow reduction ratio (*PFR*) and total exfiltration ratio in the water balance (*Exfil*). During the calculation, all the volume was converted from L to mm by dividing the cell surface area. These performance indicators help to provide an understanding of how a bioretention affect the water balance and local flow regime. Definitions of the selected hydrological performance indicators are listed as follow:

- $VRR[\%] = 1 - \frac{V_{out}}{V_{in}}$, V_{out}: outflow volume (mm) of an event, V_{in}: incoming water (mm) of an event.
- $VRR_{Total}[\%] = 1 - \frac{\sum V_{out}}{\sum V_{in}}$, $\sum V_{out}$: total outflow volume (mm), $\sum V_{in}$: total incoming water (mm).
- $\overline{VRR_{Event}}[\%] = \frac{\sum_{i=1}^{N}(1-\frac{V_{out_i}}{V_{in_i}})}{N}$, N: the total number of events.
- $R_{100}[\%] = \frac{N_{100}}{N}$, N_{100}: number of events with zero outflow (or 100% VRR).
- $R_{80}[\%] = \frac{N_{80}}{N}$, N_{80}: number of events with VRR > 80%.
- $PFR[\%] = 1 - \frac{Max(Q_{out})}{Max(Q_{in})}$, Q_{out}: Outflow rate (mm/min); Q_{in}: incoming water (rainfall and runoff) flow rate (mm/min).
- Exfil [%] = $\frac{V_{recharge}}{V_{in}}$; $V_{recharge}$ is the volume of exfiltration (mm) which enters the subsoil.

4.2 RESULTS

4.2.1 Hydrological Functioning Analysis

4.2.1.1 Long-term water balance

4.2.1.1.i JdB cumulative water balance

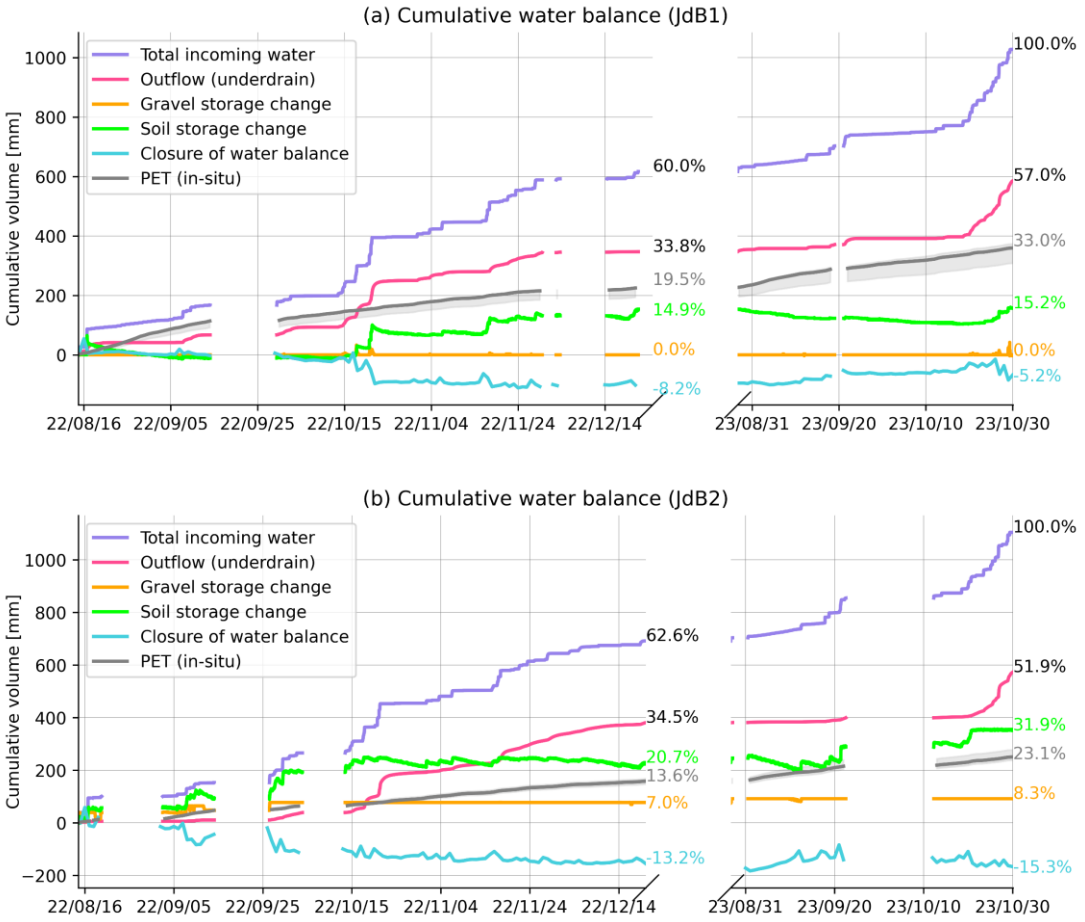

Figure 4-3: Cumulative water balance for JdB1 & JdB2. Unit: mm (per m² of bioretention area)

The long-term water balance for JdB bioretention cells is presented in Figure 4-3. Each subplot has two parts corresponding to the two monitoring periods (period 1 in 2022 and period 2 in 2023). JdB1 has more gaps in 2022, while JdB2 has a larger gap in 2023. The numbers displayed for the different curves at the end of each period indicate the contribution of each water balance term to the total cumulative incoming volume over the two periods. The PET curve with uncertainty interval indicates the variation between the 3 *in-situ* solar radiation sensors (as mentioned in 3.2.2), and the grey line represents the PET calculated from the sensors within the mentioned cell. Due to the gaps in the data, the long-term water balance of the two cells does not exactly cover the same events, and the values of the different terms are hence not directly comparable. The soil and gravel storage change in Figure 4-3 represent the

volume difference from the initial storage conditions. The closure of the water balance (calculated using Eq. 5-7) can be interpreted as an error term encompassing unaccounted processes (e.g., storage at the surface and in the vegetation), differences between actual ET and PET, and measurement uncertainties.

For JdB2, the IWS layer rapidly filled up at the beginning of the monitoring period after several events in 2022 August and remained at maximum storage (about 171 mm) after that. After this initial filling period, saturation level (as given from the pressure sensor) generally exceeds the designed IWS thickness (outlet level), indicating that saturation extends to the soil substrate (a situation confirmed by field sampling in May 2023). The occurrence of this saturation level within the soil media, above the drainage outlet and during periods with no or negligible outflow, could indicate a clogging of the orifice or the presence another factor preventing water from draining as quickly as expected. One possibility is clogging of the geotextile layer just above the gravel. However, since the exact configuration of the outlet is not clearly known, it may also be that the outlet is positioned above the gravel layer (rather than within it), requiring water to move laterally to reach the outlet (when the vertical flow path has strong head losses due to the geotextile clogging), which would result in slower drainage.

Overall, under the current hydraulic loading ratio of 3.9, the two JdB bioretentions could abstract almost half of the incoming water (43.0% for JdB1, 48.1% for JdB2). JdB2 (with an IWS) shows slightly higher ability to abstract water compared to JdB1 (without IWS). From the Figure 4-3, this difference may however be due to the additional storage provided by the gravel layer (filling up at the beginning of the first period). However, the proportion of outflow over the first period is quite similar between the two cells and most of the difference appears to occur for the second period (when the gravel storage barely changes).

The closure term (blue curves in Figure 4-3) is not negligible in the long-term water balance. It covers the uncertainty from the direct measurement, uncertainty from different data processing (e.g., the method to estimate soil storage, or reconstruct inflow) and also the difference between Actual ET and PET. The long-term closure is very high, especially for JdB2 (-15.3%). However, several big “drops” indicate that the final negative closure are linked to a limited number of events showing inconsistencies between inflow, outflow, and soil storage. Excluding these events, the

water balance closure would not be as negative. When zooming into some specific dry periods, such as the beginning of second valid period (from 2023-08-31 to 2023-09-10), without the interference of inflow and outflow, the closure curve either remain stable (for JdB1), or increase (JdB2). This may indicate that during this dry period, the actual ET of JdB1 was close to its PET, and the actual ET of JdB2 was even higher than its PET.

4.2.1.1.ii SC cumulative water balance

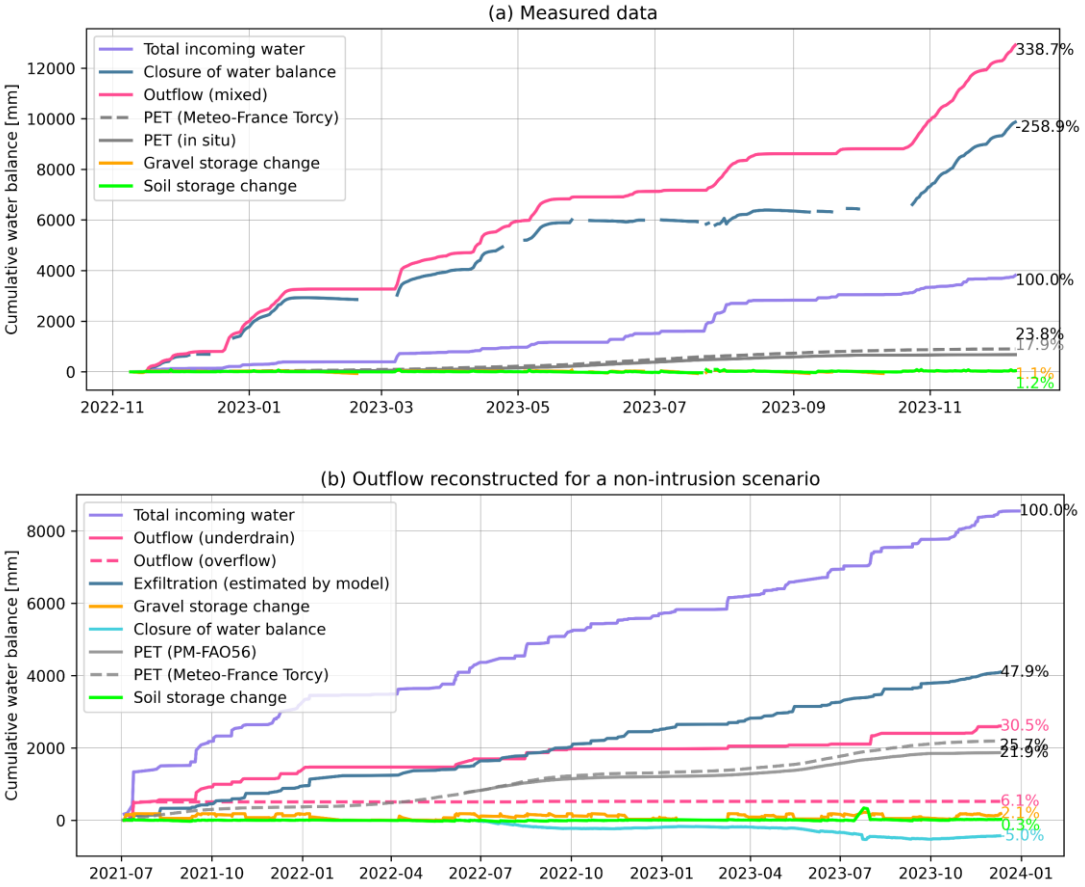

Figure 4-4: Cumulative water balance for SC bioretention (a: measured data; b: outflow reconstructed for a non-intrusion scenario); The negative closure of water balance(intrusion) is presented inversely in (a); the closure term in (b) is considered only start from 2022-06.

For SC bioretention, the long-term water balance is presented in two parts (as shown in Figure 4-4); the first one (Figure 4-4a) is from 2022/11/09 to 2023/12/10 (shaded period Figure 3-3), which has groundwater intrusion problem; the second one (Figure 4-4b) is the extended period 2021/01/21 – 2023/12/10, which has been reconstructed with the reservoir model to assess the functioning of the system without groundwater intrusion.

Figure 4-4a shows the original measurement from the monitoring system. Since the overflow pipe is connected to the underdrain, the outflow measurement encompasses both drainage and overflow (which only occurred 3 times during this period according to the surface water level sensor). During this period, the outflow is threefold the incoming water volume. Overall, the intrusion was observed at various moments of the year, suggesting it could occur at any period. It happened more often in the winter period (November to February) due to the continuous rainfall but also occurred after some large events in March and May. The summer period showed less intrusion, possibly due to a lower level of the (presumed) perched lens.

For the extended period (Figure 4-4b), the model assumes the bottom underlying soil allows the bioretention to exfiltrate at a rate of 0.22 mm/h (estimated based on the gravel water level drawdown rate during the non-intrusion periods) if there is water in the bottom gravel storage. According to the reconstructed water balance, the SC bioretention can theoretically exfiltrate 48.1% of total incoming water over the studied period even though the underground soil has a very low permeability. The exfiltration process is rather constant throughout the year and only interrupts during the few long dry periods. Outflow represents 36.6 % of incoming water and mainly occurs as underdrain flow (30.5 % vs 6.1% for overflow). The PET calculated with *in-situ* data is lower than the reference PET from the Météo France meteorological station situated at Torcy (5 km away from the site) for their common period (2022-06-16 to 2023-12-10). The possible explanation could be the lower wind speed (at 3 m) measured at the *in-situ* meteorological station as well as higher humidity, compared to the Météo-France stations; 2) shadow effect of surround buildings can limit the global solar radiation measurement of the *in-situ* sensor.

It is notable that, since the uncertainty from measurement and data preprocessing is included in the reservoir model calculation, the closure term in Figure 4-4b only represents the difference between PET and actual ET. By selecting only for the period where *in-situ* PET is available, the closure reaches up to 5%. This indicates that the actual ET in the cell is slightly lower than PET, which may be explained by: 1) the sunken design of SC cell reduces dissipation of humidity; 2) shadow from the walls near SC cell is very likely to reduce real ET. However, another possible explanation is the uncovered uncertainty from monitoring and data processing. Further details on ET

are discussed in the dry period performance analysis in the following dry period analysis.

4.2.1.2 Dry period analysis

Evapotranspiration estimated during dry periods lasting more than two days are shown in Figure 4-5 and Figure 4-7. For each period, 3 bars are used to represent the ET estimated by water balance, PET calculated from the *in-situ* sensor and PET from a reference meteorological station. For JdB, the reference meteorological station is right next to cells, while for SC the reference station is Torcy weather station (around 5 km away). The "variability" bar on top of each column indicates the variation of daily ET over the corresponding dry period (the unrealistic ETs, such as <0 mm/d or > 10 mm/d were excluded during the data processing). The daily average of soil moisture is also presented as dots following the right y axis.

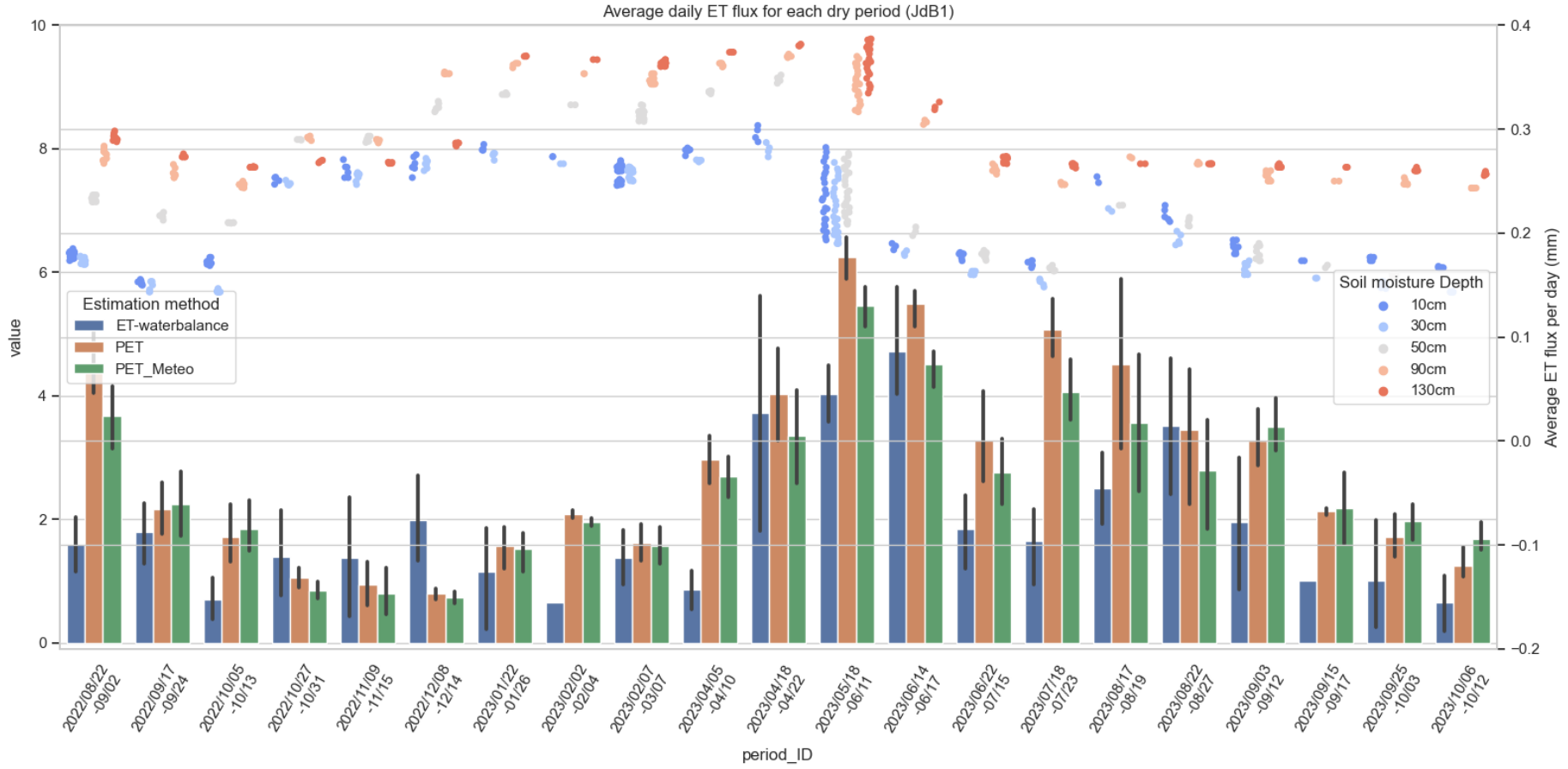

Figure 4-5: Estimated ET and PET during dry period for JdB1 bioretentions (average daily flux per each dry period)

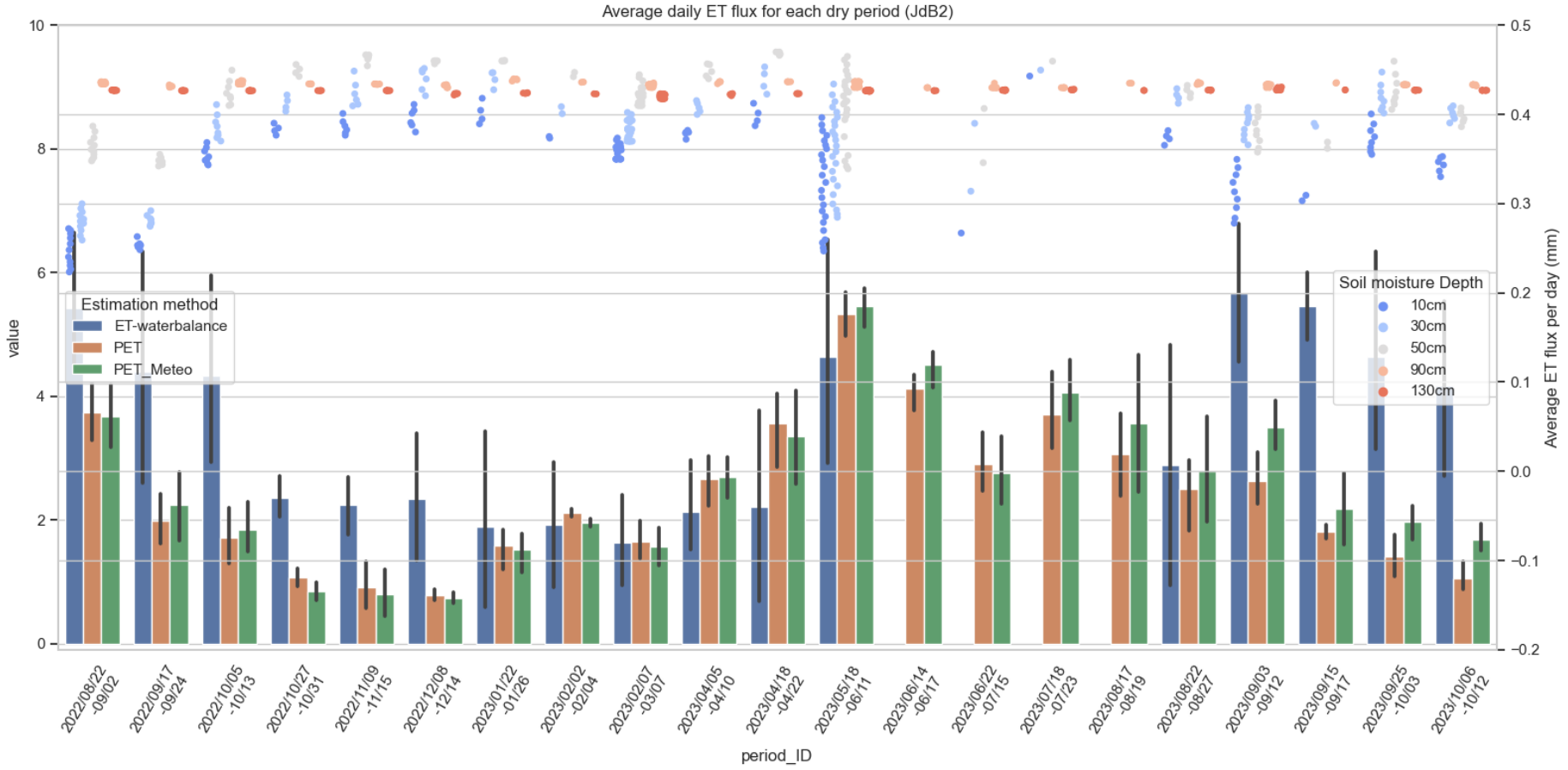

Figure 4-6: Estimated ET and PET during dry period for JdB2 bioretentions (average daily flux per each dry period)

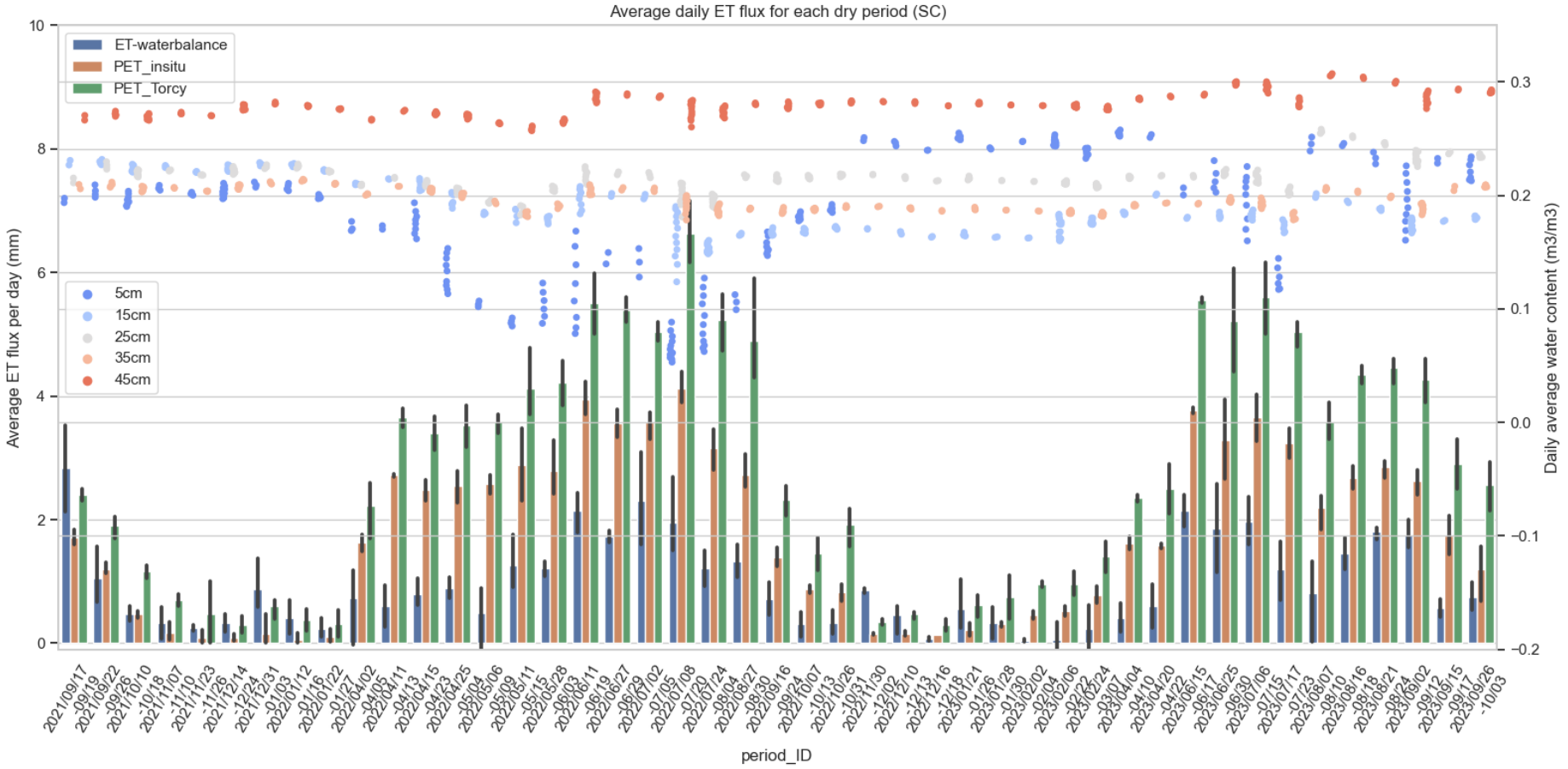

Figure 4-7: Estimated ET and PET during dry period for SC bioretentions (average daily flux per each dry period)

The uncertainty and possible errors in the estimation of ET need to be noted. For JdB2, several periods are missing due to the failure in the monitoring system. Several periods in September 2023 also show very high ET values, sometimes largely exceeding local PET values. While these high ETs may originate from uncertainties in water balance calculations, a noticeable source of water balance uncertainty is the inability to completely capture soil water storage variation with a limited number of sensors, especially when there are localised high moisture zone. In SC, the calibration of soil moisture sensors indicates the direct measured moisture can be overestimated (see 3.2.4), therefore the ET estimated by soil moisture change is probably slightly overestimated. However, even though the absolute value of soil moisture measurements has high uncertainty, their continuous variation still captures the dynamics of soil moisture changes at the different depths.

Overall, JdB2 has the highest ET over the three cells. It has more periods where ET is higher than PET. For SC and JdB1, the ET is overall lower than PET (except a few winter periods, as shown in Figure 4-5 and Figure 4-7). This situation is consistent with the high water content in JdB2, which results from the direct contact between the IWS and the substrate layer. In contrast, the IWS in SC is located well below the transition layer, and JdB1 does not have an IWS. In addition, this situation can also be due to the *in-situ* radiation sensor in JdB1 providing higher value compared to the sensor in JdB2 (possibly due to the reflection from the metal roof catchment), which leads to a relatively higher PET value in JdB1. However, this should also impact the ET as well. For SC, these deviations between estimated ET and *in-situ* PET may be due to the system being set below the ground surface, with vertical sides that likely limit incoming light and air circulation.

For JdB1 and SC, some periods with low ET/PET ratios are observed during the growing season (April to October). These periods also coincide with lower topsoil water content. Therefore, it is a reasonable guess that the vegetations during these periods were experiencing water stress. During the growing period (when the vegetation was well covering the system), the ET/PET periods show up with the decreasing of soil moisture. For JdB1, the three consecutive dry periods between 2023-06-14 and 2023-07-18, suggest that dry surface conditions are not necessarily associated with water stress, which rather coincides/shows up with the decrease of soil moisture content below 50 cm. Depending on the period of the year, stress ET

limitation will occur under different soil moisture condition due to the specific dynamic of deeper root species. In this case, those behaviours may be caused by the different action patterns of deeper-rooted plant (i.e., tree) and shallow roots plants (shrubs and ground-covering plants). In the case of SC, the ratio of ET/PET, seems to more closely follow the decrease of surface water content, despite the presence of herbaceous plants with roots extending beyond 20 cm, this may be due to the limited uptake capacity of the surface fine root system. However, as mentioned earlier, there was no sign of water stress on the plants from the frequent visual inspection on SC. Therefore, the discussion that the SC was subjected to water stress remains doubtful, and it is more likely that the maximum ET if SC cell was limited (by the design). For JdB2, the water stress barely occurred. This is due to the presence of IWS which maintains high soil moisture, especially the deep soil (90 cm and 130 cm) is saturated all the time.

Considering only periods common to JdB1 and JdB2 (i.e. excluding periods with missing data in either of the two cells), the cumulative ET were 58 mm (JdB1) and 132 mm (JdB2), while for the observation period 2023 were 71 mm (JdB1) and 194 mm (JdB2). The ET difference between IWS cell and non-IWS cell are more than 128% (for 2022) and 172% (for 2023). In a weight-lysimeter study in the same region with same hydraulic loading ratio (Ouédraogo et al., 2022), ET for the bioretention cell with IWS was reported to be 87% higher than for the non-IWS cell in summer and 18% higher during the autumn. However, the substrate used in Ouédraogo's study is silt clay, which may have a higher water retention capacity and therefore help mitigate differences in ET caused the presence or absence of IWS. In another study from Hess et al. (2017), the IWS cell has 63% more ET than non-IWS cell with both sandy substrate. Compared to these weight-lysimeter studies, the difference on ET between JdB1 and JdB2 seems overly large, which may indicate the estimation of water balance in JdB1 and JdB2 is not entirely robust (especially for the soil water storage).

4.2.1.3 Event-scale performance

4.2.1.3.i Event-scale volume reduction ratio

Table 4-1: Statistic of event-scale volume reduction ratio (VRR) in JdB1, JdB2 and SC

ID	Total event numbers	VRR-Range [%]	VRR-Median [%]	Ratio of event with >80% VRR (R_{80}) [%]
JdB1	46	10 - 100	64	33
JdB2	48	3.3 - 100	91	58
SC	185	10 - 100	100	76

Table 4-1 shows the statistics of event-based VRR over the three cells. Based on the reconstruction using the reservoir model, with exfiltration taken into account, SC shows the best VRR, with a high median value of 100% (fully retained), and the largest ratio of events with more than 80% of VRR. Between the two cells in JdB, although JdB2 shows a higher median value, an extremely low VRR (3.3%) are also observed in this cell due to continuous wet weather in November 2023 that saturated the whole substrate and IWS of JdB2.

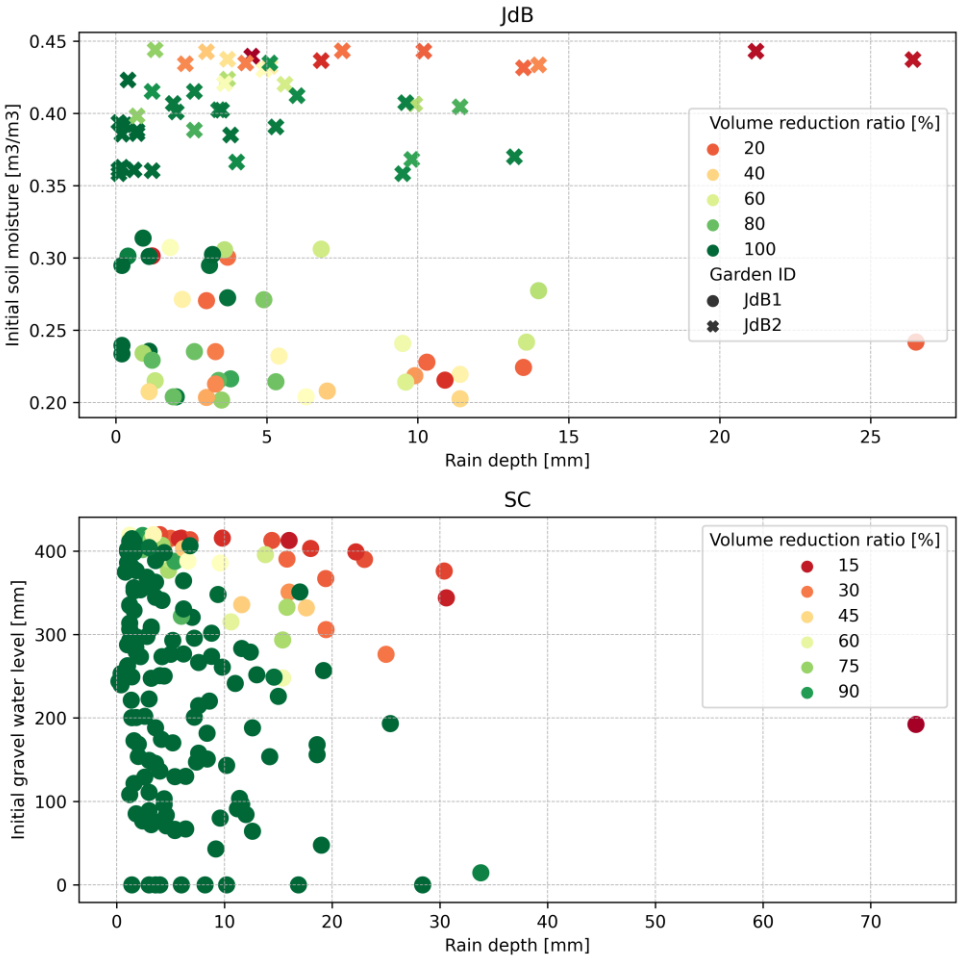

Figure 4-8: Event-scale volume reduction ratio related to different initial average soil moisture over the whole substrate layer (upper: JdB) and different bottom gravel water level (lower: SC)

Figure 4-8 shows how the event-based volume reduction from the different cells varies depending on rainfall depth and initial conditions (initial soil moisture content for JdB and initial water depth in the gravel layer for SC).

Expectably, higher rain depths lead to lower VRR for all three cells. Overall, JdB1 shows significantly lower initial water contents than JdB2. For JdB2 and SC, volume reduction efficiency tends to be higher under dry initial conditions (i.e., low soil water content or a low water level in the gravel layer), which are associated with higher storage capacity. Surprisingly, this is not the case for JdB1, where water content does not show a clear influence on volume reduction. This situation may result from the possible preferential flow caused by cracks, as identified along the wall close to the inflow through a tracer experiment in 2024-07 (conducted by E. Berthier, Cerema), although other locations might also be affected. Those cracks may have formed as a result of the shrinkage of the silty substrate s during the dry period. They allow the water to reach quickly and directly the underdrain flow with limited control from the substrate media (evidence of these preferential flow from sensor reactions and field photos can be found in Appendix 6 – Evidence of Preferential Flow and Substrate Crack in JdB). This interpretation in terms of preferential flow is also consistent with the generally lower volume reduction efficiency from JdB1 compared to JdB2 (although this lower volume reduction efficiency, may also be explained by the possible the clogging issue at the JdB2 outlet). In this case, higher initial water content can help achieve a more even distribution of water on and in the substrate. The presence of IWS (JdB2) can prevent this drying out of the soil, and hence avoid soil cracks to form and create preferential flows.

4.2.1.3.ii IWS impact on Peak flow reduction rate

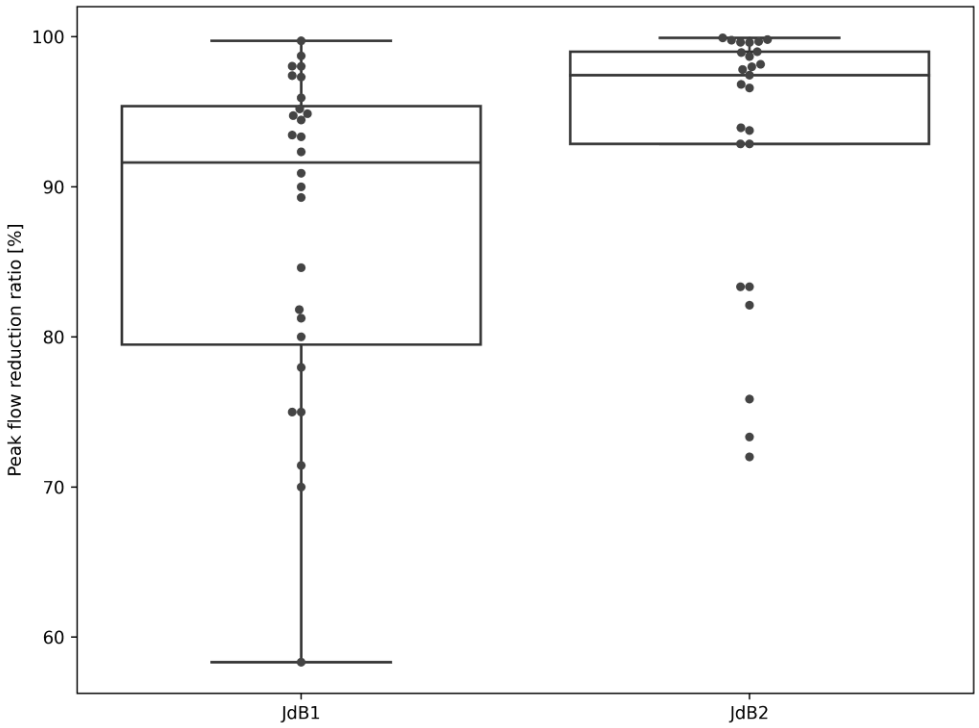

Figure 4-9: Boxplot on peak flow reduction ratio for JdB1 and JdB2

As shown in Figure 4-9, the distribution of peak flow reduction ratios for JdB1 and JdB2 shows difference in both their range and median. Both cells demonstrate a high median peak-flow reduction, exceeding 90%. Such high peak-flow reduction values are consistent with those reported by Lucke & Nichols (2015), for a similar system design (lined, 90 cm of substrate) with higher permeability substrate and loading ratio (sandy loam with loading ratio >8). In contrast, some events exhibit significantly lower peak-flow reduction, especially for JdB1. The low reduction ratio in JdB1 may be due to the preferential flow near the inlet, as described previously.

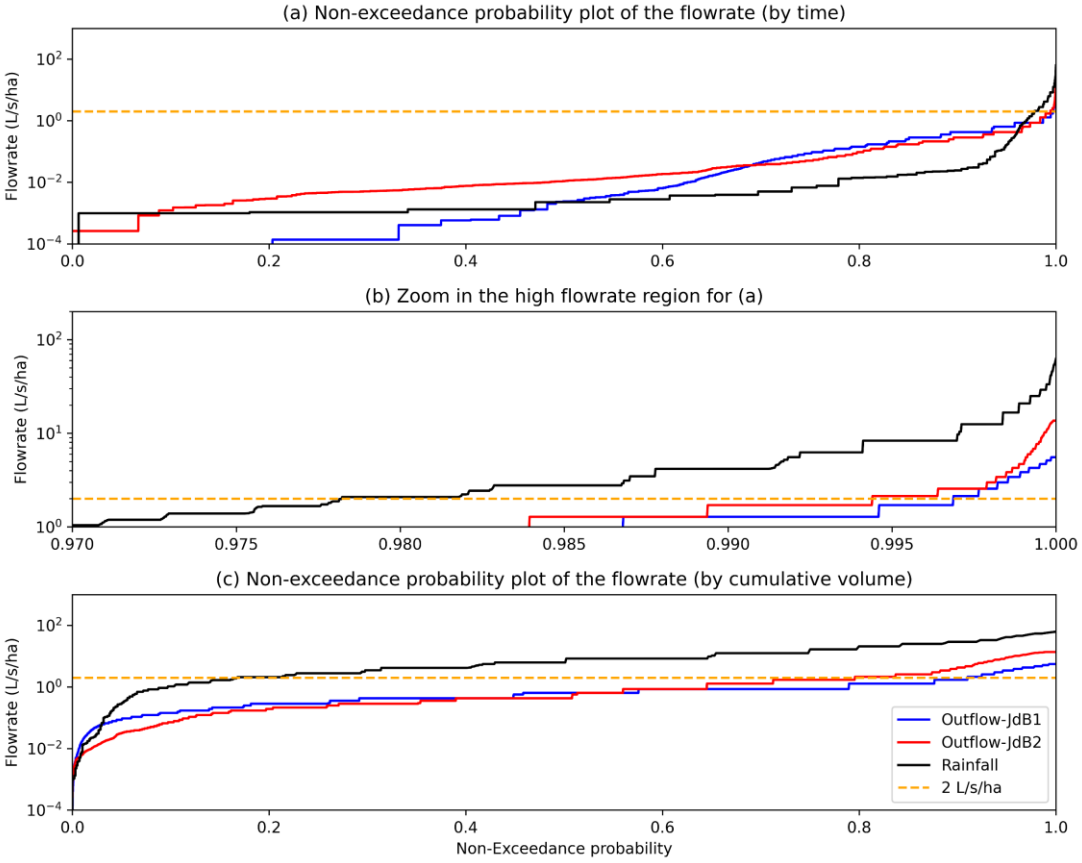

Figure 4-10: Non-exceedance probability of the total incoming flow (rainfall) and outflow from JdB1 and JdB2 (2-min time step); (a) time-based non-exceedance probability of the flowrate; (b) zoom in the high flowrate region for (a); (c) cumulative volume-based non-exceedance probability of the flowrate

Figure 4-10 presents the flow distribution of outflow of JdB1 and JdB2 compared to the pre-treatment flow (direct rainfall above the whole catchment) and a reference discharge rate of 2 L/s/ha which represents a lower range of French flow discharge regulations. In a time-based non-exceedance probability plot, the value at a given probability indicates the flowrate that is not exceeded for that proportion of time; in a volume-based non-exceedance probability plot, the value at a given probability indicates the flowrate below which that proportion of the total cumulative volume was conveyed.

As expected, infiltration trough the bioretention substrate media modifies the flow distribution curves: maximum flows are attenuated, and runoff volume is redistributed over longer periods of time. For instance, flow lower than 2 L/s/ha represents 20% of the incoming rainfall but 80% of JdB2 outflow and 90% of JdB1 outflow (according to Figure 4-10c).

Overall, the distribution curves for JdB1 and JdB2 are similar but small difference can be noted:

- JdB2 shows a longer tail of very low flow values then JdB1. This could be linked to some clogging effect (of geotextile or of the outlet), or to the drainage condition (with outlet higher than the bottom of substrate layer).
- However, from the distribution based cumulative volume (Figure 4-10c), the drainage volume associated with this long tail can be found to be very small (the approx. 40% of time steps with flow $<1e^{-2}$ L/s/ha represent less than 5% in cumulated volume)
- JdB2 shows higher flow than JdB2 for the upper 2% of flow values, with maximum flow rates reaching up to 14 L/s/ha compared to 6 L/s/ha for JdB1 (Figure 4-10a). Thus, from this graph quick flow through cracks cannot be identified. Note that the max value of 14L/s/ha in JdB2 is consistent with the soil hydraulic conductivity over the whole bioretention area (*median Ks 20 mm/h * cell surface 25.1 m² / whole catchment surface 97.6 m² =15 L/s/ha*), and might be reach when the JdB2 is completely saturated. Lower maximum flow values on JdB1 probably means that only a limited portion of the garden area contributes to infiltration and that the cracks only allow for a limited part of flow to directly access the outlet.

Compared to JdB1, the presence of an IWS in JdB2 ensures higher soil moisture content that prevents the formation of cracks. At the same time, higher water content limits the storage capacity of the substrate and is less favourable in terms of peak flow control, this can be evidenced from the several low peak-flow reduction events in JdB2. In addition, the outlet in JdB2 is a simple hole located in a corner at the top of gravel layer (covered by a gravel pit) instead of a long underdrain located at the bottom of gravel with an elbow towards the outlet. Hence, the design in JdB2 hence requires water to move vertically through a thin low permeability saturated substrate media situated below outlet level to reach the gravel drainage. Or when the geotextile separation gets clogged, the water to flow laterally trough the bottom of substrate. It may impede water evacuation or cause clogging, which can result in lower peak-flow (and thus higher peak flow reductions). While some clogging was already observed during maintenance in March 2024, the specific role of the lateral outflow setting on drainage dynamics could also be further investigated through modelling.

4.2.2 Vegetation Development in Bioretention Cells

According to the image classification of the top-view drone photos from 2021 to 2023, the vegetation in JdB shows clear differences between the two experimental cells JdB1 and JdB2 (Figure 135).

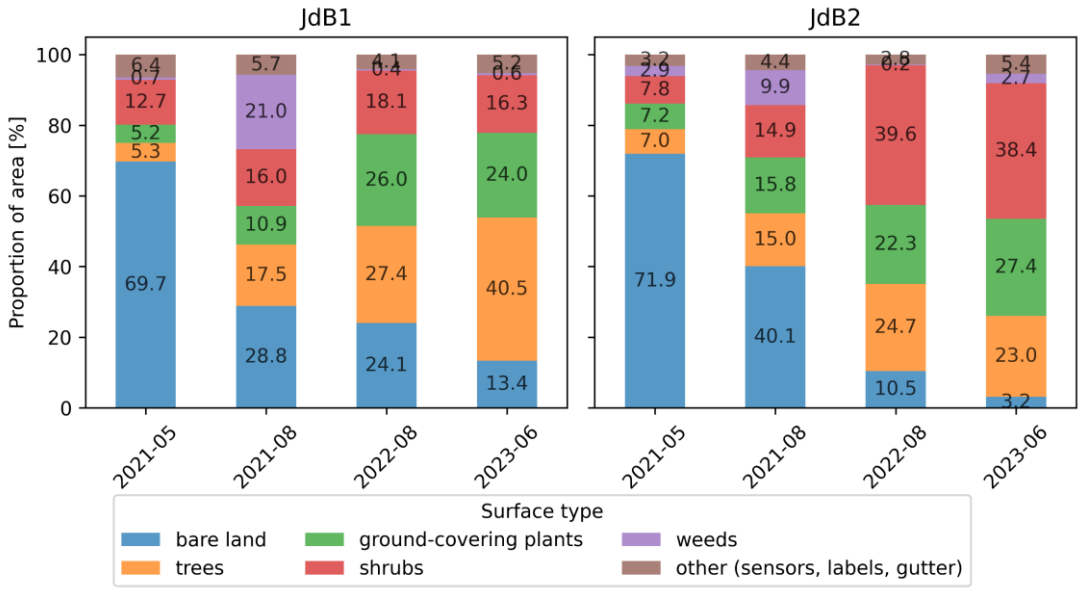

Figure 4-11: The surface coverage proportion for different vegetation types in JdB1 & JdB2

Figure 4-11 shows two subplots for JdB1 and JdB2, each subplot shows the variation of vegetation and uncovered surface from 4 different dates. The stacked column of May 2021 represents the initial situation (right after planting the vegetation), which was relatively similar between both cells with ~ 70% of bare soil. During the first growing season after planting (2021-05 to 2021-08), JdB1 and JdB2 already showed noteworthy development for all plants. From the long-term management perspective, JdB2 (with IWS) has higher vegetation coverage than JdB1.This difference was not seen for the first growing season, possibly because of the IWS was not filled during the first growing season. In addition, the dominant vegetation between JdB1 and JdB2 is different. While trees covered most of the projection area in JdB1 after 27 months of operation, shrubs became the dominant vegetation in JdB2. This difference was specifically seen in the competition between *Cornus sanguineum* (shrub) and *Carpinus betulus* (tree) (from visual inspection). Potential reason can be the water distribution over the soil depth as trees can reach out deeper soil while shrubs rely more on the middle and shallow soil water. The first hypothesis is thus that shrubs may suffer water shortage in JdB1. The second possibility is that water logging in JdB2 may limit the development of *Carpinus betulus* (trees). *Carpinus* can tolerate wet

heavy clay, but growth quite fast in wet but well-drained soils (Sikkema et al., 2016). This is proved also during the observation in 2024, a rainy year, persistent water logging conditions in JdB2 were clearly detrimental to most of species in JdB2 (except *Pyrus*), *Lonicera nitida* has practically disappeared.

For SC cell, the available photo records show the turnover of herbaceous plants during the past three years. Initial planting in Nov 2019 involved *Carex Oshimensis* 'Evergold' (along the edge), *Miscanthus Sinensis* (inner ring), *Carex grayi* (ring) and *Iris* (centre). No weeds control was applied until the beginning of 2022. In March 2022, three new herbaceous plants, i.e., *Lobelia fulgens* (in the centre), Rudbeckia (in the inner ring) and *Lychinis coronaria* (along the edge) were introduced into the garden, to complete vegetation coverage and replace some plants that had disappeared or did not thrive (especially *Carex Oshimensis* 'Evergold'). The *Carex Oshimensis* 'Evergold' progressively declined over the first two years of operation and finally disappeared after the winter of 2022/2023. From 2022 to 2023, the dominant specie in the summer period changed from *Carex grayi* to *Miscanthus Sinensis*, and the former did not grow back in 2023. The disappearance of *Carex grayi* might be due to the dry early spring in 2023, accentuated by the competitive pressure from the *Miscanthus Sinensis* with its extensive rhizomatous root system. It's worth noting that the *Miscanthus Sinensis* became the absolutely dominant species in SC cell since the summer 2023, its canopy covers most of other plants (as shown in Figure 7-4, Appendix 7). with its height (as shown in Figure 4-12) and density of foliage, it takes up the entire surface area from the top-view. Another hypothesis could be that the well-developed and dense coverage of *Miscanthus sinensis* limited the sunlight of *Carex grayi*, which has a higher demand.

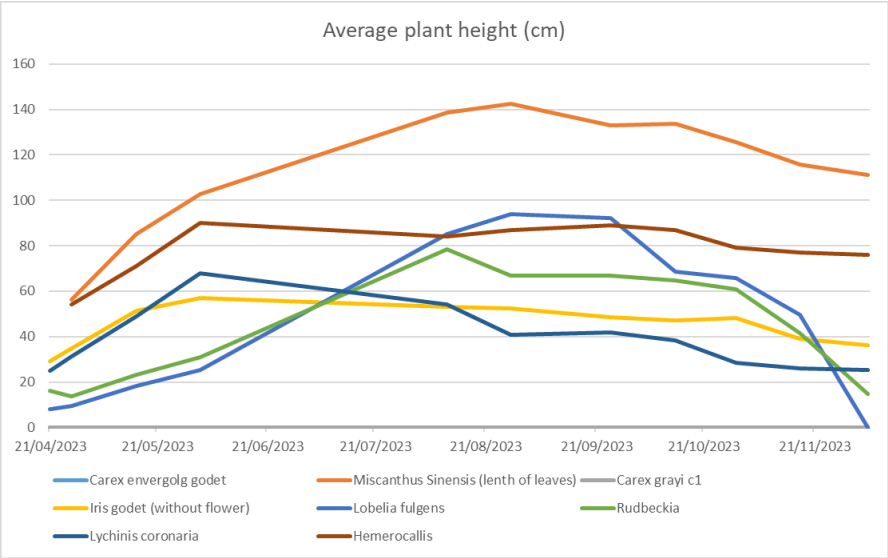

Figure 4-12: Average plant height change for different plants in SC in 2023

Furthermore, seasonal variations on vegetations exist in both JdB and SC. During the winter, SC almost completely loses all greenery on the surface (due to the dominant species Miscanthus senescence in winter). In JdB, some evergreen species (*Lonicera nitida*, *Hedera helix* and *Abelia x grandiflora*) keep their leaves in winter, while others, such as *Carpinus betulus*, are deciduous but retain their dead leaves throughout the cold season.

Whether plant community diversity and growth trends, including seasonal variations, could affect water fluxes, especially ET, would require more field-based investigation and needs to be further investigated (e.g. sap flow monitoring for trees and/or assessment of transpiration from leaf to the canopy scale, using porometry methods (Askari et al., 2021)).

4.2.3 Scenario Analysis Based on Reservoir Model

For SC, the reservoir model used to reconstruct hydrological processes allows testing alternatives scenarios regarding the extension of the gravel storage layer and underlying soil permeability. The following table (Table 4-2) presents the results obtained with the original configuration (S0) along with alternative settings, based on different bottom storage depths (S1, S2, S3) or on the lining of the drainage layer (S4).

Table 4-2: Hydrological performance of different design configuration scenarios for SC bioretention (Avg. VRR-Event = average event scale volume reductions, VRR-Total = total volume reduction over the sum of all events).

Model scenarios	Avg. VRR-Event	VRR-Total	Completely retained events	Total exfiltration
S1 (620 mm IWS, unlined)	87%	66%	136/185	51.5%
S0 (420 mm IWS, unlined)	85%	62%	128/185	49.3%
S2 (220 mm IWS, unlined)	82%	55%	118/185	43.5%
S3 (20 mm IWS, unlined)	61%	27%	59/185	15.9%
S4 (no IWS, lined)	22%	11%	2/185	0.0%

Lining (scenario S4) significantly limits the volume reduction performance of the bioretention cell (total volume reduction is only 11%), which means for soil and hydraulic loading conditions in SC, the ET alone is not an efficient mean to reduce runoff volume. An unlined system implemented on a low permeability clay underlying soil can still reduce by 27% the total runoff volume by applying a 20 mm very thin bottom storage. This performance can increase if a deeper bottom gravel storage is applied, however, since 220 mm of IWS already encountered for 55% of VRR-Total, there is not much benefit to increase the storage depth when it is above 220 mm (for instance from 220 mm to 420 mm, the VRR-Total only increase 7% more).

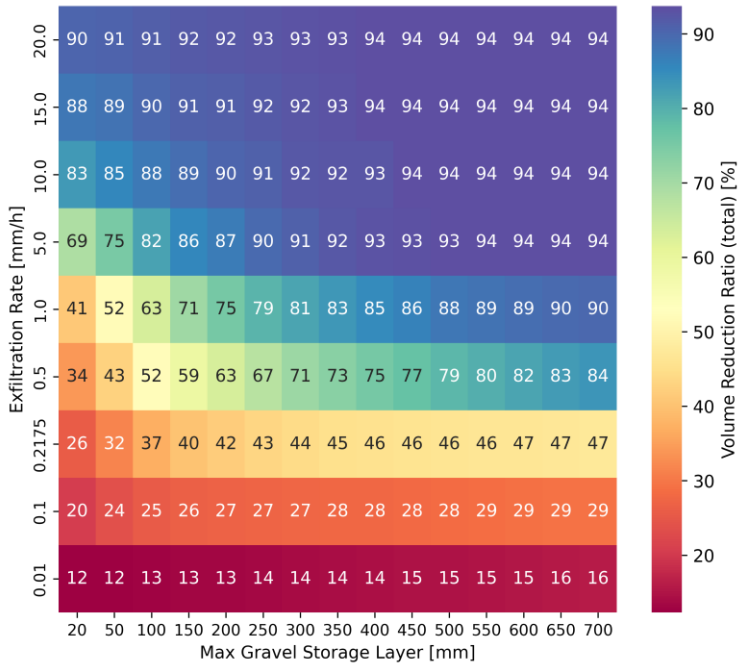

Figure 4-13: Heatmap of different max gravel storage layer thickness and bottom exfiltration rate impact on VRR-Total for SC bioretention (the number in each square: VRR-Total under a certain scenario)

By applying grid search on bottom gravel storage layer thickness and exfiltration rate of underlying soil, a VRR heatmap can be generated (see Figure 4-13). As shown in Figure 4-13, higher bottom exfiltration rate and higher gravel storage layer thickness can provide higher volume reduction ratio, but the benefit from extending gravel layer thickness largely depends on the bottom exfiltration rate. For high exfiltration rates, significant volume reduction can be achieved with a minimal storage layer thickness. For the lowest permeability settings, increasing the gravel storage thickness cannot compensate for the limited exfiltration rates.

4.3 DISCUSSION

4.3.1 Uncertainties and Limitations

The analysis conducted in this study is subject to various (and possibly significant) uncertainties, arising from different factors. For measurement uncertainty, evaluations have been conducted for most of the sensors in the three bioretention prototypes as shown in 3.2.4. However, uncertainty of the measurement is not presented directly in the result figures due to the following reasons.

For some terms (such as inflow or water level), elementary uncertainty assessments were based on the OLS regression and prediction intervals (Eq. 3-10). However, for soil water storage, this approach is not applicable since the study focuses more on variations than the absolute measurement. Also, the OLS analysis did not make sense for soil moisture and thus cannot be used here (as discussed in 3.2.4.3.iii and 3.2.4.3.iv). Hence, the impact of measurement uncertainties is not directly/explicitly accounted for in the analysis. It is worth noting that since the event end in SC bioretention is identified based on soil moisture change (introduced in 3.2.5.4.ii), not taking the uncertainty into account can lead to difference in the event durations, numbers and even the overall water balance. Moreover, the water balance calculation for SC (partition between seepage and transpiration) is completely depends on soil moisture measurements. The situation is different for JdB, where having both inflow and outflow theoretically allows better capturing the water balance (however there were issues in inflow data for JdB).

Alternative propagation methods for a more robust assessment of water balance other approaches would be needed: 1) outflow monitoring and/or weighting (but this is not always possible) 2) increasing the number of soil moisture sensors, or on the

contrary use sensors with bigger measurement volume (although this may lose profile information but can gain a better average soil moisture evaluation).

In addition of the measurement uncertainty, the data analysis methods conducted in the study could also introduce additional uncertainty. For instance, inflow data for JdB consist of both measurements and estimates from precipitation, with their specific uncertainties, this may lead to the "drops" in the water balance closure. For the dry period analysis, the removal of the first 2 days of each dry period to ensure the seepage/drain is finished could result in ignoring high transpiration-rates at the beginning of dry periods, thereby putting more emphasis on water limited conditions. In the hydrological event identification/separation procedure, the threshold for end one event can lead to less than 5 % of uncertainty in the seepage volume of SC (See 3.2.5).

The inability of the monitoring system to fully capture soil storage variations could also introduce some biases into the analysis. These biases are more problematic at the event-scale or for dry period analysis: for JdB, makes it difficult to detect water balance issues when defining "valid observation periods"; in SC, biases in soil moisture storage can lead to overestimation of seepage if the sensor fails to detect the response to inflow, or underestimation if only the surface sensor is wetted.

As mentioned in 4.2.1, the water level in JdB2 often exceeds the level of the outflow orifice saturation therefore extends and fluctuates within the soil layer, resulting in alternance of between saturated and unsaturated condition for lower soil moisture probes, that probably can cause uncertainty in soil water storage estimation. However, the comparison of water storage estimates with those obtained using an alternative method combining soil moisture sensors and water level for soil storage calculations shows only limited differences, suggesting that this uncertainty remains moderate. More generally, the ability of discrete soil measurements (15 sensors for 38 m^3 in the case of JdB) to assess water storage variations within studied systems may be questionable, particularly when inflow occurs from only one side (as for JdB). During the operation, uneven soil moisture distribution was found in the soil profile (Figure 3-17). Besides, fast reaction (quick increase water content) of deeper soil sensors was also observed. This evidence support the existence of preferential flow along the soil sensor cable or cracks (and perhaps roots) in the soil.

4.3.2 Impact of Bioretention Design On its Hydrological Performance

4.3.2.1 Bioretention design impact on ET

4.3.2.1.i Role of IWS

The primary difference between JdB1 and JdB2 lies in the presence or absence of IWS. This design variation leads to large differences in how the two bioretention cells are functioning, particularly in terms of ET. As mentioned in the result part, existing literature reports the ability of IWS to enhance ET. However, the ET difference reported between JdB2 and JdB1 was significantly higher than that reported in previous studies. Here, the difference in ET may be exacerbated by: 1) For JdB1, the non-uniform distribution of inflow resulting in uneven water content, with increasing water stress as the distance from the water inlet increases, whereas, for JdB2, the presence of the IWS ensures more uniform humidification and higher water availability for plants; 2) preferential flows due to cracks in the JdB1 substrate (personal observation), causing large amount of water to bypass the system. Here, the presence of an IWS is not relevant as additional storage for volume control (as it always remains full), but it could be beneficial to ensure proper hydrodynamic functioning and sustain vegetation growth. However, the design of IWS needs to ensure that plants can access to the water, which means the combination of substrate textures and thickness need to allow a suitable IWS depth, or suitable capillary fringe table for plant roots.

4.3.2.1.ii Role of soil characteristics

Two different substrate types were used in the three experimental prototypes. One was sandy as commonly recommended for bioretention filter media (sandy loam in SC); the other was a fine-texture planting soil, used for gardens in Paris (silt loam in JdB). According to the frequent visual inspection, vegetations in SC have been remaining healthy conditions. Combine with the high moisture at the substrate below 15 cm, the substrate in SC was found to be good for water holding capacity. This may be due to the combine effect of fine particles added into the SC sandy substrate, capillary barrier near the bottom of substrate, and the high HLR. For JdB, as expected, the fine media also support well the vegetation growth

For the bioretention designed with limited loading ratios and aiming for ET, common garden soil such as silt loam can be a potential option, but it needs to be carefully managed. For instance, the use of such fine-textured soils requires caution

due to the potential for crack formation (as observed for JdB1), which may lead to infiltration bypassing the substrate. The observations from JdB2 suggest that this issue could be solved with the implementation of an IWS connecting to the substrate layer. However, in JdB2 the significative wetting of the substrate observed for JdB2, with saturation above the level of the outlet, was likely reinforced by the specific drainage condition of this cell (easily get clogged). While this may be beneficial for the vegetation during dry periods, poor soil drainage can also in turn limit the growth of some plants. Besides, the inclusion of IWS ensuring substrate humidification may not really be compatible with exfiltration (which is desirable for volume reduction). In addition, clogging will always be an issue under such high proportion of clay. Thus, if greater water retention capacity is required, it may be more effective to increase the organic matter content rather than using very fine-textured soil. Another possibly for preventing the formation of cracks is the addition of a mulch layer at the surface, as done during the operation of JdB. The large difference on surface moisture results from the two field sampling works in 2022 and 2023 also confirmed this function of mulch layer. The implementation of mulch layer efficiently increased the moisture of the surface soil.

4.3.2.1.iii Role of vegetation

The role of plants remains difficult to quantify due to the variety of factors involved (e.g., plant diversity, maintenance etc.). In this study, it is mainly addressed through the assessment of evapotranspiration. In SC, the occurrence of low ET/PET ratios during the growing season, together with surface drying but wet deeper substrate conditions, suggests that the root zone is primarily related to the shallow soil.

However, the above hypothesis is established on the maximum ET within SC is equal to the PET. In fact, the cell has shadow effect from its own structure (mainly from the nearby wall);the low-lying shape of the cell which can limit atmospheric exchanges et increase locally the humidity; the physiology of the dominant vegetation in SC could be different from the reference grass with a crop factor < 1 (for *Miscanthus sinensis*, the crop factor is 0.8); also dense foliage cover of *Miscanthus sinensis* may reduce soil direct evaporation due to shading. The above evidence is sufficient to show that the maximum ET in the cell is smaller than the PET, thus ET/PET ratios do not 100% imply that the plant in SC was under water stress.

For the two cells in JdB, the planted shrubs seemed to better develop in the wetter soil surface (JdB2), while trees prefer higher soil water content in the deeper layer.

If the goal is to promote ET and support healthy, long-term plant development, it would be valuable to further explore how to adapt plant selection. This includes considering both the plants' ability to access water within the soil profile and their tolerance to stress periods, as well as how to better align plant selection with predicted variations in moisture throughout the entire media profile.

4.3.2.1.iv Role of HLR

According to the scenario analysis in 4.2.3, when a system like SC is lined with a drainage, ET alone is not an efficient mean to reduce runoff volume (11%) when the vegetated area represents only 8% on the inflow catchment. Such result is somewhat expectable; at the annual scale PET hardly represent more than 1000 mm, whereas with a high HLR (>10), rainfall (and runoff) would be significantly higher.

It is also expected to have more ET on JdB due to the water holding capacity of its substrate and low HLR (e.g., JdB has 25% of vegetated area). Of course, comparing the water balance is challenging due to the limited available observation period for JdB. However, in the end, despite the significantly lower HLR and the relatively favourable soil conditions, the ET ratio (23% to 33%) remains relatively low.

4.3.2.2 Bioretention design impact on exfiltration

The bioretention design impact on exfiltration is examined based on SC and the supplement reservoir model. According to the overall water balance (Figure 4-4), exfiltration plays a more important role (even three times more) compared to ET. It is also predictable that, unless the HLR is significantly reduced, exfiltration will remain the dominant process if the underlying subsoil permeability or IWS storage capacity is sufficiently high.

For a bioretention system with a low permeability underground, the scenario analysis supports that when the permeability of underlying soil is between 0.1 – 1.0 mm/h, increase the thickness of bottom gravel storage can make valid improvement of exfiltration. If the *in-situ* permeability is lower than that, a shallow (200 mm) IWS can be a significant improvement on enhancing exfiltration, but it is useless to further increase the storage thickness. However, other HLRs that different than SC are necessary to be tested.

4.3.2.3 Other suggestions on bioretention cell design

Groundwater intrusion issues, such as the one that affected SC, were also reported in previous studies (Bonneau et al., 2020). Given the highly heterogeneous (and sometimes unknown) nature of urban soils and groundwater pathways, such phenomena may also occur in other contexts. For future implementation of bioretention systems, especially where the native soil is clay, better pre-construction investigations on the underground conditions (e.g., in both dry and wet periods of a year) can help to choose appropriate depth of the cell, thus preventing the drainage layer/the bottom of the cell to be located within the temporary perched water lens.

4.4 CONCLUSION

In this study, three prototypes of bioretention systems were investigated: JdB1 and JdB2 are two lined systems with silt loam substrate and 3.9 of HLR, differing only by the presence of IWS; while SC is a system which is unlined at the bottom (contact with low permeability clay subsoil), with a IWS under a drainage layer (IWS not contact with substrate). SC has sandy loam substrate and a HLR of 13.4. The monitoring results from 3 pilot bioretention cells monitored from 2021 to 2023 (for JdB, it was the autumn of 2022 and 2023) are presented. During the experiment, due to the groundwater intrusion issue, a reservoir model has been developed to complete/fix the problematic data. This model was considered as a tool to extend the field monitoring aspect, which evaluated multiple scenarios of the bottom storage thickness and native soil $K_{s,}$

Over the long continuous observation in SC, 61.7 % of total incoming water has been controlled (by exfiltration into the ground or ET). The performance of the bioretention cell shows clear seasonal variability, with most of the overflow/high drainage flow happening between May and September (which reflects the climate characteristics of Paris, where most of large and intense events happens in the summertime, and small and frequent events happen in winter). At the event scale, significant reduction is often obtained. This reduction is depending on both initial storage conditions and rainfall characteristics, and thus small events are well retained.

The observation period in JdB1 and JdB2 is less continuous and shorter compared to SC. Over the two summer-autumn periods in 2022 and 2023, the two JdB

bioretentions could abstract 43.0% (JdB1) and 48.1% (JdB2). In an event-scale, JdB1 has a median VRR-Event of 64%, while JdB2 has a higher ratio of 91%.

Based on the monitoring results and different design configurations of bioretention cells, the impact of IWS presence, the thickness of IWS and the conductivity of underlying subsoil on hydrological performance (e.g., ET, peak flow reduction and runoff reduction) was investigated. The findings are listed as follow:

- Except from enhancing ET, when a IWS is in contact with the substrate, it can also help to protect substrate from drying and cracking, which can be an issue for low hydraulic loading ratio bioretention with silty or clay substrate.
- For SC, despite a relatively high HLR and low underground permeability, exfiltration is significant due to the presence of an unlined IWS. The benefits from increasing the extent of this layer are however limited.
- The combination of IWS contact with fine substrate raise up the risk of clogging, this might also result from JdB's special drain design and the use of geotextile as a separation layer.

Besides, although vegetations were measured via different methods during the experimental periods. These vegetation growth assessment measurements could be made more frequently and in conjunction with other plant eco-physiological parameters (e.g. leaf stomatal conductance or transpiration rate, canopy surface temperature as a proxy of stomatal conductance, etc.) to better understand plant-water relations in the soil-plant-atmosphere continuum and to better capture the influence of plant selection on water transfers. Another direction is to look at matching substrate and cell structures to create a system with more resilient moisture dynamics under drought and wet extremes. Thus, the system can support more sustainable vegetation development.

Furthermore, even the three cells were specified to be compared under variety of designs, the difference on data availability and designs between them makes the effect of some parameters on performance not directly comparable. In this case, using models that are validated on monitoring and field investigation is going to be a useful approach to further explore the different design impact on bioretention performance.

Chapter 5: Modelling the Hydrological Behaviours of Bioretention Cells with HYDRUS: Model Representativeness and Robustness Based on A Monitoring Device in Paris

5.1 INTRODUCTION

Bioretention systems are widely used today as a part of sustainable urban drainage systems, to restore a more natural water balance in urbanised area. Their corresponding benefits include reducing the runoff volume, mitigating urban heat island by evapotranspiration (ET), recharging groundwater by exfiltration. Modelling is a common tool to evaluate the hydrological performance of a bioretention system (W. A. Lisenbee et al., 2021). As introduced in Chapter 2, commonly, one type of model can conceptually represent a bioretention system and focus on the flux (e.g., ET, drainage flow, overflow, exfiltration) between the system and its surrounding environment, such as the LID module of SWMM (Storm Water Management Model) (Gironás et al., 2010). Another type of model, such as HYDRUS (Šimůnek et al., 2022), uses physical laws for water movement within the bioretention system, and thus is able to describe the hydrological processes in greater details, such as water transport between different layers and the soil moisture distribution.

In real practice, detailed knowledge of all the properties/characteristics of the modelled bioretention systems (detailed geometry, soil and vegetation properties, underground conditions, etc.) is never available. Even when field measurements are available, they might not be completely representative of the system complexity due to spatial heterogeneity. Whether these incomplete/limited data compromise the assessment of the system's hydrological performance or not remains questionable. Various studies have been conducted on testing the different input parameters, but they were mainly focused on scenarios analysis such as different rainfall return period or different media types (Meng et al., 2014), or global sensitivity analysis on detailed

parameters (Ouédraogo et al., 2025). There is still insufficient information to determine how well the model can represent a system with or without detailed knowledge. Hence, in this study, the impact of different levels of knowledge on soil hydrodynamic properties, bottom boundary condition (BC), PET and vegetation properties on the hydrological behaviour of an experimental bioretention cell modelled with a physical based approach (in HYDRUS-1D) was analysed. The sensitivity of modelling results to these uncertain modelling input parameters was assessed from both the fitting goodness and a range of hydrological performance indicators. This work was developed for the SC bioretention cell.

5.2 METHODS AND MATERIALS

5.2.1 HYDRUS-1D Model

HYDRUS-1D is a model for simulating water (also solute and heat, but these two aspects were not considered in this study) movement in saturated/unsaturated porous media (Šimůnek et al., 2013). The model uses a finite element solution to solve the Richards Equation (Richards, 1931), which is a quasilinear partial differential equation for water movement in unsaturated porous media. Hydraulic conductivity curve and water retention curve are needed to solve the Richards equation. HYDRUS-1D allows to use different empirical models, such as Van Genuchten model (Van Genuchten, 1980) or Brook and Corey (1964) to parametrise the media and create the two needed curves, also direct input of the two curves is possible through the "look-up table". HYDRUS-1D allows users to define a vertical profile with a number of different media. The upper boundary allows constant/variable pressure head or flux as input, or a time-variable input, e.g., a timeseries of precipitation and PET. The bottom boundary also allows to be set as constant/variable pressure head or flux, deep drainage, free drainage, seepage face or horizontal drains. In addition, HYDRUS-1D provides options for vegetation, including different root uptake models, root density distribution profile and root growth.

Note that the HYDRUS-1D used in this study is the 1D module of commercial HYDRUS 5.02, which allows higher print time compared to the public version HYDRUS-1D 4.17. Simulations in this study rely on a package Phydrus (Collenteur et al., 2020), which allows HYDRUS-1D simulations to be performed using a Python

interface, making it easier to conduct parameters/configurations adaptation and batch simulations.

5.2.2 Simulation Preparation

5.2.2.1 Conceptualisation of the selected bioretention cell in the model

The SC pilot bioretention cell was modelled with HYDRUS-1D. Due to the fact that only one bottom boundary condition can be represented at a time in HYDRUS, the simulation cannot be conducted with both drainage pipe and bottom exfiltration. Thus, only the surface ponding layer (14.6 cm), substrate layer (48 cm of sandy loam) and transition layer (10 cm of sand) of the selected case were modelled in HYDRUS-1D (the blue part in Figure 5-1). A complementary reservoir model (introduced in 4.1.2) was used to represent the hydrological behaviour of drainage and bottom gravel layers and obtain the volume of exfiltration and drainage (the pink part in Figure 5-1).

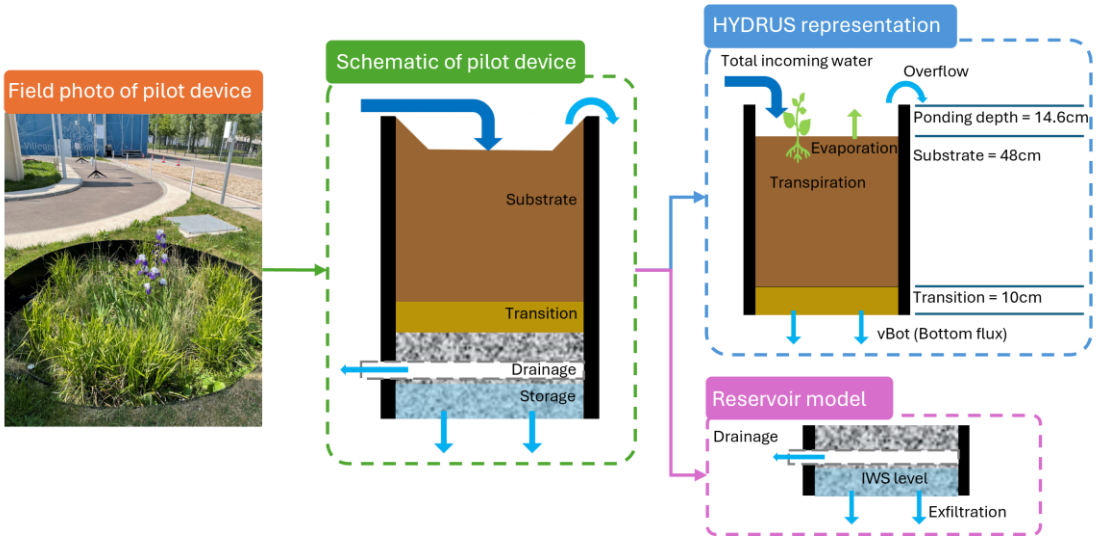

Figure 5-1: Hand-held field photo of SC pilot bioretention device, schematic of the pilot device and HYDURS and Reservoir model representation

5.2.2.2 Simulation settings

All simulations were run over a period of 14 months, from 2022-11-01 to 2024-12-31, with 1 min interval time-variable atmosphere boundary inputs. For HYDRUS, the incoming water was calculated as the sum of measured inflow (converted to water depth over bioretention surface) and direct rainfall. For each simulation, a fixed pressure head of -500cm over the whole column depth was used as initial soil condition, then the first two months of simulation (2022-11-01 to 2022-12-31, rainy winter period) were used as initialisation period to achieve a stable soil moisture profile for each simulation. The simulation results were thus analysed for a one-year

period from 2023-01-01 to 2023-12-31. For the reservoir model, inputs are the bottom flux (i.e., the flow through the bottom boundary of HYDRUS part) in 1min time step, with an underlying soil Ks of 0.2175 mm/h (calculated in 4.1.2.4) and 42 cm of gravel storage layer.

5.2.3 Uncertain Inputs For Sensitivity Analysis

5.2.3.1 Potential evapotranspiration (PET)

Atmospheric boundary condition was used in the model, which requires PET to calculate the upwards flux. Two different PET scenarios were considered in this study: 1) PET- *in-situ*: calculated with *in-situ* measured meteorological data and PM-FAO56 equation (Allen et al., 1998); 2) PET-Torcy: provided by a nearby station (6 km away) from Météo-France. The use of these two scenarios represents the situation that sometimes the PET from very *in-situ* sensors is not available, thus the simulation has to use the reference PET provided from a nearby weather station.

Note that due to the shadow effects around the radiation sensor in SC, the lower *in-situ* wind speed (3m for SC site and 10m height extrapolated to 2m based on a reference wind profile for Torcy), surrounding land use (urban area for SC site and agriculture are for Torcy) and calculation methods (PM-FAO56 for SC site and PM-Météo France for Torcy), the PET-Torcy has higher value than PET- *in-situ* (as shown in Figure 5-2). The one missing period in PET- *in-situ* was replaced by PET-Torcy.

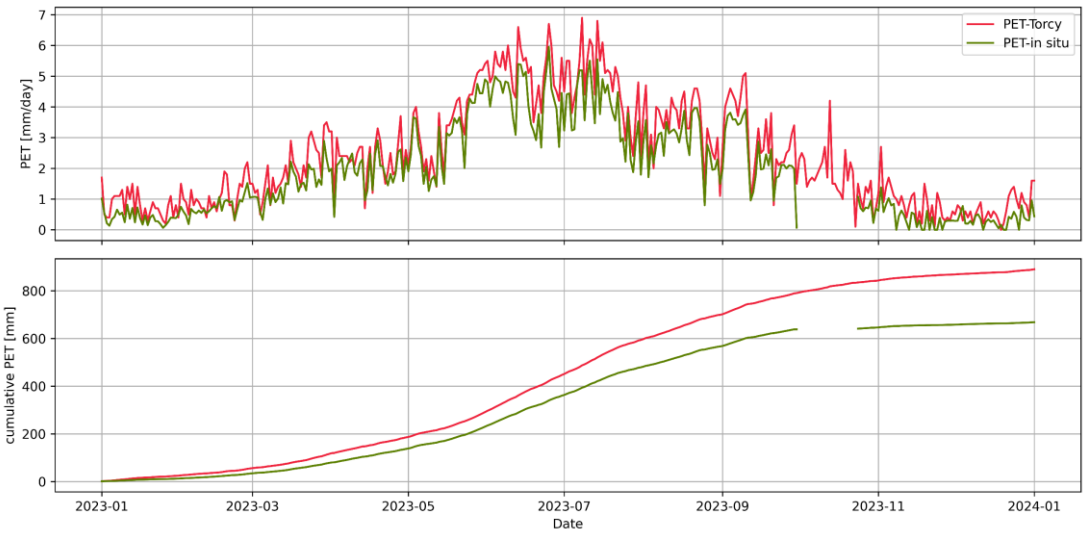

Figure 5-2: PET inputs from Torcy and *in-situ* (upper: daily PET; lower: annual PET)

5.2.3.2 Bottom boundary conditions

In HYDRUS, the seepage boundary condition needs the bottom layer to be saturated before allowing water to leave the system (atmosphere pressure under it), while the free drainage boundary allows water to move vertically at a unit hydraulic gradient (the hydraulic head decreases linearly with depth).

Normally, as atmospheric pressure condition is expected at the bottom of a transition layer connected to a gravel layer with large difference on particle size, the bottom boundary condition should be a seepage face. However, during the operation of the bioretention system, some sand from the transition layer might have migrated into the gravel layer, and thus the bottom boundary conditions could become similar to a free drainage condition. Hence, both "seepage face" and "free drainage" were considered for bottom boundary conditions.

5.2.3.3 Media hydraulic parameters

As introduced earlier, modelling water fluxes in variably saturated porous media with Richards equation requires specifying soil hydrodynamic properties. In most cases, these properties are represented by soil water retention curve and hydraulic conductivity functions. In HYDRUS, different options can be used to specify these curves and functions. For van Genuchten equation, parameters can be estimated with the Rosetta pedotransfer function, based only on the soil type information (sandy loam for substrate layer and sand for transition layer in this case), or based on grain size distribution, or on both grain size and bulk density (Y. Zhang & Schaap, 2017). Soil hydrodynamic parameters can also be estimated based on field investigations such as BEST-infiltration tests (Lassabatere et al., 2013). As presented in 3.2.3.1, the water retention curve and hydraulic conductivity functions came from two different equations, hence these hydrodynamic parameters from BEST-infiltration tests were converted into look-up tables as inputs.

14 sets of parameters (the three levels of Rosetta predictions + 11 BEST-infiltration field measurements) were used for sensitivity analysis for the substrate layer and three sets of the transition layer parameters (Rosetta predictions). The following table presents all the soil hydraulic parameters used during the simulations.

Table 5-1: Media hydraulic parameters input (parameter definitions can be found in 3.2.3.1.ii)

ID	Layer	Model	Ks (cm/min)	θr	θs	alpha (1/cm)	n	η
T3_slope	Substrate	BEST	0.032	0.000	0.413	0.083	2.324	9.165
T3_intercept	Substrate	BEST	0.046	0.000	0.413	0.127	2.324	9.165
T1_slope	Substrate	BEST	0.058	0.000	0.413	0.177	2.324	9.165
T1_steady	Substrate	BEST	0.084	0.000	0.413	0.337	2.324	9.165
T2_slope	Substrate	BEST	0.086	0.000	0.413	0.093	2.324	9.165
T2_intercept	Substrate	BEST	0.047	0.000	0.413	0.162	2.324	9.165
T4_intercept	Substrate	BEST	0.077	0.000	0.345	0.030	2.341	8.863
T5_slope	Substrate	BEST	0.078	0.000	0.434	0.217	2.319	9.265
T5_intercept	Substrate	BEST	0.081	0.000	0.434	0.229	2.319	9.265
T6_slope	Substrate	BEST	0.026	0.000	0.434	0.054	2.319	9.265
T6_intercept	Substrate	BEST	0.050	0.000	0.434	0.111	2.319	9.265
avg_bulk	Substrate	Rosetta (V-G)	0.019	0.063	0.353	0.017	1.453	
avg_nobulk	Substrate	Rosetta (V-G)	0.027	0.064	0.383	0.017	1.438	
sandy_loam	Substrate	Rosetta (V-G)	0.027	0.039	0.387	0.027	1.448	
sand_before	Transition	Rosetta (V-G)	0.346	0.057	0.411	0.027	2.305	-
sand_after	Transition	Rosetta (V-G)	0.252	0.057	0.409	0.025	2.087	-
sand_simple	Transition	Rosetta (V-G)	0.495	0.045	0.430	1.450	2.680	-

5.2.3.4 Surface coverage fraction (SCF) curves

The SCF simply represents the ratio of area covered by vegetation over the whole bioretention surface area. It can be used in HYDRUS simulation to differentiate between potential soil evaporation (E_p, cm/min), and potential vegetation transpiration (T_p, cm/min) in the total PET flux (Šimůnek et al., 2013), following the Eq. 5-1.

$$T_p = PET \times SCF$$
$$E_p = PET \times (1 - SCF) \quad \text{Eq. 5-1}$$

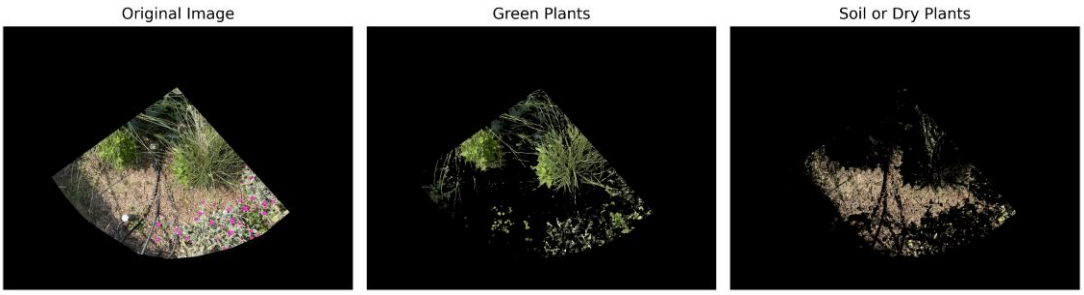

Figure 5-3: Example of SCF (a quarter of a top-view photo in June 2023)

As shown in Figure 5-3, the measured SCFs were calculated based on the top-view photos of the bioretention cell prototype every 2 to 4 weeks over the year of 2023, with the use of an open-source computer vision library OpenCV

(https://github.com/opencv/opencv?tab=readme-ov-file). Pixels in each photo were identified to group A (green plants) and group B (soil and dry plants). The ratio of group A over the sum of group A and B was thus considered as the SCF value of this individual day.

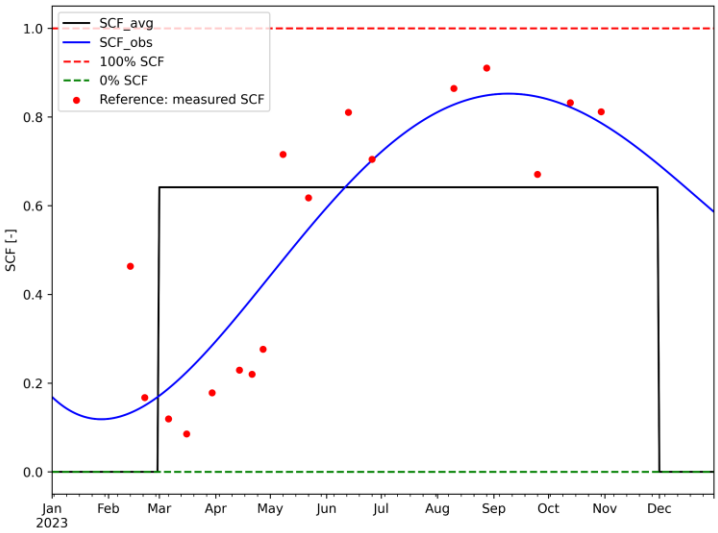

Figure 5-4: Temporal evolution of measured SCF values and SCF parameter settings tested in the Hydrus sensitivity analysis (SCF_obs: polynomial curve fitted on observed SCF in the monitoring device over 2023; SCF_avg: average SCF during growing season, 0 for the rest; 100%SCF: complete vegetation coverage of the bioretention surface; 0%SCF: no vegetation coverage of the bioretention surface)

Figure 5-4 presents the temporal evolution of measured SCF values and SCF parameter settings tested in the Hydrus sensitivity analysis. The 17 red dots represent the measured SCF values from different dates over the year. Note that the significant drop between the two dots in February is due to the trimming and removal of weeds. Overall, in 2023, the SCF started to increase from March, and reached to the highest coverage by the end of summer (September), and then slowly decreased in the winter. However, even in the winter, the green part of the dominant specie (i.e., *Miscanthus Sinensis*) still remained high.

Based on all the measured SCF values, a SCF curve can be built by fitting a 4-degree polynomial curve to these measured SCFs (i.e., SCF_obs in Figure 5-4). The fitting curve does not have special meaning, but is only trying to create a smoothed curve, to provide high resolution (1min time step) SCF input for HYDRUS-1D.

Another curve (SCF_avg) can be built by assigning a constant average value of SCF_obs for the growing season and assign 0 for the rest of the year. In addition, full vegetation coverage (100%SCF) and bare soil (0%SCF) settings were considered.

5.2.3.5 Root distribution profile

Root distribution profile can be defined as a function of root density to depth. In this study, 3 root profiles were selected for simulation: two triangle profiles (Figure 5-5b) with different depths, and one uniform profile (Figure 5-5c). The triangle distribution describes the root density as linearly decreasing from the surface to deeper soil (Prasad, 1988). According to (Jia et al., 2022), the uniform distribution is characteristic of a root taproot system with large lateral roots, e.g., Aleppo pine (Ghestem et al., 2011) and Pulsatilla pratensis (Lynch, 1995). Triangle distribution can represent root taproot system with small lateral roots, e.g., Trigonella balansae (Lynch, 1995). Other distribution, e.g., Parabolic distribution for concentrated root system, and exponential distribution for a plate-shaped root system (Jia et al., 2022), are not considered in the current stage of study to reduce the number of simulations.

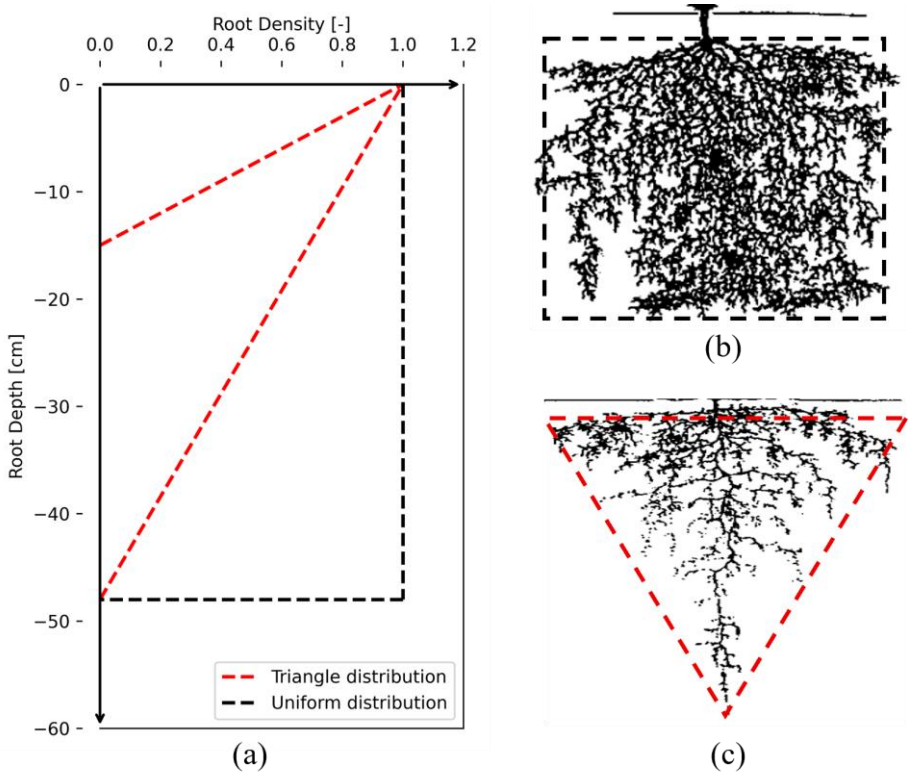

Figure 5-5: Root density distribution: (a) the 3 different root distribution inputs tested in this study; (b) uniform distribution, modified from (Lynch, 1995); (c) triangle distribution, modified from (Lynch, 1995)

As shown in Figure 5-5a, 3 root density distribution profiles were tested: triangle and uniform over the whole substrate depth (48 cm), and triangle over only 15 cm depth to represent the scenario of grass lawn. As mentioned in 4.2.2, the dominant vegetation in the pilot bioretention cell during the monitoring period is *Miscanthus Sinensis*. According to a specific site study on the spatial distribution of the roots, the root of Miscanthus distributes mostly within the top 30 cm, and the root density shows a linear decrease from the surface to 50 cm depth (Neukirchen et al., 1999). Hence, the triangle profile (48 cm) is considered here to be more representative the reality of vegetation root distribution in the pilot bioretention system over all the three input profiles. However, this profile is more of a reference, rather than a recommendation.

In HYDRUS-1D, the root distribution is highly linked to the calculation of root transpiration through a normalised water uptake distribution function Eq. 5-2. The equation established root distribution $b(x)$. Where the L_R is the region occupied by root zone (in this case, 15cm or 48cm). Eq. 5-3 is used for normalising the root density distribution to ensure $b(x)$ integrate to unity over the flow domain.

$$b(x) = \frac{b'(x)}{\int_{L_R} b'(x)dx} \quad \text{Eq. 5-2}$$

$$\int_{L_R} b(x)dx = 1 \quad \text{Eq. 5-3}$$

5.2.3.6 Root uptake models

HYDRUS provides two options of root uptake models: Feddes model and S-Shape model. In this study, Feddes model (Feddes et al., 1978) was used for vegetation root uptake estimation (Eq. 5-4, Eq. 5-5, Eq. 5-6).

$$S(h) = \alpha(h)S_p \quad \text{Eq. 5-4}$$

$$\int_{L_R} S_p dx = T_p \quad \text{Eq. 5-5}$$

$$T_a = \int_{L_R} S(h,x)dx = T_p \int_{L_R} \alpha(h,x)b(x)dx \quad \text{Eq. 5-6}$$

Where the sink term S is defined as the volume of water removed from a unit volume of soil per unit time due to root uptake, $\alpha(h)$ is sink term variable function (as introduced later in Figure 5-6), $b(x)$ is the normalised root distribution (as shown in

Eq. 5-2), T_p is the potential transpiration rate and T_a is the final actual transpiration rate calculated by HYDRUS.

The Feddes model input is directly related to $\alpha(h)$, which is the stress response function. While h increases (soil from wet to dry), α changes with soil water pressure head to reflect drought or anoxic stress. As shown in Figure 5-6, between h1 to h2, α increases linearly until 1, where the root uptake equals to the maximum transpiration rate (potential transpiration rate); between h2 and h3, α constantly equals to 1; from h3 to h4 (wilting point), α is assumed to decrease linearly until 0, under which the root can no longer extract water from the soil. The input variable h_3 is related to the atmospheric demand and thus varies with the provided potential transpiration rate T_p ($h_{3,\ low}$ to $h_{3,\ high}$ are two thresholds regarding to T_p =1 mm/d or 5 mm/d). In another word, vegetation has more difficulty to extract the water at the PET rate and thus α start decreasing for higher pressure head values.

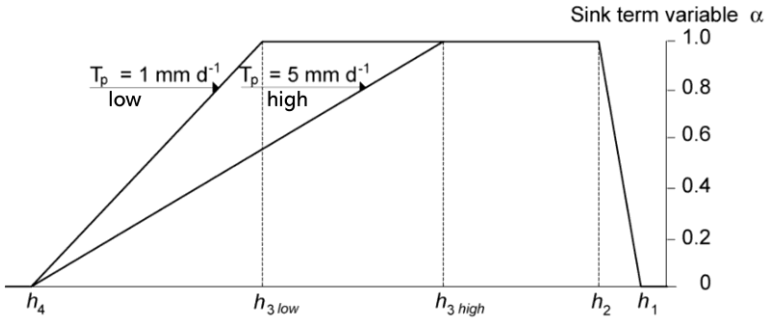

Figure 5-6: Dimensionless sink term variable α as a function of the soil water pressure head h (Figure source: (Feddes & Raats, 2004))

Four plant species or families (i.e., grass, alfalfa, wheat and corn) with contrasting root extraction behaviours were considered to assess the impacts of the uncertainties on Feddes model parameters. The characteristics of these four plant types can be summarized as follows. Grass: commonly used in urban areas (thus as a reference); Alfalfa: wide pressure head range of maximum root uptake rate; Wheat: strong extraction ability even when the soil is wet; Corn: able to extract water even when the soil is dry.

Table 5-2: Feddes model input for different vegetations

Vegetation	h_1 [cm]	h_2 [cm]	$h_{3,high}$ [cm]	$h_{3,low}$ [cm]	h_4 [cm]	$T_{p,high}$ [cm/day]	$T_{p,low}$ [cm/day]
Grass (Šejna et al., 2022)	-15	-25	-300	-1000	-8000	0.5	0.1
Alfalfa (Taylor & Ashcroft, 1972)	-15	-30	-1500	-1500	-8000	0.5	0.1
Wheat (Wesseling et al., 1991)	0	-1	-500	-900	-16000	0.5	0.1
Corn (Feddes & Raats, 2004)	-15	-30	-325	-600	-15000	0.5	0.1

5.2.4 Model Accuracy Indicator

To evaluate how well the HYDRUS outputs match monitoring results, the dynamics of substrate moisture at different depths was considered. The Kling–Gupta efficiency (KGE), which involves three terms, i.e., correlation, bias and variability (Kling et al., 2012), was used as an indicator of goodness of fit. The equation of KGE is shown in Eq. 5-7.

$$KGE = 1 - \sqrt{(r-1)^2 + (\beta-1)^2 + (\gamma-1)^2} \quad \text{Eq. 5-7}$$

- r: The Pearson correlation coefficient (linear correlation between observed and simulated values).
- β: The bias ratio, calculated as the mean of the simulated data over the mean of the observed data.
- γ: The variability ratio, which is the standard deviation of simulated data over the standard deviation of the observed data.

For each simulation, five KGE values were calculated based on the monitored soil moisture at different depths (2.5 cm, 7.5 cm, 17.5 cm, 27.5 cm, 37.5 cm) and the simulation soil moisture at the corresponding simulation depth. The average of those KGEs were taken as the KGE of this simulation.

5.2.5 Two-step Sensitivity Analysis

To address the impact of different input variables to the model fitting and model performance, a sensitivity analysis is necessary. It is conducted in two steps in order to reduce the number of simulations and facilitate the interpretation of the results.

As shown in Table 5-3, Step1 focused on testing the variables on bottom boundary conditions, media hydrological parameter sets and PET scenarios, with a fixed vegetation parameter setting (i.e., Observed SCF, grass root uptake models and 48 cm of triangular root distribution profiles). Based on the result of step1, for each

bottom boundary condition and PET, a most suitable media hydrological parameter set (the one with the highest KGE) was selected to test vegetation inputs (4 SCF scenarios, 4 root uptake models and 3 root distribution profiles) for Step2.

Table 5-3: Variables used in HYDRUS sensitivity analysis

Required model inputs	Input variables	Number of sets
Bottom boundary condition[1]	Seepage face; Free drainage	2
Media hydrological parameters[1]	(substrate: 11 BEST-infil test + 3 Rosetta settings) × (transition: 3 settings with Rosetta)	42
PET[1]	PET- *in-situ*; PET-Torcy	2
SCF[2]	Observed SCF[1]; average SCF (growing season); 1; 0 (no transpiration)	4
Root uptake model[2]	Grass[1]; Alfalfa; Wheat; Corn	4
Root distribution profile[2]	Triangular (48cm[1]; 15cm); Uniform (48cm)	3

[1]Tested in Step1 of analysis; [2]Tested in Step2 of analysis

5.2.6 Hydrological Performance Indicators

Different hydrologic performance indicators were used for HYDRUS and the supplement reservoir model, those indicators represented different terms of annual water balance (i.e., ET, volume which leaves from substrate layer, exfiltration and drainage), water stock in the soil and indicator for drought stress. Definitions of the selected hydrological performance indicators are listed as follow:

- ET [%]: $\frac{ET}{V_{in}}$; ET = Total ET (cm) calculated by HDRUS over the 1 year simulation period, V_{in}= total inflow (cm) over the 1 year simulation period.
- vBot [%]: $\frac{V_{Bot}}{V_{in}}$; V_{Bot}= the volume (cm) leaves from the bottom boundary face of HYDRUS model, calculated by HYDRUS.
- Average media water content [cm^3/cm^3]: average water content in substrate and transition layer, calculated by HYDRUS.
- Exfiltration [%]: $\frac{V_{recharge}}{V_{in}}$; $V_{recharge}$ the volume of exfiltration (mm) which enters the surround soil, calculated by reservoir model (4.1.2.4).
- Drainage [%]: $1 - \frac{V_{underdrain}}{V_{in}}$, calculated by reservoir model (4.1.2.4).
- Drought period [%]: $\frac{T_{soil\ moisture<0.2}}{T_{total}}$, $T_{\text{soil moisture}}$ <0.2 indicates the period when the soil moisture at 15 cm depth is lower than 0.2 cm^3/cm^3, calculated from HYDRUS output.

When comparing the indicators calculated by the reservoir model (i.e., exfiltration and drainage), the bottom gravel storage can be different among different simulations as well as the monitoring results. To minimize the impact of initial bottom gravel storage, the performance comparison between monitored results and simulated results was chosen to start after a long dry period in February 2023, thus ensuring near-zero initial gravel storage level for both simulations and observations.

5.3 RESULTS

5.3.1 Model Fit Goodness

5.3.1.1 Step1: boundary conditions, PET and media hydraulic parameters

5.3.1.1.i Dynamic of soil moisture change

Figure 5-7 presents the average soil moisture over the substrate and transition layer for both simulated and monitored results. The simulations can be grouped according to corresponding bottom boundary conditions. Each group contains curves that represent different sets of hydrodynamic parameter inputs for substrate and transition layer. Note that some of parameter sets did not allow the model to converge, thus the number of curves under each group is different. To show the details of the changes in the curves more clearly, only part of the results (four months) is shown in Figure 5-7.

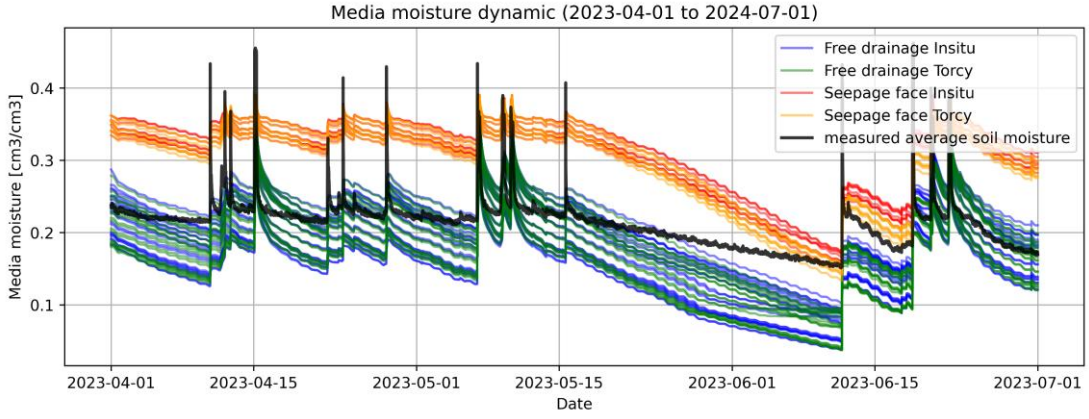

Figure 5-7: The dynamic of average soil water content in different simulations for Step1 (period: 2023-04-01 to 2023-07-01)

According to Figure 5-7, simulations with free drainage (blue) and seepage face (red) bottom boundary conditions lead to significantly different mean soil water content. Soil water content during dry weather periods is much higher for seepage face simulations compared to both field measurements and free drainage simulations. The

decrease of soil storage after each rain event shows different trends depending on the two bottom boundary conditions. For seepage face, the fast decrease of water content immediately after a rain event (associated with drainage) interrupts after a few hours at relatively high-water contents. For free drainage, this initial stage persists for a longer period until reaching lower water content values. Hence, seepage face leads to an important overestimation of ET during long dry periods (as shown by the significant difference in decreasing slope between measured and modelled soil water content) and free drainage leads to water stress conditions that do not exist in reality. The impact of soil hydrodynamic parameters is also important. When combined with seepage face bottom boundary condition, BEST infiltration test parameter sets lead to near saturated storage (the top two red curve). In half of the cases with BEST parameters, simulations fail to converge due to a full saturation of the soil profile (that cannot be handled by HYDRUS-1D), a behaviour that is in any case not consistent with field observations.

5.3.1.1.ii Cumulative bottom flux

Aside from the soil moisture variation, the flux of the bottom boundary (in this case, the interface between the transition and its underlying gravel layer) is a direct indicator to represent the outgoing flow rate and quantity. In Figure 5-8, the vBot flux from the first step simulation is compared to the vBot flux calculated from the monitored soil moisture and reservoir model (as introduced in 4.1.2.3). In general, for same boundary conditions, vBot associated with different PET scenarios show similar dynamics and only essentially differ in their cumulative values (15 to 18cm more vBot for *in-situ* scenario than Torcy).

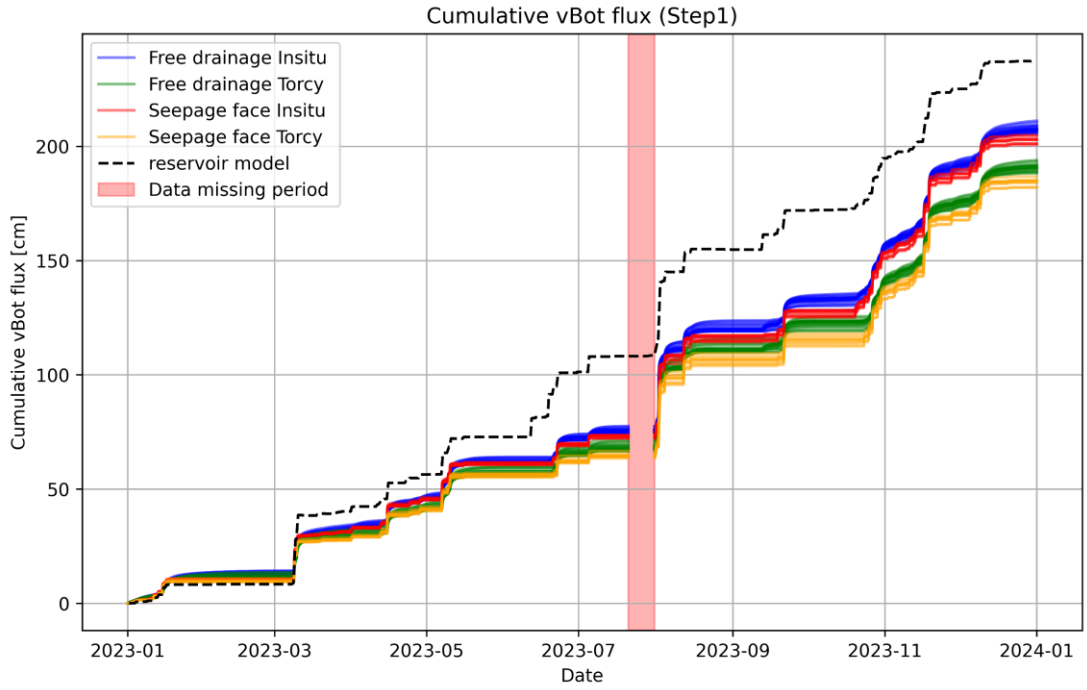

Figure 5-8: Cumulative vBot flux for Step1 (a period of 10 days is missing in the monitored soil moisture data, therefore same period of simulation results is removed and replaced with a shaded gap)

When comparing the two bottom boundary conditions under a same PET (for example "Free drainage *in-situ*" vs "Seepage face *in-situ*"), vBot exhibit different dynamics: the curves of free drainage increase gradually instead of showing a sharp turn after each event as it is the case for seepage face (more clearly indicated in Figure 5-9). This indicates that the water outflow through free drainage boundary lasts longer. However, the cumulative vBot value does not show a large difference between free drainage and seepage face (< 4%) when the PET is the same.

The annual cumulative vBot of all the simulations are 11% to 23% lower than values calculated based on the variation of the measured substrate moisture values. However, when looking into individual events, the amount of increased vBot from measurements can be either similar or very different from simulations. Two periods are presented in the following figure as examples.

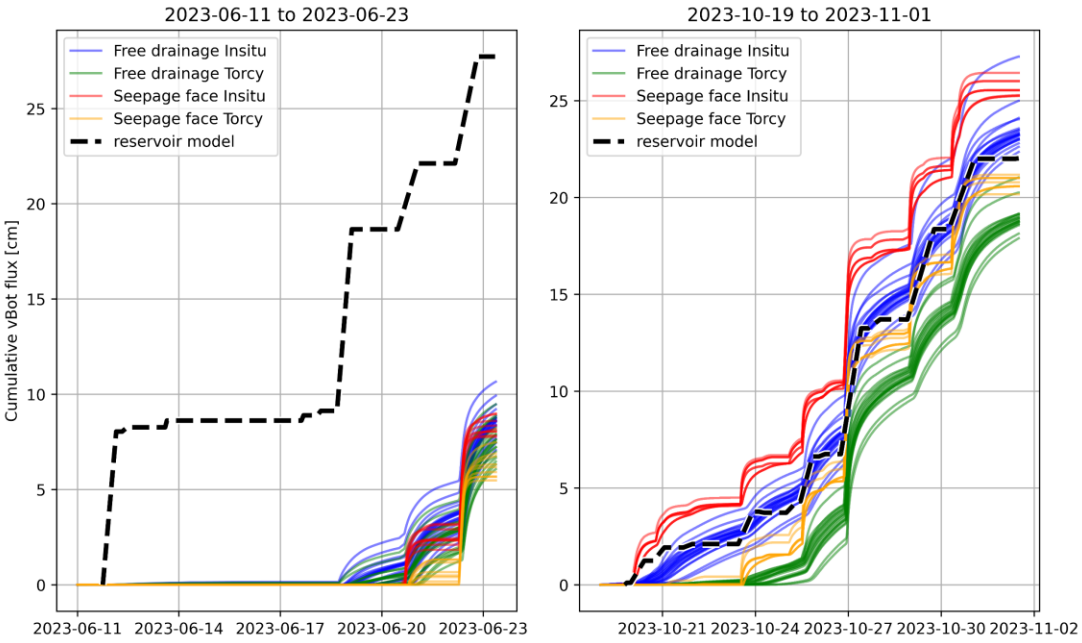

Figure 5-9: Cumulative vBot flux for two specific periods in Step1(left: events after a dry period in June; right: events during wet period in October)

For events with long pre-dry period, the vBot from simulations are lower than field monitoring and sometimes even no vBot from simulations (e.g., for the event in June shown in Figure 5-9, left subplot); while during wet periods, the increase of vBot is similar (Figure 5-9, right subplot). This difference may indicate that: 1) in all the HYDRUS simulations, the substrate becomes too dry after a long dry period, and therefore has the ability to absorb an important part of the water from the next rain event, thus limiting the vBot flux; 2) there may be preferential flow (e.g., cracks in the substrate or along the soil moisture sensor) after long dry periods, allowing the water to quickly bypass the system and being counted as vBot in the monitoring.

5.3.1.1.iii KGE on moisture variation at different depths

Not all the combinations of inputs were able to conduct a converged simulation. In the 168 simulations from Step1 of sensitivity analysis, only 65 simulations successfully converged. As shown in Figure 5-10, the proportion of converging simulations was higher for the free drainage boundary condition than seepage face boundary. For not converged simulations where seepage face boundary was applied, the whole soil profile and the surface storage were observed to be saturated at some point. This is a situation that HYDRUS model cannot mathematically solve. Besides, near half of simulations with free drainage have low (negative) KGE values, which also leads to wider distribution of KGE. On the contrary, simulations with seepage

face are more concentrated and have overall higher KGE compared to free drainage, possibly also due to the higher soil moisture content yielded by the seepage face boundary.

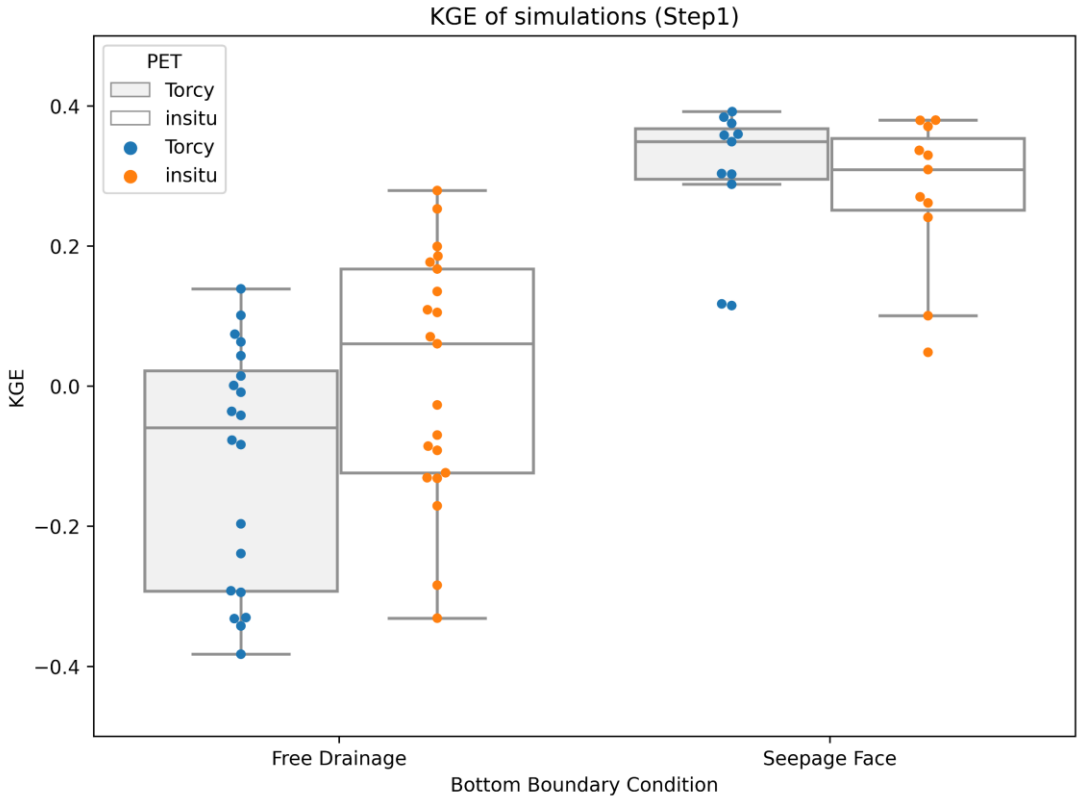

Figure 5-10: Boxplot of KGEs calculated for simulation Step1

For each combination of bottom boundary condition and PET, a set of best fitted (with highest KGE value) media hydraulic parameters were identified. Note that KGE values are very low for all simulations, even the best fitted simulation. This situation is due to a part of poorly fitted curves at certain depths of soil (as shown in Figure 5-11). For instance, the free drainage simulations underestimate the soil moisture for soil deeper than 17.5cm during the dry summer period. While simulations with seepage face boundary overestimate the soil moisture for layers deeper than 17.5cm.

Overall, the free drainage bottom boundary condition has better fit when combined with *in-situ* PET than Torcy PET, while for seepage face, Torcy has better fit goodness than *in-situ* PET. This indicates that the seepage face leads to higher water storage and hence needs higher PET to compensate, while the free drainage is the opposite. Surprisingly, the best fitted hydraulic parameters of substrate media are all from the Rosetta prediction. For free drainage bottom boundary condition (both for Torcy and *in-situ* PET), the simulation which uses Rosetta prediction based on soil

grain size distribution (Sand: Silt: Clay = 65.9: 23.7: 10.4) without providing bulk density has the highest KGE. Similarly, the best fitted seepage face simulations are all based on the default texture input “sandy loam” from HYDRUS as the substrate input. Figure 5-11 compares on the simulated and monitored soil moisture variation at different depths of those input combination. In summary, the most important difference between simulations is induced by the boundary conditions.

According to the soil moisture comparison, the difference brought by different PETs is not very pronounced. While in the surface layers of soil (2.5 cm and 7.5 cm), free drainage shows similar or even better fit goodness than seepage face, large difference can be found in the soil profile deeper than 15 cm (17.5 cm, 27.5 cm and 37.5 cm), where the KGEs of free drainage simulations are extremely low. This situation is possibly due to the “over-drying” in some dry periods created by simulations with free drainage and thus causes lower overall KGE values.

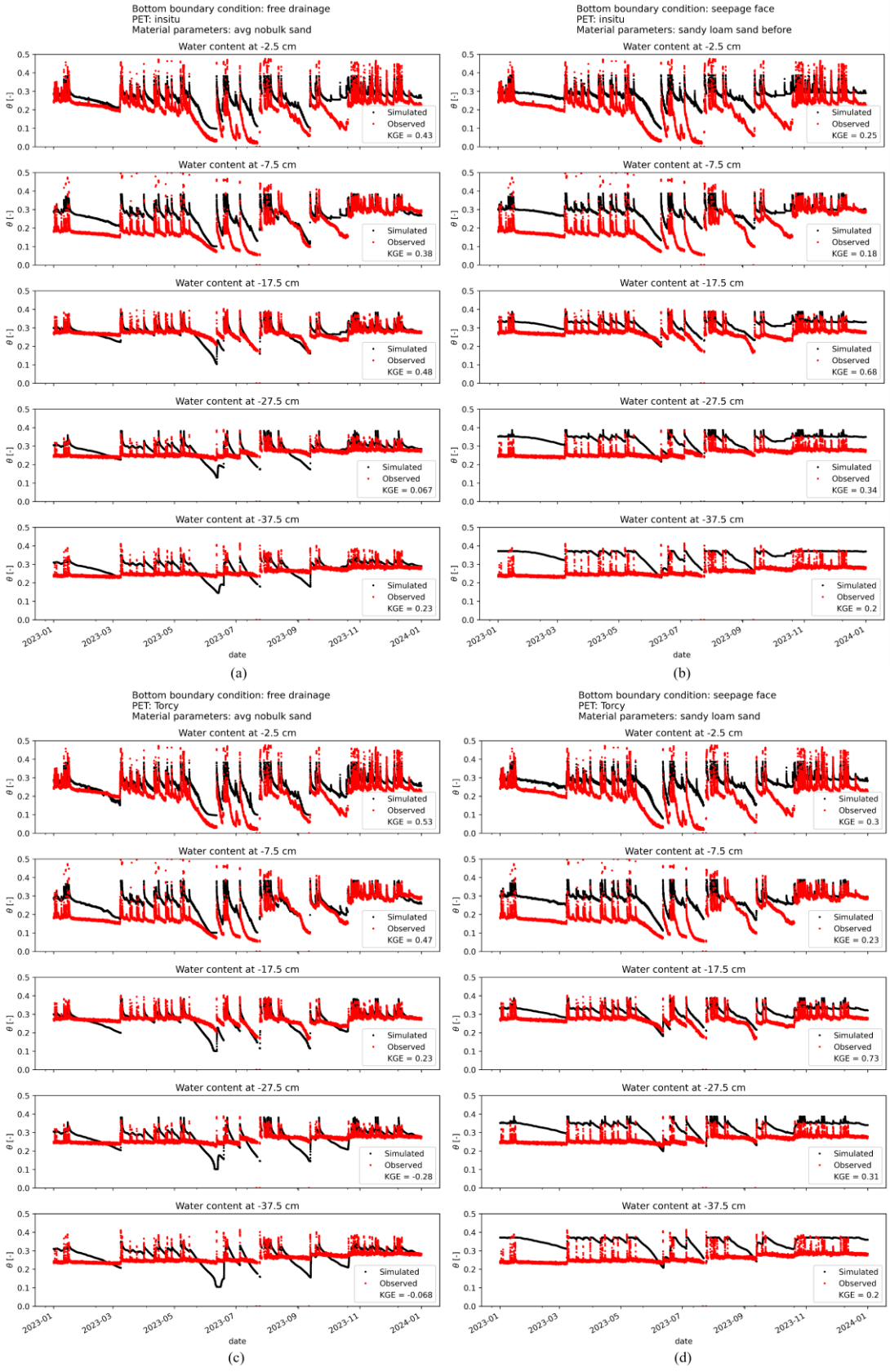

Figure 5-11: Simulated and monitored soil moisture at different depths of best fitted combinations in Step1

5.3.1.2 Step2: SCF, root uptake models and root density distribution

5.3.1.2.i Dynamic of soil moisture change

The four input combinations (1: Free drainage with Torcy PET; 2: Free drainage with *in-situ* PET; 3: Seepage face with Torcy PET; 4: Seepage face with *in-situ* PET) were used for batch simulations in Step 2, employing the best-fitted media hydraulic parameters (i.e., those yielding the highest KGE) for each combination. The dynamic of average media moisture is shown in Figure 112.

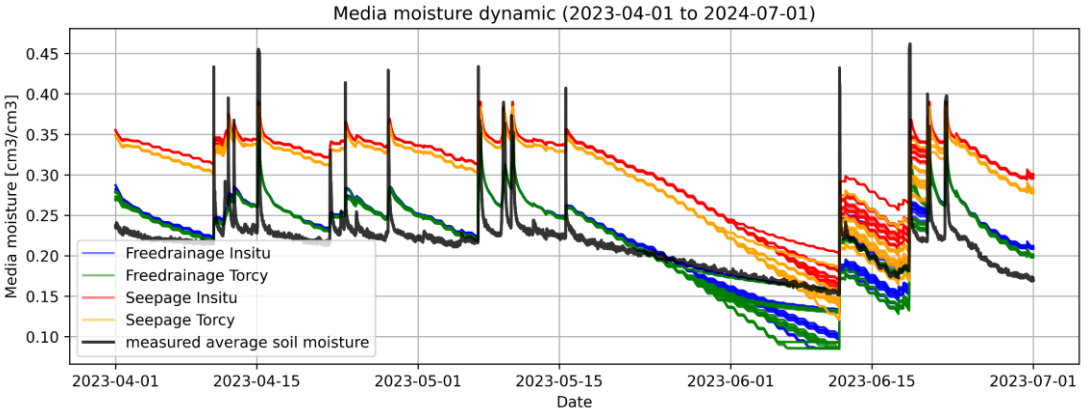

Figure 5-12: The dynamic of average media water content in different simulations for Step2 (period: 2023-04-01 to 2023-07-01)

Compared to Step1, where the different substrate media hydraulic parameters show large variation in the dynamic of moisture, the vegetation parameters do not induce pronounced differences in the dynamic of moisture in Step2. Most of time, curves with the same bottom boundary-PET combination are overlapped, the only limited differences are shown in the end of a long dry period in June.

5.3.1.2.ii Cumulative bottom flux

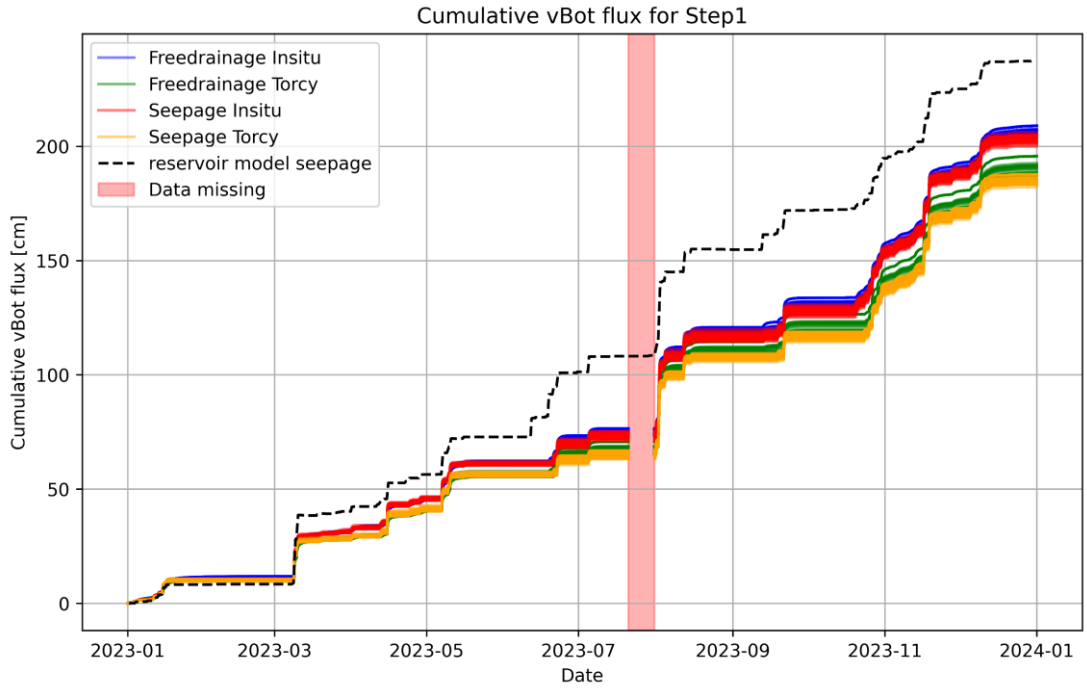

Figure 5-13: Cumulative vBot flux for Step2 (a period of 10 days is missing in the monitored soil moisture data, therefore same period of simulation results is removed and replaced with a shaded gap)

Similar to Step1, different vegetation parameters do not introduce large variations on the cumulative bottom flux. For the annual cumulation, the simulated vBot in Step2 is 12% to 23% less than the monitored vBot. Within each boundary condition and PET combination (each colour), the variation of cumulative vBot caused by vegetation characteristics is less than 10 cm (< 6% of the lowest cumulative vBot)

5.3.1.2.iii KGE on moisture variation at different depths

Figure 5-14 presents the KGE of simulations of Step2. Since the results do not significantly differ between the two PET options, the impact of plant related parameters of KGE values is shown for PET *in-situ* only. Root uptake models (vegetation types) induce nearly no differences and therefore they are not labelled.

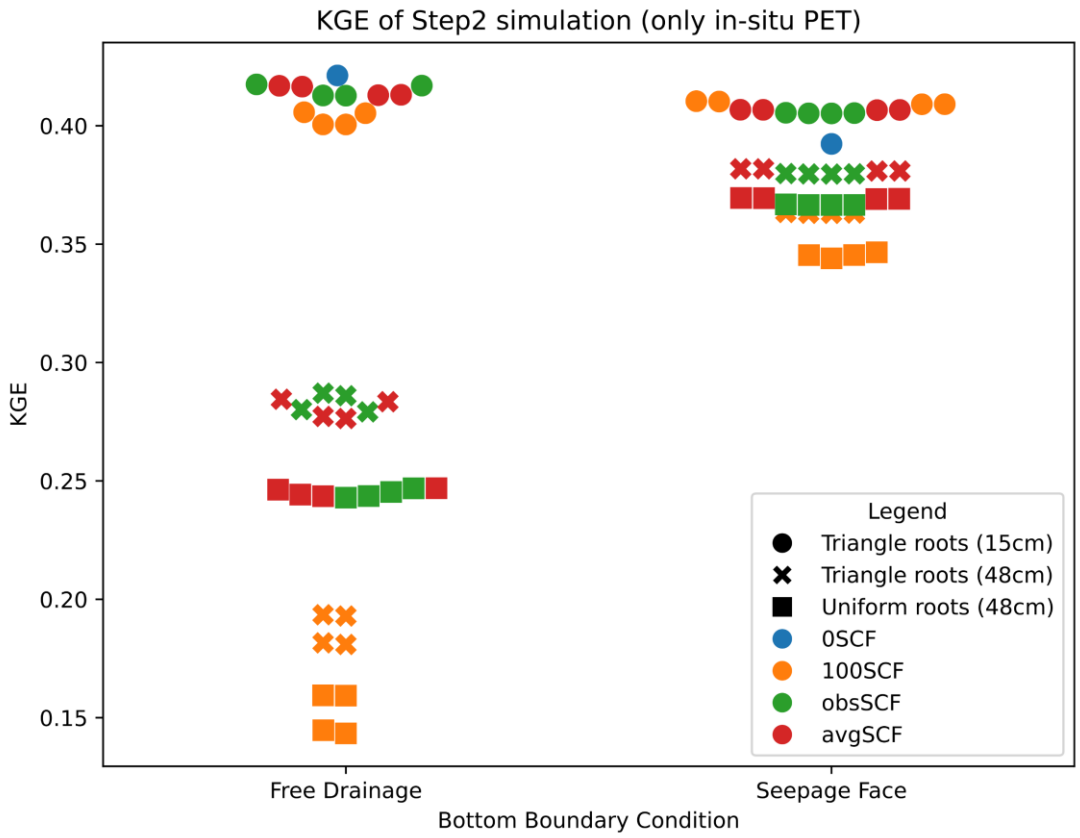

Figure 5-14: KGEs calculated for simulation Step2 (only *in-situ* PET)

Overall, under the current climate input and substrate type, the vegetation type (root uptake model parameters) does not have large impact on the fit goodness. Especially for seepage condition, the effect is very limited, while it is more visible for free drainage. Vegetation parameters have more impact in the case of free drainage boundary conditions than for seepage face. The two vegetation characteristics that have the highest impact on fit goodness are: 1) the maximum root depth (15 cm root depth fits best); 2) the SCF (best fits for 0 coverage and lowest fits for 100% coverage). Aside from these characteristics, the shape of root distribution has more limited impact. Overall, the best fits are obtained for vegetation scenarios that enhance surface drying, but limit water uptake (thus soil drying) in the deeper layers. This result is not in line with initially judged as the most plausible setting to describe the bioretention prototype system.

5.3.2 Model Robustness

5.3.2.1 Drought resilience

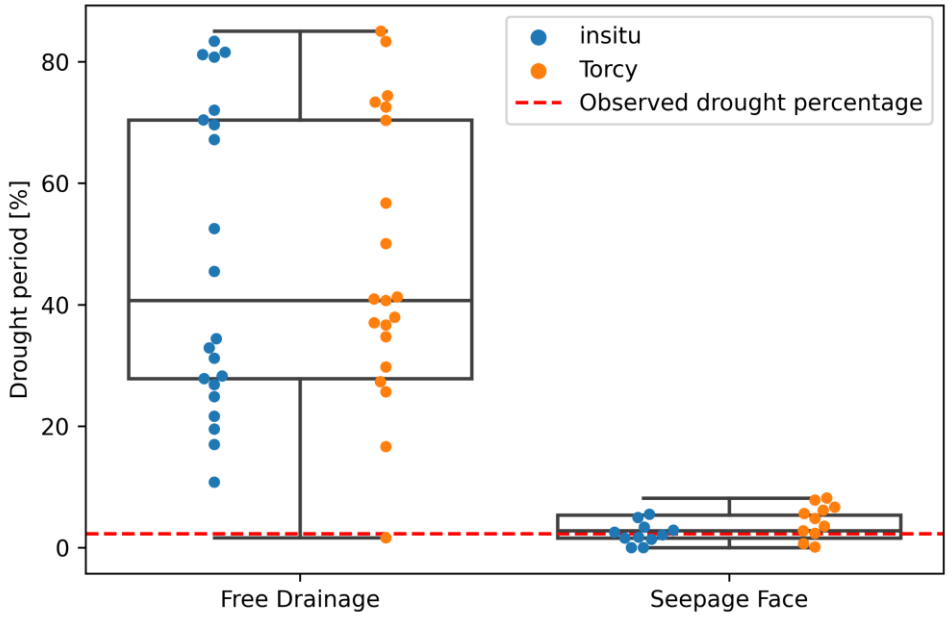

Figure 5-15: Drought period percentage (Step1)

Drought periods (introduced in 5.2.6) can be computed for both by field monitoring and HYDRUS simulations. The percentage of the simulation/monitoring period associated with drought periods is shown in Figure 5-15. In Step1 (upper subplot), free drainage simulation shows much higher proportions of drought period than observations under most of soil hydraulic parameter sets, which is contrary to the field monitoring. On the other hand, the simulations with seepage face boundary show smaller variations, and are overall in line with the monitoring results. Step1 indicates that the drought period percentage estimation is very sensitive to bottom boundary conditions. However, when facing with different media hydraulic parameters, drought period percentage is robust for seepage condition, but has more variation under free drainage condition.

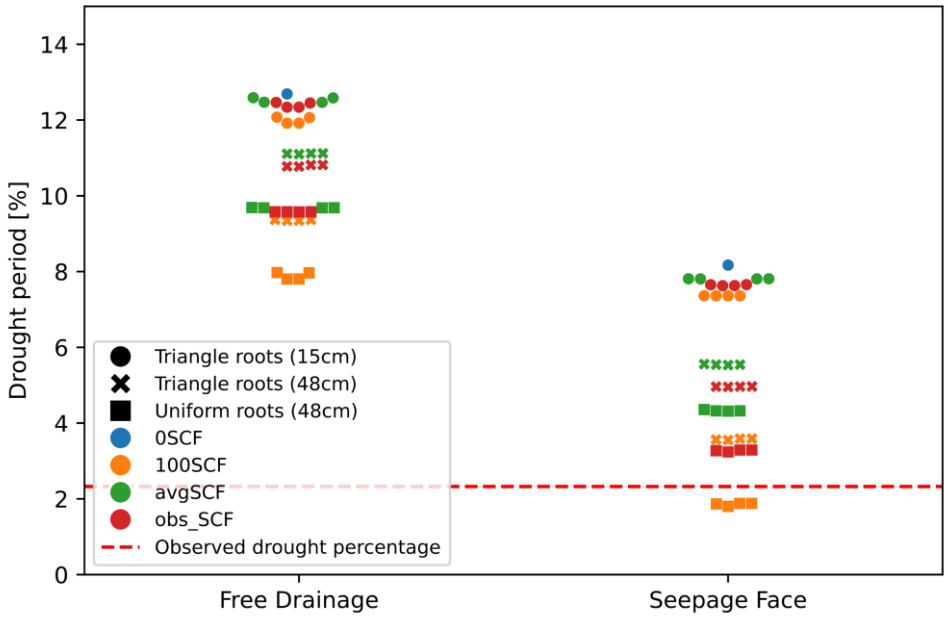

Figure 5-16: Drought period percentage (Step2)

In Step2 (Figure 5-16), shallow root profile simulations are associated with a higher proportion of drought periods compared to the deeper or more uniformly distribution. Compared to uniform root, triangle root has higher drought period percentage, which indicates its better ability to extract water from the surface media (<15cm). In addition, lager variation on drought period percentage between different root depths (triangle 15cm and 48cm) is found under seepage face condition than free drainage, which is due to the difference on the moisture at 15cm (as shown in Figure 5-17 and Figure 5-18).

For SCF, the highest drought period percentage is from 0%SCF (no vegetation and root uptake), this is expectable as surface evaporation becomes limited at much lower water content (hCritA) than transpiration (h3) and never really interrupts (0%SCF also means the model will consider the value of PET as the potential transpiration). But this might also be very related to the ability of water to move upwards from 15cm to the surface. Similarly, when SCF is set to 100%, the given PET is thus considered as only potential transpiration (maximum rate of root uptake), which can be very limited when the soil moisture goes down. This might be the reason of lower drought period percentage for 100SCF in Step2 (also can be supported in in Figure 5-17 and Figure 5-18).

Figure 5-17 (free drainage boundary) and Figure 5-18 (seepage face boundary) present the comparison of soil moisture at 15cm depth provided by different

simulations in Step2 and the monitored moisture at 17.5cm, to limit the number of curves for clear display, only *in-situ* PET and grass root uptake model is taken here. Since no field sensor is available at 15cm, the measurements from a 17.5cm probe is taken, thus the observe moisture here is supposed to be slightly higher than 15cm moisture in reality. For each figure, three subplots are used to present the three root density distributions, different SCF curves are represented in each subplot.

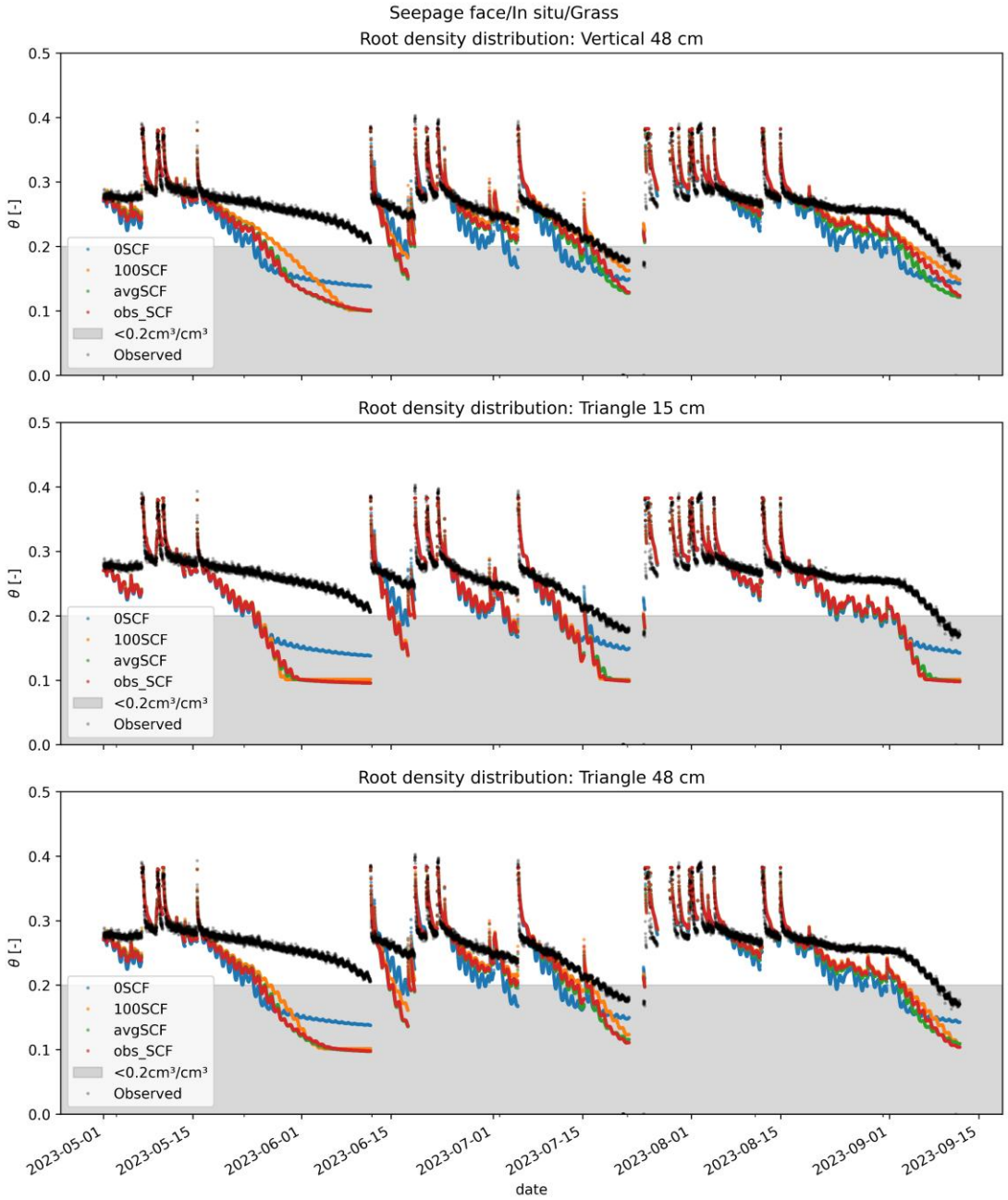

Figure 5-17: Simulated (15cm) and monitored (17.5cm) soil moisture under different root density distribution profiles and SCFs for Free drainage boundary (Period: 2023-05-01 to 2023-09-12)

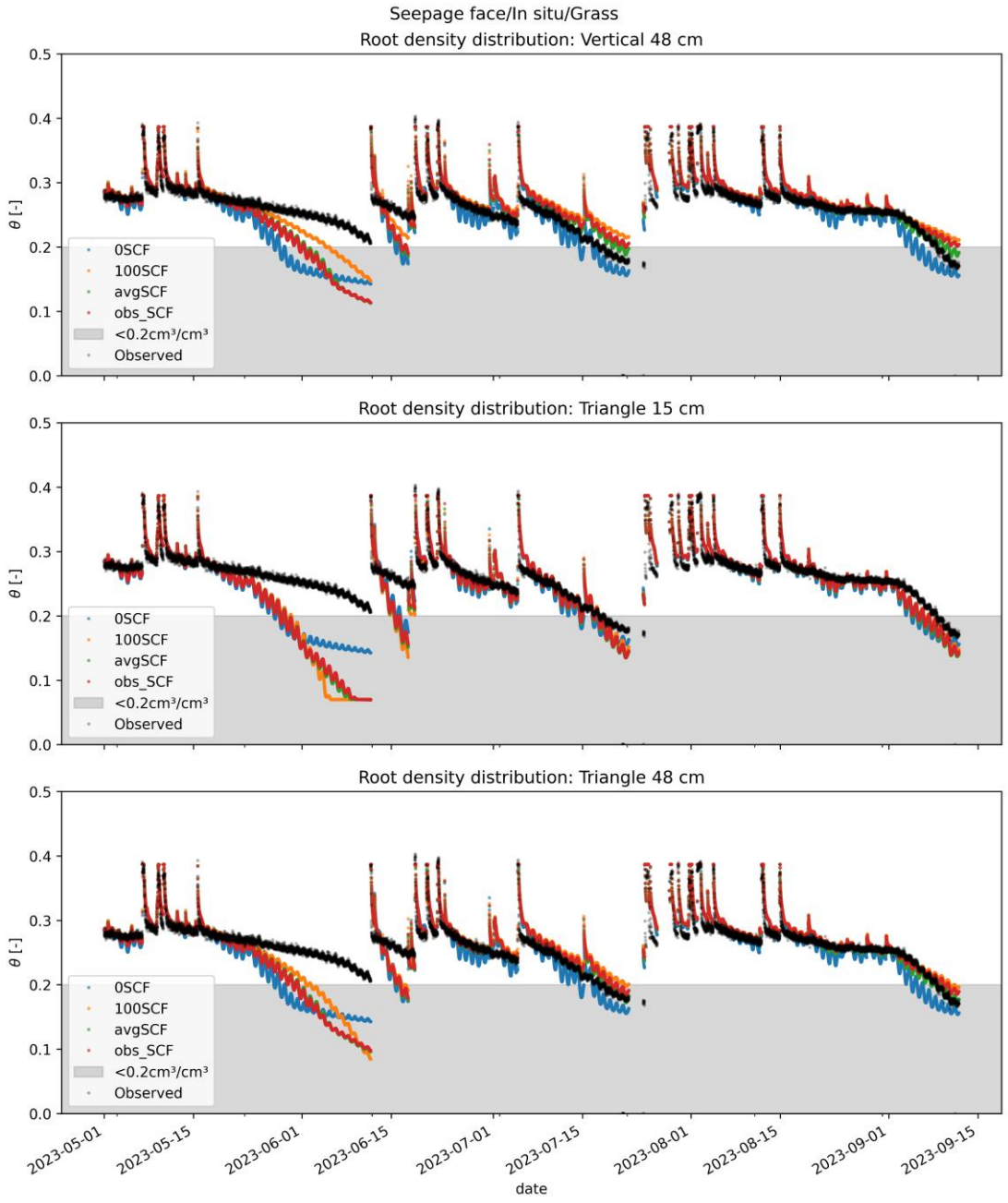

Figure 5-18: Simulated (15cm) and monitored (17.5cm) soil moisture under different root density distribution profiles and SCFs for Seepage face boundary (Period: 2023-05-01 to 2023-09-12)

From Figure 5-17 and Figure 5-18, the overall simulation curves variation trend is similar to the observation curve (with a “shift”), except for the long-dry period starting from the middle of May 2023. This difference can be more related to the difference between PET and ET at this period. From the moisture variation at 15cm, it is difficult to have a clue on which root density distribution profile and the correlation extraction behaviour is closer to the sensor observation (also given the consideration of measurement uncertainties in the field soil moisture). Same conclusion can also be

drawn for the SCF, where the 0%SCF is not realistic but has the highest KGE in Figure 5-16.

5.3.2.2 Water balance

5.3.2.2.i Evapotranspiration

The ET ratio (over the total incoming water) provides a more direct perspective on the vegetation impact on water balance (as shown in Figure 5-19). For Step1, the different bottom boundary conditions and PETs shows clear impact on ET ratio, and simulations with seepage face are closer to the corresponding PET, which is consistent with their lower drought period percentages (in Figure 5-15).

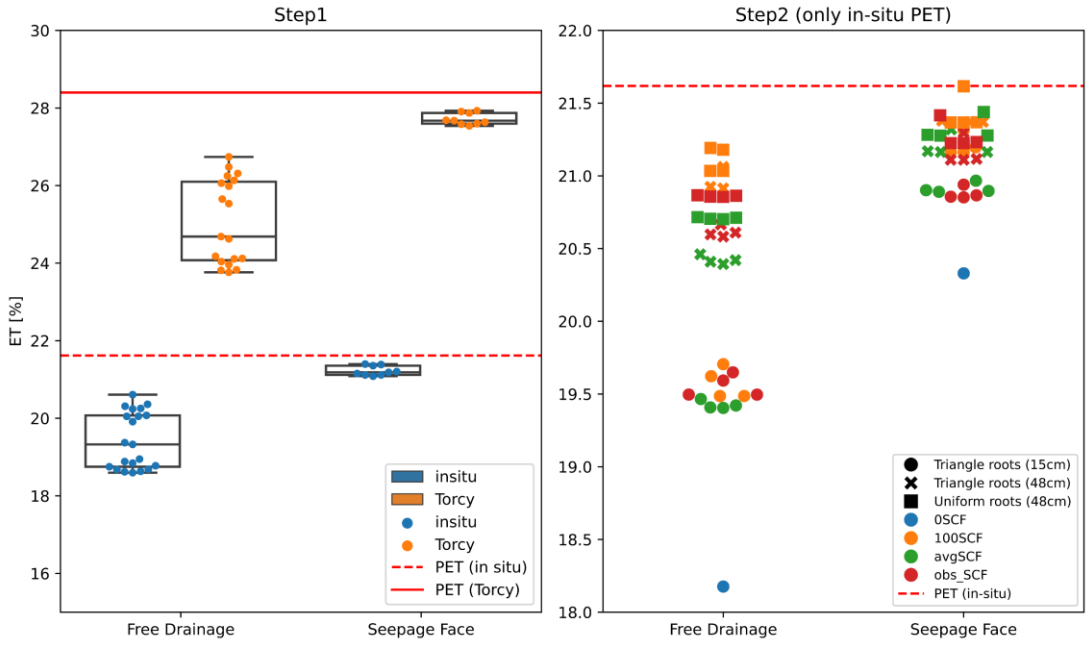

Figure 5-19: Evapotranspiration ratio for Step1 and Step2

Unlike Step1, vegetation parameters tested in Step2 have limited impact of the ET ratio: overall it varies between 18% and 21.5% of the total incoming water, and for seepage boundary the variation is even lower, between 20.3 and 21.6%.

In Step2, higher SCFs (more transpiration) and deeper root density profile lead to higher ET ratios, especially for free drainage boundary. This situation is reasonable since the deeper root and higher transpiration provide the ability to extract water from deeper media, thus unlike the evaporation-dominated case (e.g., 0%SCF), it can avoid the possible limitation on water upwards movement caused by the too-dry media near the very surface. Very dry periods was also found at 15cm (as shown in Figure 5-17 and Figure 5-18). In this case, higher drought period percentage for 0%SCF is not

contradiction with less ET , since the water cannot leave by gradient and evaporation (the slope of moisture decreasing is flatter for 0SCF than others at the first week of June 2023 in Figure 5-17 and Figure 5-18).

Besides, the uniform root (48cm) provides higher ET than triangle root (48cm) and triangle root (15 cm). This difference between root profiles shows larger variation when the bottom boundary is free drainage, which might be due to the higher water stress in the substrate layer during the simulation. Lower water content under free drainage conditions likely indicates greater sensitivity to parameters that control transpiration reduction due to drought stress, especially root depth in this case.

5.3.2.2.ii Volume reduction and groundwater recharge

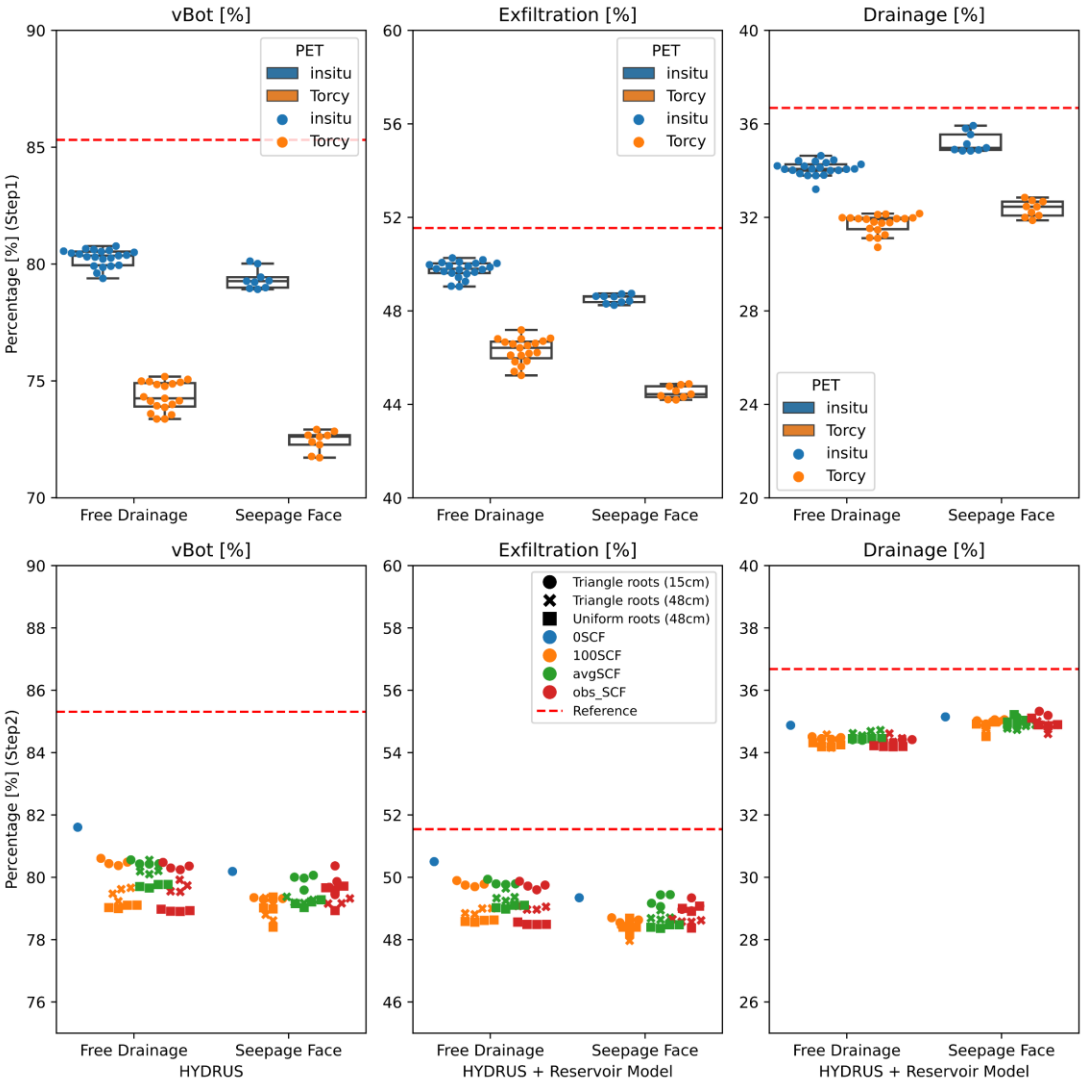

Figure 5-20: Volume reduction and groundwater recharge performance provided by HYDRUS and HYDRUS + Reservoir model. (Step1: the upper row; Step2: the lower row)

In Figure 5-20, the left column subplots are direct outputs from HYDRUS, while the right two columns of subplots are recalculated exfiltration and underdrain flow by using the reservoir model and vBot from HYDRUS. For each column, the upper subplot represents Step1, and the lower subplot is for Step2 (only for *in-situ* PET). Reference values, derived from the observations (as detailed in 4.1.2) is provided for exfiltration and drainage. For Step1, when considering the long-term water balance, the differences brought by bottom boundary conditions (1%) are less than differences brought by PETs (6%). Even though values of vBot flux from HYDRUS are lower than the reference vBot, those differences become smaller after the reservoir model calculations for exfiltration and drainage, especial when the *in-situ* PET is taken. The result of Step2 indicate that the model performance on exfiltration and drainage volume is not sensitive to vegetation characteristics: only 2% difference on exfiltration and less than 1% on drainage. The impact of different root density profiles on vBot and exfiltration is consistent with the results for ET (vBot even mirrors ET). Overall, the combination of HYDRUS and reservoir model shows great robustness on exfiltration and drainage.

5.3.3 Summary of Findings

In this study, a field monitored bioretention cell was represented by combining HYDRUS model with a reservoir model. Different model inputs were tested to evaluate their impact on model fit goodness and hydrological performance. In summary, compared to the field monitoring result, the modelling approach is overall good at representing cumulative flux in water balance (i.e., ET, exfiltration and drainage), but not robust at representing the moisture variation at different depths in the substrate media. Depending on the output considered (and thus the intended use of the model or performance aspect considered), the most influential factors change. If the aim is to evaluate the water balance, only bottom boundary conditions and PET inputs have visible impact. The impact of media hydraulic parameters and vegetation characteristics (i.e., root uptake model, root distribution and SCF) is almost neglectable. When the model is used to evaluate the performance in link to media moisture variation (e.g., drought stress for vegetation), it is mainly sensitive to different bottom boundary conditions and media hydraulic parameters, while PET and vegetation characteristics do not have significant impacts.

The bottom boundary condition directly influences the moisture variation and the residual water within the substrate. Seepage face condition tracts water quickly after the bottom layer of media reaches saturation but retains more water during the dry period, while free drainage boundary takes longer time to drain out and retains less water.

In the case of PET, the two PET inputs (*in-situ* and Torcy) are essentially only different in values, so their effects are generally predictable. However, under prolonged drying, the combination of higher PET and free drainage boundary causes the media within the top 15cm to approach the wilting point, thus make difference. Except that, most of the time the effect of the two PETs does not cause large difference on variation pattern of moisture at different depths.

The differences in soil hydraulic parameters produce more significant output variability in the free drainage lower boundary setting than in the seepage face setting. This impact of soil hydraulic parameters is significant for simulated water content (and thus the model performance assessed from observed water contents), but tends to be more limited for the long term water balance. Note that the analysis on media hydraulic parameters does not involve all possible configurations as convergence could not be achieved for some of them. Additional consideration needs to be given to the fact that we have a more limited number of converging simulations.

For vegetation characteristics, this study indicated that under the case of SC: 1) the contribution of ET to the overall water balance is limited and 2) the system does not undergo significant stress (or drought periods). 3) when the system is not facing significant drought stress, the impact of root uptake models on media moisture is not very visible compared to SCF and root density distribution.

From the perspective of fit goodness, although despite an extensive knowledge of the system, the model failed to accurately replicate soil moisture variations. And the "better" knowledge on media hydraulic parameters (i.e., BEST infiltration test) and surface coverage fraction (vegetation coverage measurement) is no better than simply applying a Rosetta prediction and average SCF. However, given the fact that the appropriate boundary condition is not really able to be identified, it is not surprising that "having more precise" media hydraulic parameter estimation does not change much. Based on KGE and drought indicators, seepage face seems to be slightly more realistic than free drainage. But still, it is far from perfect (and not obvious at all from

Figure 5-17). There may be different explanations to that: 1) the actual lower boundary setting is more complex than a sharp transition (seepage) or perfect continuity (free drainage) and 2) the tested simple media hydrodynamic functions (single permeability and porosity) fail to accurately capture drying dynamics.

One thing that is notable is that for media hydraulic parameters, HYDRUS model handles Rosetta prediction and BEST infiltration inputs differently. For Rosetta prediction, HYDRUS generates high resolution table of water retention curve and hydraulic conductivity function through van-Genuchten equation. While for BEST-infiltration test, the table of water retention curve and hydraulic conductivity function is generated outside of HYDRUS, then entered as a look-up table. However, more frequent convergence issues and also unrealistic ET jumps were observed only for look-up tables. For this reason, the "best knowledge" settings may not always be accurately handled by HYDRUS.

Regardless of the parameters and boundary conditions, the ability of the current modelling approach to replicate water content is quite limited. Thus, although the seepage face shows greater robustness on drought period assessments (based on 15 cm moisture) comparing to free drainage, the overall water storage is inaccurately represented for both boundary conditions. For vegetation parameters, different SCF and root density profiles had a visible effect on drought period percentage, but there was little difference between the different root uptake model inputs (under current climate conditions). However, when assessing long term water balance, e.g., volume reduction (drainage volume) and groundwater recharge (exfiltration volume) , models are quite robust for all the tested inputs. This means that although the flow dynamics simulated through the substrate vary from one configuration to another (and noticeably differ from the observed dynamics), these differences do not lead to significant discrepancies in the partitioning between ET and exfiltration (vBot). This result is potentially related to the fact that, regardless of the configuration, the media moisture in the root zone remains relatively high (due to the nature of the substrate and loading ratio). It may also be due to the fact that the volume available to be evaporated and transpired (i.e., PET) represents only a limited fraction of the incoming volume, hence ultimately the water balance is not very sensitive to variations in different PET inputs.

5.4 CONCLUSIONS

5.4.1 Discussion and Limitations

The first conclusion of this study is that, despite being a quite detailed model, supposedly proving a close description of the physical processes involved in bioretention, the model fails to accurately replicate water content variations. In particular, it seems that there is an issue in our conceptualization of the physics of the system, either in the bottom boundary conditions, the media properties, or both. Under these conditions, using a "better knowledge" of the system or not, does not have much importance.

Regarding to the modelling tool itself, HYDRUS is robust in describing the physical process such as water flow within the media with the build-in van Genuchten model, but shows limitation (and more specifically convergence issues) when using look-up table to specify soil hydraulic properties. In addition, the representation of underdrain and the interaction with underlying soils still needs to be completed with a complementary model (in this case, a reservoir model).

As a summary, the current developed HYDRUS and reservoir model can robustly predict the annual water balance without very different detailed knowledge on the input. Hence, the approach is useful to understand a bioretention's the long-term water balance indicators (e.g., groundwater recharge and volume reduction), However, for event-based water balance indicators, the current modelling approach is very sensitive to the initial condition, thus performed better during wet period but sometimes be highly inaccurate after a prolonged drying period. However, the current model is not robust when being used to evaluate the drought resilience without knowing the specific bottom boundary conditions, SCF and root distribution profile. For media moisture-based indicators related to drought resilience, it is necessary to better conceptualize the bottom boundary condition, and thus some vegetation parameters may also have a significant influence.

Considering the current model is insensitivity to better knowledge inputs, in practical implementations (e.g., to evaluate drainage volume), simulation with a simpler model may be an option and needs further tests. Further investigation could be done on representing the dynamic of soil moisture, and applying different fit goodness indicators for different stages of soil water content change. Besides, even though KGE

is a comprehensive indicator for model fit goodness, it is still not the perfect indicator to evaluate the fitting of soil moisture, particularly because it places less emphasis on the moisture levels during dry period between events, which often deviate from the average.

5.4.2 Perspectives

A key perspective of this study is the need to further investigate the physical processes, which may explain why neither boundary conditions (free drainage and seepage face) can adequately represent the observed media moisture dynamic. One possible explanation is that the complexity of the actual soil system, which may include a combination of capillary barrier, preferential flow, or regions of continuous porous media without exhibit capillary rupture. Whose effect may not be captured by hydraulic parameters derived from texture information or very local measurements. Thus, dual-porosity or dual-permeability models could be more appropriate for capturing the observed behaviour under these contexts. However, a significant challenge is to define parameters for such models. Even inverse modelling can be used in this case, but issues on such inverse modelling are remaining: it simply compensates wrong physical processes by “tuning” soil parameters, which has no transferability to any other site, and also the physical processes might even change over time but not be predictable under inverse modelling.

Another alternative modelling strategy could involve combining the outputs of two separate simulations: one with a free drainage boundary condition and another with a seepage face. Then weighting their proportions over the bioretention area according to hydraulic behaviour across.

Finally, as an extension of this work, the sensitivity analysis should be applied to alternative bioretention designs, particularly those expected to exhibit drier conditions, such as systems with lower HLR or sandier soils. Even in the absence of monitoring data from the specific design site, such an analysis could provide valuable insight into whether water balance evaluations remain robust under a broader range of design configurations.

Chapter 6: Conclusions and Perspectives

This research was conducted under the main objective of elucidating the impacts of various bioretention design characteristics on their hydrological performance, with special focuses on their ability to limit runoff volumes and potential for restoring components of the natural water balance that have been altered by urbanisation (e.g., infiltration, ET).

The first part of the work was based on a thorough literature review, which focused on the hydrological behaviour and performance of bioretention systems worldwide. This review attempted to estimate the linkages between the design and local context of a bioretention system and its hydrological performance, not only through direct takeaway messages synthetised from the various articles, but also based on the construction and analysis of a database with detailed information on 128 bioretention devices extracted from 75 articles and dissertations.

The second part of this work involved experiments on three bioretention cell prototypes (JdB1, JdB2 and SC) in Paris region. JdB1 and JdB2 are lined systems with small HLR (3.9), thick substrate layer (~140 cm) and fine substrate media (silt loam). The design purpose of these two cells was to test a typical garden design in Paris with underground constraints (situations where exfiltration is not allowed or should be limited), as well as to test the impact of the presence (JdB2) or absence (JdB1) of IWS. SC is a partly lined (bottom unlined) cylindric cell with high HLR (13.4), shallower substrate (48 cm) and engineered substrate media (sandy loam). It represents a more conventional bioretention cell design but has a low permeability clay subsoil. This experiment part included continuous hydrological monitoring and field/lab investigations. Based on corresponding data and results, aspects of bioretention system behaviours that were underrepresented in the current literature, were explored, especially the case of unfavourable underground conditions.

Lastly, one prototype (i.e., the SC bioretention cell) has been modelled with the physical-based model HYDRUS-1D. Model's robustness, more specifically the validity of calculated performance indicators, was assessed to better understand its applicability for simulating other design scenarios. In reality, the system is far more

complex than how it is represented in the model due to factors such as media and vegetation heterogeneity. Thus, the modelling part of this research was primarily focused on assessing the model's robustness under these various input types (e.g., different boundary conditions, media hydraulic parameters, PET and vegetation characteristics). This study examined the extent to which the results of such a model can be relied upon, considering the uncertainties and knowledge gaps inherent in bioretention implementation.

6.1 MAIN FINDINGS

6.1.1 Literature Review (Chapter 2)

The investigation on literature indicated several key gaps in the current bioretention studies: 1) Underrepresentation of local contexts and designs. Some local contexts (e.g., regions with high seasonal rainfall variability) are underexplored in existing literature. 2) Lack of long-term or overall water balance monitoring and performance evaluation. Due to the difficulty on long-term monitoring or complete water balance monitoring, current research often focuses on short-term runoff control (e.g., volume reduction or peak flow reduction) while neglecting long-term and overall water balance performance. In this situation, the result might be misleading since part of water balance is not captured (e.g., overestimation in volume reduction when the water bypasses the system through urban karst). 3) Interactions with surrounding soil. In the case of unlined systems, the interaction between bioretention systems and the surrounding soil is not adequately studied, these interactions can potentially make large difference in their water balance. 4) Call for more environmental-friendly bioretention designs. Use local materials instead of the non-renewable or non-biodegradable materials resource (e.g. gravel or geotextile).

6.1.2 Field Experiment (Chapter 3&4)

Over the long continuous observation period on SC, a shallow groundwater intrusion issue was founded, which brought massive of perched groundwater into the system and led failure on the drainage flux measurement. A reservoir model was developed to reconstruct the drainage flux. Based on this model, if the intrusion phenomenon had not occurred, 63% of the total incoming water could have been expected to be controlled (through exfiltration into the ground or evapotranspiration). While for lined systems (where water can be controlled only by ET) this proportion

reaches 43% (JdB1) and 48% (JdB2). From the event-based perspective, the median of volume reduction ratio for JdB1, JdB2 and SC during the experiment period is 64%, 91%, 100%. Additionally, 33%, 58% and 76% of events has volume reduction ratio > 80% for JdB1, JdB2 and SC. Comparing the two cells in JdB, the ET (calculated by closure of water balance) in the IWS cell are 128% (for 2022) and 172% (for 2023) higher than in non-IWS cell. For SC, the reservoir model for drainage flux reconstruction was extended to test different underlying subsoil Ks. Results indicate that a lining would significantly limit the volume reduction performance (total volume reduction falling to 11% instead of 62% for the current setting with low permeability clay soil).

6.1.3 Model Representing (Chapter 5)

The modelling work on SC bioretention system indicates that: 1) compared to the field monitoring result, the modelling approach is overall good at representing cumulative flux in water balance (i.e., ET, exfiltration and drainage), but not robust at representing the moisture variation at different depths in the substrate media; 2) for water balance (flux) simulation, only bottom boundary conditions and PET inputs have visible impact. The impact of media hydraulic parameters and vegetation characteristics (i.e., root uptake model, root distribution and SCF) is almost neglectable; 3) for media moisture variation simulation, the most sensible factors are bottom boundary conditions and media hydraulic parameters, while PET and vegetation characteristics have limited impacts. Thus, considering the knowledge on bottom boundary condition and soil hydraulic parameters are commonly very limited, this modelling approach can be used on water balance flux (e.g., drainage) evaluation, but still needs further testing before extending to other design scenarios (e.g., lower HLR), especially for ET and media moisture evaluation.

6.2 IMPLICATION ON DESIGN

6.2.1 Soil Characteristics

The choice of substrate media is always challenging; coarse media have high conductivity but poor water retention, whereas fine media have good water retention ability but low conductivity. This study tested two different types of media, a conventional engineered media (sandy loam) and a less commonly used fine media (silt loam). As shown in the study, the sandy loam was well suited for vegetation

growth and water requirement, possibly due to the relatively high clay and silt component in the chosen sandy loam media which may have improved water retention. Also, the high HLR and the capillary barrier observed in the substrate-transition interface also helped to maintain the substrate moisture. On the other hand, the finer media in JdB supported nicely the vegetation growth under a low HLR, but it also caused problems such as clogging and cracks for the cell without IWS, and sometimes prolonged surface ponding for the cell with IWS. While an increased proportion of clay generally leads to increased adsorption capacity for the treatment of micropollutants, such soil is also very likely to emit colloids (clay particles) in the percolation water and thus are at risk of increased pollutant transfer to the underground or drainage.

6.2.2 IWS

For an unlined system but with low permeability underground, even a small IWS can improve runoff volume reduction (for example in SC reservoir scenario, a 22 cm of bottom water storage can increase total volume reduction from 11% to 55% compared to a lined case). However, it is needed for a survey of local underground conditions, and ensure the level of the drain is above possible saturation level of surrounding soils. For a lined system with an IWS configurated to maintain permanent saturation at the bottom of the substrate, it allows better water distribution within the substrate (avoids preferential flow due to soil shrinking) and increased ET. To achieve these benefits, it is important to consider whether the outlet height allows the water in the IWS to reach the bottom of the substrate or whether the HLR provides enough water to maintain the IWS level at the substrate bottom. Otherwise, adjusting the substrate media depth may be necessary to ensure that roots can extend into the IWS (but in this case it won't help much for wetting the substrate).

6.2.3 HLR

The ratio between the receiving catchment and the bioretention surface (i.e., HLR) is directly linked to the system water balance. To promote ET, lower HLR should be preferred. For the studied systems, the high HLR (>10) in SC led to lower ET ratio and a large fraction of water cannot be extracted. Finer substrate might be considered as another way to promote ET by ensuring soil moisture under lower HLR. In any case, it is worth noting that, due to the limitation of ET by PET, ET alone is unlikely to provide sufficient volume control to meet current stormwater management

targets under the climate considered - unless considering HLR ratios approaching one. In this case, it is necessary to be careful on the surface size of a bioretention system, especially when the system is dry. When a low HLR is applied to a larger bioretention surface, it may result in an uneven distribution of incoming water. This can leave parts of the cell dry, making them less favourable for supporting ET.

6.2.4 Vegetation

In the modelling results, differences in vegetation characteristics (e.g., root density distribution, root uptake model and SCF) showed neglectable impacts on the bioretention water balance performance. To enhance ET and ensure healthy long-term vegetation development, it is nevertheless valuable to further explore plant selection strategies, which includes considering their ability to extract water within the soil profile and their tolerance to water stress. In another words, optimizing plant selection to better match with predicted water content variations in the whole soil profile could also be interesting to investigate.

6.3 PERSPECTIVES

6.3.1 Further Refinements

This PhD thesis could be further refined based on the following tasks. The first part would be to further investigate the existing experimental bioretention systems. For JdB, we suggest analysing longer periods based on the more reliable monitoring data in 2024 and 2025 (after the issue of inflow monitoring system was solved). A longer and more continuous observation period would allow for a more effective comparison of the long-term performance of the two cells, especially for performance during drought periods. For SC, since the whole experiment site is going to be removed, an "autopsy" could be done: 1) measuring root density profiles (e.g., root length density, root mass density, root length, root diameter); 2) taking soil samples at different depths to check if there has been an evolution in grain size, bulk density and organic matter content; 3) additional infiltration tests to evaluate the heterogeneity at the soil surface, or cover different plant species in order to check the root-mediated effect on the higher/lower local infiltration rate; 4) check the interfaces between substrate media/ sand and sand / gravel to see if the substrate was mixed into the gravels.

Another task would be further exploring the modelling scope. Based on the current HYDRUS-1D modelling work on SC, the sensitivity analysis on SC structure

could be extended to scenarios with lower HLR, and possibly also different substrates (sandier media or JdB silt loam). The main objective of this task would be to assess whether the results related to volume reduction and water balance remain robust under these scenarios. However, for lower HLR, or higher permeability media, the bias between the 1D model and reality may increase due to inhomogeneous infiltration and soil moisture distribution. Moreover, 2D modelling on SC should be done to address the following topics: 1) analysing heterogeneity of infiltration and soil moisture over the area of the garden, and potential consequences on drainage volumes and volume reduction under different HLR ratios; 2) analysing the importance of lateral exfiltration and its effect on the water balance for different surrounding subsoil conditions. For JdB, we suggest modelling the two more complicated systems in HYDRUS-2D for a better understanding of the hydrologic processes in these systems (effect of the bottom IWS condition, spatial heterogeneity of infiltration and soil moisture) and of the factors of divergence between modelling and reality (preferential flow through cracks, surface microtopography, possible clogging of the geotextile). Such modelling would allow for a better assessment of whether and how IWS improves the distribution of infiltration across the entire bioretention area. The influence of the outflow level, whether above or below the substrate-gravel interface, on the hydrodynamics of the system (in the case in JdB2) could especially be checked.

6.3.2 Building on This Work

Three topics can be brought as potential research projects building upon this PhD thesis.

6.3.2.1 Topic1: Towards a flexible assessment tool for evaluating bioretention hydrological performance under various designs and contexts

The first topic is to develop a flexible assessment tool for evaluating bioretention hydrological performance under various designs and contexts. Based on the modelling work in this thesis, HYDRUS demonstrates robust performance in simulating water balance even though the soil moisture profile is not very well represented. This suggests that a simpler model for representing water balance may be feasible. The objective of this study is to create a modelling tool which can adjust its mathematic solution based on the available knowledge of inputs from the users and its intended usage, and also able to represent various designs and contexts. This study can be conducted by:

1) Applying the current sensitivity framework from this study on other more conceptual models such as SWMM, check their difference on representing capability and sensitivity to the various input knowledge levels (based on the work from the current PhD project). Exploring the possibility of simplifying physical-based solutions (HYDRUS) to simpler equations (SWMM) and eventually building a flexible framework which allows choosing the suitable calculation method for different hydrological processes.

2) Based on this framework, the influence of local contexts, design parameters and configurations can be explored. This step can provide design recommendations or guidelines. Optionally, this framework can also serve the construction of a design tool based on meta-models adjusted from a large dataset generated from simulations, over a wide range of designs and contexts. This approach can be similar to the one developed by Sage et al. (2024).

6.3.2.2 Topic2: Choosing the right combination of vegetation and substrate: towards a resilient vegetation development

The role of plants, although mentioned in the current study, was not comprehensively evaluated due to the complexity of the plant species and time limitation. Knowledge of the physiological responses of different types of vegetation to bioretention conditions, under various design configurations and future climate extremes related to climate change, is needed. To ensure a bioretention system have a good functioning over the long term and limited maintenance issues, plant have to survive and develop correctly. Thus, the objectives of this study are 1) understand how bioretention hydrologic conditions impact plant physiology, and thus resilience of the system and ecosystem services; 2) investigate how plant development affects the hydrology of bioretention systems, with a focus on the impact of roots (e.g., infiltration rates, preferential flow). A possible methodology would be to have the bioretention columns in a greenhouse, under controlled irrigation conditions that allow to simulate different scenarios of drought or water excess, and then measure key vegetation parameters (e.g., stomatal conductance, leaf area index, plant height, canopy cover, and root density distribution). Lastly, combining with the hydrological flux and stock measurements, the impact of different irrigation scenarios on plant ecophysiology (to identify if the plant is under drought/wet stress) could be evaluated. The impact of

plant species and root traits on bioretention system hydrodynamics, such as infiltration rates or volume reduction ratio, could also be assessed.

6.3.2.3 Topic3: Low carbon footprint designs for climate extremes resilient bioretention systems

This topic aims to extend the current research by further exploring how to simultaneously ensure runoff control, water availability and vegetation growth. The objective is to investigate strategies or bioretention designs to ensure water availability for vegetation, enhancing its resilience to future climate extremes. It will explore methods for water storage to mitigate drought while preventing waterlogging during heavy rainfall, using environmentally friendly solutions with a limited carbon footprint. The general approach can be based on the following ideas: 1) Coupling international benchmarking and identifying climate-resilience strategies; 2) Narrowing down the selection of solution based on hydrodynamic modelling; 3) Assessing environmental impacts and carbon footprint of each solution to ensure long-term sustainability (life cycle analysis).

6.3.2.4 Topic4: Alternative hydraulic functions for water movement modelling in bioretention systems

Preliminary findings from the current study suggest that HYDRUS (with single porosity models e.g., Richards equation coupled with van Genuchten and Brooks and Correy models, and conventional free drainage or seepage face bottom conditions) cannot accurately reproduce observed soil moisture dynamics. This research would aim to evaluate the ability of different water flow models in simulating soil moisture content variations within bioretention systems (further developed from Asra, 2023). The potential limitations of current hydraulic parameterization and functions in representing a system with heterogeneous substrate (with roots and other possibilities to cause preferential flows) would need to be investigated. This study could address the following aspects:

1) Compare and evaluate other water flow models (e.g., dual-permeability models) in HYDRUS on their performance on reproducing the soil moisture dynamic at different depths.

2) Test invert solution from the field monitoring data and compare the soil hydraulic parameters from invert solutions with BEST-infiltration tests and Rosetta prediction. Check the physical meaning of these invert solution

parameters and the possibility to extend them for other studies cases (if logical pattern is found).

6.3.3 Future Research Outlook

Looking forward, based on the findings from the existing literature and the experimental and modelling work in this study, future research could also focus on:

1) High-efficiency field surveys or wider implementation of low-cost sensor on real-world bioretention systems to evaluate their long-term behaviour and maturing.

2) Examine whether a system designed to enhance ET, reduce outflow, and increase retention time can also improve pollutant retention, particularly for those micropollutants that are not easily absorbed by substrate media. The main idea here is limiting bottom flux to reduce pollutant leaching, as well as increasing the residence time within the substrate to enhance biodegradation effects.

3) Examine the consequences of the interactions between bioretention systems and groundwater. While some studies have already addressed this issue (K. Zhang et al., 2018; K. Zhang & Chui, 2019), a specific focus could be placed on: i) how to adapt their design and deployment strategies in such contexts; or ii) the risk of forming localized saturated water lenses beneath bioretention systems in layered soil systems. A systematic analysis of the hydrological impact and performance of bioretention (across a variety of climate, hydrogeology contexts, etc.) could also be conducted, following the approach developed in (Pophillat et al., 2022).

Chapter 7: Appendices

7.1 APPENDIX 1 - AI USAGE STATEMENT

In this study, AI tools have been used mainly in two aspects: 1) coding assistant (GitHub Copilot Education subscription), including automatic code generation and debugging; 2) language polishing, including very limited number of sentences rephrasing, words choosing and translation (ChatGPT and DeepL).

Additionally, a customized ChatGPT-4.0 model (https://chat.openai.com/g/g-eRlJew2v3-research-article-extractor-experimental-setting) was developed specifically to collect information on experimental setting from literature in the literature review. The model was built on technical instruction and a knowledge base document summarized from 57 human-read articles from the selected literature list. 16 articles were tested on this model, the model shows good capability on text mining especially for long text documents, but the accuracy of the model output varied each time even on the same article and hence could not be directly used. However, with human validation, the ChatGPT-assistant could provide a "search using a clue" approach for information extraction for a research article showing the potential of this type of approach for literature screening. The instruction and knowledge base document are provided as the supplementary S4 together with the article (https://ars.els-cdn.com/content/image/1-s2.0-S0048969725003183-mmc4.docx). However, no results generated from the above AI model was eventually used in the final literature review.

7.2 APPENDIX 2 – SEARCHING TERMS

TITLE-ABS-KEY (bioretention OR biofiltration OR bioinfiltration OR biofilter OR "rain garden" OR raingarden OR bioswale) AND ((storm* OR rain* OR runoff) OR (hydrau* OR hydrolog* OR infiltration OR evapo* OR percolation)) AND NOT TITLE-ABS-KEY (wastewater OR sewage) AND PUBYEAR > 1999 AND PUBYEAR < 2023 AND PUBYEAR > 1999 AND PUBYEAR < 2023

7.3 APPENDIX 3 – LITERATURE DATABASE

Database for monitored bioretentions:

https://ars.els-cdn.com/content/image/1-s2.0-S0048969725003183-mmc2.zip

Database for real-world bioretentions:

https://ars.els-cdn.com/content/image/1-s2.0-S0048969725003183-mmc3.zip

7.4 APPENDIX 4 – TABLES IN SENSOR CALIBRATION

Table 7-1: The prediction interval boundary of CS451_4 water level sensor

lab [mm]	sensor average [mm]	lower error [mm]	upper error [mm]	upper error [%]	lower error [%]	Prediction [mm]
6.8	14.8	1.7	1.7	23.7	23.7	7.1
18.8	28.2	1.7	1.7	8.1	8.1	20.1
28.0	34.0	1.7	1.7	6.3	6.3	26.4
68.3	75.2	1.7	1.7	2.5	2.5	67.9
138.5	145.1	1.7	1.7	1.2	1.2	138.2
260.8	266.4	1.7	1.67	0.6	0.6	260.4
404.0	409.0	1.7	1.7	0.4	0.4	403.9
477.0	482.1	1.7	1.7	0.4	0.4	477.5

Table 7-2: The prediction interval boundary of Q_IFC100_DN25 flowmeter

injection [L/min]	sensor average [L/min]	lower error [L/min]	upper error [L/min]	upper error [%]	lower error [%]	Prediction [L/min]
0.026	0.056	0.056	0.056	122.3	122.3	0.036
0.132	0.167	0.056	0.056	38.5	38.5	0.148
0.311	0.296	0.056	0.056	20.2	20.2	0.278
0.849	0.850	0.056	0.056	6.7	6.7	0.837
1.317	1.324	0.056	0.056	4.3	4.3	1.315
1.889	1.884	0.057	0.057	3.0	3.0	1.879
2.433	2.467	0.058	0.058	2.3	2.3	2.468
2.435	2.430	0.058	0.058	2.4	2.4	2.431

Table 7-3: The prediction interval boundary of SoilVUE50_4 &100_2 (unit: cm3/cm3)

Sample results	Sensor average	Sensor depth	Sample depth	Sensor ID	Lower error	Upper error	Prediction
9.45	3.93	0.5	2.5	50_4	5.67	5.67	9.94
9.2	5.39	4.5	4.5	100_2	5.54	5.54	11.04
16.79	11.16	5.5	8.5	50_4	5.20	5.20	15.40
16.7	11.98	14.5	15.5	100_2	5.17	5.17	16.02
15.90	14.42	45.5	50	50_4	5.12	5.12	17.87
25.1	17.61	34.5	35	100_2	5.12	5.12	20.28
21.45	17.62	15.5	17.5	50_4	5.12	5.12	20.28
19.7	17.73	24.5	25	100_2	5.12	5.12	20.37
23.74	23.77	25.5	27.5	50_4	5.34	5.34	24.93
24.2	25.91	44.5	45.5	100_2	5.49	5.49	26.55
27.64	26.77	35.5	35	50_4	5.55	5.55	27.20

Table 7-4: The prediction interval boundary of CS650-VS (unit: cm3/cm3)

Sample results	Sensor average	Sensor depth	Sample depth	Sensor ID	Lower error	Upper error	Prediction
14.60	25.00	30.00	29.50	S20	10.06	53.81	18.70
15.90	22.50	20.00	19.75	S5, S17	9.98	50.28	19.86
16.10	15.00	10.00	10.00	S2	9.97	49.78	20.04
16.80	19.00	50.00	50.00	S9	9.94	48.10	20.66
17.88	16.00	30.00	30.00	S4	9.89	45.73	21.63
18.04	23.00	10.00	11.00	S3	9.88	45.39	21.77
19.10	19.00	50.00	50.00	S7	9.84	43.32	22.72
19.80	28.00	90.00	90.00	S10	9.82	42.06	23.34
20.51	20.00	10.00	10.00	S1	9.80	40.86	23.98
21.11	24.00	50.00	50.00	S8	9.78	39.90	24.52
21.80	22.00	30.00	30.50	S6	9.77	38.87	25.13
23.10	30.00	70.00	71.00	S15, S3	9.75	37.09	26.29
23.20	30.00	130.00	130.00	S13	9.75	36.96	26.38
23.50	19.00	50.00	50.50	S9	9.75	36.58	26.65
24.44	27.00	10.00	13.00	S2	9.74	35.44	27.49
26.70	27.00	10.00	12.50	S16	9.76	33.06	29.51
29.30	33.00	90.00	91.00	S10	9.81	30.82	31.84
29.90	30.00	50.00	47.50	S22	9.83	30.37	32.37
30.40	33.00	20.00	21.75	S1, S19	9.85	30.01	32.82
33.00	43.00	90.00	89.50	S25	9.96	28.35	35.14
35.50	38.00	130.00	124.00	S14	10.11	27.06	37.38
36.00	38.00	90.00	90.00	S11	10.15	26.83	37.83
36.87	43.00	130.00	124.00	S28	10.21	26.45	38.61
42.20	37.00	130.00	130.00	S13	10.68	24.63	43.37

7.5 APPENDIX 5 – TABLES OF DRY PERIODS STATISTICS

Table 7-5: Dry periods statistics for JdB1

ID	dry_start	dry_end	outflow (mm)	delta_soil_storage (mm)	delta_gravel storage (mm)	ET_total (mm)	ET_daily (mm)	duration	avg soil moisture (start)	avgsoil moisture (end)
0	8/22/2022	9/2/2022	0.12	-17.74	0.00	17.63	1.60	11 days	0.25	0.24
1	9/13/2022	9/14/2022	0.12	0.03	0.00	-0.15	-0.15	1 days	0.23	0.23
2	9/17/2022	9/24/2022	0.00	-12.56	0.00	12.56	1.79	7 days	0.23	0.22
3	10/5/2022	10/13/2022	0.68	-4.64	0.00	3.96	0.50	8 days	0.22	0.22
4	10/27/2022	10/31/2022	0.60	-4.56	0.00	3.96	0.99	4 days	0.28	0.27
5	11/9/2022	11/15/2022	1.04	-7.53	0.00	6.49	1.08	6 days	0.28	0.27
6	12/1/2022	12/2/2022	0.60	-4.54	0.00	3.94	3.94	1 days	0.31	0.31
7	12/8/2022	12/14/2022	4.58	-11.69	0.00	7.11	1.19	6 days	0.31	0.30
8	12/17/2022	12/18/2022	0.12	-2.39	0.00	2.27	2.27	1 days	0.30	0.30
9	1/22/2023	1/26/2023	2.39	-7.62	3.00	2.23	0.56	4 days	0.34	0.33
10	1/29/2023	1/30/2023	0.32	-0.86	0.00	0.54	0.54	1 days	0.33	0.33
11	2/2/2023	2/4/2023	0.48	-0.86	0.00	0.38	0.19	2 days	0.33	0.33
12	2/7/2023	3/7/2023	3.55	-18.09	0.00	14.54	0.52	28 days	0.33	0.32
13	3/13/2023	3/14/2023	2.03		-171.00			1 days		0.35
14	4/5/2023	4/10/2023	1.63	-4.78	0.00	3.15	0.63	5 days	0.34	0.34
15	4/18/2023	4/22/2023	2.79	-17.66	0.00	14.88	3.72	4 days	0.35	0.34

16	5/4/2023	5/5/2023	0.20	-7.22	0.00	7.02	7.02	1 days	0.33	0.33
17	5/18/2023	6/11/2023	2.71	-99.31	0.00	96.60	4.03	24 days	0.33	0.27
18	6/14/2023	6/17/2023	0.00	-14.16	0.00	14.16	4.72	3 days	0.26	0.25
19	6/22/2023	7/15/2023	66.05		0.00			23 days		0.22
20	7/18/2023	7/23/2023	1.12	-9.35	0.00	8.24	1.65	5 days	0.22	0.21
21	8/10/2023	8/11/2023	0.16	-6.33	0.00	6.17	6.17	1 days	0.26	0.26
22	8/17/2023	8/19/2023	0.32	-5.31	0.00	4.99	2.50	2 days	0.25	0.25
23	8/22/2023	8/27/2023	1.39	-12.26	0.00	10.86	2.17	5 days	0.25	0.24
24	9/3/2023	9/12/2023	0.04	-15.66	0.00	15.62	1.74	9 days	0.23	0.22
25	9/15/2023	9/17/2023	0.04	-1.00	0.00	0.96	0.48	2 days	0.22	0.22
26	9/25/2023	10/3/2023	0.04	-8.09	0.00	8.05	1.01	8 days	0.22	0.21
27	10/6/2023	10/12/2023	0.08	-3.24	0.00	3.16	0.53	6 days	0.21	0.20
28	10/17/2023	10/18/2023	0.00	-0.54	0.00	0.54	0.54	1 days	0.20	0.20

Table 7-6: Dry periods statistics for JdB2

ID	dry_start	dry_end	outflow (mm)	delta_soil_storage (mm)	delta_gravel storage (mm)	ET_total (mm)	ET_daily (mm)	duration	avg soil moisture (start)	avgsoil moisture (end)
0	8/22/2022	9/2/2022	0.00	-34.53	-10.80	45.33	4.12	11 days	0.39	0.36
1	9/13/2022	9/14/2022	0.00	-7.59	-1.50	9.09	9.09	1 days	0.39	0.39
2	9/17/2022	9/24/2022	0.00	-13.28	-3.90	17.18	2.45	7 days	0.38	0.37
3	10/5/2022	10/13/2022	0.36	-30.18	0.00	29.82	3.73	8 days	0.43	0.41
4	10/27/2022	10/31/2022	3.74	-13.14	0.00	9.40	2.35	4 days	0.43	0.42
5	11/9/2022	11/15/2022	8.84	-19.82	0.00	10.97	1.83	6 days	0.44	0.43
6	12/1/2022	12/2/2022	2.79	-3.49	0.00	0.70	0.70	1 days	0.44	0.44
7	12/8/2022	12/14/2022	11.75	-20.15	0.00	8.40	1.40	6 days	0.44	0.42
8	12/17/2022	12/18/2022	0.72	-1.64	0.00	0.93	0.93	1 days	0.42	0.42
9	1/22/2023	1/26/2023	9.88	-15.10	0.00	5.22	1.31	4 days	0.44	0.43
10	1/29/2023	1/30/2023	1.23	-0.93	0.00	-0.31	-0.31	1 days	0.43	0.43
11	2/2/2023	2/4/2023	1.79	-5.63	0.00	3.83	1.92	2 days	0.43	0.42
12	2/7/2023	3/7/2023	9.12	-28.05	0.00	18.93	0.68	28 days	0.42	0.41
13	3/13/2023	3/14/2023	2.67		0.00			1 days		0.44
14	4/5/2023	4/10/2023	4.06	-14.68	0.00	10.62	2.12	5 days	0.43	0.42
15	4/18/2023	4/22/2023	7.41	-16.28	0.00	8.87	2.22	4 days	0.44	0.43
16	5/4/2023	5/5/2023	0.64	-5.09	-32.40	36.86	36.86	1 days	0.43	0.43
17	5/18/2023	6/11/2023	4.54		-14.40			24 days	0.44	

18	6/14/2023	6/17/2023	0.00		-4.20			3 days		
19	6/22/2023	7/15/2023	12.03		-8.10			23 days		
20	7/18/2023	7/23/2023	0.24		-9.00			5 days		
21	8/10/2023	8/11/2023	1.16		0.00			1 days		
22	8/17/2023	8/19/2023	2.71		-8.40			2 days		
23	8/22/2023	8/27/2023	2.43		-6.30			5 days		0.42
24	9/3/2023	9/12/2023	0.52	-42.48	-9.00	50.96	5.66	9 days	0.42	0.39
25	9/15/2023	9/17/2023	0.40	-11.30	0.00	10.90	5.45	2 days	0.40	0.39
26	9/25/2023	10/3/2023	3.55	-40.60	0.00	37.05	4.63	8 days	0.44	0.41
27	10/6/2023	10/12/2023	1.43	-8.03	0.00	6.59	1.10	6 days	0.41	0.40
28	10/17/2023	10/18/2023	0.24	-4.24	0.00	4.00	4.00	1 days	0.41	0.40

Table 7-7: Dry periods statistics for SC

ID	dry_start	dry_end	delta_soil_storage (mm)	ET_total (mm)	ET_daily (mm)	duration	avg soil moisture (start)	avgsoil moisture (end)
0	9/13/2021	9/14/2021	-0.78	0.78	0.78	1 days	0.23	0.23
1	9/17/2021	9/19/2021	-5.30	5.30	2.65	2 days	0.25	0.24
2	9/22/2021	9/26/2021	-4.19	4.19	1.05	4 days	0.25	0.24
3	10/7/2021	10/8/2021	-1.14	1.14	1.14	1 days	0.25	0.25
4	10/10/2021	10/18/2021	-4.03	4.03	0.50	8 days	0.25	0.24
5	10/24/2021	10/25/2021	-0.68	0.68	0.68	1 days	0.25	0.25
6	10/28/2021	10/29/2021	-0.72	0.72	0.72	1 days	0.25	0.25
7	11/7/2021	11/10/2021	-1.12	1.12	0.37	3 days	0.25	0.25
8	11/12/2021	11/13/2021	0.04	-0.04	-0.04	1 days	0.25	0.25
9	11/20/2021	11/21/2021	-0.24	0.24	0.24	1 days	0.25	0.24
10	11/23/2021	11/26/2021	-1.02	1.02	0.34	3 days	0.25	0.24
11	12/14/2021	12/24/2021	-3.65	3.65	0.37	10 days	0.25	0.25
12	12/31/2021	1/3/2022	-2.48	2.48	0.83	3 days	0.26	0.25
13	1/6/2022	1/7/2022	-2.21	2.21	2.21	1 days	0.26	0.25
14	1/12/2022	1/16/2022	-2.09	2.09	0.52	4 days	0.26	0.25
15	1/18/2022	1/19/2022	-0.16	0.16	0.16	1 days	0.25	0.25
16	1/22/2022	1/27/2022	-0.96	0.96	0.19	5 days	0.25	0.25
17	1/31/2022	2/1/2022	-0.50	0.50	0.50	1 days	0.25	0.25
18	2/3/2022	2/4/2022	-0.23	0.23	0.23	1 days	0.25	0.25
19	2/9/2022	2/10/2022	-0.37	0.37	0.37	1 days	0.25	0.25
20	2/13/2022	2/14/2022	-0.20	0.20	0.20	1 days	0.25	0.25
21	4/2/2022	4/5/2022	-2.30	2.30	0.77	3 days	0.25	0.24
22	4/11/2022	4/13/2022	-1.04	1.04	0.52	2 days	0.25	0.24
23	4/15/2022	4/23/2022	-6.16	6.16	0.77	8 days	0.25	0.23
24	4/25/2022	5/4/2022	-7.91	7.91	0.88	9 days	0.24	0.23

25	5/6/2022	5/9/2022	-1.22	1.22	0.41	3 days	0.23	0.22
26	5/11/2022	5/15/2022	-4.73	4.73	1.18	4 days	0.21	0.20
27	5/18/2022	5/19/2022	-1.49	1.49	1.49	1 days	0.22	0.21
28	5/28/2022	6/3/2022	-7.16	7.16	1.19	6 days	0.22	0.21
29	6/11/2022	6/19/2022	-17.23	17.23	2.15	8 days	0.24	0.20
30	6/27/2022	6/29/2022	-3.47	3.47	1.74	2 days	0.23	0.23
31	7/2/2022	7/5/2022	-6.92	6.92	2.31	3 days	0.24	0.22
32	7/8/2022	7/20/2022	-22.47	22.47	1.87	12 days	0.22	0.16
33	7/24/2022	8/4/2022	-13.32	13.32	1.21	11 days	0.22	0.19
34	8/27/2022	8/30/2022	-3.91	3.91	1.30	3 days	0.23	0.22
35	9/1/2022	9/2/2022	-1.12	1.12	1.12	1 days	0.22	0.21
36	9/4/2022	9/5/2022	-1.22	1.22	1.22	1 days	0.22	0.21
37	9/13/2022	9/14/2022	-0.74	0.74	0.74	1 days	0.24	0.24
38	9/16/2022	9/24/2022	-5.36	5.36	0.67	8 days	0.24	0.22
39	10/4/2022	10/5/2022	2.44	-2.44	-2.44	1 days	0.20	0.20
40	10/7/2022	10/13/2022	-2.25	2.25	0.38	6 days	0.20	0.19
41	10/19/2022	10/20/2022	-2.35	2.35	2.35	1 days	0.23	0.22
42	10/23/2022	10/24/2022	-1.88	1.88	1.88	1 days	0.23	0.22
43	10/26/2022	10/31/2022	-2.36	2.36	0.47	5 days	0.22	0.22
44	11/30/2022	12/2/2022	-1.65	1.65	0.82	2 days	0.24	0.23
45	12/10/2022	12/13/2022	-1.59	1.59	0.53	3 days	0.23	0.23
46	12/16/2022	12/18/2022	-0.15	0.15	0.07	2 days	0.23	0.23
47	1/21/2023	1/26/2023	-2.63	2.63	0.53	5 days	0.24	0.23
48	1/28/2023	1/30/2023	-0.81	0.81	0.41	2 days	0.23	0.23
49	2/2/2023	2/4/2023	-0.05	0.05	0.02	2 days	0.23	0.23
50	2/6/2023	2/22/2023	-0.89	0.89	0.06	16 days	0.23	0.22
51	2/24/2023	3/7/2023	-2.64	2.64	0.24	11 days	0.22	0.22
52	3/16/2023	3/17/2023	-0.97	0.97	0.97	1 days	0.24	0.23

53	3/29/2023	3/30/2023	-0.90	0.90	0.90	1 days	0.23	0.23
54	4/4/2023	4/10/2023	-2.56	2.56	0.43	6 days	0.23	0.22
55	4/17/2023	4/18/2023	-0.33	0.33	0.33	1 days	0.23	0.23
56	4/20/2023	4/22/2023	-1.19	1.19	0.59	2 days	0.22	0.22
57	4/30/2023	5/1/2023	-1.28	1.28	1.28	1 days	0.23	0.23
58	5/4/2023	5/5/2023	-0.62	0.62	0.62	1 days	0.22	0.22
59	6/15/2023	6/17/2023	-4.39	4.39	2.19	2 days	0.20	0.18
60	6/25/2023	6/30/2023	-9.22	9.22	1.84	5 days	0.22	0.18
61	7/3/2023	7/4/2023	-1.63	1.63	1.63	1 days	0.18	0.17
62	7/6/2023	7/15/2023	-17.58	17.58	1.95	9 days	0.23	0.16
63	7/17/2023	7/23/2023	-7.21	7.21	1.20	6 days	0.16	0.15
64	8/7/2023	8/10/2023	-2.24	2.24	0.75	3 days	0.25	0.26
65	8/16/2023	8/18/2023	-2.86	2.86	1.43	2 days	0.27	0.26
66	8/21/2023	8/24/2023	-5.13	5.13	1.71	3 days	0.26	0.24
67	8/30/2023	8/31/2023	-1.53	1.53	1.53	1 days	0.23	0.22
68	9/2/2023	9/12/2023	-18.28	18.28	1.83	10 days	0.23	0.17
69	9/15/2023	9/17/2023	-1.15	1.15	0.57	2 days	0.26	0.25
70	9/20/2023	9/21/2023	-1.59	1.59	1.59	1 days	0.26	0.26
71	9/26/2023	10/3/2023	-4.99	4.99	0.71	7 days	0.26	0.24

7.6 APPENDIX 6 – EVIDENCE OF PREFERENTIAL FLOW AND SUBSTRATE CRACK IN JDB

Figure 7-1: Crack along the inlet of JdB1 (taken in 2022-08, after refill the crack)

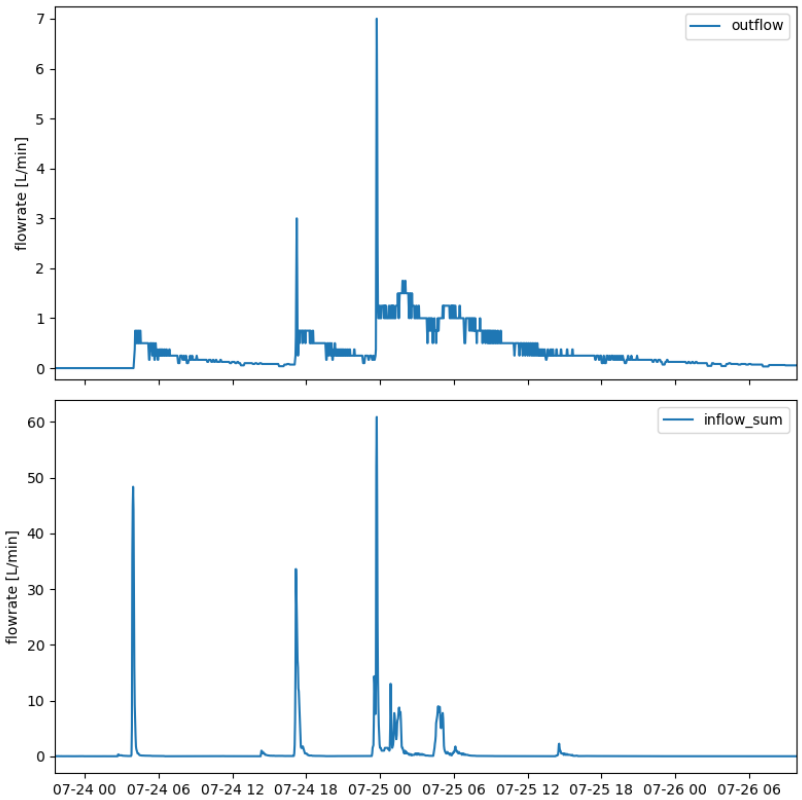

Figure 7-2: Fast reaction and high peak of outflow in 2023 summer

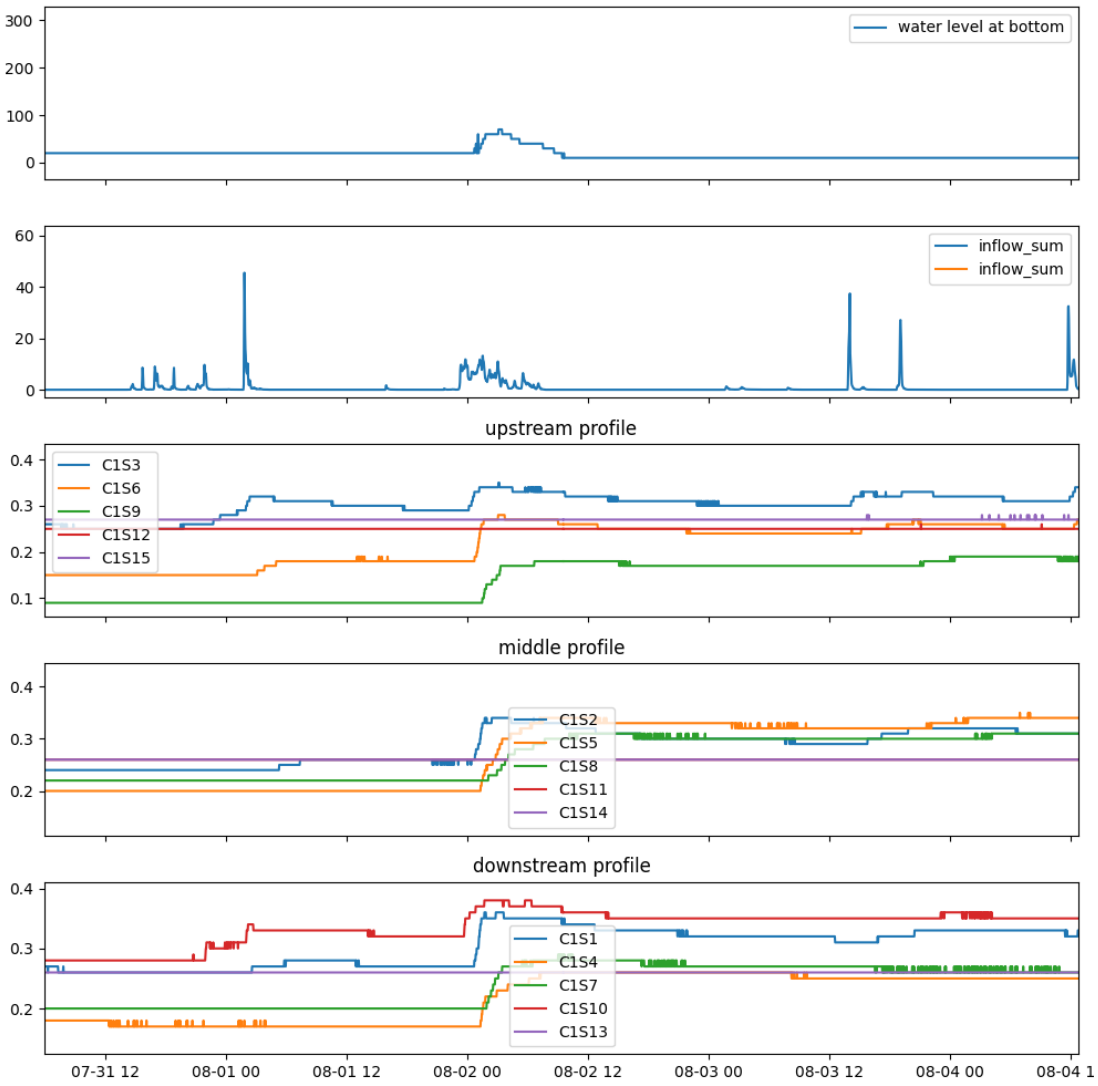

Figure 7-3: Preferential flow along the cable or crack next the soil sensor (faster reaction at downstream 90cm sensor C1S10 than the upstream sensors in JdB1)

7.7 APPENDIX 7 – MISCANTHUS SINENSIS CANOPY IN THE SUMMER 2023

Figure 7-4: The well developed *Miscanthus Sinensis* in the summer 2023, SC

Bibliography

Allen, R. G., Pereira, L. S., Raes, D., & Smith, M. (1998). FAO Irrigation and drainage paper No. 56. *Rome: Food and Agriculture Organization of the United Nations*, *56*(97), e156.

Aravena, J. E., & Dussaillant, A. (2009). Storm-water infiltration and focused recharge modeling with finite-volume two-dimensional Richards equation: Application to an experimental rain garden. *Journal of Hydraulic Engineering*, *135*(12), 1073–1080. Scopus. https://doi.org/10.1061/(ASCE)HY.1943-7900.0000111

Askari, S. H., De-Ville, S., Hathway, E. A., & Stovin, V. (2021). Estimating Evapotranspiration from Commonly Occurring Urban Plant Species Using Porometry and Canopy Stomatal Conductance. *Water*, *13*(16), 2262. https://doi.org/10.3390/w13162262

Asra, A. (2023). *Modélisation hydrologique de l'infiltration des eaux pluviales dans les sols urbains en prenant en compte les chemins préférentiels*.

Attivissimo, F., Cataldo, A., Fabbiano, L., & Giaquinto, N. (2011). Systematic errors and measurement uncertainty: An experimental approach. *Measurement*, *44*(9), 1781–1789. https://doi.org/10.1016/j.measurement.2011.07.011

Bacys, M., Khan, U., Sharma, J., & Bentzen, T. R. (2018). An evaluation of global bioretention cell design guidelines. *Geophysical Research Abstracts*, *20*, 17987. https://meetingorganizer.copernicus.org/EGU2018/EGU2018-17987-1.pdf

Bacys, M., Khan, U. T., Sharma, J., & Bentzen, T. R. (2019). Hydrological Efficacy of Ontario's Bioretention Cell Design Recommendations: A Case Study from North York, Ontario. *Journal of Water Management Modeling*, *27*. Scopus. https://doi.org/10.14796/JWMM.C468

Baek, S.-S., Choi, D.-H., Jung, J.-W., Yoon, K.-S., & Cho, K.-H. (2015). Evaluation of a hydrology and run-off BMP model in SUSTAIN on a commercial area and a public park in South Korea. *Desalination and Water Treatment*, *55*(2), 347–359. Scopus. https://doi.org/10.1080/19443994.2014.939502

Barlow, D., Burrill, G., Nolfi, J. R., & Self-Sufficiency, V. I. of C. I. C. for S. in F. (1977). *A Research Report on Developing a Community Level Natural Resource Inventory System*. Center for Studies in Food Self-Sufficiency, Vermont Institute of Community Involvement. https://books.google.fr/books?id=ypHtAAAAMAAJ

Batalini de Macedo, M., Ambrogi Ferreira do Lago, C., Mendiondo, E. M., & H. Giacomoni, M. (2019). Bioretention performance under different rainfall regimes in subtropical conditions: A case study in São Carlos, Brazil. *Journal of Environmental Management*, *248*. Scopus. https://doi.org/10.1016/j.jenvman.2019.109266

Benedict, M. A., & McMahon, E. T. (2002). Green infrastructure: Smart conservation for the 21st century. *Renewable Resources Journal*, *20*(3), 12–17.

Bertolotto, C. S., & Clark, A. (2017, February). *Rain Garden and Bioretention Literature Review: An Assessment of Functional Parameters, BMPs and Landowner Perspectives*.

Bertrand-Krajewski, J.-L. (2021). Integrated urban stormwater management: Evolution and multidisciplinary perspective. *Journal of Hydro-Environment Research*, *38*, 72–83. https://doi.org/10.1016/j.jher.2020.11.003

Beryani, A., Goldstein, A., Al-Rubaei, A. M., Viklander, M., Hunt, W. F., III, & Blecken, G.-T. (2021). Survey of the operational status of twenty-six urban stormwater biofilter facilities in Sweden. *Journal of Environmental Management*, *297*. Scopus. https://doi.org/10.1016/j.jenvman.2021.113375

Bethke, G. M., William, R., & Stillwell, A. S. (2022). Rain Garden Performance as a Function of Native Soil Parameters. *Journal of Sustainable Water in the Built Environment*, *8*(1). Scopus. https://doi.org/10.1061/JSWBAY.0000967

Boening-Ulman, K. M., Tirpak, R. A., Martin, J. F., Braswell, A. S., Iii, W. F. H., & Winston, R. J. (2024). *Observing the 'Urban Karst' phenomenon and its effects on infiltration based stormwater control measures*. 16th International Conference on Urban Drainage, Delft, The Netherlands.

Bonneau, J., Fletcher, T. D., Costelloe, J. F., Poelsma, P. J., James, R. B., & Burns, M. J. (2020). The hydrologic, water quality and flow regime performance of a bioretention basin in Melbourne, Australia. *Urban Water Journal*, *17*(4), 303–314. Scopus. https://doi.org/10.1080/1573062X.2020.1769688

Bonneau, J., Lipeme Kouyi, G., Lassabatere, L., & Fletcher, T. D. (2021). Field validation of a physically-based model for bioretention systems. *Journal of Cleaner Production*, *312*. Scopus. https://doi.org/10.1016/j.jclepro.2021.127636

Bortolini, L., & Zanin, G. (2018). Hydrological behaviour of rain gardens and plant suitability: A study in the Veneto plain (north-eastern Italy) conditions. *Urban Forestry and Urban Greening*, *34*, 121–133. Scopus. https://doi.org/10.1016/j.ufug.2018.06.007

Brooks, R. H., & Corey, A. T. (1964). *Hydraulic properties of porous media*. Colorado State University.

Brown, R. A., & Hunt, W. F. (2010). Hydrologic Impact of an Internal Water Storage (IWS) Layer on Bioretention Performance. *2010 Pittsburgh, Pennsylvania, June 20 - June 23, 2010*. 2010 Pittsburgh, Pennsylvania, June 20 - June 23, 2010. https://doi.org/10.13031/2013.29676

Brown, R. A., & Hunt, W. F. (2011a). Impacts of Media Depth on Effluent Water Quality and Hydrologic Performance of Undersized Bioretention Cells. *Journal of Irrigation and Drainage Engineering*, *137*(3), 132–143. Scopus. https://doi.org/10.1061/(ASCE)IR.1943-4774.0000167

Brown, R. A., & Hunt, W. F. (2011b). Underdrain configuration to enhance bioretention exfiltration to reduce pollutant loads. *Journal of Environmental*

Engineering, *137*(11), 1082–1091. Scopus. https://doi.org/10.1061/(ASCE)EE.1943-7870.0000437

Burdine, N. (1953). Relative permeability calculations from pore size distribution data. *Journal of Petroleum Technology*, *5*(03), 71–78.

Clar, M. (2010). In Situ Bioretention Design Concept. *Low Impact Development 2010*, 96–103. https://doi.org/10.1061/41099(367)10

Collenteur, R., Vremec, M., & Brunetti, G. (2020). *Interfacing FORTAN Code with Python: An example for the Hydrus-1D model* [Other]. pico. https://doi.org/10.5194/egusphere-egu2020-15377

Craven, B. D., & Islam, S. M. (2011). Ordinary least-squares regression. *The SAGE Dictionary of Quantitative Management Research*, *1*, 224–228.

Davis, A. P. (2008). Field performance of bioretention: Hydrology impacts. *Journal of Hydrologic Engineering*, *13*(2), 90–95. Scopus. https://doi.org/10.1061/(ASCE)1084-0699(2008)13:2(90)

Davis, A. P., Traver, R. G., Hunt, W. F., Lee, R., Brown, R. A., & Olszewski, J. M. (2012). Hydrologic Performance of Bioretention Storm-Water Control Measures. *Journal of Hydrologic Engineering*, *17*(5), 604–614. Scopus. https://doi.org/10.1061/(ASCE)HE.1943-5584.0000467

De Feo, G., Antoniou, G., Fardin, H., El-Gohary, F., Zheng, X., Reklaityte, I., Butler, D., Yannopoulos, S., & Angelakis, A. (2014). The Historical Development of Sewers Worldwide. *Sustainability*, *6*(6), 3936–3974. https://doi.org/10.3390/su6063936

De Feo, G., Antoniou, G. P., Mays, L. W., Dragoni, W., Fardin, H. F., El-Gohary, F., Laureano, P., Kanetaki, E. I., Zheng, X. Y., & Angelakis, A. N. (2014). Historical development of wastewater management. In *Handbook of Engineering Hydrology* (pp. 163–217). CRC Press.

De-Ville, S., & Deeprose, G. (2024). *Bioretention Inlet Efficiency: A Left Turn for Stormwater Runoff*. 16th International Conference on Urban Drainage, Delft, The Netherlands.

Dhalla, S., & Zimmer, C. (2010). *Low impact development stormwater management planning and design guide* [Design Guideline]. TRCA&CVC. https://cvc.ca/wp-content/uploads/2014/04/LID-SWM-Guide-v1.0_2010_1_no-appendices.pdf

Dietz, M. E., & Clausen, J. C. (2005). A Field Evaluation of Rain Garden Flow and Pollutant Treatment. *Water, Air, and Soil Pollution*, *167*(1–4), 123–138. https://doi.org/10.1007/s11270-005-8266-8

Ding, N., Zhu, Q., Cherqui, F., Walcker, N., Bertrand-Krajewski, J., & Hamel, P. (2024). Laboratory Performance Assessment of Low-cost Water Level Sensor for Field Monitoring in the Tropics. *Water Research X*, 100298. https://doi.org/10.1016/j.wroa.2024.100298

Donaghue, A. G., Morgan, N., Toran, L., & McKenzie, E. R. (2022). The impact of bioretention column internal water storage underdrain height on denitrification

under continuous and transient flow. *Water Research, 214*, 118205. https://doi.org/10.1016/j.watres.2022.118205

DPU. (2024, May). *DPU STORM WATER DRAINAGE MANUAL*. The City of Columbus Department of Public Utilities. https://www.columbus.gov/files/sharedassets/city/v/2/utilities/documents/sewer-publications/2024-columbus-stormwater-drainage-manual.pdf

Dumont, E., Sage, J., Branchu, P., & Monnier, E. (2023). *Faisabilité de l'infiltration des eaux pluviales en zone d'aléa dissolution du gypse – apport de la modélisation numérique*.

Durmont, J. F., Sage, J., & Gromaire, M. C. (2024). *How far can we rely on lined green infrastructures for urban runoff control? A case study in Paris conurbation*. 16th International Conference on Urban Drainage, Delft, The Netherlands.

Dussaillant, A. R., Cuevas, A., & Potter, K. W. (2005). Raingardens for stormwater infiltration and focused groundwater recharge: Simulations for different world climates. *Water Supply*, *5*(3–4), 173–179. https://doi.org/10.2166/ws.2005.0097

Dussaillant, A. R., Wu, C. H., & Potter, K. W. (2004). Richards equation model of a rain garden. *Journal of Hydrologic Engineering*, *9*(3), 219–225. Scopus. https://doi.org/10.1061/(ASCE)1084-0699(2004)9:3(219)

Dussaillant, A., Wu, C., & Potter, K. W. (2005). Infiltration of stormwater in bioretention cells: Numerical model and field experiment. *Ingenieria Hidraulica En Mexico*, *20*(2), 5–17.

Ebrahimian, A., Wadzuk, B., & Traver, R. (2019). Evapotranspiration in green stormwater infrastructure systems. *Science of The Total Environment*, *688*, 797–810. https://doi.org/10.1016/j.scitotenv.2019.06.256

Eich, G., & Wierecky, N. (2002). *Vom Hasenmoor zum Transportsiel: 160 Jahre Hamburger Stadtentwässerung*. Hamburger Stadtentwässerung.

Emerson, C. H., & Traver, R. G. (2008). Multiyear and Seasonal Variation of Infiltration from Storm-Water Best Management Practices. *Journal of Irrigation and Drainage Engineering*, *134*(5), 598–605. https://doi.org/10.1061/(ASCE)0733-9437(2008)134:5(598)

Feddes, R. A., Kowalik, P. J., & Zaradny, H. (1978). *Simulation of field water use and crop yield*. Wageningen : Centre for agricultural publishing and documentation. http://lib.ugent.be/catalog/rug01:000032129

Feddes, R. A., & Raats, P. A. C. (2004). *Parameterizing the soil – water – plant root system*. https://edepot.wur.nl/35358

Feldman, A., Foti, R., & Montalto, F. (2019). Green Infrastructure Implementation in Urban Parks for Stormwater Management. *Journal of Sustainable Water in the Built Environment*, *5*(3). Scopus. https://doi.org/10.1061/JSWBAY.0000880

Flanagan, K., Branchu, P., Boudahmane, L., Caupos, E., Demare, D., Deshayes, S., Dubois, P., Meffray, L., Partibane, C., Saad, M., & Gromaire, M.-C. (2020). Vers une maîtrise à la source de la contamination des eaux pluviales urbaines:

Rétention et devenir de micropolluants dans deux ouvrages de filtration végétalisés. *Techniques Sciences Méthodes*, *12*, 65–88. https://doi.org/10.36904/tsm/201912065

Flanagan, K., Branchu, P., & Gromaire, M.-C. (2017). Les ouvrages de biorétention: Synthèse des guides internationaux de conception et de mainte - nance des filtres plantés pour le traitement à la source des eaux de ruissellement urbaines. *Techniques Sciences Méthodes*, *12*, 89–126. https://doi.org/10.1051/tsm/201712089

Fletcher, T. D., Andrieu, H., & Hamel, P. (2013). Understanding, management and modelling of urban hydrology and its consequences for receiving waters: A state of the art. *Advances in Water Resources*, *51*, 261–279. https://doi.org/10.1016/j.advwatres.2012.09.001

Fletcher, T. D., Shuster, W., Hunt, W. F., Ashley, R., Butler, D., Arthur, S., Trowsdale, S., Barraud, S., Semadeni-Davies, A., Bertrand-Krajewski, J.-L., Mikkelsen, P. S., Rivard, G., Uhl, M., Dagenais, D., & Viklander, M. (2015). SUDS, LID, BMPs, WSUD and more – The evolution and application of terminology surrounding urban drainage. *Urban Water Journal*, *12*(7), 525–542. https://doi.org/10.1080/1573062X.2014.916314

Gao, J., Pan, J., Hu, N., & Xie, C. (2018). Hydrologic performance of bioretention in an expressway service area. *Water Science and Technology*, *77*(7), 1829–1837. Scopus. https://doi.org/10.2166/wst.2018.048

Géhéniau, N., Fuamba, M., Mahaut, V., Gendron, M. R., & Dugué, M. (2015). Monitoring of a Rain Garden in Cold Climate: Case Study of a Parking Lot near Montréal. *Journal of Irrigation and Drainage Engineering*, *141*(6), 04014073. https://doi.org/10.1061/(ASCE)IR.1943-4774.0000836

Ghestem, M., Sidle, R. C., & Stokes, A. (2011). The Influence of Plant Root Systems on Subsurface Flow: Implications for Slope Stability. *BioScience*, *61*(11), 869–879. https://doi.org/10.1525/bio.2011.61.11.6

Gironás, J., Roesner, L. A., Rossman, L. A., & Davis, J. (2010). A new applications manual for the Storm Water Management Model(SWMM). *Environmental Modelling & Software*, *25*(6), 813–814.

Goor, J., Cantelon, J., Smart, C. C., & Robinson, C. E. (2021). Seasonal performance of field bioretention systems in retaining phosphorus in a cold climate: Influence of prolonged road salt application. *Science of the Total Environment*, *778*. Scopus. https://doi.org/10.1016/j.scitotenv.2021.146069

Guo, C., Li, J., Li, H., Zhang, B., Ma, M., & Li, F. (2018). Seven-year running effect evaluation and fate analysis of rain gardens in Xi'an, Northwest China. *Water (Switzerland)*, *10*(7). Scopus. https://doi.org/10.3390/w10070944

Guo, J. C. Y., & Luu, T. M. (2015). Operation of Cap Orifice in a Rain Garden. *Journal of Hydrologic Engineering*, *20*(10), 06015002. https://doi.org/10.1061/(ASCE)HE.1943-5584.0001184

Hamel, P., Ding, N., Cherqui, F., Zhu, Q., Walcker, N., Bertrand-Krajewski, J.-L., Champrasert, P., Fletcher, T. D., McCarthy, D. T., Navratil, O., & Shi, B.

(2024). Low-cost monitoring systems for urban water management: Lessons from the field. *Water Research X*, *22*, 100212. https://doi.org/10.1016/j.wroa.2024.100212

Hanley, P. A., Livesely, S. J., Fletcher, T. D., & Szota, C. (2023). *Water Use Strategy Determines the Effectiveness of Internal Water Storage for Trees Growing in Biofilters Subject to Repeated Droughts*. https://doi.org/10.2139/ssrn.4402784

Heasom, W., Traver, R. G., & Welker, A. (2006). Hydrologic modeling of a bioinfiltration best management practice. *Journal of the American Water Resources Association*, *42*(5), 1329–1347. https://doi.org/10.1111/j.1752-1688.2006.tb05304.x

Herrera, J., Bonilla, C. A., Castro, L., Vera, S., Reyes, R., & Gironás, J. (2017). A model for simulating the performance and irrigation of green stormwater facilities at residential scales in semiarid and Mediterranean regions. *Environmental Modelling and Software*, *95*, 246–257. Scopus. https://doi.org/10.1016/j.envsoft.2017.06.020

Hess, A., Wadzuk, B., & Welker, A. (2017). Evapotranspiration in rain gardens using weighing lysimeters. *Journal of Irrigation and Drainage Engineering*, *143*(6). Scopus. https://doi.org/10.1061/(ASCE)IR.1943-4774.0001157

Houdeshel, D., & Pomeroy, C. (2014). Storm-Water Bioinfiltration as No-Irrigation Landscaping Alternative in Semiarid Climates. *Journal of Irrigation and Drainage Engineering*, *140*(2), 06013004. https://doi.org/10.1061/(ASCE)IR.1943-4774.0000663

Huang, J., Yu, Z., Qin, Y., Wang, L., Huang, Y., & Huang, Y. (2021). A case in subtropical climate city: Assessing the bioretention hydraulic performance on storm in response to poor permeability soil. *Journal of Environmental Management*, *293*, 112952. https://doi.org/10.1016/j.jenvman.2021.112952

Huang, T., Sage, J., Técher, D., & Gromaire, M.-C. (2025). Hydrological performance of bioretention in field experiments and models: A review from the perspective of design characteristics and local contexts. *Science of The Total Environment*, *965*, 178684. https://doi.org/10.1016/j.scitotenv.2025.178684

Hunt, W. F., Passeport, E., & Brown, R. A. (2008). Water Quality and Hydrologic Benefits of Five Bioretention Cells in North Carolina. *World Environmental and Water Resources Congress 2008*, 1–10. https://doi.org/10.1061/40976(316)6

Ice, G. (2004). History of Innovative Best Management Practice Development and its Role in Addressing Water Quality Limited Waterbodies. *Journal of Environmental Engineering*, *130*(6), 684–689. https://doi.org/10.1061/(ASCE)0733-9372(2004)130:6(684)

IUSS WG. (2014). *World Reference Base for Soil Resources 2014—International soil classification system for naming soils and creating legends for soil maps*. LCC MAKS Press. https://doi.org/10.29003/m4174.978-5-317-07235-3

J. Šimůnek, M. Šejna, H. Saito, M. Sakai, & M. Th. van Genuchten. (2013). *The HYDRUS-1D Software Package for Simulating the One-Dimensional*

Movement of Water, Heat, and Multiple Solutes in Variably-Saturated Media. DEPARTMENT OF ENVIRONMENTAL SCIENCES UNIVERSITY OF CALIFORNIA RIVERSIDE RIVERSIDE, CALIFORNIA.

Jia, X., Zhang, W., Wang, X., Jin, Y., & Cong, P. (2022). Numerical Analysis of an Explicit Smoothed Particle Finite Element Method on Shallow Vegetated Slope Stability with Different Root Architectures. *Sustainability*, *14*(18), 11272. https://doi.org/10.3390/su141811272

Jiang, C., Li, J., Li, H., Li, Y., & Zhang, Z. (2020). Low-impact development facilities for stormwater runoff treatment: Field monitoring and assessment in Xi'an area, China. *Journal of Hydrology*, *585*. Scopus. https://doi.org/10.1016/j.jhydrol.2020.124803

Kanso, T. (2021). *Mesure et modélisation du bilan hydrologique de dispositifs rustiques de gestion à la source des eaux de ruissellement de chaussées*. Paris Est.

Kanso, T., Tedoldi, D., Gromaire, M.-C., Ramier, D., Saad, M., & Chebbo, G. (2018). Horizontal and vertical variability of soil hydraulic properties in roadside sustainable drainage systems (SuDS)-nature and implications for hydrological performance evaluation. *Water (Switzerland)*, *10*(8). Scopus. https://doi.org/10.3390/w10080987

Karnatz, C., Thompson, J. R., & Logsdon, S. (2019). Capture of stormwater runoff and pollutants by three types of urban best management practices. *Journal of Soil and Water Conservation*, *74*(5), 487–499. Scopus. https://doi.org/10.2489/jswc.74.5.487

Kasprzyk, M., Szpakowski, W., Poznańska, E., Boogaard, F. C., Bobkowska, K., & Gajewska, M. (2022). Technical solutions and benefits of introducing rain gardens – Gdańsk case study. *Science of the Total Environment*, *835*. Scopus. https://doi.org/10.1016/j.scitotenv.2022.155487

Kim, H., Mallari, K. J. B., Baek, J., Pak, G., Choi, H. I., & Yoon, J. (2019). Considering the effect of groundwater on bioretention using the Storm Water Management Model. *Journal of Environmental Management*, *231*, 1270–1276. Scopus. https://doi.org/10.1016/j.jenvman.2018.03.032

Kling, H., Fuchs, M., & Paulin, M. (2012). Runoff conditions in the upper Danube basin under an ensemble of climate change scenarios. *Journal of Hydrology*, *424–425*, 264–277. https://doi.org/10.1016/j.jhydrol.2012.01.011

Kluge, B., Markert, A., Facklam, M., Sommer, H., Kaiser, M., Pallasch, M., & Wessolek, G. (2018). Metal accumulation and hydraulic performance of bioretention systems after long-term operation. *Journal of Soils and Sediments*, *18*(2), 431–441. https://doi.org/10.1007/s11368-016-1533-z

Kridakorn Na Ayutthaya, T., Suropan, P., Sundaranaga, C., Phichetkunbodee, N., Anambutr, R., Suppakittpaisarn, P., & Rinchumphu, D. (2023). The influence of bioretention assets on outdoor thermal comfort in the urban area. *Energy Reports*, *9*, 287–294. https://doi.org/10.1016/j.egyr.2023.05.257

Lassabatere, L., Angulo-Jaramillo, R., Yilmaz, D., & Winiarski, T. (2013). BEST method: Characterization of soil unsaturated hydraulic properties. In *Advances in Unsaturated Soils. CRC Press, London* (pp. 527–532).

Le Coustumer, S., Fletcher, T. D., Deletic, A., Barraud, S., & Poelsma, P. (2012). The influence of design parameters on clogging of stormwater biofilters: A large-scale column study. *Water Research*, *46*(20), 6743–6752. https://doi.org/10.1016/j.watres.2012.01.026

Le Monde, & AP. (2024, July 30). *Paris Olympics: Understanding the issue with Seine water quality*. https://www.lemonde.fr/en/sports/article/2024/07/30/paris-olympics-understanding-the-issue-with-seine-water-quality_6705160_9.html

Lee, J., Bae, S., Lee, W. H., & Gil, K. (2022). Effect of surface area to catchment area ratio on pollutant removal efficiency in vegetation-type facilities. *Ecological Engineering*, *179*. Scopus. https://doi.org/10.1016/j.ecoleng.2022.106609

Li, H. (2007). *Urban particle and pollutant capture via stormwater filter facilities and the concomitant water quality and hydrological benefits*. University of Maryland, College Park.

Li, H., Sharkey, L. J., Hunt, W. F., & Davis, A. P. (2009). Mitigation of Impervious Surface Hydrology Using Bioretention in North Carolina and Maryland. *Journal of Hydrologic Engineering*, *14*(4), 407–415. https://doi.org/10.1061/(ASCE)1084-0699(2009)14:4(407)

Li, J., Li, F., Li, H., Guo, C., & Dong, W. (2019). Analysis of rainfall infiltration and its influence on groundwater in rain gardens. *Environmental Science and Pollution Research*, *26*(22), 22641–22655. Scopus. https://doi.org/10.1007/s11356-019-05622-z

Li, J., Liu, F., & Li, Y. (2020). Simulation and design optimization of rain gardens via DRAINMOD and response surface methodology. *Journal of Hydrology*, *585*. Scopus. https://doi.org/10.1016/j.jhydrol.2020.124788

Li, J., Zhao, R., Li, Y., & Li, H. (2020). Simulation and optimization of layered bioretention facilities by HYDRUS-1D model and response surface methodology. *Journal of Hydrology*, *586*. Scopus. https://doi.org/10.1016/j.jhydrol.2020.124813

Lisenbee, W. A., Hathaway, J. M., Burns, M. J., & Fletcher, T. D. (2021). Modeling bioretention stormwater systems: Current models and future research needs. *Environmental Modelling & Software*, *144*, 105146. https://doi.org/10.1016/j.envsoft.2021.105146

Lisenbee, W., Hathaway, J., Negm, L., Youssef, M., & Winston, R. (2020). Enhanced bioretention cell modeling with DRAINMOD-Urban: Moving from water balances to hydrograph production. *Journal of Hydrology*, *582*. Scopus. https://doi.org/10.1016/j.jhydrol.2019.124491

Lu, J., Zhang, Q., Werner, A. D., Li, Y., Jiang, S., & Tan, Z. (2020). Root-induced changes of soil hydraulic properties – A review. *Journal of Hydrology*, *589*, 125203. https://doi.org/10.1016/j.jhydrol.2020.125203

Lucke, T., & Nichols, P. W. B. (2015). The pollution removal and stormwater reduction performance of street-side bioretention basins after ten years in operation. *Science of the Total Environment*, *536*, 784–792. Scopus. https://doi.org/10.1016/j.scitotenv.2015.07.142

Lynch, J. (1995). Root Architecture and Plant Productivity. *Plant Physiology*, *109*(1), 7–13. https://doi.org/10.1104/pp.109.1.7

Machusick, M., Welker, A., & Traver, R. (2011). Groundwater Mounding at a Storm-Water Infiltration BMP. *Journal of Irrigation and Drainage Engineering*, *137*(3), 154–160. Scopus. https://doi.org/10.1061/(ASCE)IR.1943-4774.0000184

Mai, Y., & Huang, G. (2021). Hydrology and rainfall runoff pollutant removal performance of biochar-amended bioretention facilities based on field-scale experiments in lateritic red soil regions. *Science of the Total Environment*, *761*. Scopus. https://doi.org/10.1016/j.scitotenv.2020.143252

Massoudieh, A., Maghrebi, M., Kamrani, B., Nietch, C., Tryby, M., Aflaki, S., & Panguluri, S. (2017). A flexible modeling framework for hydraulic and water quality performance assessment of stormwater green infrastructure. *Environmental Modelling and Software*, *92*, 57–73. Scopus. https://doi.org/10.1016/j.envsoft.2017.02.013

Meng, Y., Wang, H., Chen, J., & Zhang, S. (2014). Modelling hydrology of a single bioretention system with HYDRUS-1D. *Scientific World Journal*, *2014*. Scopus. https://doi.org/10.1155/2014/521047

Météo-France. (2023, September 22). *Le climat en France métropolitaine*. Le climat en France métropolitaine. https://meteofrance.com/comprendre-climat/france/le-climat-en-france-metropolitaine

MOHURD. (2014). *海绵城市建设技术指南（Technical Guidelines for Sponge City Construction）*.

MPCA. (2022, August 15). *Bioretention terminology—Minnesota Stormwater Manual* [Guideline]. Bioretention Terminology - Minnesota Stormwater Manual. https://stormwater.pca.state.mn.us/index.php?title=Bioretention_terminology

Muerdter, C. P., Wong, C. K., & LeFevre, G. H. (2018). Emerging investigator series: The role of vegetation in bioretention for stormwater treatment in the built environment: pollutant removal, hydrologic function, and ancillary benefits. *Environmental Science: Water Research & Technology*, *4*(5), 592–612. https://doi.org/10.1039/C7EW00511C

Muthanna, T. M., Viklander, M., & Thorolfsson, S. T. (2008). Seasonal climatic effects on the hydrology of a rain garden. *Hydrological Processes*, *22*(11), 1640–1649. https://doi.org/10.1002/hyp.6732

Nakamura, H., & Oosawa, M. (2021). Effects of the underground discharge channel/reservoir for small urban rivers in the Tokyo area. *IOP Conference Series: Earth and Environmental Science*, *703*(1), 012029. https://doi.org/10.1088/1755-1315/703/1/012029

Nasrollahpour, R., Skorobogatov, A., He, J., Valeo, C., Chu, A., & van Duin, B. (2022). The impact of vegetation and media on evapotranspiration in bioretention systems. *Urban Forestry & Urban Greening*, *74*, 127680. https://doi.org/10.1016/j.ufug.2022.127680

NCDEQ. (2024). *NCDEQ stormwater design manual*. North Carolina Department of Environmental Quality. https://www.deq.nc.gov/about/divisions/energy-mineral-and-land-resources/stormwater/stormwater-program/stormwater-design-manual

Neukirchen, D., Himken, M., Lammel, J., Czypionka-Krause, U., & Olfs, H.-W. (1999). Spatial and temporal distribution of the root system and root nutrient content of an established Miscanthus crop. *European Journal of Agronomy*, *11*(3–4), 301–309. https://doi.org/10.1016/S1161-0301(99)00031-3

Nichols, W., Welker, A., Traver, R., & Tu, M.-C. P. (2021). Modeling Seasonal Performance of Operational Urban Rain Garden Using HYDRUS-1D. *Journal of Sustainable Water in the Built Environment*, *7*(3). Scopus. https://doi.org/10.1061/JSWBAY.0000941

Nocco, M. A., Rouse, S. E., & Balster, N. J. (2016). Vegetation type alters water and nitrogen budgets in a controlled, replicated experiment on residential-sized rain gardens planted with prairie, shrub, and turfgrass. *Urban Ecosystems*, *19*(4), 1665–1691. https://doi.org/10.1007/s11252-016-0568-7

NSC. (2008). *North Shore City Bioretention Guidelines*. https://www.scribd.com/document/73716036/New-ZealandBioretention-Guidelines-Rain-Garden-North-ShoreCity-Council

O, S., & Foelsche, U. (2019). Assessment of spatial uncertainty of heavy rainfall at catchment scale using a dense gauge network. *Hydrology and Earth System Sciences*, *23*(7), 2863–2875. https://doi.org/10.5194/hess-23-2863-2019

Öhrn Sagrelius, P., Blecken, G., Hedström, A., Ashley, R., & Viklander, M. (2022). Environmental impacts of stormwater bioretention systems with various design and construction components. *Journal of Cleaner Production*, *359*, 132091. https://doi.org/10.1016/j.jclepro.2022.132091

Olszewski, J. M., & Davis, A. P. (2013). Comparing the Hydrologic Performance of a Bioretention Cell with Predevelopment Values. *Journal of Irrigation and Drainage Engineering-Asce*, *139*(2), 124–130. https://doi.org/10.1061/(ASCE)IR.1943-4774.0000504

Osman, M., Wan Yusof, K., Takaijudin, H., Goh, H. W., Abdul Malek, M., Azizan, N. A., Ab. Ghani, A., & Sa'id Abdurrasheed, A. (2019). A Review of Nitrogen Removal for Urban Stormwater Runoff in Bioretention System. *Sustainability*, *11*(19), 5415. https://doi.org/10.3390/su11195415

Ouédraogo, A. A., Berthier, E., Durand, B., & Gromaire, M.-C. (2022). Determinants of Evapotranspiration in Urban Rain Gardens: A Case Study with Lysimeters under Temperate Climate. *Hydrology*, *9*(3). Scopus. https://doi.org/10.3390/hydrology9030042

Ouédraogo, A. A., Berthier, E., Sage, J., & Gromaire, M.-C. (2025). Modelling evapotranspiration in urban green stormwater infrastructures: Importance of sensitivity analysis and calibration strategies with a hydrological model. *Environmental Modelling & Software*, *185*, 106319. https://doi.org/10.1016/j.envsoft.2025.106319

Pan, J., Liu, J., Hu, G., Su, J., & Qin, G. (2022). Long Term Hydrological Effects of Bioretention on Expressway Service Area. *Polish Journal of Environmental Studies*, *31*(2), 1271–1283. Scopus. https://doi.org/10.15244/pjoes/142384

Payne, E., Hatt, B., Deletic, A., Dobbie, M., McCarthy, D., & Chandrasena, G. (2015a). *Adoption Guidelines for Stormwater Biofiltration Systems*. Melbourne, Australia: Cooperative Research Centre for Water Sensitive Cities.

Payne, E., Hatt, B., Deletic, A., Dobbie, M., McCarthy, D., & Chandrasena, G. (2015b). *Adoption Guidelines for Stormwater Biofiltration Systems – Summary Report*. Melbourne, Australia: Cooperative Research Centre for Water Sensitive Cities.

Penman, H. L. (1948). Natural evaporation from open water, bare soil and grass. *Proceedings of the Royal Society of London. Series A. Mathematical and Physical Sciences*, *193*(1032), 120–145.

Perales-Momparler, S., Andrés-Doménech, I., Hernández-Crespo, C., Vallés-Morán, F., Martín, M., Escuder-Bueno, I., & Andreu, J. (2017). The role of monitoring sustainable drainage systems for promoting transition towards regenerative urban built environments: A case study in the Valencian region, Spain. *Journal of Cleaner Production*, *163*, S113–S124. Scopus. https://doi.org/10.1016/j.jclepro.2016.05.153

Petrucci, G., Rioust, E., Deroubaix, J.-F., & Tassin, B. (2013). Do stormwater source control policies deliver the right hydrologic outcomes? *Journal of Hydrology*, *485*, 188–200. https://doi.org/10.1016/j.jhydrol.2012.06.018

Petrucci, G., Rodriguez, F., Deroubaix, J.-F., & Tassin, B. (2013). Linking the management of urban watersheds with the impacts on the receiving water bodies: The use of flow duration curves. *Water Science and Technology*, *70*, 127–135. https://doi.org/10.2166/wst.2014.206

PGCDER. (2007, December). *Bioretention Manual*. The Prince George's County Department of Environmental Resources.

Pophillat, W., Sage, J., Rodriguez, F., & Braud, I. (2022). Consequences of interactions between stormwater infiltration systems, shallow groundwater and underground structures at the neighborhood scale. *Urban Water Journal*, *19*(8), 812–823. https://doi.org/10.1080/1573062X.2022.2090382

Prasad, R. (1988). A linear root water uptake model. *Journal of Hydrology*, *99*(3–4), 297–306. https://doi.org/10.1016/0022-1694(88)90055-8

Premarathna, K. S. D., Biswas, J. K., Kumar, M., Varjani, S., Mickan, B., Show, P. L., Lau, S. Y., Novo, L. A. B., & Vithanage, M. (2023). Biofilters and bioretention systems: The role of biochar in the blue-green city concept for

stormwater management. *Environmental Science: Water Research & Technology*, *9*(12), 3103–3119. https://doi.org/10.1039/D3EW00054K

Prince George's County Department of Environmental Resources. (2000, January). *Low-Impact Development Design Strategies—An ontegrated Design Approach*.

PUB. (2024). *ABC Waters Design Guidelines* (Version 5TH EDITION). https://www.pub.gov.sg/-/media/PUB/Reservoirs/ABC/PDF/ABC_Waters_Design_Guidelines.pdf

Qiu, F., Zhao, S., Zhao, D., Wang, J., & Fu, K. (2019). Enhanced nutrient removal in bioretention systems modified with water treatment residuals and internal water storage zone. *Environmental Science: Water Research & Technology*, *5*(5), 993–1003. https://doi.org/10.1039/C9EW00093C

Quinn, R., Rougé, C., & Stovin, V. (2021). Quantifying the performance of dual-use rainwater harvesting systems. *Water Research X*, *10*, 100081. https://doi.org/10.1016/j.wroa.2020.100081

Ramier, D. (2005). *Bilan hydrique des voiries urbaines: Observations et modélisation*. Nantes.

Ramier, D., Caupos, E., Bak, A., Branchu, P., Dubois, P., Flanagan, K., Georgel, P., Neveu, P., Paupardin, J., Ratovelomanana, T., Saad, M., Seidl, M., Thomas, E., & Gromaire, M.-C. (2016). *Mesurer l'efficacité des techniques alternatives pour la maîtrise des flux polluants: Un challenge métrologique. Le cas de quatre dispositifs innovants suivis dans le cadre du projet ROULÉPUR*. NOVATECH 2019, Lyon, France.

Richards, L. A. (1931). CAPILLARY CONDUCTION OF LIQUIDS THROUGH POROUS MEDIUMS. *Physics*, *1*(5), 318–333. https://doi.org/10.1063/1.1745010

Roy-Poirier, A., Champagne, P., & Filion, Y. (2010). Review of Bioretention System Research and Design: Past, Present, and Future. *Journal of Environmental Engineering*, *136*(9), 878–889. https://doi.org/10.1061/(ASCE)EE.1943-7870.0000227

Sage, J., Berthier, E., & Gromaire, M.-C. (2015). Stormwater Management Criteria for On-Site Pollution Control: A Comparative Assessment of International Practices. *Environmental Management*, *56*(1), 66–80. https://doi.org/10.1007/s00267-015-0485-1

Sage, J., Berthier, E., Gromaire, M.-C., & Chebbo, G. (2024). Supporting the Design of On-Site Infiltration Systems: From a Hydrological Model to a Web App to Meet Pluriannual Stormwater Volume Reduction Targets. *Journal of Hydrologic Engineering*, *29*(3), 04024005. https://doi.org/10.1061/JHYEFF.HEENG-6092

Schaap, M. G., Leij, F. J., & Van Genuchten, M. Th. (2001). rosetta: A computer program for estimating soil hydraulic parameters with hierarchical pedotransfer functions. *Journal of Hydrology*, *251*(3–4), 163–176. https://doi.org/10.1016/S0022-1694(01)00466-8

Schlea, D., Martin, J. F., Ward, A. D., Brown, L. C., & Suter, S. A. (2014). Performance and water table responses of retrofit rain gardens. *Journal of Hydrologic Engineering*, *19*(8). Scopus. https://doi.org/10.1061/(ASCE)HE.1943-5584.0000797

Seddon, N., Chausson, A., Berry, P., Girardin, C. A. J., Smith, A., & Turner, B. (2020). Understanding the value and limits of nature-based solutions to climate change and other global challenges. *Philosophical Transactions of the Royal Society B: Biological Sciences*, *375*(1794), 20190120. https://doi.org/10.1098/rstb.2019.0120

Šejna, M., Šimůnek, J., & van Genuchten, M. Th. (2022). *HYDRUS User Manual (Version5)*. PC-Progress, Prague, Czech Republic. https://www.pc-progress.com/downloads/Pgm_Hydrus3D5/HYDRUS_user_Manual_V5.pdf

Shen, R., Pennell, K. G., & Suuberg, E. M. (2013). Influence of Soil Moisture on Soil Gas Vapor Concentration for Vapor Intrusion. *Environmental Engineering Science*, *30*(10), 628–637. https://doi.org/10.1089/ees.2013.0133

Shuster, W. D., Bonta, J., Thurston, H., Warnemuende, E., & Smith, D. R. (2005). Impacts of impervious surface on watershed hydrology: A review. *Urban Water Journal*, *2*(4), 263–275. https://doi.org/10.1080/15730620500386529

Shuster, W., Darner, R., Schifman, L., & Herrmann, D. (2017). Factors Contributing to the Hydrologic Effectiveness of a Rain Garden Network (Cincinnati OH USA). *Infrastructures*, *2*(3), 11. https://doi.org/10.3390/infrastructures2030011

Sikkema, R., Caudullo, G., & de Rigo, D. (2016). *Carpinus betulus in Europe: Distribution, habitat, usage and threats*.

Šimůnek, J., Van Genuchten, M. T., & Šejna, M. (2022). The HYDRUS Software Package for Simulating One-, Two-, and Three-Dimensional Movement of Water, Heat, and Multiple Solutes in Variably-Saturated Porous Media, Technical Manual II, Hydrus 2D/3D. Version 5.0. *PC Progress*, *1*, 283.

Skorobogatov, A., He, J., Chu, A., Valeo, C., & Van Duin, B. (2020). The impact of media, plants and their interactions on bioretention performance: A review. *Science of The Total Environment*, *715*, 136918. https://doi.org/10.1016/j.scitotenv.2020.136918

Smith, C., Connolly, R., Ampomah, R., Hess, A., Sample-Lord, K., & Smith, V. (2021). Temporal Soil Dynamics in Bioinfiltration Systems. *Journal of Irrigation and Drainage Engineering*, *147*(11). Scopus. https://doi.org/10.1061/(ASCE)IR.1943-4774.0001617

Smolek, A. P., Anderson, A. R., & Hunt, W. F. (2018). Hydrologic and Water-Quality Evaluation of a Rapid-Flow Biofiltration Device. *Journal of Environmental Engineering (United States)*, *144*(2). Scopus. https://doi.org/10.1061/(ASCE)EE.1943-7870.0001275

SOILMOISTURE EQUIPMENT CORP. (2016, February). *Operating Instructions 2816 G1/G5*. SOILMOISTURE EQUIPMENT CORP. https://soilmoisture.com/wp-

content/uploads/2024/07/Resource_Instructions_0898-2816_2816-Chameleon.pdf

Spraakman, S., & Drake, J. A. P. (2021). Hydrologic and soil properties of mature bioretention cells in Ontario, Canada. *Water Science and Technology*, *84*(12), 3541–3560. Scopus. https://doi.org/10.2166/wst.2021.464

Spraakman, S., Rodgers, T. F. M., Monri-Fung, H., Nowicki, A., Diamond, M. L., Passeport, E., Thuna, M., & Drake, J. (2020a). A Need for Standardized Reporting: A Scoping Review of Bioretention Research 2000–2019. *Water*, *12*(11), 3122. https://doi.org/10.3390/w12113122

Spraakman, S., Rodgers, T. F. M., Monri-Fung, H., Nowicki, A., Diamond, M. L., Passeport, E., Thuna, M., & Drake, J. (2020b). A Need for Standardized Reporting: A Scoping Review of Bioretention Research 2000–2019. *Water*, *12*(11), 3122. https://doi.org/10.3390/w12113122

Stewart, R. D., Lee, J. G., Shuster, W. D., & Darner, R. A. (2017a). Modelling hydrological response to a fully-monitored urban bioretention cell. *Hydrological Processes*, *31*(26), 4626–4638. https://doi.org/DOI: 10.1002/hyp.11386

Stewart, R. D., Lee, J. G., Shuster, W. D., & Darner, R. A. (2017b). Modelling hydrological response to a fully-monitored urban bioretention cell. *Hydrological Processes*, *31*(26), 4626–4638. https://doi.org/10.1002/hyp.11386

Stewart, R. D., Rupp, D. E., Abou Najm, M. R., & Selker, J. S. (2016). A Unified Model for Soil Shrinkage, Subsidence, and Cracking. *Vadose Zone Journal*, *15*(3), 1–15. https://doi.org/10.2136/vzj2015.11.0146

Stovin, V. (2024). *Utilising Multiple Stormwater Control Metrics to Design Vegetated SuDS with Continuous Rainfall Inputs*. 16th International Conference on Urban Drainage, Delft, The Netherlands.

STU. (1982). *La Maîtrise du des eaux pluviales: Quelques solutions pour l'amélioration du cadre de vie (The management of urban stormwater: Solutions for environmental improvement)*. Ministère de l'Urbanisme et du Logement, Direction de l'Urbanisme et des ….

Su, J., Wang, M., Razi, M. A. M., Dom, N. M., Sulaiman, N., & Tan, L.-W. (2023). A Bibliometric Review of Nature-Based Solutions on Urban Stormwater Management. *Sustainability*, *15*(9), 7281. https://doi.org/10.3390/su15097281

Tahvonen, O. (2018). Adapting bioretention construction details to local practices in Finland. *Sustainability (Switzerland)*, *10*(2). Scopus. https://doi.org/10.3390/su10020276

Tang, S., Luo, W., Jia, Z., Liu, W., Li, S., & Wu, Y. (2016). Evaluating Retention Capacity of Infiltration Rain Gardens and Their Potential Effect on Urban Stormwater Management in the Sub-Humid Loess Region of China. *Water Resources Management*, *30*(3), 983–1000. Scopus. https://doi.org/10.1007/s11269-015-1206-5

Tansar, H., Duan, H.-F., & Mark, O. (2023). Statistical evaluation on hydrologic performance of bioretention design parameters under different rainfall

conditions. *IOP Conference Series: Earth and Environmental Science*, *1136*(1), 012024. https://doi.org/10.1088/1755-1315/1136/1/012024

Taylor, S. A., & Ashcroft, W. H. (1972). *Physical Edaphology—The Physics of Irrigated and Nonirrigated Soils* (Vol. 38). https://acsess.onlinelibrary.wiley.com/doi/10.2136/sssaj1974.03615995003800010002x

Técher, D. (2022). Using superpixel- or pixel-based segmentation for efficient green roof digital image classification and rapid estimation of plant species cover. *Urban Forestry & Urban Greening*, *76*, 127722. https://doi.org/10.1016/j.ufug.2022.127722

Técher, D., & Berthier, E. (2023). Supporting evidences for vegetation-enhanced stormwater infiltration in bioretention systems: A comprehensive review. *Environmental Science and Pollution Research*. https://doi.org/10.1007/s11356-023-25333-w

Tedoldi, D., Pierlot, D., Kovacs, Y., & Gromaire, M.-C. (2019). *Urban pollution control and soil contamination in Sustainable Drainage Systems: Insights gained from an extensive field study*. NOVATECH 2019, Lyon, France.

Tirpak, R. A., Afrooz, A. N., Winston, R. J., Valenca, R., Schiff, K., & Mohanty, S. K. (2021). Conventional and amended bioretention soil media for targeted pollutant treatment: A critical review to guide the state of the practice. *Water Research*, *189*, 116648. https://doi.org/10.1016/j.watres.2020.116648

Trowsdale, S. A., & Simcock, R. (2011). Urban stormwater treatment using bioretention. *Journal of Hydrology*, *397*(3–4), 167–174. https://doi.org/10.1016/j.jhydrol.2010.11.023

UDFCD. (2015). *Urban Storm Drainage Criteria Manual Volume 3*.

US EPA. (1990). *Pollution Prevention Act of 1990*. https://www.epa.gov/p2/pollution-prevention-act-1990

USDA Forest Service. (1980). *An Approach to Water Resources Evaluation of Non-point Silvicultural Sources*. U.S. Environmental Protection Agency Environmental Research Laboratory.

USKH. (2008, December). *LOW IMPACT DEVELOPMENT DESIGN GUIDANCE MANUAL*. Watershed Management Services Municipality of Anchorage.

Van Genuchten, M. Th. (1980). A Closed-form Equation for Predicting the Hydraulic Conductivity of Unsaturated Soils. *Soil Science Society of America Journal*, *44*(5), 892–898. https://doi.org/10.2136/sssaj1980.03615995004400050002x

Venvik, G., & Boogaard, F. C. (2020). Infiltration capacity of rain gardens using full-scale test method: Effect of infiltration system on groundwater levels in Bergen, Norway. *Land*, *9*(12), 1–18. Scopus. https://doi.org/10.3390/land9120520

Vinck, E., & Bock, B. D. (2024). *Lessons learnt from the continuous monitoring of infiltration systems*. 16th International Conference on Urban Drainage, Delft, The Netherlands.

Viviani, G., & Iovino, M. (2004). Wastewater Reuse Effects on Soil Hydraulic Conductivity. *Journal of Irrigation and Drainage Engineering*, *130*(6), 476–484. https://doi.org/10.1061/(ASCE)0733-9437(2004)130:6(476)

Wadzuk, B. M., Hickman, J. M., & Traver, R. G. (2015). Understanding the Role of Evapotranspiration in Bioretention: Mesocosm Study. *Journal of Sustainable Water in the Built Environment*, *1*(2), 04014002. https://doi.org/10.1061/JSWBAY.0000794

Walmsley, A. (1995). Greenways and the making of urban form. *Landscape and Urban Planning*, *33*(1–3), 81–127. https://doi.org/10.1016/0169-2046(95)02015-L

Wang, J., Chua, L. H. C., & Shanahan, P. (2019). Hydrological modeling and field validation of a bioretention basin. *Journal of Environmental Management*, *240*, 149–159. Scopus. https://doi.org/10.1016/j.jenvman.2019.03.090

Wang, M., Zhang, D., Li, Y., Hou, Q., Yu, Y., Qi, J., Fu, W., Dong, J., & Cheng, Y. (2018). Effect of a Submerged Zone and Carbon Source on Nutrient and Metal Removal for Stormwater by Bioretention Cells. *Water*, *10*(11), 1629. https://doi.org/10.3390/w10111629

Water by Design. (2014). *Bioretention Technical Design Guidelines* [Guideline]. https://www.newwaterways.org.au/downloads/Resources%20-%20Policy%20and%20Guidelines/SW%20and%20GW%20Mgmt/wbd_2014_bioretentiontdg_mq_online.pdf

Wen, X., Hu, Z., Jing, Y., Li, X., Zhang, X., & Chai, S. (2021). Influence of rainwater infiltration in partial anti-seepage bioretention on adjacent municipal roads in different collapsible grades loess sites. *Water (Switzerland)*, *13*(15). Scopus. https://doi.org/10.3390/w13152055

Wesseling, J. G., Elbers, J. A., Kabat, P., & Van den Broek, B. J. (1991). SWATRE: instructions for input. *Internal Note, Winand Staring Centre, Wageningen, the Netherlands*, *1991*, 700.

Whelans, C., Maunsell, H. G., & Palmer, T. (1994). Planning & management guidelines for water sensitive urban (residential) design: Consultants report prepared for the Department of Planning and Urban Development, the Water Authority of Western Australia and the Environmental Protection Authority. *Mount Hawthorn, WA: Whelans and Halpern Glick Maunsell in Association with Thompson Palmer and Institute for Science and Technology Policy, Murdoch University*.

William, R., Gardoni, P., & Stillwell, A. S. (2019). Reliability-Based Approach to Investigating Long-Term Clogging in Green Stormwater Infrastructure. *Journal of Sustainable Water in the Built Environment*, *5*(1). Scopus. https://doi.org/10.1061/JSWBAY.0000875

William, R., Gardoni, P., & Stillwell, A. S. (2021). Predicting rain garden performance under back-to-back rainfall conditions using stochastic life-cycle analysis. *Sustainable and Resilient Infrastructure*, *6*(3–4), 143–155. https://doi.org/10.1080/23789689.2019.1660549

Winston, R. J., Dorsey, J. D., & Hunt, W. F. (2016). Quantifying volume reduction and peak flow mitigation for three bioretention cells in clay soils in northeast Ohio. *Science of The Total Environment*, *553*, 83–95. https://doi.org/10.1016/j.scitotenv.2016.02.081

Woods Ballard, B., Wilson, S., Udale-Clarke, H., Illman, S., Scott, T., & Ashley, R. M. (2015). *The SuDS manual*. CIRIA.

Woods-Ballard, B., Kellagher, R., Martin, P., Jefferies, C., Bray, R., & Shaffer, P. (2007). *The SUDS manual* (Vol. 697). Ciria.

Xiong, J., Liang, L., Shi, W., Li, Z., Zhang, Z., Li, X., & Liu, Y. (2022). Application of biochar in modification of fillers in bioretention cells: A review. *Ecological Engineering*, *181*, 106689. https://doi.org/10.1016/j.ecoleng.2022.106689

Yang, F., Fu, D., Zevenbergen, C., & Rene, E. R. (2022). A comprehensive review on the long-term performance of stormwater biofiltration systems (SBS): Operational challenges and future directions. *Journal of Environmental Management*, *302*, 113956. https://doi.org/10.1016/j.jenvman.2021.113956

Zhang, H., Ahmad, Z., Shao, Y., Yang, Z., Jia, Y., & Zhong, H. (2021). Bioretention for removal of nitrogen: Processes, operational conditions, and strategies for improvement. *Environmental Science and Pollution Research*, *28*(9), 10519–10535. https://doi.org/10.1007/s11356-020-12319-1

Zhang, K., & Chui, T. F. M. (2017). Evaluating hydrologic performance of bioretention cells in shallow groundwater. *Hydrological Processes*, *31*(23), 4122–4135. Scopus. https://doi.org/10.1002/hyp.11308

Zhang, K., & Chui, T. F. M. (2018). Interactions between shallow groundwater and low-impact development underdrain flow at different temporal scales. *Hydrological Processes*, *32*(23), 3495–3512. Scopus. https://doi.org/10.1002/hyp.13272

Zhang, K., & Chui, T. F. M. (2019). A review on implementing infiltration-based green infrastructure in shallow groundwater environments: Challenges, approaches, and progress. *Journal of Hydrology*, *579*, 124089. https://doi.org/10.1016/j.jhydrol.2019.124089

Zhang, K., Chui, T. F. M., & Yang, Y. (2018). Simulating the hydrological performance of low impact development in shallow groundwater via a modified SWMM. *Journal of Hydrology*, *566*, 313–331. https://doi.org/10.1016/j.jhydrol.2018.09.006

Zhang, K., Liu, Y., Deletic, A., McCarthy, D. T., Hatt, B. E., Payne, E. G. I., Chandrasena, G., Li, Y., Pham, T., Jamali, B., Daly, E., Fletcher, T. D., & Lintern, A. (2021). The impact of stormwater biofilter design and operational variables on nutrient removal—A statistical modelling approach. *Water Research*, *188*, 116486. https://doi.org/10.1016/j.watres.2020.116486

Zhang, L., Lu, Q., Ding, Y., Peng, P., & Yao, Y. (2018). Design and Performance Simulation of Road Bioretention Media for Sponge Cities. *Journal of Performance of Constructed Facilities*, *32*(5). Scopus. https://doi.org/10.1061/(ASCE)CF.1943-5509.0001209

Zhang, L., Oyake, Y., Morimoto, Y., Niwa, H., & Shibata, S. (2019). Rainwater storage/infiltration function of rain gardens for management of urban storm runoff in Japan. *Landscape and Ecological Engineering*, *15*(4), 421–435. Scopus. https://doi.org/10.1007/s11355-019-00391-w

Zhang, L., Oyake, Y., Morimoto, Y., Niwa, H., & Shibata, S. (2020). Flood mitigation function of rain gardens for management of urban storm runoff in Japan. *Landscape and Ecological Engineering*, *16*(3), 223–232. Scopus. https://doi.org/10.1007/s11355-020-00409-8

Zhang, Y., & Schaap, M. G. (2017). Weighted recalibration of the Rosetta pedotransfer model with improved estimates of hydraulic parameter distributions and summary statistics (Rosetta3). *Journal of Hydrology*, *547*, 39–53. https://doi.org/10.1016/j.jhydrol.2017.01.004

Zhou, J., Xiong, J., Xu, Y., Zhang, F., & Zhang, F. (2023). Performance evaluation of a low-cost loess-based filler for bioretention cells. *Journal of Environmental Management*, *344*, 118542. https://doi.org/10.1016/j.jenvman.2023.118542